Florida International University

FIU Digital Commons

3-28-2019

Control and Optimization of Energy Storage in AC and DC Power Grids

Samy Mohamed
sfadd002@fiu.edu

Follow this and additional works at: https://digitalcommons.fiu.edu/etd

Part of the Electrical and Electronics Commons

FLORIDA INTERNATIONAL UNIVERSITY

Miami, Florida

CONTROL AND OPTIMIZATION OF ENERGY STORAGE IN AC AND DC POWER

GRIDS

A dissertation submitted in partial fulfillment of the

requirements for the degree of

DOCTOR OF PHILOSOPHY

in

ELECTRICAL AND COMPUTER ENGINEERING

by

Samy Gamal Faddel Mohamed

2019

To: Dean John Volakis
      College of Engineering and Computing

This dissertation, written by Samy Gamal Faddel Mohamed, and entitled Control and Optimization of Energy Storage in AC and DC Power Grids, having been approved in respect to style and intellectual contents, is referred to you for judgment.

We have read this dissertation and recommend that it be approved.

_____
Ahmed Ibrahim

_____
Mohammed Hadi

_____
Sakhrat Khizroev

_____
Osama A. Mohammed, Major Professor

Date of Defense: March 28, 2019

The dissertation of Samy Gamal Faddel Mohamed is approved.

_____
Dean John Volakis
College of Engineering and Computing

_____
Andrés G. Gil
Vice President for Research and Economic Development
and Dean of the University Graduate School

Florida International University, 2019

ii

DEDICATION

For their endless support, love, and sacrifice, I dedicate this work.

To my Beloved Parents, my Sisters and Dear Wife Haneen.

ACKNOWLEDGMENTS

ABSTRACT OF THE DISSERTATION

CONTROL AND OPTIMIZATION OF ENERGY STORAGE IN AC AND DC POWER

GRIDS

by

Samy Gamal Faddel Mohamed

Florida International University, 2019

Miami, Florida, USA

Professor Osama A. Mohammed, Major Professor

Energy storage attracts attention nowadays due to the critical role it will play in the power generation and transportation sectors. Electric vehicles, as moving energy storage, are going to play a key role in the terrestrial transportation sector and help reduce greenhouse emissions. Bulk hybrid energy storage will play another critical role for feeding the new types of pulsed loads on ship power systems. However, to ensure the successful adoption of energy storage, there is a need to control and optimize the charging/discharging process, taking into consideration the customer preferences and the technical aspects. In this dissertation, novel control and optimization algorithms are developed and presented to address the various challenges that arise with the adoption of energy storage in the electricity and transportation sectors.

Different decentralized control algorithms are proposed to manage the charging of a mass number of electric vehicles connected to different points of charging in the power distribution system. The different algorithms successfully satisfy the preferences of the customers without negatively impacting the technical constraints of the power grid. The developed algorithms were experimentally verified at the Energy Systems Research

Laboratory at FIU.

In addition to the charge control of electric vehicles, the optimal allocation and sizing of commercial parking lots are considered. A bi-layer Pareto multi-objective optimization problem is formulated to optimally allocate and size a commercial parking lot. The optimization formulation tries to maximize the profits of the parking lot investor, as well as minimize the losses and voltage deviations for the distribution system operator. Sensitivity analysis to show the effect of the different objectives on the selection of the optimal size and location is also performed.

Furthermore, in this dissertation, energy management strategies of the onboard hybrid energy storage for a medium voltage direct current (MVDC) ship power system are developed. The objectives of the management strategies were to maintain the voltage of the MVDC bus, ensure proper power sharing, and ensure proper use of resources, where supercapacitors are used during the transient periods and batteries are used during the steady state periods. The management strategies were successfully validated through processor in the loop simulations.

TABLE OF CONTENTS

LIST OF TABLES

LIST OF FIGURES

LIST OF ACRONYMS

ACRONYMS	DETAILS
AES	All Electric Ship
AGC	Automatic Generation Control
AIMD	Additive Increase - Multiplicative Decrease
BESS	Battery Energy Storage Station
BEV	Battery Electric Vehicle
COP	Conference of the Parties
CPP	Critical Peaking Pricing
DA	Day-Ahead
DDS	Data Distribution Service
DG	Distributed Generation
DSM	Demand-Side Management
DSO	Distribution System Operator
EMALS	Electromagnetic Aircraft Launch System
ERCOT	Electric Reliability Council of Texas
ESS	Energy Storage Systems
EV	Electric Vehicle
EVA	Electric Vehicle Aggregator
FLC	Fuzzy Logic Controller
FR	Frequency Regulation
G2V	Grid to Vehicle

HEV	Hybrid Electric Vehicle
ICE	Internal Combustion Engine
IEC	International Electrotechnical Commission
LA	Load Aggregator
LFC	Load Frequency Control
LSE	Load-Serving-Entity
LVAC	Low Voltage Alternative Current
LVDC	Low Voltage Direct Current
MMGA	Mathematical Morphology Gradient Algorithm
MTOU	Multi-Group Time-of-Use
MTOUCP	Multi-Group TOU with Critical Peaking
MOOP	Multi-Objective Optimization Problem
MVAC	Medium Voltage Alternative Current
MVDC	Medium Voltage Direct Current
NSGA	Non-dominated Sorting Genetic Algorithm
PEV	Plug-in Electric Vehicle
PF	Pareto Front
PHEV	Plug-in Hybrid Electric Vehicle
PL	Parking Lot
PO	Pareto Optimality
POC	Point of Charging
PV	Photo-Voltaic

PWM	Pulse Width Modulation
RT	Real-Time
SOC	State of Charge
TOU	Time-of-Use
V2B	Vehicle to Building
V2G	Vehicle to Grid
V2V	Vehicle to Vehicle

Chapter 1   Introduction

Energy storage will be the cornerstone in the future energy transition, providing services throughout the electricity system value chain and into the end-user sector [1]. The increasing demand for more flexibility in the power system, the dramatic changes in the transportation sector to mitigate the climate change, and the important inter-linkages between sectors are the major drivers behind the evolving interest in the energy storage in the energy transition map.

A considerable renewable energy curtailment has been reported in recent years [2]. The power curtailment is primarily driven by the unmatched generation and demand hours, where the increase in the electricity generation, coming from renewable resources, occurs during the low-demand period. This represents a waste of energy and inefficient operation of the overall resources in the power sector. Energy storage can greatly reduce the level of power curtailment by charging during the high generation periods and discharging during the low generation periods.

The increasing concerns about climate change and the need to decarbonize the transportation sector, as a major reason for CO_2 emission, is also pushing toward more adoption of energy storage in the future transportation sector. The increasing role and interest in batteries can be witnessed by examining the new production capacity for batteries of electric vehicles (EVs). For example, the projected annual production of 35 GWh of cells by Tesla Gigafactory captured the news in 2016. The planned capacity expansion of energy storage by 2021 now totals over 220 GWh, with more than half planned in China.

Energy storage can also provide additional services to the energy system by integrating the electricity, heating & cooling, gas, and transportation sectors. Such technologies can help provide competitive flexibility to the electricity system and can transfer the share of renewables originally generated in the electricity sector to other sectors.

To see the different applications where energy storage can be used, the types of different energy storage devices and their capabilities will be briefly presented. Then, the applications of the different energy storage devices will be discussed.

1.1   Types of Different Energy Storage Devices

Generally speaking, the different technologies of energy storage devices can be classified based on their storage principle, as shown in Figure 1.1. The members of each type may change with the technological developments. However, these five types reflect the main storage principles. The provided examples under each type are not meant to be comprehensive. The different types of energy storage are:

1. Mechanical energy storage, which combines several principles ranging from potential energy in pumped hydro storage, the volume and pressure work of air/liquid in compressed air/liquid energy storage to the rotational energy of a mass in flywheels.

2. Electrical energy storage, which stores electricity in the form of electrons. It can be stored as an electric field in the case of supercapacitors and a magnetic field in the case of a super conducting magnetic coil. Usually the energy capacity of this electrical storage is limited, but it has a high-power density.
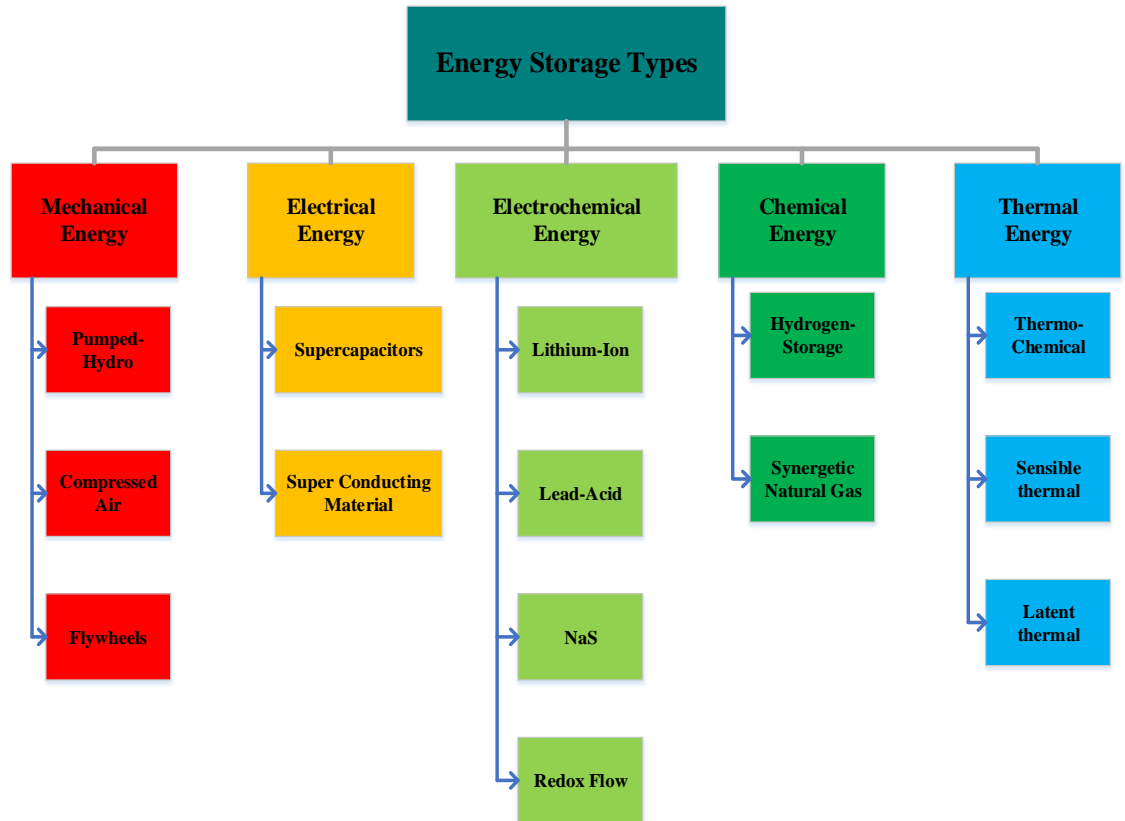
Figure 1.1: Energy storage classifications

3. Electrochemical energy storage that covers the different types of batteries. In this type of storage, the chemical energy is stored and converted to electrical energy and vice-versa in electrochemical reactions. The batteries can be conventional ones or flow batteries. Flow batteries differ from conventional rechargeable batteries in that the electroactive materials are not all stored within the electrode but, instead, are dissolved in electrolyte solutions that are stored in tanks [3]. Flow batteries offer valuable operational advantages, since they work at ambient temperatures, and their power and energy storage characteristics are independently scalable.

4. Chemical energy storage, which stores the energy in a chemical form that might be liquid, gaseous or solid, and the energy is also released in chemical reactions. The most common form of it is the hydrogen storage and synergetic natural gas. They usually have a high-energy density and provide a variety of transport options.

5. Thermal energy storage, where the energy can be stored in the sensible heat or the latent heat or using a thermos-chemical process. In general, thermal storage is quite cost-effective compared to other storage options.

While each storage type can be used on its own, hybrid types of storage devices can also be used. They are usually used to combine the different advantages of each type in a complementary way, which can result in a better utilization, and increase the lifetime and efficiency of the storage system. For example, a high-energy density storage like batteries can be combined with a high-power density, such as supercapacitors or flywheels, to form a complementary hybrid energy storage system. Figure 1.2 shows the characteristics of the different types of energy storage. The figure shows that they vary greatly in the charging/discharging time (from seconds to days) and their output power (from watts to gigawatts). Pumped storage and compressed air energy storage systems are often termed "bulk energy storage," since they generally store larger amounts of energy than battery storage systems. Some energy storage technologies and applications are well established, while others are in various stages of research and development [4].

The current worldwide usage of the different storage types is shown in Table 1.1. The Table shows that the current capacity of energy storage is 196.348 GW. Although the

4

dominant type of energy storage is pumped hydro storage, representing 94.3% of the total installed capacity, it is not expected that pumped hydro technology will evolve and develop more in the future since it is already a mature technology that has been used for decades. Electrochemical energy storage is expected to dominate the future sales of the storage market. This is basically driven by the fast expansion in the transportation sector, with the Lithium-Ion battery as the most promising battery type so far. The cost of Li-Ion batteries fell by as much as 73% between 2010 and 2016 for transportation applications [3].
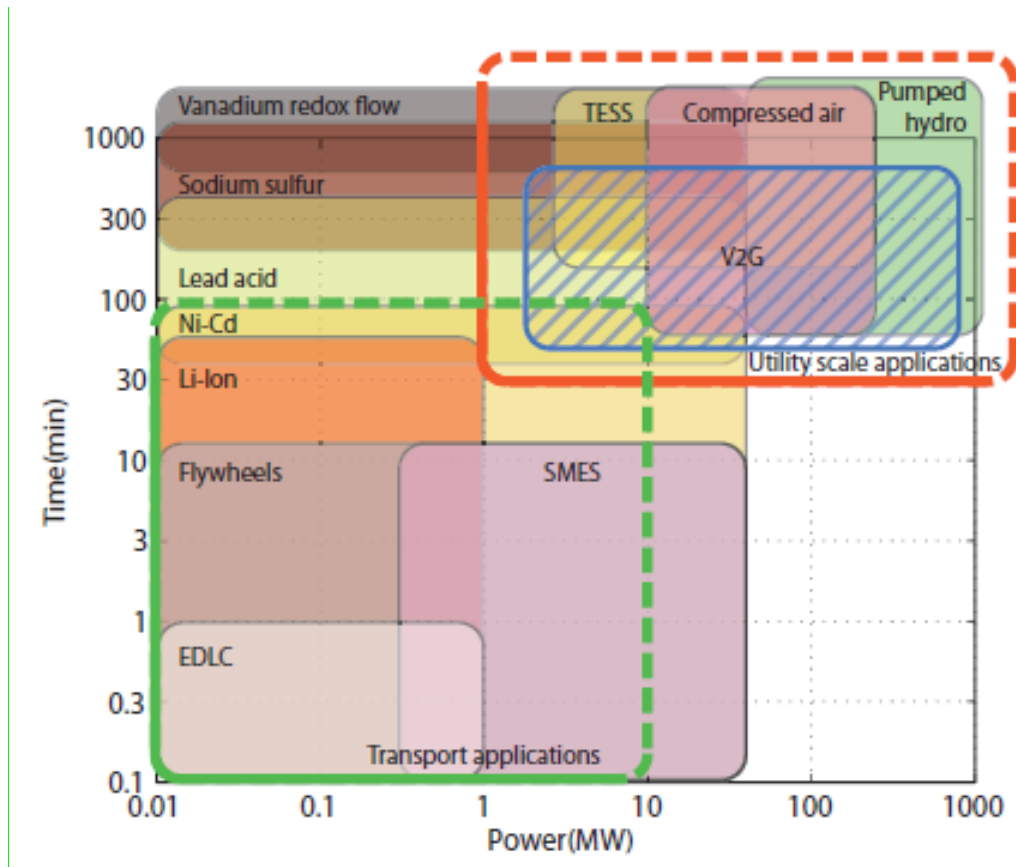
Figure 1.2: Performance characteristics of different energy storage types [6]

Table 1.1: Current usage of storage technologies [a]

Technology Type	Projects	Rated Power (MW)
Electro-chemical	1074	4460
Pumped Hydro Storage	352	185193
Thermal Storage	220	4031
Electro-mechanical	73	2588
Hydrogen Storage	14	22
Liquid Air Energy Storage	2	5

1.2 Applications of Energy Storage

Energy storage devices have many applications in the energy sector. However, the majority of applications are in the electricity sector, where the energy storage can provide many capacity and ancillary services. The main services that can be provided by the energy storage in the electricity sector are shown in Figure 1.3. Broadly speaking, the application of energy storage can be divided into utility applications and transportation applications.

1.2.1 Utility Applications

The adoption of energy storage in modern power systems is growing due to the increasing levels of stability problems. The main job of a storage plant in the power grid is to enhance the power quality and ensure load-generation balance. Although renewable energy sources are environmentally beneficial, their intermittent nature causes voltage and frequency fluctuations in the grid. This represents a significant barrier to their widespread adoption and replacement of fossil-fuel-based generation [5].

[a] DOE online visualization: https://www.energystorageexchange.org/projects/data_visualization

With high penetration of renewable energy resources, the ability of the conventional generators to match the intermittent generation and demand becomes an important concern. Utilities in the United States have expressed concerns about their systems "bottoming out" due to the minimum generation requirements during overnight hours, and being unable to accommodate more intermittent renewable generation during these times. The repetitive cycling and high-frequency MW power changes are another pressing issue because they can cause damage to the generation plants. With the exception of fast-starting reciprocating engines, most conventional plants have minimum up-and-down times, and require several hours to restart—at considerable cost [1]. When used in the power system, energy storage can provide multiple benefits to the electric utility, helping them integrate more renewable resources. Energy storage can be used to ensure the frequency stability of system and provide more system inertia.
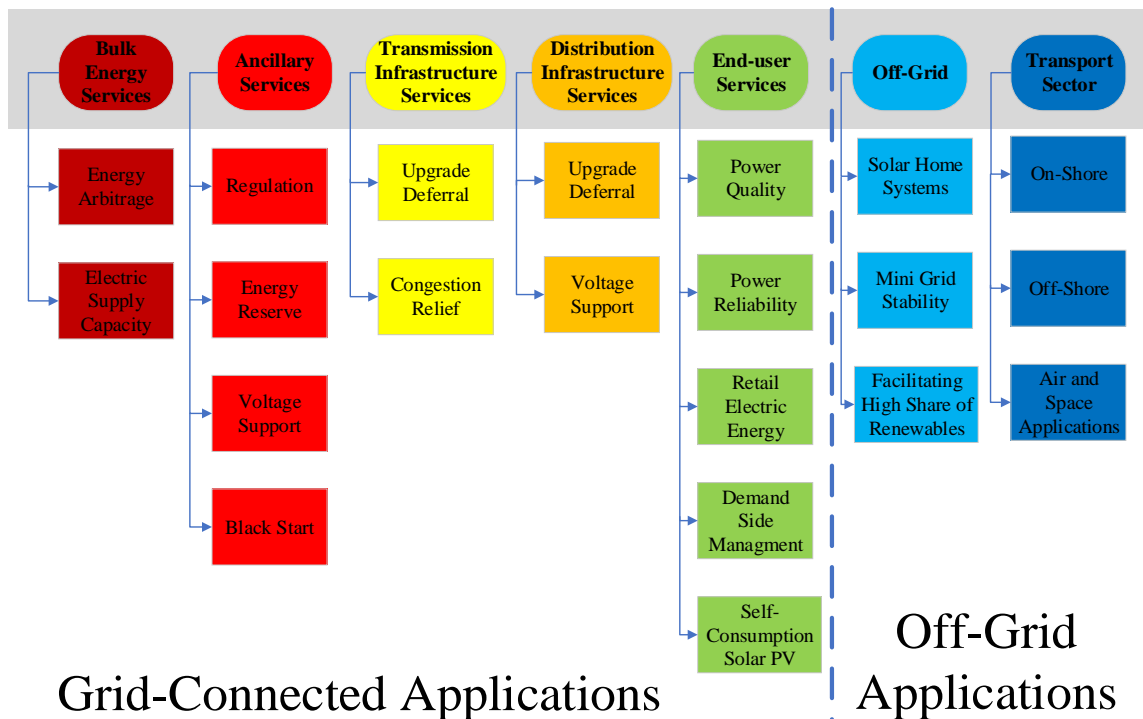
Figure 1.3: Services that can be provided by the energy storage

Energy storage can provide multiple services to electric utilities, ranging from bulk service, such as the energy arbitrage, deferring the transmission and distribution upgrades to power quality and behind-the-meter end-users services. In addition, energy storage can provide regulation and spinning reserve services in the whole-sale market, providing more opportunities and more room for revenue.

1.2.2 Transportation Applications

Energy storage devices will play a critical role in the future transportation sector. Electric vehicles, as moving energy storage, are going to play a key role in the terrestrial transportation sector. Other energy storage devices, such as large batteries, flywheels and supercapacitors, will play another key role in space and maritime ship power systems.

The main drivers behind electrifying the transportation sector are to reduce oil-dependency, reduce the greenhouse emissions, and increase the overall efficiency of the system. When it comes to the terrestrial transportation sector, there are two ways to store electricity and shift from the oil-driven internal combustion engines (ICE). One way is to switch from oil-derived fuels to one of several electricity-derived fuels, either gaseous or liquid, with hydrogen receiving the most attention in recent years. The other way is to store the electricity on-board, primarily using batteries, and use the stored electricity to drive an electric motor. Based on the way of generating the on-board electricity and the type of the driving engine, the vehicle can be either a pure battery electric vehicle (BEV) or a plugin hybrid electric vehicle (PHEV) that uses both stored electricity and an ICE or fuel cell engine. The required power and discharging/charging periods for the different terrestrial transportation means are shown in Figure 1.4.
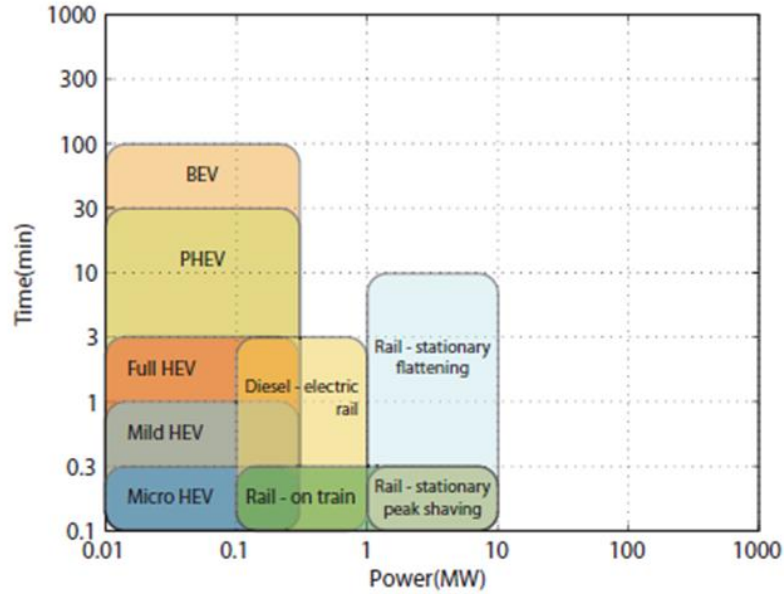
Figure 1.4: Characteristics of the different terrestrial transportation means [6]

At the end of 2016, the global electric vehicle fleet reached a total size of 2 million vehicles (including battery EVs and plugin hybrid vehicles). A representative from the Natural Resources Defense Council estimated that the Chinese electric vehicle regulation could result in the production of more than 1 million electric vehicles per year by 2020 [4].

In the case of maritime applications, the presence of on-board energy storage will be critical in the next generation of all electric ships [7]. This is driven by the growth of the on-board auxiliary electric loads, the emerging types of pulsed loads, and the capacity needed to support the propulsion system. Energy storage will be needed in both the commercial sector and for military applications.

For the commercial sector, the major driver will be the fuel economy. Instantaneous fluctuations of the on-board demand (e.g, dynamic positioning) will break the balance between the power generation and demand. Since the currently used diesel generators are

9

designed to work in their fixed high-efficiency area and modulate the number of running engines to achieve optimal load matching, the instantaneous fluctuations will reduce the fuel efficiency. Thus, the use of fast controllable storage devices will help meet the load fluctuations and increase the efficiency of the system.

For military applications, energy storage devices will be mainly used to increase ship survivability and to enable high-energy pulsed loads. Without the energy storage devices, the shipboard generators would need to be significantly oversized to support the emerging high-energy pulsed loads, which will increase the initial and operational costs of the system.

1.3   Problem Statement

Adopting a large number of different storage devices in the transportation sector will bring many benefits to the energy sector in general, and will greatly change the current electricity sector, bringing more opportunities and challenges.

On the one hand, the impacts of vehicles' electrification on the distribution system will be magnificent and complex. A large number of electric vehicles that are charging at the same time might overload the system, which could reduce the lifetime of distribution transformers, and cause repetitive connection/disconnection of voltage control units. In addition, distribution system upgrades might be necessary, causing large investments in the infrastructure.

Moreover, providing charging stations for residential and commercial parking lots needs to be carefully studied and addressed. Electric vehicles' charging stations are more

10

complicated than conventional gas stations because electricity is a commodity that will not be stored, and the operator of the parking lot needs to satisfy multiple charging requests from different vehicles with different preferences. In addition, the vehicles are expected to be parking for longer time periods.

Also, when parked, electric vehicles can provide multiple grid services. With smart control of the charging process, electric vehicles can be considered as dispatchable-loads. If the vehicles are allowed to discharge, they can be considered as prosumers in the distribution system, providing valuable services to the operator of the system.

On the other hand, future electric ships will be a large-scale power system with complex and different loads. One potential solution to ensure load-generation balance and increase fuel efficiency will be a distributed energy storage system, which is based on a cluster of large or small storage systems, using different kinds of energy storage devices. At present, the most promising, dominant energy storage devices for maritime applications are batteries, supercapacitors, and flywheels [7]. Energy management and control of the system will be a crucial task for the successful adoption of the storage devices. The on-board storage system should enable multiple functions, such as providing power to un-interruptible loads during power outages, supporting mission loads, and providing system stability.

1.4   Research Objectives

The main objective of this dissertation is to develop control and optimization algorithms to facilitate the adoption of storage devices in the transportation sector without negatively impacting the power grid. Also, the dissertation investigates how the storage

11

devices can help improve the power system's efficiency. The dissertation focuses on the use and management of batteries in electric vehicles and the use of hybrid energy storage in shipboard power systems.

The control and management strategies should satisfy the customer and/or operator preferences, the system technical constraints, and the involved economic issues. From that perspective, decentralized control algorithms are appropriate solutions that can reduce the drawbacks of centralized algorithms, such as the large investment required for the communication infrastructure. Also, they do not suffer from the single-point failure problem, in case of the loss of the main communication link. In decentralized or distributed control algorithms, the charging/discharging reference decision is not processed and generated using the aggregator or the system operator. Instead, the aggregator or the system operator generates some sort of a signal to incentivize the participating storage units to do a certain action. However, each unit decides on its charging/discharging rate based on its own preferences, and no private information is sent back to the aggregator or the operator [7]. Based on that, the major aspects of the dissertation are:

1. Studying the effect of uncoordinated charging of a substantial number of electric vehicles that are dispersed in the power grid.

2. Developing a proper control framework and evaluating it experimentally.

3. Designing an intelligent control algorithm to make the best use of distributed electric vehicles in demand-side management.

4. Formulating a multi-objective optimization problem to optimally allocate and size an electric vehicles' parking lot.

5. Developing an energy management framework for multiple sources and energy storage to meet the pulsating load demand of a ship power system.

1.5 Original Contribution of this Dissertation

The main goal of the research work in this dissertation is to facilitate the integration of electric vehicles (EVs) into the transportation sector without negatively impacting the power grid, and to make the best use of energy storage in shipboard power systems in the presence of the high demand of pulsed loads. To achieve that, a thorough analysis of the impacts of the uncoordinated charging of electric vehicles dispersed in different locations of the distribution system is done. The analysis is done, using simulation, on an 18-bus distribution system, including the modelling of both the primary and secondary distribution system. Also, the analysis is verified experimentally using a small-scale laboratory distribution system with multiple Lithium-Ion batteries and converters. The results showed that the uncontrolled charging of electric vehicles will have severe impacts on the distribution system, causing high system peaks and severe under-voltage problems. The results also emphasized the fact that future charging stations must follow the standard charging arrangement at unity or 0.95 capacitive power factors, or repetitive operations will be needed from the voltage control units in the system, which will reduce the lifetime of the power system components.

To mitigate the negative impacts of the uncoordinated charging of EVs, an autonomous control algorithm is developed to ensure the proper charging of EVs without negatively affecting the power system. The algorithm takes into consideration the preferences of the

EV owners, as well as the system's technical constraints, such as voltage limits. The algorithm is validated experimentally. In addition, the algorithm is verified in the presence of distributed generation units. The results showed that the proposed algorithm can ensure fair charging among the different EVs connected to the system without violating the grid's technical constraints.

For electric utilities that incorporate demand-side management (DSM) programs, EVs could become either a burden or an advantage, depending on their charging control strategy and the signaling of the DSM program. Therefore, a decentralized fuzzy-based controller is proposed to successfully integrate and coordinate the charging of EVs, while providing grid services, if needed by the power grid operator. Also, a new DSM scheme that is capable of benefiting from EVs as prosumers, which can provide grid services, is suggested and tested. The new scheme effectively helped mitigate the system peaking and avoided introducing new peaks "the rebound effect." The new scheme is compatible with the current DSM infrastructure and does not need any further investments.

Usually, the EV owners will primarily prefer to charge their vehicles at homes. However, many EV owners do not have a private parking space. Therefore, there will be a need for non-residential charging stations in other places, such as work, business districts, near bulky public transportation stations, and other public facilities. To that end, this dissertation proposes a multi-objectives optimization methodology to optimally allocate and size future EV parking lots. The proposed algorithm takes into consideration the economic aspects of the parking lots, such as maximizing the profits of the investor of the

parking lot, and at the same time the technical aspects of the distribution system, such as minimizing the voltage deviations and power losses in the system.

In addition to the control and optimization of the charging of EVs, investigating the use of hybrid energy storage in a shipboard power system is performed.

Due to the nature of the emerging pulsed loads connected to the shipboard medium voltage direct current (MVDC) power systems, conventional generators are not able to respond to the high ramping rate of these types of loads. Therefore, the existence of energy storage systems will be mandatory for the successful and smooth operation of the MVDC system.

To ensure a satisfactory performance of a MVDC power system with pulsed loads, an energy management strategy to control the operation of a combination of supercapacitors and batteries is developed. The objectives of the management strategy are to maintain the voltage of the MVDC bus, ensure proper power sharing, and ensure proper use of resources, where supercapacitors are used during the transient periods and the batteries are used during the steady state periods. To achieve these objectives, a modified droop-based control algorithm supported by a signal processing tool, such as the mathematical morphology gradient algorithm (MMGA), and state machine logic were designed and tested on a notional MVDC shipboard power system. The management strategy is validated through FPGA in the loop.

Also, an artificial intelligence-based algorithm is developed to add a level of robustness and intelligence to the shipboard power system. The algorithm is tested under different loading conditions and different states of charges of the storage devices.

The results showed that the proposed algorithms can successfully insert/remove the appropriate storage device during the transient and the steady state periods. In addition, they are able to maintain the voltage of the MVDC bus in the case of an overcharged/undercharged storage unit, while not negatively affecting the storage devices.

1.6   Dissertation Organization

Chapter 2 provides an overview about the different types of EVs and their different applications in the power grid. Also, the chapter presents a comprehensive literature review about the different control and optimization techniques that are used to manage the charging of EVs.

Chapter 3 studies the impact of the uncontrolled charging of EVs on the distribution system using MATLAB/Simulink. In this chapter, an automated charge controller is also proposed to ensure fair charging among the different EVs without mitigating the distribution system.   Sensitivity analysis is performed to study the effect of the controller parameters on the charging of EVs and the distribution system.

Chapter 4 provides an experimental verification of the impacts of the uncontrolled charging of EVs. In addition, an experimental validation of the automated controller, discussed in chapter 3, is presented.

Chapter 5 introduces a decentralized fuzzy-based controller to successfully integrate and coordinate the charging of EVs. The chapter also investigates the effect of the charging of

EVs under different DSM schemes. In addition, a new DSM scheme that is capable of benefiting from EVs, as prosumers that can provide grid services, is proposed and tested.

Chapter 6 proposes a Pareto-based multi-objective optimization formulation to optimally size and allocate a commercial EV parking lot. The optimization formulation tries to maximize the profits of the investor of the EV parking lot, as well as minimize the losses and voltage deviations for the distribution system operator. Sensitivity analysis to show the effect of the different objectives on the selection of the optimal size and location is also performed.

Chapter 7 presents an improved decentralized control algorithm for the charging of EVs in a microgrid. The algorithm is based on the Additive Increase - Multiplicative Decrease (AIMD) algorithm, which is commonly used for the management of communication network congestions. The algorithm is tested using a co-simulation platform, where a real-communication network is used with MATLAB via the Data Distribution Service (DDS) middleware.

Chapter 8 provides an overview about the MVDC ship power system and its different components. Also, the effect of the pulsed loads on the system is investigated and mitigated using a battery system as an initial study.

Chapter 9 provides a decentralized droop-based control algorithm with the MMGA as a signal processing technique. The algorithm is used to manage a hybrid energy storage system that is used to mitigate the effect of integrating the pulsed loads into the MVDC ship power system. The control algorithm is validated using FPGA in the loop simulation.

Chapter 10 adds a level of intelligence to the shipboard power system by using fuzzy logic as an expert system to decide on the charging/discharging reference for the different storage devices on the shipboard.

Chapter 11 concludes this dissertation and gives insight on the future work.

Chapter 2   Charge Control and Operation of Electric Vehicles in Power

Grids

Electric Vehicles (EVs) and hybrid Electric vehicles (HEVs) are going to reshape the future of the transportation sector. However, adopting large numbers of EVs and HEVs will impact the electric utilities as well. Managing the charging/discharging of substantial numbers of distributed batteries will be critical for the successful adoption of EVs and HEVs. Therefore, this chapter presents a literature review about the recent control and optimization strategies for managing the charging/discharging of EVs. The chapter covers different control and operation strategies reported in the literature, as well as issues related to the real time dispatching of EVs in the smart grids. In addition, challenges related to the stochastic nature of the driving characteristics of EVs are considered.

2.1   Introduction

The increased concerns about greenhouse emissions and the signing of the 21st Conference of the Parties (COP21) agreement in Paris in December 2015 by 175 countries [8], [9] reaffirms the urgent need to strengthen the global response to climate change. The electricity and transportation sectors are major players in achieving the objective of limiting the rise of the average earth temperature to 2 °C. Electric Vehicles (EVs) and hybrid EVs (HEV) are seen as the main contributors to achieving that objective, as they reduce the carbon emissions in the transportation sector, which are responsible for almost one quarter (23%) of greenhouse emissions [10]. EVs help increase the energy efficiency since the electric motors used in EVs are more efficient than the internal combustion engines used in conventional vehicles. Also, EVs will help in the reduction of greenhouse

emissions in the electricity sectors by supporting the integration of renewable energy resources in the global power generation mix. As such, EVs can increase the energy independence of nations by reducing the need for oil in the transportation sectors. They also help in increasing the quality of air in large polluted cities, which was one of the reasons for the Chinese national plan of "ten cities and thousands units" to promote the penetration of EVs into the public transportation sector (e.g., buses and taxis) across more than 25 cities.

With that increasing interest and growing deployment of electric vehicles, there will be a need to develop algorithms to control the charging/discharging of large numbers of EVs. EVs, from the power system point of view, can be regarded as a producer or consumer (known as prosumer), depending on their operational mode of charging or discharging. Considerable numbers of EVs bring challenges or opportunities to the smart grid, depending on their control strategy. On one hand, they can cause negative impacts on the grid. These impacts can range from line overloading in both primary and secondary distribution systems to transformers overloading [4,5], line losses [13], low voltages and voltage unbalances [14]. On the other hand, EVs, as controllable loads, can provide more flexibility to the system operator in demand-side management by better valley filling, peak shaving, and increasing the system efficiency [15]. Also, they can provide ancillary services to the grid, such as regulation and reserve services [16]. This is especially important for power systems in the presence of a high share of intermittent renewable energy resources, where the system inertia is a big challenge. A considerable group of EVs

can help mitigate the inertial loss by behaving as a large storage unit [17]. EVs can also be valuable for local voltage and reactive power support [18].

2.2 Types and Usage of Vehicles

At the beginning of the 20th century, the automobile began to dominate transportation, with three types of vehicles competing for market share, which are steam-powered engines, internal combustion engines (ICEs) and electric vehicles (EVs). Initially, electric vehicles fared well in comparison to competitors, with a smooth, quiet ride, no tailpipe emissions, and relatively reliable starting for higher expense [19]. Despite the general acceptance with the public, EVs faced several drawbacks, some of which are still present to date, including relatively short driving range and unavailability of convenient, cost-effective charging stations beyond the major population centers. Because of these shortcomings, ICEs became much more attractive in comparison to EVs when the electric starter was invented in 1912, replacing a difficult to operate and often dangerous crank starter [19]. With ICEs' easy starting and EVs' limited distance per battery charge, the EV was fast becoming a niche market.

However, nowadays, with the rapid improvements in the battery technology in terms of higher battery density and lower costs (as shown in Figure 2.1), EVs have come into the picture again. In addition to these technological improvements, the need to mitigate climate change and air pollution will lead to deploying more EVs in the future. Figure 2.2 shows the evolution of the global EV stock and the distribution of EVs in different countries. The pattern shown in Figure 2.2 depicts that more EVs will be adopted in the future. Also, the

21

introduction of more public charging stations, which will be explained later, helped make the EVs more acceptable.
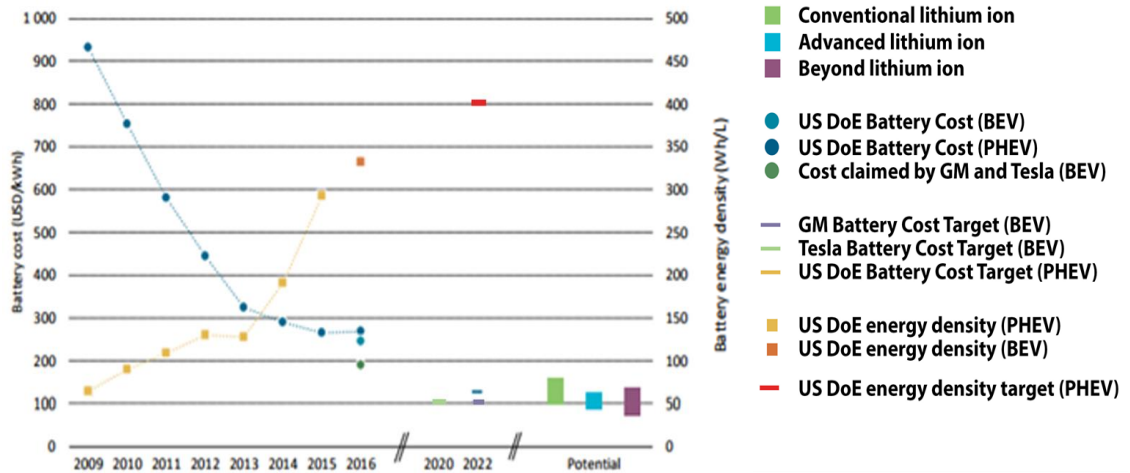
Figure 2.1: Evolution of battery energy density and cost [10]

When only considering plug-in electric vehicles (PEVs), electric vehicles whose batteries can be charged by plugging into the electricity grid, vehicles can be divided into battery electric vehicles (BEVs) and plug-in hybrid electric vehicles (PHEVs) [20]. The rated capacity, maximum charging rate and electric mileage range of some types of commercially available EVs [21] are shown in Table 2.1. Other types are available in [21] as well.

To increase the acceptance of EVs, EV manufacturers and different municipalities started to install and provide incentives for the installation of EV charging stations. Mainly, there are three types of charging stations, which are AC level 1, AC level 2, and DC fast charging. AC level 1 and 2 charging stations feed the EV with an AC current that is

22

converted to DC current using the onboard charging equipment, where the charger is onboard in the vehicle. They differ in their voltage and current ratings. The third type, DC fast charging, provides high DC current to the vehicle. Due to the large current, the DC fast charger must be off-board [22]. Details about the different charging stations are given in Table 2.2. The expected spread of the different charging stations according to their convenience is illustrated in Figure 2.3.
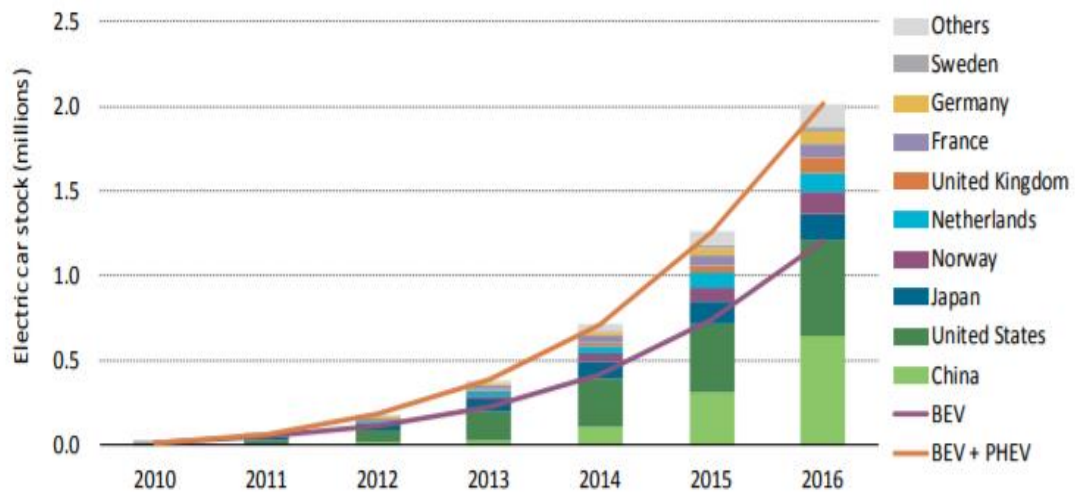
Figure 2.2: Evolution of the global electric car stock, 2010-16 [10]

Table 2.1. Commercial EV examples [21]

Model	Type	Capacity (kWh)	Charging Rate (kW)	Electric Range (miles)	Price ($)
Nissan Leaf	BEV	30	6.6	107	$29,000
Tesla model S	BEV	100	10	315	$71,000
Chevrolet Bolt	BEV	60	7.2	238	$37,500
Toyota Prius	PHEV	9	3.3	25	$28,000
Ford Fusion Energy	PHEV	7	3.3	19	$33,900

Table 2.2. Charging stations characteristics [22]

Charging Level	Vehicle Range Added per Charging Time and Power	Supply Power	Unit Cost Range Per (Single Port)
AC Level 1	4 miles/h @ 1.4 kW	120 V/20 A (14–16 A continuous)	$300–$1500
	6 miles/h @ 1.9 kW		
AC Level 2	10 miles/h @ 3.4 kW	(208/240)VAC (16–80 A continuous)	$400–$6500
	20 miles/h @ 6.6 kW		
	60 miles/h @ 19.2 kW		
DC Fast Charging	24 miles/h @ 24 kW	208/240)VAC 3-phase ~(20–400 A AC)	$10,000–$40,000
	50 miles/h @ 50 kW		
	90 miles/h @ 90 kW		

Figure 2.3: Likelihood of the use of charging infrastructure [22]

2.3   Control and Operation of Electric Vehicles

To date, most EVs operate in the unidirectional energy flow only, where the energy is coming from the grid or the source to charge the EVs in what is known as grid to vehicles (G2V) [23], [24]. However, in the future, with more EVs on the road and more development in the communication infrastructure, other operational modes that allow for bidirectional energy flow to and from the vehicles can be feasible. These other operational modes can be divided into vehicle to grid mode (V2G), vehicle to building mode (V2B) [25]–[27], and vehicle to vehicle mode (V2V) [28]. In the V2G mode, aggregated power from a group of EVs can be used to support the grid by providing regulation services (to stabilize the voltage and frequency) or reserve services (to meet the sudden increase in demand or outage of generation unit) [29]–[32]. In these cases, the EV owners must be given proper incentives to allow the discharging of their EVs. However, the management of such process will not be done through the owners themselves since a single EV cannot provide sufficient power to the grid. This can be done through a third party, or agent. This third party can be an aggregator or a parking lot operator, which coordinates the charging of EVs.

In the V2B mode, the EV or the EVs can be integrated in the building energy management to minimize the cost of electricity for the owner or to use the EV as a storage to store excess power from renewable energy resource that might be on the top of the building (e.g., photovoltaic modules), and provide this energy back when there is a deficit in the supply.

In the V2V mode, energy flow among different EVs is allowed. This can be used by a parking lot operator that tries to maximize its profits by purchasing energy from the energy market and allocating this energy among the EVs according to the different owners' preferences. In all cases of bidirectional power flow, battery degradation costs and reduced life time should be taken into consideration. Therefore, to control and coordinate the power flow, different control and optimization algorithms have been introduced in the literature. These algorithms vary widely between just mitigating the negative impacts of EVs' charging on the power grid to making profits by the EV owners via participating as distributed resources [33].

In the first part of this chapter, a general categorization for EV charge management algorithms is discussed. In the second part, the stochastic and the real-time dispatching issues related to EV charge management are explored.

2.3.1 Deterministic Control Approaches

Integrating large numbers of EVs to the smart grid can cause considerable negative impacts. While the global, or system-wide, negative impacts on the bulk power system are likely only at large EV penetration levels [34], localized impacts on the distribution system are expected to be more significant even at moderate penetration levels. However, it was shown that with adequate management, the negative impacts of EVs can be reduced and the penetration depth of electric vehicles can be increased [35]. Several strategies have been introduced in order to control EV charging to prevent negative impacts on the grid. These can be classified into centralized, decentralized, and autonomous charging control strategies.

2.3.1.1 Centralized Charging Control

Many methods of EV charge management have focused on centralized control methods [29]–[32]. In centralized scheduling and control, the control algorithm of EVs is done centrally after collecting all the information about the EVs' status and owners' preferences, as well as other system data, such as market prices, system constraints, and loading. The central controller can be an aggregator or the system operator. Centralized controllers usually result in the optimal utilization of the system resources but need a mature communication infrastructure [36]. Figure 2.4 shows a schematic for the centralized control method, where all data from the different participants in the system are sent to the main controller that processes all the data and sends back reference signals to be followed by different entities.
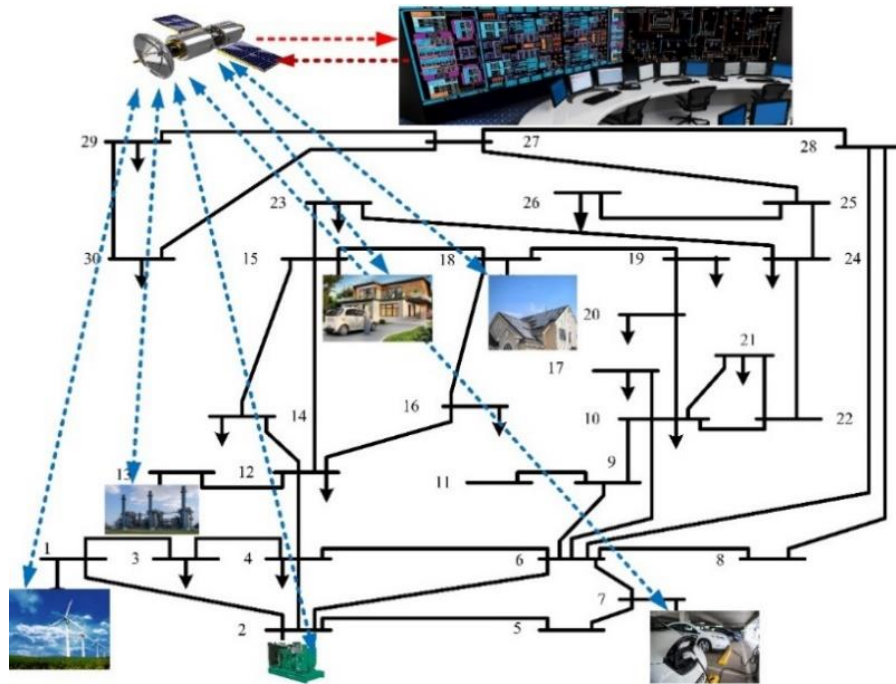
Figure 2.4: Centralized controller schematic

In [29], the authors used a control algorithm that uses the EV as another voltage control device in the system to mitigate the intermittency of distributed solar generations. The control algorithm consists of two stages, where the coordination between the EVs and the on-line tap changing transformer is done in the first stage. Then, in the second stage, a correction is made to the EV charging/discharging to provide a fast response to the fluctuation in the solar energy. The algorithm performed well in mitigating the over-voltage/under-voltage problems in the system. However, the mobility of the EVs was not taken into consideration.

Electric vehicles on a large scale were used to provide frequency regulation (FR) in the utility grid in [30], in which the authors presented a coordinated control strategy for large-scale EVs, BESSs (Battery Energy Storage Station) and traditional FR resources involved in automatic generation control (AGC). It was shown that EVs and BESS can provide a fast response in the case of a disturbance of short period but if the disturbance continued for longer period, only the AGC will participate in the response continuously. In [31], the effect of EVs in providing ancillary services with wind integration was investigated. It was shown that the regulation power requirements from conventional generators were greatly reduced with the integration of a V2G system participating in load frequency control. In [32], a V2G algorithm was developed to optimize energy and ancillary services scheduling for a third party, called the aggregator. An optimal bidding formulation for EVs performing regulation up and down with only unidirectional power flow was developed. The simulations were performed on a simulated market with constant prices of regulation services over the study year.

None of the V2G studies in [30]–[32], however, addressed charging impacts on the distribution system and they require significant communication bandwidth to frequently dispatch the EVs . Additionally, the optimization requires significant computational power by the centralized controller

In [37], a multi-objective optimization was used to coordinate the charging of the plug-in EVs in a way that satisfies the network technical constraints, as well as the customer convenience. Heavy communication between the EV customers, vehicle coordinator and energy hub operator at the distribution system company is required. It also requires the knowledge of load profiles.

In [38], [39], economic-based charge control was investigated. It was found that price-based methods can sometimes cause distribution system overloads in the night hours due to low system prices. The method requires good communication infrastructure to perform well. In [40], a three-level hierarchical control algorithm was proposed for coordinating EVs' charging at the provincial-level in China. The user preferences are sent from the lower level from the different charging stations to a higher level on the municipals level, where these data are added to other non-EV loads and pricing times, and finally all the data from the different municipals are sent and processed by the provincial-level operator. The algorithm is good for a vertically integrated utility system, where the conventional power system architecture is still being followed. Rebound effects, where there is a sudden load increase/decrease due to the instantaneous connection/disconnection of a considerable number of EVs in the low/high price period, were considered. The rebound effects were

solved using the proper coordination from the upper municipal level coordinator. However, there was no consideration for the generation and network constraints.

Three approaches were studied in [41]; dumb charging, dual tariff policy and smart charging. Voltage profiles and line congestion levels were evaluated, for the peak load hour, and for grid technical limits checking. Also, network power losses were evaluated for a typical daily load profile. Smart charging with hierarchical centralized control showed the best performance, and it showed that the voltage is the limiting factor for higher integration of EVs.

Communication with the transformer substation for the sake of fair charging of electric vehicles as soon as possible was investigated in [42]. The connection rate of EVs keeps increasing until the set point limit is reached, and then it varies up and down to maintain the set point level. At the end of each minute interval, the chargers will again attempt to connect with a connection rate probability. The random process, used for connecting the electric vehicles, ensures that each of the EVs has fair access to the available power. In [43], the authors proposed a centralized charging control that allows the EVs to find, via a distributed communication network, either the closest charging station, and then only be allowed to charge if there are no network constraints, or the charging station that will allow for the quickest charge.

In [44], an algorithm that provides real time energy management for a grid connected charging park was proposed. The algorithm uses a fuzzy controller to yield the charging rate of each PHEV based on the current and estimated power needed by the PHEVs, the estimated power generated by the PV, and the daily energy tariff. In case of high system

loading, the output of the fuzzy controller is modified to avoid negative impacts on the grid.

A market mechanism for the optimal allocation of the charging capacity to the vehicles was proposed in [45]. The main purpose of the developed mechanism was to allow the owners of the vehicles to express their individual preference, as well as ensure network stability. The author tried to open the door for multi-tiered user plans, in which different users can be offered different resource allocation based on their preference, and their willingness to pay. At the same time, network constraints, such as total network loading, voltage drop and phase unbalance, were taken into consideration.

In [46], a central electric vehicle charging optimization algorithm was proposed. The optimization was based on a receding horizon linear optimization problem. The authors took into consideration constraints such as the transformer and line limitations, phase unbalance and voltage stability within the network. As a simplification for the problem, the authors used a DC-equivalent model for the distribution network. Later, the algorithm was applied to the actual distribution network. In making this decision, the authors were looking not just at the current point in time, but at the best possible solution for a finite future charging horizon in discrete intervals, since underlying conditions may change unexpectedly (such as vehicles arriving or departing).

Although centralized control strategies can result in the optimal utilization of the system resources, they have a number of disadvantages:

1. The need for large investment in the communication infrastructure, especially at the distribution level.

2. An enormous number of messages need to be communicated within a very limited period of time, which might cause communication issues, such as high latency and low quality of service.

3. High computation burden for processing a large amount of data.

4. Loss of the main communication link or problems with the central controller might have severe consequences on the system integrity.

5. User privacy issues since the central controller has access to the data of all users.

2.3.1.2 *Decentralized Charging Control*

Other EV charge strategies have focused on decentralized control algorithms that use reduced communication infrastructure and computational burden. In decentralized, or distributed control, the charging/discharging reference decision is not processed and generated using the aggregator or the system operator. Instead, the operator generates some sort of a signal to incentivize the participating EVs to do a certain action [47]. However, each EV decides on its charging/discharging rate based on its own preference, and no private information is sent back to the aggregator or the operator [48]. Other works use multi-agent control algorithms [49]. A multi-agent system consists of two or more intelligent virtual or physical entities that cooperate and interact with each other to achieve certain objectives related to their environments [50]. A schematic for the multi-agent approach is shown in Figure 2.5.
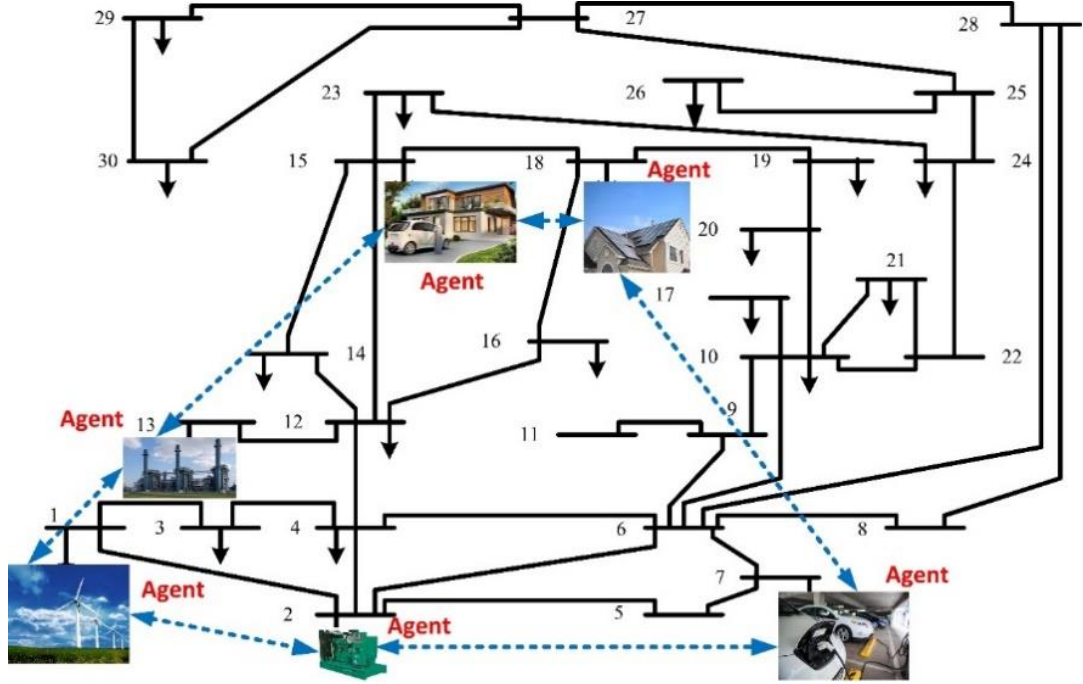
Figure 2.5: Decentralized controller schematic

A decentralized controller using price-driven coordination between the utility and the EVs was considered in [11]. The authors used two gradient optimization methods, one that is based on the cost and the other based on a primal-dual approach, to minimize the total load variance in the distribution network. They assumed a uniform fleet with each car having a maximum capacity of 1.96 kW. The proposed approach changes the feedback control signal of each EV, taking into consideration the state of the feeder supplying the EV. Although the method converges to a near-optimal load variance while ensuring that the capacity of the feeders are not overloaded, special care should be given to the algorithm step size to ensure convergence.

An electric vehicle for charging and discharging in the household was considered in [48]. In this study, the impact of price-based demand response strategies on smart household load pattern variations was assessed. A forecasting procedure using a hybrid

wavelet transform-based artificial neural network was considered to accurately consider the price elasticity of demand. The household load datasets are acquired to perform optimal appliance scheduling, considering an hourly varying price tariff scheme. The algorithm presented in [51] was based on EVs setting their own charge profiles according to price forecasts. In [52], a two-stage control algorithm was used to coordinate the charging of EVs in the presence of multiple aggregators. The algorithm takes into consideration the network constraints. A third-party price coordinator was introduced to generate a fair price signal between the distribution system operator, who tries to efficiently operate the system without violations, and the aggregators, which try to charge the EVs according to their preferences and with the lowest cost. Although the method achieves satisfactory results, the used linear programming model and assumptions did not accurately characterize the charging process of the EVs by neglecting mobility aspects and battery efficiency.

In [53], a large population of plug-in electric vehicles was used to mitigate wind intermittency and frequency regulation. Each EV adjusts its charging or discharging power in response to a communal virtual price signal and based on its own urgency level of charging. The proposed scheme created a cost-saving opportunity for both the EV owner and the utility. In [54], a pricing scheme that conveys price and quantity information to the load aggregator (LA) was developed and compared with the pricing-only scheme. It was shown that the price/quantity scheme is insensitive to the regularization penalty and requires less computation capability than the pricing-only scheme. The pricing scheme was used to minimize the charging costs for the EV owner. If the objective was changed to profit maximization for the utility, the method loses its beneficial properties.

Game theory has been recently used by multiple researchers [55]–[60] to coordinate the charging process of EVs by achieving the Nash equilibrium, where no player has anything to gain by changing his/her own strategy. In [55], the coordination of EVs was performed using non-cooperative games to minimize generation cost. In [56], optimal demand-side management (DSM) is achieved using a model derived from game-theory. Each consumer's scheduler is required to broadcast its consumption schedule to all other participants in the DSM program. In [60], a mean field game theoretic approach was proposed to control the charging of the EVs without increasing the grid peak and taking the customers` preferences into consideration.

In [61], a distributed framework was suggested to charge the EVs at comparable charging rates without overloading the upstream service transformer. In [62], two electric vehicle charging algorithms were proposed, one centralized and one distributed. Their performances, in simulations that used real vehicle data, were compared on a model that is based on a real low-voltage network in northern Melbourne, Australia. The proposed algorithm for distributed charging used probability criteria to decide whether the vehicle will be charged or not. This probability is based on the node voltage and the state of charge (SOC) of the battery. It does not take into consideration the maximum charging rate. The method can be used only up to 25% penetration level, and it is sensitive to the location of vehicles in the network; when vehicles are connected near the far ends of the network, there is a significantly increased risk of voltage drop.

In [63], [64], control of energy flow between EVs and the grid has been demonstrated using fuzzy logic controllers (FLC), mainly for voltage compensation and load flattening.

The proposed technique assumes that the EVs are available to be charged and discharged. It also assumes that all EVs in a certain area will charge from a certain charging station, and the charging station will work most likely as an aggregator. In [65], the effectiveness of distributed additive increase and multiplicative decrease (AIMD) charging algorithms at mitigating the impact of domestic charging of EVs on low-voltage distribution networks was investigated. The proposed method tries to achieve fair charging among different vehicles without violating the voltage constraint or overloading the substation, and, at the same time, it took into consideration the time-of-use prices. To achieve the mentioned objectives, a simple radial communication between the distribution station and the vehicles is used.

These, and other similar decentralized charging methods, rely on reduced communication infrastructure from the utility or the aggregator, even if there is no communication from the EVs back to the grid. Although, the decentralized control algorithms reduce the need for expensive communication infrastructure and the computation burden, they have the following disadvantages:

1. They do not always ensure optimality and best use of resources.
2. They may result in a rebound effect, which can be harmful to the system.
3. They have a limited ability in participating in ancillary service markets.
4. They are vulnerable to changes in customers' behavior.

2.3.1.3 *Autonomous Charging Control*

Autonomous charging control algorithms were considered in the literature as a part of decentralized algorithms but with no communication at all. However, due to the increased

work in that type of controllers, it is preferred to consider them as a third type of control algorithm. Autonomous controllers can be the first step for integrating a considerable number of EVs in the absence of communication infrastructures in the distribution systems in many countries. An autonomous controller mainly depends on local inputs to decide on the charging/discharging rate. Also, an autonomous controller can be viewed as a lower layer of a more comprehensive decentralized strategy, where decisions should be taken on the secondary distribution system instantaneously. An example of an autonomous droop controller is shown in Figure 2.6.
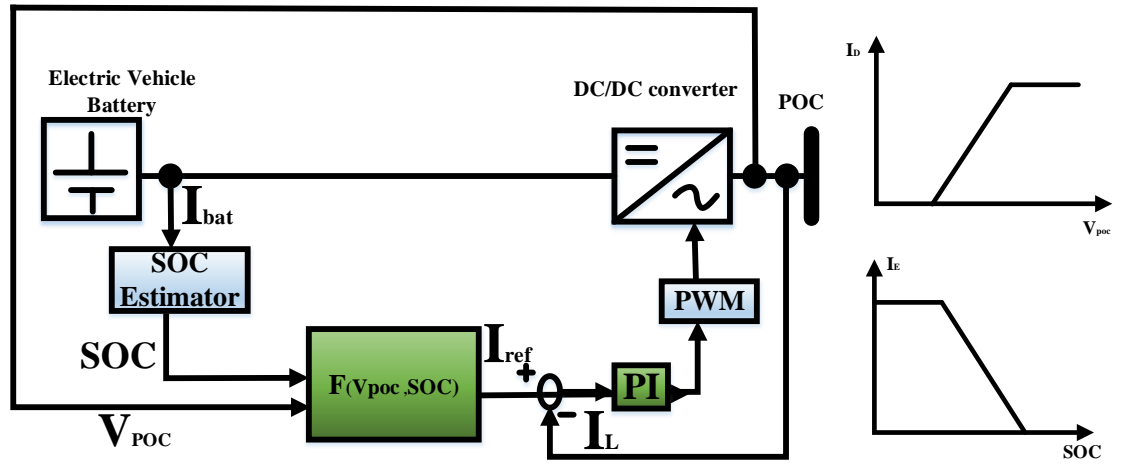
Figure 2.6 : Autonomous droop controller (POC: point of charging)

In [66], a voltage-constrained local optimization of EV charging was suggested. Each EV in the system optimizes its own charging, aiming to maximize its charging rate while not violating nodal voltage or feeder loading constraints. However, it does not consider the fairness of charging and battery SOC of each EV. In fact, a comparable performance can be obtained using simpler control structures.

In an autonomous controller, provision of ancillary services, such as secondary and tertiary frequency regulation, are harder to do due to the absence of communication, hence the direct coordination of the charging/discharging of EVs. However, the primary frequency and voltage regulations are possible using the droop controllers [67], [68]. A voltage-feedback control structure for EVs in a distribution system was suggested in [69]. However, the issue of fairness among EVs connected to different buses in the system was not addressed. SOC dependency of charging rate was not considered, either. Fair charging means that EVs with similar initial SOC should charge at the same charging rate irrespective of their location in the distribution system. Since some of the EVs are connected to the upstream buses near the substation, they have the advantage of having a higher charging rate due to the higher voltage than those connected to downstream buses. In [70], the authors propose an active power/frequency (P—f) droop control strategy to be implemented at the EV coupling inverter, where the EV will autonomously adapt its power output based on the microgrid frequency. This work proposed the use of this control strategy during service restoration. In [71], the authors proposed an autonomous distributed V2G control scheme, where electric vehicles supply a distributed spinning reserve according to the frequency deviation at the plug-in terminal. The authors in [72] proposed a method that uses only local information, which is the node voltage, SOC and the time of required charging given by the user. Based on that information, the algorithm controls the charging rate. It uses an averaging technique method to find the set-point voltages used in the controller that mainly depend on historical data. Fairness was not completely proved in the results. In [73], the author proposed an effective, autonomous, voltage-based control scheme for charging electric vehicles. This control scheme coordinates the charging among

38

the EVs connected to the distribution nodes in a fair manner so that voltage violations are avoided. The proposed method uses constant gain values and the upstream point charges faster than the downstream one. In [74], the author developed an autonomous voltage feedback control structure for EV charging based on the model in [73]. This control structure relies on the local voltage measurement, where the EV is plugged in. It compares the system measured voltage at the point of charging with a predefined reference voltage. The drawback of the proposed algorithm is that it needs to update the reference set point with each seasonal variation, and the upstream point charges relatively faster than the downstream one. In [75], [76], a new voltage-based EV charger was proposed. The controller used local voltage as one of the inputs and the state of charge as the second input. Then, a nonlinear exponential controller decides on the charging rate based on the inputs. The aim of this work was to eliminate the need for seasonal changing of the controller set-points mentioned in the previous autonomous work. This is done by keeping the voltage set-point as a constant value for all the EVs at the different buses, and relaxing the controller sensitivity to the voltage to ensure fair charging among the EVs.

Fuzzy-based controllers were introduced in [77] to maintain the MVDC voltage and the battery SOC within proper thresholds, and to keep the power balance stable among the units of fast charge and the rest of the charging stations.

Autonomous charging algorithms eliminate the need for the communication infrastructure and can also be used as the first layer of hierarchical control algorithms, where decisions should be done at the local levels. Also, an autonomous control algorithm is the only option for utilities with no available communication infrastructure at the

distribution level. However, if an autonomous control algorithm is used alone, it will have the following disadvantages:

1. Lack of the optimal operation of the system.

2. Lack of ability to participate in ancillary service markets.

3. May result in a rebound effect.

4. Vulnerable to changes in customers' behavior.

Based on the above discussion about the different types of controllers that are used to manage the charging of EVs, a summary of the different papers discussed above is given in Table 2.3 below. Also, proper classification of control algorithms and their compatibility with both vertically integrated and restructured utility systems can be reached.

Depending on the utility structure, communication infrastructure, electricity market design and the level of sector liberalization, one or more of the controllers` types can be used. On one hand, multiple central aggregators can be used in a restructured utility system to achieve the reliable and cost-effective operation of their zones. On the other hand, one central controller can be used to control the vertically integrated system.

As the future electric utilities move toward more deregulated ones, decentralized and multi-agent systems will be more suitable due to their several advantages. For instance, current demand-side management programs can send minimum signals to provide guidance to a decentralized controller that makes the final decision locally.

Autonomous controllers can be the first step for integrating a considerable number of EVs in the absence of communication infrastructure in the distribution system in many countries. Also, having autonomous control at the lowest level of the

centralized/decentralized controller is advantageous since it reduces the communication

traffic with the V2G aggregator.

Table 2.3: Summary of the discussed control techniques

Ref. Number	Technique Used	Bidirectional Battery Flow	Utility Constraints Consideration
Centralized Techniques			
[29]	Rolling Scheduling Using Linear Programming	✓	✓
[30]	Tie-Line Bias Control	✓	✗
[31]	Tie-Line Bias Control	✓	✗
[32]	Linear Programming	✓	✗
[37]	Multi-Objective Optimization Using Particle Swarm	✗	✗
[38]	Non-Linear Programming Using GAMS	✗	✓
[39]	Linear Programming	✗	✗
[40]	Quadratic Optimization	✗	✗
[41]	Linear Programming	✗	✓
[42]	Additive Increase, Multiplicative Decrease Algorithm	✗	✓
[44]	Fuzzy Control	✗	✗
[45]	Linear Programming	✗	✓
[46]	Receding Horizon Using Linear Programming	✗	✓
Decentralized Techniques			
[10]	Gradient Optimization	✗	✓
[48]	Artificial Neural Networks- Wavelet Transform	✓	✗
[49]	Hybrid-PSO& Linear Programming	✗	✗
[51]	Linear Programming	✗	✗
[52]	Linear Programming	✗	✓
[53]	Congestion Pricing Algorithm	✓	✓
[54]	Game Theory	✗	✗
[55]	Non-Cooperative Game Theory	✗	✗
[56]	Game Theory	✗	✗
[57]	Game Theory	✗	✗

[58]	Non-Cooperative Game Theory	✗	✗
[59]	Normalized Nash Game	✗	✗
[60]	Stochastic Mean Field Game Theory	✗	✗
[61]	Additive Increase, Multiplicative Decrease Algorithm	✗	✗
[62]	Probability Theory	✗	✓
[63]	Fuzzy Control	✓	✓
[64]	Fuzzy Control	✓	✓
[65]	Additive Increase, Multiplicative Decrease Algorithm	✗	✓
Autonomous Techniques			
[66]	Linear Programming	✗	✓
[67]	Droop Controller	✓	✓
[68]	Droop Controller	✓	✓
[69]	Droop Controller	✗	✓
[70]	Droop Controller	✓	✓
[71]	Droop Controller	✓	✓
[72]	If-Then Rules	✗	✓
[73]	Proportional Controller	✗	✓
[74]	Droop Controller	✗	✓
[75]	Exponential Controller	✗	✓
[76]	Exponential Controller	✗	✓
[77]	Fuzzy Controller	✗	✓

2.3.2 Real-Time and Stochastic Operation Approaches

When dealing with real-world scenarios, the optimal operation of EV charging becomes more challenging. Since in real-time (RT), the aggregator or the operator receives a regulation signal update once every 2–6 s, the RT strategy needs to be computationally efficient. In addition, this strategy must ensure meeting the regulation signal while considering EV characteristics and EV owners' preferences.

Moreover, different kinds of uncertainties are involved in the scheduling process. Generally, there are three major types of uncertainties when dealing with EV charging.

These types are: renewable energy uncertainties [78], market uncertainties [79], and EV mobility uncertainties [80]. An aggregator or system operator should take into account these kinds of uncertainties during the scheduling of EV charging/discharging. Also, the communication latency and EV owner preference should be considered.

As a market participant who contributes to energy and ancillary service markets, an electric vehicle aggregator (EVA) or operator is required to submit energy schedules to the wholesale energy market and capacity schedules, e.g., frequency regulation and reserves. These schedules are submitted to the concerned markets on the day-ahead. In real-time, if no ancillary service is requested by the system operator, the EVA is expected to abide by its own energy schedules. However, if an ancillary service, e.g., frequency regulation, is requested, the EVA is expected to follow the ancillary service command signal. This is performed by moving some or all EVs above or below their scheduled charging rates. A brief timeline for the operation of the electric vehicle aggregator or the system operator is shown in Figure 2.7.

The EVA, therefore, needs day-ahead (DA) and real-time (RT) charge management strategies. The DA strategy concerns the optimal schedules of energy and regulation capacities that the EVA sends to the corresponding markets on the day-ahead. Then, the EVA needs a RT strategy for EV dispatching that helps deciding which EVs should be moved from their DA scheduled charging rates and by how much.
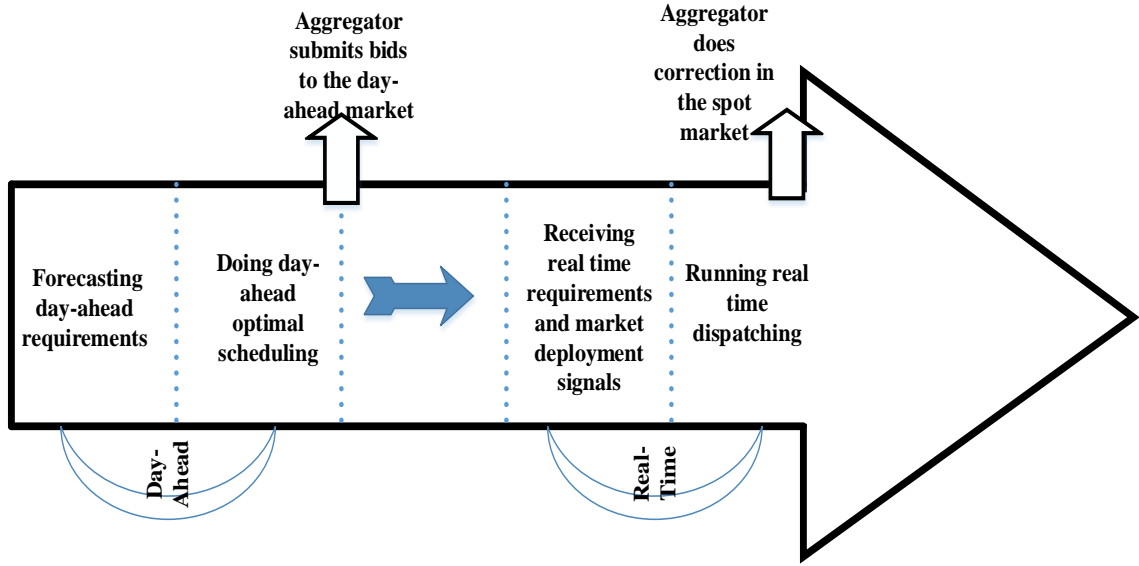
Figure 2.7: Timeline of the day-ahead and real-time markets

2.3.2.1 Day-Ahead Scheduling with Uncertainties

Uncertainties, if not included in the day-ahead scheduling, might greatly affect the system performance from the economic and technical standpoints. To deal with uncertainties, several modelling methodologies have been developed, such as probabilistic methods [81], stochastic optimization [82], robust optimization [83], and fuzzy optimization [24], [84].

Managing a large number of hybrid EVs at a city parking lot was considered in [81]. The authors tried to maximize the available energy in the EV for the next time step, taking into account the different uncertainties of the driving characteristics, such as the arrival time, departure time, and initial state of charge.

These data were based on normal distribution curves that were validated using actual transportation statistics. The drawback of the proposed algorithm is the need for a high

computation requirement to process large amount of data. Minimizing the overall load variance in the presence of demand response was considered in [82]. The stochastic nature of the availability (arrival and departure times) of the EVs was considered, but the energy uncertainties were not taken into consideration. In [85], a binary particle swarm optimization with adapting differential evolution was proposed to handle the uncertainties associated with renewable energy. The authors tried to minimize the cost of generating the electric power from the conventional fossil units by using the flexibility of the EVs to accommodate as much renewable power as possible. In [86], the authors used unidirectional V2G to mitigate the risk of energy trading by a load-serving-entity (LSE), which uses thermal and wind power sources, and has a high penetration of EVs. Mixed-integer stochastic programming is used to formulate the problem of coordinating V2G with energy trading with an objective of finding the optimal bids that will maximize the LSE profits. In [87], [88], a bi-layer optimization technique was used to accommodate renewable energy to enhance the gird performance in the presence of EVs. Robust optimization that handles the uncertainties in prices for V2G optimization was considered in [89]. In [85]–[89], EV mobility and energy uncertainties were not taken into consideration. In [83], robust optimization was suggested to coordinate EVs scheduling with thermal generators to provide ancillary services to the grid. The proposed robust optimization algorithm can lead to conservative solutions.

A hierarchical optimization algorithm for scheduling the EVs for profit maximization while satisfying the transformer constraints was considered in [90]. It was assumed that the energy and the availability of the EVs are stochastic based on probability distribution. The

drawback of the proposed algorithm is that the computation burden increases exponentially with the number of the EVs and the length of the operating time frame.

Most of the algorithms mentioned previously focus on a large number of EVs, whether they were coordinated by the utility or an aggregator. For these cases, the EV characteristics and mobility can be forecasted with a reasonable accuracy due to the law of large number. This is not the case for a small number of EVs, like the case of a parking garage, with a limited number of EVs. This problem still needs more investigation.

EV parking garage scheduling in a city using historical data of EV mobility and parking patterns was considered in [91]. The authors tried to maximize the total profits and the total number of EVs that fulfill their requirements. The operator schedules the charging from the time point at which the electricity price is the cheapest, irrespective of the EV time availability, which is risky and sub-optimal. In [80], fuzzy optimization was used for dealing with the uncertainties associated with EV mobility and market prices. The authors turned the deterministic optimization problem into a fuzzy optimization problem to handle the different uncertainties of EVs, while trying to maximize the profits of an EV parking lot. Although the methodology took into consideration the uncertainties of EVs and market prices, renewable energy uncertainties were not considered. A stochastic model for capturing the behavior of EVs was considered in [92]. To simplify the model, the whole EV fleet was considered to be the same.

2.3.2.2 *Real-Time Dispatching*

Once day-ahead scheduling has been submitted, the aggregator or the operator needs to abide by his bidding in the real-time; otherwise, a penalty will be applied. Therefore,

there is a need for real-time dispatching algorithms to ensure proper operation of the system.

A number of studies reported in the literature relied on real-time incremental dispatch methods in the context of optimal schedules. That is, it was assumed that the aggregator would send dispatch signals to all participating EVs in order to respond to regulation/reserve deployment commands requested by the system operator. A major issue with incremental dispatch, also called droop-based dispatch, is that the charging stations required for incremental power changes are more expensive than the simpler charging stations that accept on/off commands only. This is because additional hardware is needed to modulate charge rates continuously. Also, standard charging stations commercially available today do not support the communication requirements needed for continuous modulation of charge rates [93]. Another issue is that a new dispatch signal needs to be sent to every EV participating in V2G at every regulation command instance, which has a high resolution of 2–6 s.

Lately, some authors presented algorithms for managing EV charging that are suitable for RT adoption. In [94]–[97], RT charge management mechanisms were proposed. However, provision of regulation services was not considered in [94]–[96], and market mechanisms were not considered in [97]. In [98], a three-stage framework for DA and RT charge management for an EVA providing regulation services is presented. However, it involves a large number of parameters that need to be set carefully to warrant a successful outcome. In [99], the suggested framework employs model predictive control (MPC) to obtain the RT charging set point for each EV. In [98], [99], all participating EVs have to be updated every time a regulation signal is received by the EVA, which increases the

communication burden. In [100], another framework for DA and RT EV charge management is proposed in the presence of significant renewable penetration.

Considerable attention has been paid in the literature to the impact of communication on the power system control. This is motivated by the fact that higher communication traffic can result in higher latency, which may have a de-stabilizing effect on the power system. This is especially true for frequency regulation, or load frequency control (LFC), of bulk power systems and microgrids. In addition, a high communication traffic requires communication channels with high bandwidths and gives rise to high communication power consumption.

New emerging concepts that use developments in radio frequency identification and the 5G technologies have started to gain traction in the literature [101]. To address the abovementioned challenges, there must be robust and low-cost communication infrastructures that can support rapid and secure information exchange, as well as consistent and efficient design of communication protocols and architectures. The internet of things and cloud computing, based on the 5G technologies, as new computing models, could accelerate the establishment of such infrastructures. The internet of things is a new concept that attempts to combine multiple aspects and technologies coming from different approaches. According to the International Telecommunication Union, the internet of things is defined as "a technological revolution that represents the future of computing and communications, and its development depends on dynamic technical innovation in a number of important fields, from wireless sensors to nanotechnology" [102]. Omnipresent computing, pervasive computing, internet protocol, sensing technologies, communication

technologies, and embedded devices are merged together in order to form a system where the real and digital worlds meet and are continuously in symbiotic interaction [103], [104].

In [105], the authors proposed the use of internet of things to provide an automatic EV charging management. The objective of their scheme was to coordinate the charging of large-scale EVs in multiple residential buildings by leveraging the fast-distributed optimization capability of the alternating direction method of multipliers.

A platform that allows battery analysis and control of the charging and discharging processes through a web application using pre-defined profiles was introduced in [106]. A new communication architecture based on cloud computing was proposed in [107], where the authors presented a scheduling algorithm in order to attribute priority levels and optimize the waiting time to plug-in at each charging station. The potential of V2G services supported by the fog-based and cloud-based hybrid computing model in 5G networks was investigated in [108]. The authors considered the high mobility of EVs and the dynamics of the mobile computing resources in their investigation, and some possible solutions were suggested. To enable flexible and efficient connections, quality of service guarantee, and multiple concurrent support requests, the authors in [109] proposed the software-defined internet of vehicles, which is able to tackle the above-mentioned issues by adopting the software-defined networking framework. Despite the initial work to employ the advantages of the 5G and the internet of things in EV charging, more work is needed to fully explore the potential of these innovative technologies.

In addition to the internet of things, other studies have addressed the impact that the performance of the communication infrastructure has on the smart grid. In [110], LFC performance has been examined, considering a number of communication-network

49

characteristics, such as latency, bandwidth, and change in communication topology. The need for strict latency requirements in smart grids was emphasized in [111]. A model for communication latency as applied to the smart grid was introduced in [112]. A method was presented in [113] for estimating the delay margin requirements for the stability of the LFC loop. In [114], the impact of communication delays on the LFC of islanded microgrids is studied.

Recognizing the impact of communication networks' performance on the smart grid, few studies have presented methods for scheduling EV charging with low dispatch signal traffic. The main focus of [115] was to provide a valley-filling schedule for typical peak-valley daily residential profiles. It offered a user-oriented approach designed to satisfy the EV owner, while minimizing the variance and peak of the aggregated load profile as desired by the grid operator. In [116], another approach to manage the charging for valley-filling was put forward. The work presented in [115],[116] did not tackle the provision of frequency regulation, which is very challenging due to the high resolution of the regulation signals.

In [117], a simple discrete algorithm was proposed for an aggregator-driven RT charge dispatch of an EV fleet that provides regulation services. The suggested algorithm used a few heuristic rules to decide which EVs sholud be turned ON/OFF in order to meet the regulation signal under reduced dispatch traffic. Because it was based on heuristics, dispatch traffic optimality and fairness were not guaranteed. Generally, there are potential gains that can be made through optimizing the EV dispatch to perform regulation and reserves services. If EVs are charged more efficiently, additional savings in the communication bandwidth requirements can be achieved.

2.4 Conclusion

This chapter surveyed the recent research activities related to charge management of electric vehicles in a smart grid environment. The impact of EV charge management on the smart grid is first presented. Then, EV charge management strategies are divided into three categories. Centralized EV charge control, which requires a well-developed communication infrastructure, is highlighted. Decentralized charge control, which has limited communication requirements, is then discussed. In addition, communication-free, autonomous EV charge control is explored. The different approaches reported in the literature for addressing the stochastic nature of EV charge control process are overviewed. Special emphasis is also given to the issue of strategies suitable for real-time EV charge dispatch.

Chapter 3   An Automated Charger for Large Scale Adoption of Electric Vehicles

The penetration of electric vehicles (EVs) is expected to increase in the future. With more EVs on the road, more loads will be added to the distribution system, which will affect the system voltage and loading. This chapter studies the impact of the EVs on the distribution system and provides an automated controller that satisfies the customer requirements and mitigates the negative impacts of the charging of EVs on the system. The controller takes into consideration the system voltage, the customer requirements and the state of charge (SOC) of the battery. The controller is tested using a large-scale distribution system in MATLAB/Simulink. To show the interaction between the local distributed generation and the EV charging, the controller is tested in the presence of distributed generation units. Sensitivity analysis is also performed to study the effect of the controller parameters on the charging of EVs and the distribution system.

3.1   Introduction

Electric vehicles (EVs) have attracted a lot of attention in the recent years and their adoption is expected to increase soon. This is mainly due to the several advantages associated with EVs in the transportation sector. For example, EVs are more energy efficient and they can use the clean energy, such as renewable energies for charging, and thus can significantly reduce the consumption of fossil fuels. However, with the increase in the number of EVs in the power grid, there will be a need for charging algorithms that can manage the charging of a substantial number of EVs connected to the power grids. Distribution systems will be the first part of the power grid where the impacts of EVs will be witnessed. As mentioned in the previous chapter, these impacts can range from line

overloading in both primary and secondary distribution systems to transformers overloading [11], line losses [13], low voltages, and voltage unbalances [14]. In the literature, many charging control algorithms were developed.

Generally, the suggested centralized controllers have the advantage of ensuring the most efficient and optimal use of the system. However, they have major drawbacks, such as the loss of the main communication link with the system operator, which could paralyze the entire system. Also, centralized controllers need large investments in the communication infrastructure, associated security measures, and high computation capabilities. Therefore, the decentralized controllers were developed in the literature as an alternative to the centralized ones. Decentralized controllers require less communication infrastructure and the amount of the exchanged information is less, thus the computation burden is reduced. In addition, the privacy of the EV owners is protected since there is no need to exchange all the information with system operator.

As mentioned before, decentralized controllers can be divided into decentralized controllers with communication and decentralized controllers without communication (called autonomous). A two-stage control algorithm for the coordination of energy between multiple EV aggregators was proposed in [52]. A third-party price coordinator is introduced to generate an appropriate price signal between the system operator and the different aggregators so that each party satisfies its objective in a non-discriminatory way. Fuzzy logic controllers were used in [118], [119] to control the flow of energy between the grid and the EVs.

Since the communication infrastructure is not mature in many distribution systems and a substantial number of the owners of EVs are expected to charge their EVs at their homes, decentralized controllers without communication (autonomous) have been developed. In [73], [120] the authors have proposed an autonomous voltage-based control scheme for charging EVs. This control scheme effectively coordinates charging among the EVs connected to the distribution buses. However, the proposed algorithm needs to update the set-points of the controller with each seasonal variation, and the upstream point charges relatively faster than the downstream one. In [75], a technique for EV charge management with variable gain is introduced to manage the EV charging. The controller depends on a non-linear empirical exponential function that might cause delay in the real-time operation, and there is no systematical method to derive the controller-governing equations.

In [121], an autonomous charging control algorithm that enables flexible charging of EVs is proposed. The algorithm decides on the charging rate of the EV according to the free capacity between the feeder maximum current limit and the non-EV load currents. The proposed algorithm was validated experimentally using an EV that is connected to the home charger. Although the method provides charging flexibility for the home owner, if it is widely used, its impacts on distribution grids are not favorable from the distribution system operator's (DSO) point-of-view.

In [66], a voltage-constrained local optimization of EV charging was suggested. Each EV in the system optimizes its own charging, aiming at maximizing its charging rate, while not violating the nodal voltage limits or the feeder loading constraints. However, it does not consider the charging fairness and battery state of charge (SOC) of each EV. In fact,

comparable performance can be obtained using simpler control structures. A voltage-feedback control structure for EVs in a distribution system was suggested in [122]. However, the issue of fairness among EVs connected to different buses in the system was not addressed in [122]. SOC dependency of charging rate was not considered, either.

Fair charging means that EVs with similar initial SOC should charge at the same charging rate, irrespective of their location in the distribution system. Since some of the EVs are connected to the upstream buses near the substation, they have the advantage of having higher charging rates due to the higher voltage compared to those connected to the downstream buses.

In [123], the authors proposed an autonomous approach for the management of local voltages, utilizing the concept of sensitivity analysis. Results from time-series analyses reveal its effectiveness in managing the constraints. In [69], a droop-based controller was proposed to manage the charging of EVs in distribution systems. However, the problem of the sensitivity of EV charging with the location was not considered. This resulted in a discriminatory charging among the EVs. Also, the SOC of the battery was not considered, which reduces the lifetime of the battery.

In this chapter, an autonomous linear controller is proposed to manage the charging of a substantial number of EVs in a residential distribution system. The charger and its embedded controller require no communication. Unlike the droop controller in [69], the fairness of charging among different EVs, where the charging process is very sensitive to the charging location, is considered. Also, state of charge dependency is taken into consideration as well. The charger takes into consideration the owner requirements and

mitigates overloading and under-voltage problems in the distribution system. The controller and the charger are tested on a large-scale system through simulation.

3.2 Electric Vehicle Charging Control

The EV charger converts the AC current coming from the grid to a controlled DC current in order to charge the batteries. Therefore, the EV is seen from the grid as a current source [124]. EV battery charging control aims at charging the EVs by satisfying the customer requirements, and without violating the voltage standard of the grid. Taking the grid status into consideration will help ensure that the feeder losses are reduced and overloads are avoided [13].

For a given distribution transformer, the loads consist of both controllable and non-controllable loads. By controlling the loading level, the voltage profile of the system can be improved since it is in a direct relation with its loading levels. In this chapter, it is assumed that the only controllable loads are the EVs.

Figure 3.1 shows a block diagram for the proposed EV controller, which decides on the charging rate I_{ref} based on the voltage at the point of connection (POC) and the state of charge (SOC) of the EV connected to that POC. The SOC of the battery is estimated using the Coulomb counting method, where the charging energy in the battery can be monitored through the common procedure of summing the current exchanged versus the usable capacity. Coulomb-counting uses a timing reference and integrates the current over a fixed sampling period to determine the capacity that was added [125]. The $SOC(t)$ online algorithm is:

$$SOC(t) = SOC_x(t_0) + \int_0^t \frac{I_{bat}}{3600E_{usable}}(\tau)d\tau \qquad (3.1)$$

where $SOC_x(t_0)$ is the initial SOC voltage-based assessment of the battery that is added to current integrated over a 1-second $d\tau$. I_{bat} is the battery current and E_{usable} is the usable capacity in Ampere-hours. Once the SOC is known, it will be converted to a percentage, which will be used by the controller, by dividing it by the maximum usable capacity of the battery.

$$SOC_i(p.u) = \frac{SoC(t)}{E_{usable}} \qquad (3.2)$$
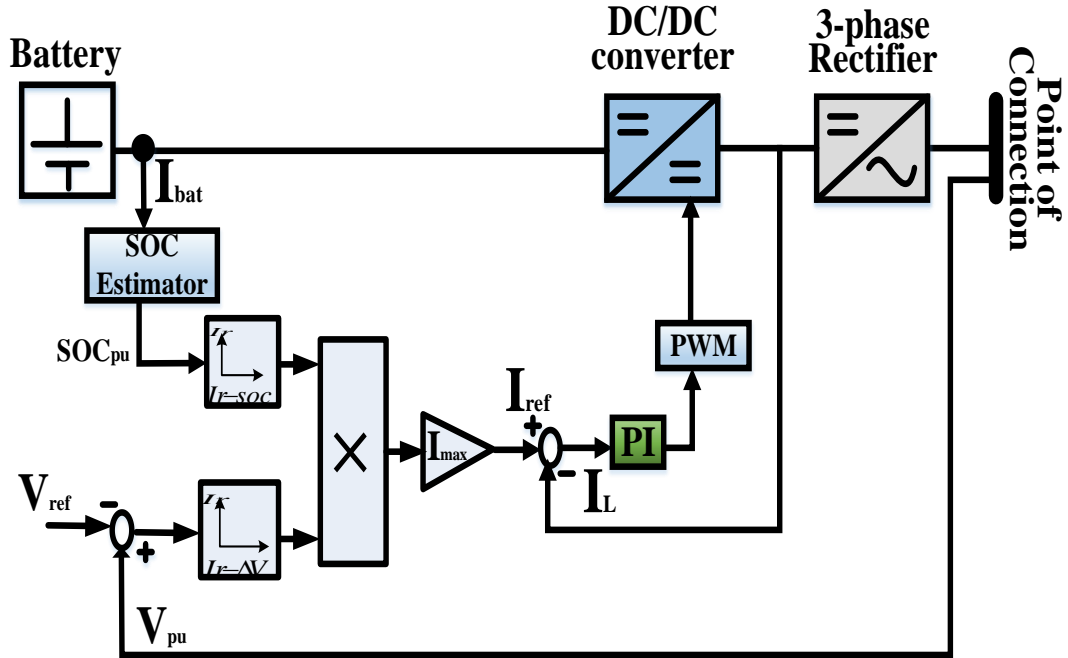
Figure 3.1: Proposed EV controller

Once the SOC is known, it will be used by the controller, along with the voltage at the POC in per unit, to decide on the charging current in per unit. The output from the controller

is multiplied by the maximum charging current of the battery I_{max} to obtain the real charging reference I_{ref}. When the reference current is obtained, it will be compared with the output current from the DC-DC converter I_L, and the error between them will go to a PI controller that will enforce the converter to follow the reference value.

The proposed controller represents a linear relationship between the EV charging rate and the voltage at the POC. The output of the controller is continuous as long as the state of charge $SOC_i < 80\%$, and there is no voltage violation (the voltage is higher than 0.95 p.u). The value of 0.95 p.u voltage was chosen since it satisfies the ANSI standards [126], and 80% state of charge was chosen as the maximum value of charging to increase the lifetime of the battery [127], [128].

The regulated charging rate I_r, can be represented as a function of the voltage variation (ΔV_i), as shown in Figure 3.2 (a), and described as follows:

$$
I_{r\_\Delta v} = \begin{cases}
I_{min} & \Delta V \leq \Delta V_{min} \\
m_1 \Delta V + k_1 & \Delta V_{min} < \Delta V \leq \Delta V_c \\
m_2 \Delta V + k_2 & \Delta V_c < \Delta V \leq \Delta V_{max} \\
I_{max} & \Delta V > \Delta V_{max}
\end{cases} \tag{3.3}
$$

where,

$$
m_1 = \frac{I_c - I_{min}}{\Delta V_c - \Delta V_{min}}, \qquad k_1 = I_{min} - m_1 \Delta V_{min}
$$

$$
, m_2 = \frac{I_{max} - I_c}{\Delta V_{max} - \Delta V_c}, k_2 = I_c - m_2 \Delta V_c \tag{3.4}
$$

where

$\Delta V_i = V_i - V_{ref,i}$, $V_{ref,i}$ is the voltage reference set-point.

Note that the voltage reference, V_{ref},i, will be constant at 0.95 p.u for all the EVs in the system. This eliminates the need for the seasonal changing and the extra tuning proposed in [120]. This voltage reference will be kept constant in all cases regardless of seasonal variations, which is highly desirable.

(a)

(b)
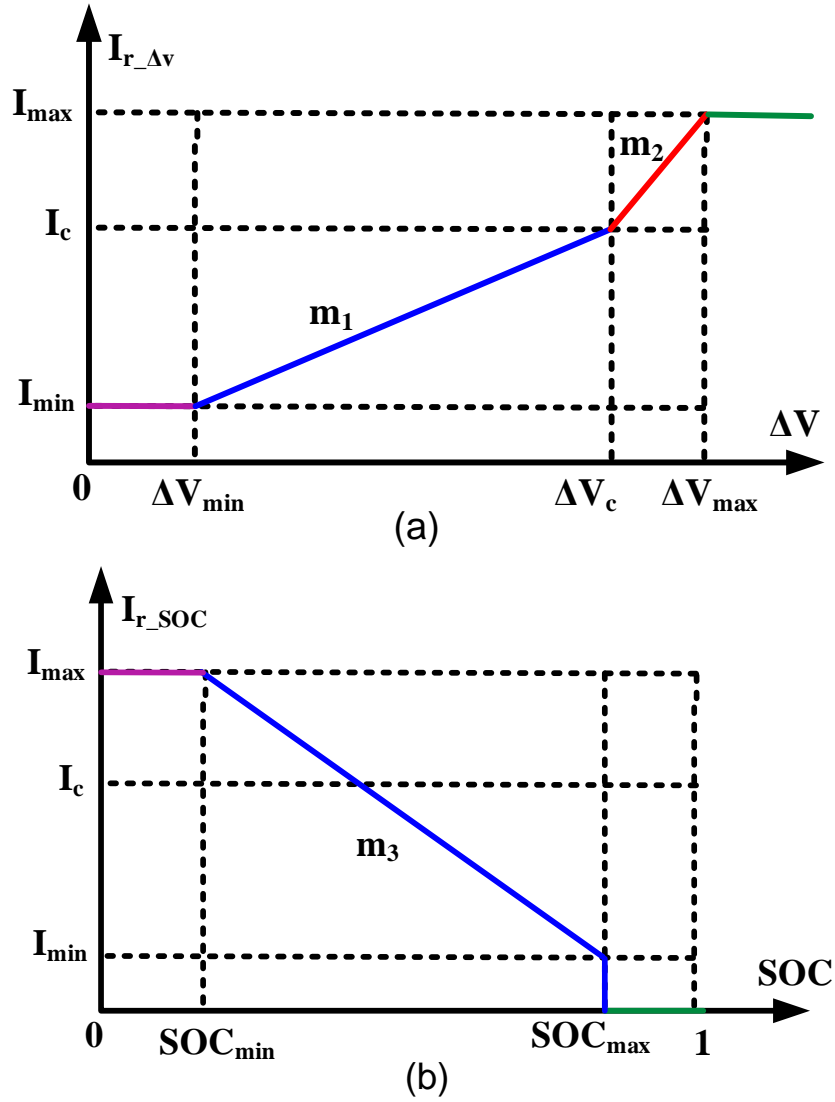
Figure 3.2 a) Rate of charge voltage control logic   b) Rate of charge SOC control logic

I_{min} and I_{max} are the minimum and maximum acceptable limits of charging rate, which are defined based on the charger limits. I_c is the current that corresponds to the voltage point ΔV_c, which is the critical point where the voltage at the POC is high enough to allow increasing the charging rate of the EV near the maximum value. ΔV_{min} and ΔV_{max} are the minimum and maximum acceptable limits of the voltage variations. From the system's point of view, the first objective of the controller is to avoid under-voltage problems in the system. It is not preferred that the EV charger increases the charging when the bus system voltage is near the minimum system standard voltage (0.95 p.u). Therefore, ΔV_{min} is set to start the increase of the charging rate if the voltage is higher than 0.954 p.u. ΔV_c, is set to increase the charging rate near the maximum charging when the system voltage is high enough, in that case 1.04 p.u and above. If the voltage is higher than the maximum system standard voltage (1.05 p.u) and ΔV_{max} is reached, the charger will charge at the maximum charging rate in order to absorb the extra power in the system.

Fairness is another important objective during the charging of the EVs. The charging of each EV to obtain acceptable bus voltages should be decided in a way that it does not consistently make the charging of one EV comparably faster than another EV according to its location in the network. It is not appropriate that EVs connected to downstream load bus, i.e. lower voltage, suffer from much lower regulated charging rates than those connected to the upstream load bus, i.e. higher voltage. Therefore, the charging can be improved by using a charging rate function that is not excessively sensitive to the voltage level. It is only when the voltage is considerably high that the charging rate should increase. This is done by choosing the appropriate values of ΔV_c and I_c.

A third objective, that will contribute to decide on the charging rate of the EV, is the dependence on the SOC of the EV. It is desirable that the EV having lower SOC should be allowed to charge at a higher charging rate, and as its SOC increases, the charging rate decreases slowly, as depicted in Figure 3.2 (b). This also helps increase the battery lifetime by reducing the charging rate greatly when the battery is near the maximum capacity. Therefore, for an EV with a current SOC_i, the current draw as a function of the SOC_i is stated as follows:

$$I_{r\_soc} = \begin{cases} I_{max} & SOC \leq SOC_{min} \\ m_3 SOC + k_3 & SOC_{min} < SOC \leq SOC_{max} \\ I_{min} & SOC > SOC_{max} \end{cases} \tag{3.5}$$

where,

$$m_3 = -\left(\frac{I_{max} - I_{min}}{SOC_{max} - SOC_{min}}\right), k_3 = I_{min} - m_3 SOC_{max} \tag{3.6}$$

SOC_{min} and SOC_{max} are the actual apparent SOC limits to the EV owners, which are usually different from the physical zero and full SOC. SOC_{min} is usually in the range (10%-20%) of the battery capacity since it is harmful to fully discharge the battery, and SOC_{max} is in the range (80%-90%) of the battery capacity since it is harmful to overcharge the battery. The final rate of charge I_{rt} from the above equations is given in (3.7).

$$I_{rt} = k * I_{r\_\Delta v} * I_{r\_soc} * I_{max} \tag{3.7}$$

where, k is an empirical factor that was determined by trial and error. It is used to tune the final charging rate based on the battery type. $I_{r\_\Delta v}, I_{r\_SOC}$ are the reference current components coming from the voltage and SOC logics. I_{max} is the maximum charging current of the battery. It is used to change the per unit reference current into an actual one. The control scheme is further modified in order to include any possible preference of the

61

EV owner. Accommodating the owner preference is done by making the EV current draw dependent on the remaining uncharged battery capacity, if needed. Thus, the minimum current draw for each EV is defined as the average value required over the remaining charging interval given in (3.8), where $SOC_x(t_{end})$ and $SOC_x(t_0)$ are the required final and the initial SOC, respectively. *dt* and *st* are the required departure and start times.

$$I_{ref} = \max(I_{rt}, \frac{SOC_x(t_{end}) - SOC_x(t_0)}{dt - st}) \ , \ I_{ref} \leq I_{max} \tag{3.8}$$

3.3   Simulation Benchmark Description

This section describes the simulation system that is used to test the impact of the EVs and the validity of the proposed controller on the power grid, where the EVs are connected to different buses. Figure 3.3 (a) shows a 3-phase unbalanced primary residential distribution system that has 18 buses. This system was introduced in [129] and was used for testing the EVs in [13]. Figure 3.3 (b) shows the secondary distribution system, which has multiple splice boxes and houses connected directly to the distribution transformer through triplex lines at a nominal service voltage of 240 V. The parameters of the system are presented in Table 3.1. The system consists of 1020 houses with load profiles based on Residential High Winter Ratio (ResHiWR) found in the system of the Electric Reliability Council of Texas (ERCOT) [130]. The loads have five-minute resolution data. The system is assumed to have 510 EVs connected at different houses. This corresponds to a 50% penetration depth. This level of penetration depth is reported to cause significant problems to the distribution system [13]. It is assumed that each EV has 24 kWh maximum capacity and 6.6 kW maximum charging rate, which emulates the 2013 Nissan Leaf. For the steady

state analysis in the distribution system, the EVs are modeled as controlled current sources, where each source is fed by its reference from the controller. This is done to reduce the computational burden and time of the simulation.

3.4   Simulation Results

The controller performance is validated through simulation on MATLAB/Simulink. Multiple simulation cases are done to show the validity of the proposed controller.

3.4.1   Control Performance in the Absence of Distributed Generation Units

To show the merits of the proposed controller, it will be compared to the case of uncontrolled charging, and the case of using a traditional droop-based control proposed in [69], where the charging rate is a constant multiplied by the voltage at the point of connection. Since the droop controller in [69] resulted in under-voltage problems, it has been modified in this chapter to stop charging if there is an under-voltage problem in the system.

Table 3.1: Secondary network parameters

Parameter	Value
EV Charger Penetration	50%
Distribution Service Transformer	150 kVA, %Z = 1.8
Secondary Conductor (transformer to splice	350 Al, 4/0 Al Neutral
Service Conductor (to the houses)	#2 Al
No. of customers	1020

138 KV

Upstream buses: 2,3,10

Downstream buses: 6,7,8,13,17,18

12.47 KV

17

10

16

18

1

3

2

9

4

11

15

12

14

5

8

6

13

7

(a)

150 KVA
Transformer

Splice Box

Splice Box

Splice Box

Splice Box

(b)
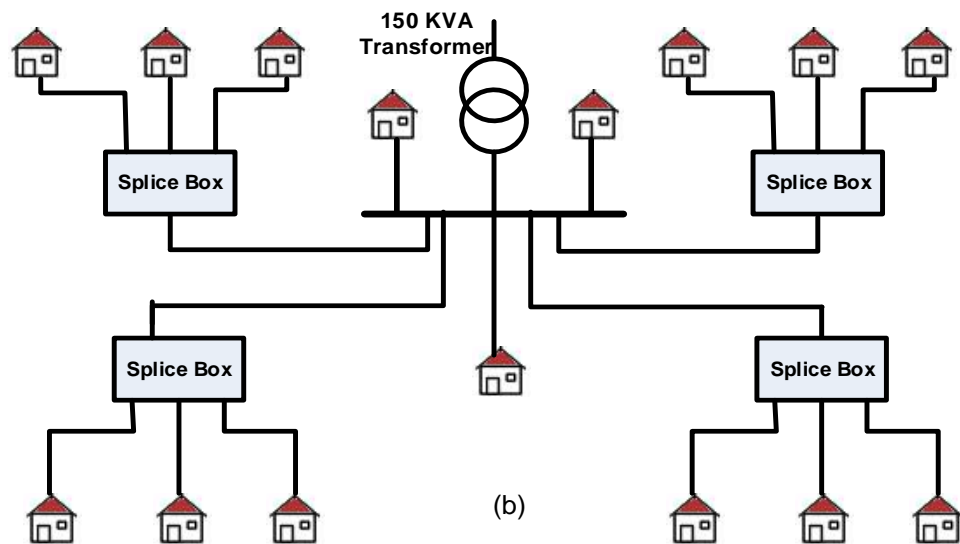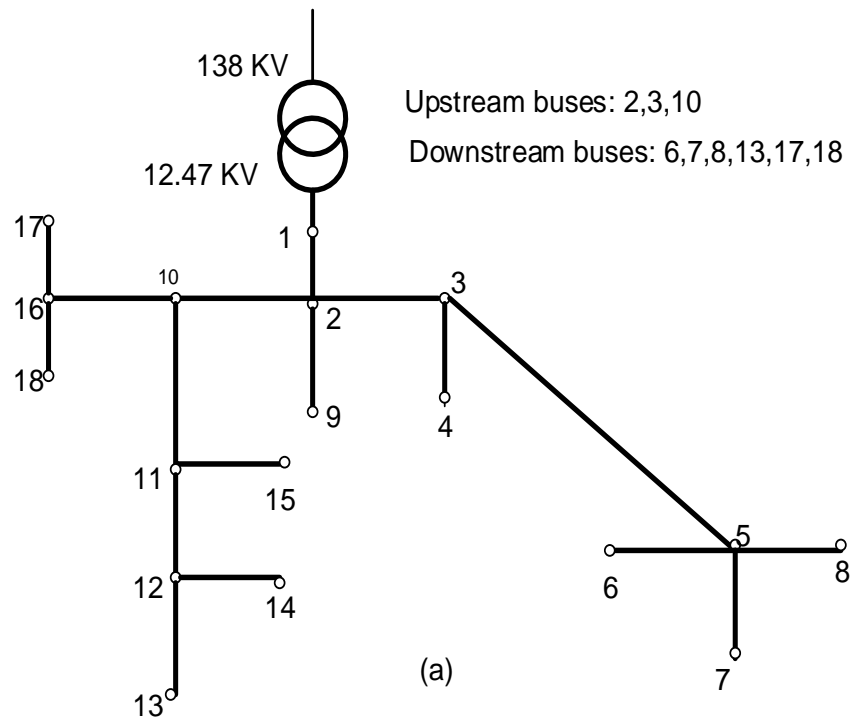
Figure 3.3: a) Primary distribution systems   b) secondary distribution systems

The penetration depth of EVs is assumed to be 50%, which represents a high penetration level of EVs that will cause negative impacts on the grid. The EVs are connected randomly to the different houses at the secondary distribution transformer. It is assumed that the owners of the EVs will prefer to charge their vehicles after they come back from work during the night hours, where the low time-of-use tariff is applied. Therefore, the plug-in times of the EVs are assumed to follow a normal distribution centered around 8 pm with a standard deviation of one hour. The initial SOCs of the batteries are assumed to be in the range of 30-50%. The number of owners with a preferred charging preference is assumed to be 20%. Other owners are assumed to desire to fully charge their batteries by early morning. The battery will be charged to a maximum of 80% of its rated capacity. This is to increase the lifetime of the battery.

Figure 3.4 shows the primary transformer loading in the different cases, which are the uncontrolled charging, the droop-based controlled charging, and the proposed controller. It can be seen from the figure that the total loading (PEV+PNonEV) is significantly increased when the EVs are allowed to charge without any control. The system peak increases from merely 3000 kW to 4000 kW. This will cause significant voltage drops, below 0.95 p.u, as depicted in Table 3.2, which violates the ANSI C84.1 standards [126]. This also increases the losses and the operating cost of the system due to the need for operating a number of expensive, fast generators. When a control is applied, the system peak becomes around 3500. This reduces the operating cost of the system and does not negatively impact the system voltages, as shown in Table 3.2. Figure 3.5 shows the voltage at two selected houses in the system. The upper one, shown in Figure 3.5 (a), corresponds

to a house that is connected to the most upstream bus 2 in the system, which is connected directly to the primary distribution transformer. The later, shown in Figure 3.5 (b), is connected to a downstream bus 6, which suffers from voltage drops across the feeders. Figure 3.5 clearly shows that without any control, the voltages at the houses' level will be negatively impacted. However, most of the negative impacts will be at the downstream houses, where the voltage can go as low as 0.92 p.u. The figure also shows that the droop and the proposed controllers succeed in limiting the under-voltage problems in the system, where the lowest voltage does not go below 0.95 p.u. This is also shown in Table 3.2. So far, both the droop-based and the proposed controllers succeed in shaving the system peak and limiting the voltage drops in the system. However, a major difference between the two controllers can be seen in Figure 3.6 and Table 3.3.
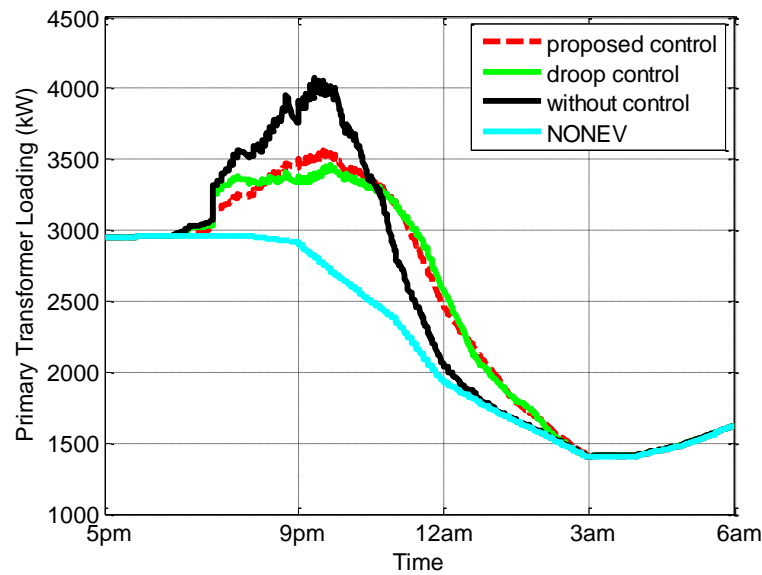
Figure 3.4: Primary transformer loading in kW
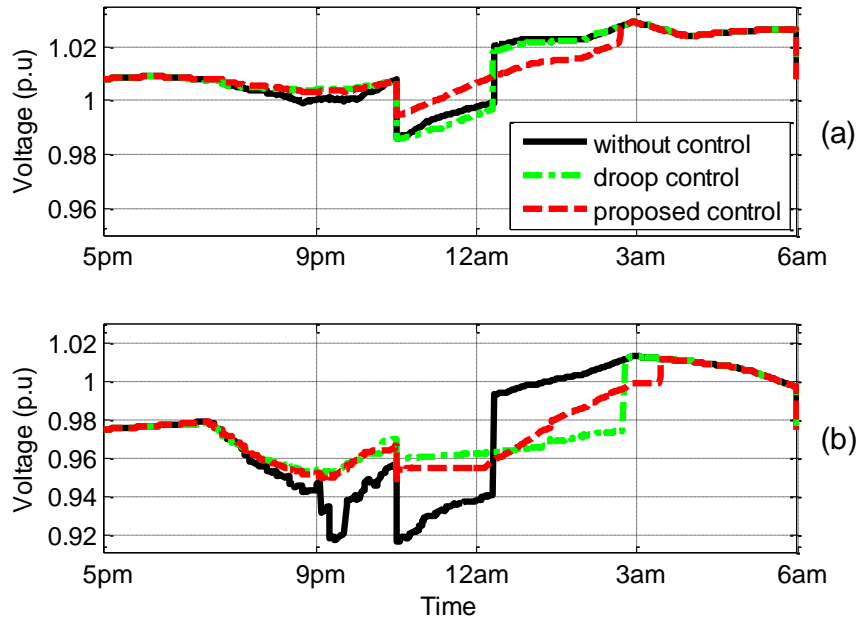
Figure 3.5: Voltages at the secondary distribution transformer
a) Upstream house   b) Downstream house
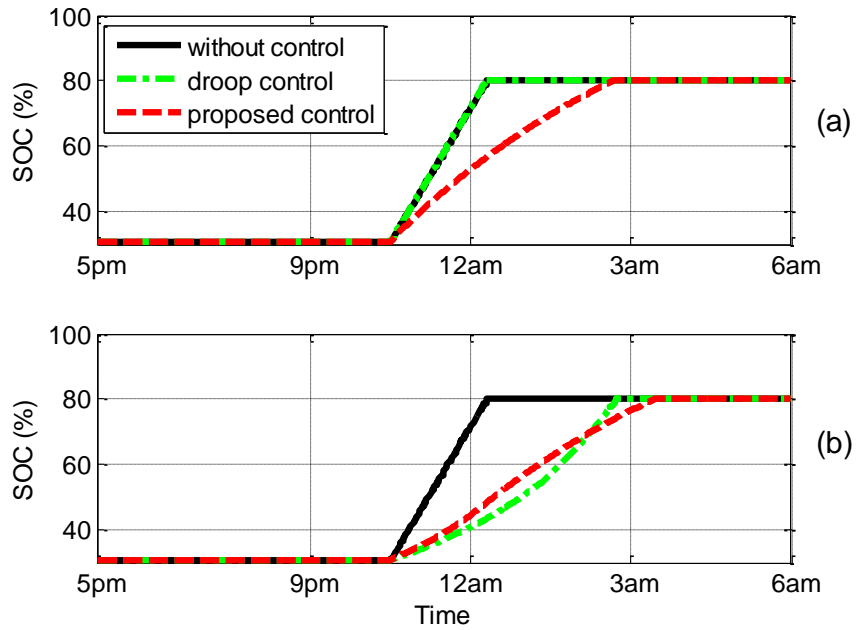
Figure 3.6: SOC of a) EVup   b) EVdown

Table 3.2: Lowest voltages at the buses of the Primary distribution system in p.u.

Bus No#	Uncontrolled case	Droop controller	Proposed controller	Proposed/Renewable
2	0.975	0.981	0.980	0.982
3	0.959	0.970	0.969	0.971
4	0.958	0.969	0.969	0.971
5	0.936	0.956	0.954	0.956
6	0.933	0.953	0.952	0.954
7	0.932	0.953	0.952	0.953
8	0.931	0.953	0.952	0.953
9	0.975	0.980	0.980	0.981
10	0.962	0.969	0.969	0.971
11	0.956	0.964	0.964	0.967
12	0.954	0.962	0.962	0.965
13	0.953	0.961	0.961	0.964
14	0.954	0.962	0.962	0.965
15	0.956	0.964	0.963	0.967
16	0.955	0.965	0.964	0.967
17	0.955	0.964	0.964	0.967
18	0.955	0.964	0.964	0.967

Table 3.3: Time to finish charging for the up and downstream EVs in hours

	EVup	EVdown	Time
Uncontrolled case	1.783	1.783	0
Droop controller	1.783	4.233	2.45
Proposed controller	4.175	4.925	0.75
Proposed/Renewable	4.142	4.383	0.242

Figure 3.6 shows that in the case of no control on the charging, both EVs charge as fast as possible with the same charging rate without any consideration to the status of the grid. When the droop-based control (dashed green curve) is used, the EV that is connected to the upstream house (EVup) charge much faster than the downstream one (EVdown). This is unfair. This happens because the upstream EVup has the advantage of higher supply voltage compared to the downstream EVdown. Since the droop-based controller is highly sensitive to voltage variations, it results in a discriminatory charging among the EVs, where the EVs that are connected to higher voltage buses in the system charge much faster than others. When the proposed controller is used (dashed red curves), both EVup and EVdown charge with a semi-equal charging rate. These results are also depicted in Table 3.3, which shows the time difference between the two EVs with extreme cases. It is obvious from Table 3.3 that the droop-based control results in a great bias to the upstream EV, where the time difference between the two EVs is 2.45 hours. When the proposed controller is used, the time difference between the two EVs becomes less than one hour (45 minutes). It is worth mentioning that all EVs finish charging before early morning.

3.4.2   Control Performance in the Presence of Distributed Generation Units

So far, the results discussed the performance of the proposed controller without the presence of distributed generation (DG) units. However, future distribution systems are expected to have more penetration of local distributed generation units. The presence of the DG, especially when the DG share is significant, will impact the power distribution system operation and control. It is therefore deemed necessary to evaluate the impact of increased DG on the distribution systems. Among the different DG technologies, the effect

of wind energy will be evaluated in this chapter. Wind energy is chosen due to the high potential of wind energy and its significant share in many countries nowadays. Also, wind is a very variable resource. Solar energy is not investigated here due to the assumption that the EVs are charging according to the time-of-use tariff, where the electricity prices are low during the night, and the EVs are charging at homes from 6 pm to 6 am.

The performance of the proposed controller with and without wind energy is compared. A sample power generation from the ERCOT system that is used in this work is shown in Figure 3.7. Since there is local generation at the house level, the loading on the primary distribution transformer will be less. This is shown in Figure 3.8, where the primary transformer loading in the presence of wind energy is less when compared to the case of the proposed controller without renewable. Since some of the loads will be fed locally, the voltage drop across the feeders will be less. This will result in improving the voltages at the downstream houses, as shown in Figure 3.9. Due to the voltage improvement, the EVs at the downstream houses will charge faster.

It should be noted that the improvements in voltage will affect the charging of the most vulnerable EVs more, and will have less impact on the EVs that are already at a good voltage condition, which is desired. This is shown in Figure 3.10 and Table 3.3, where the time difference between the two EVs has reduced from 45 minutes to only 14 minutes, which is highly recommended for non-discriminatory charging among the EVs.
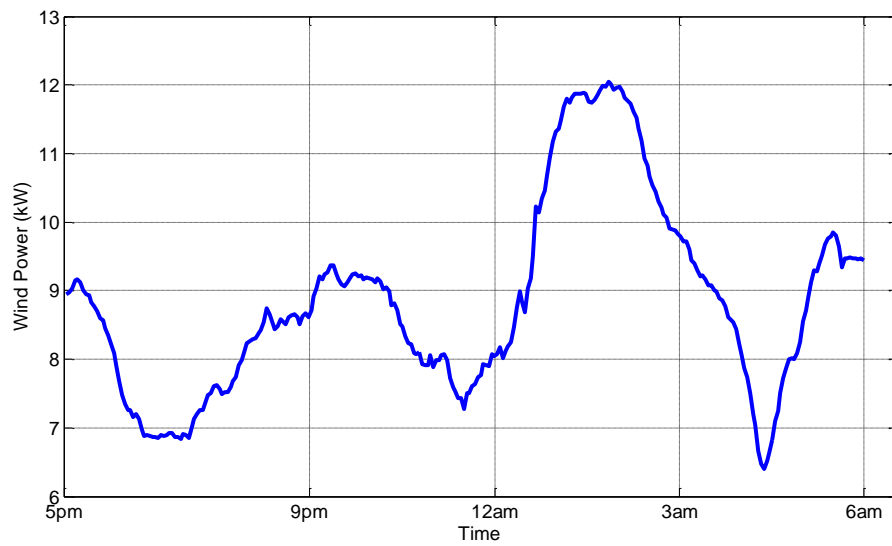
Figure 3.7: Wind power generation
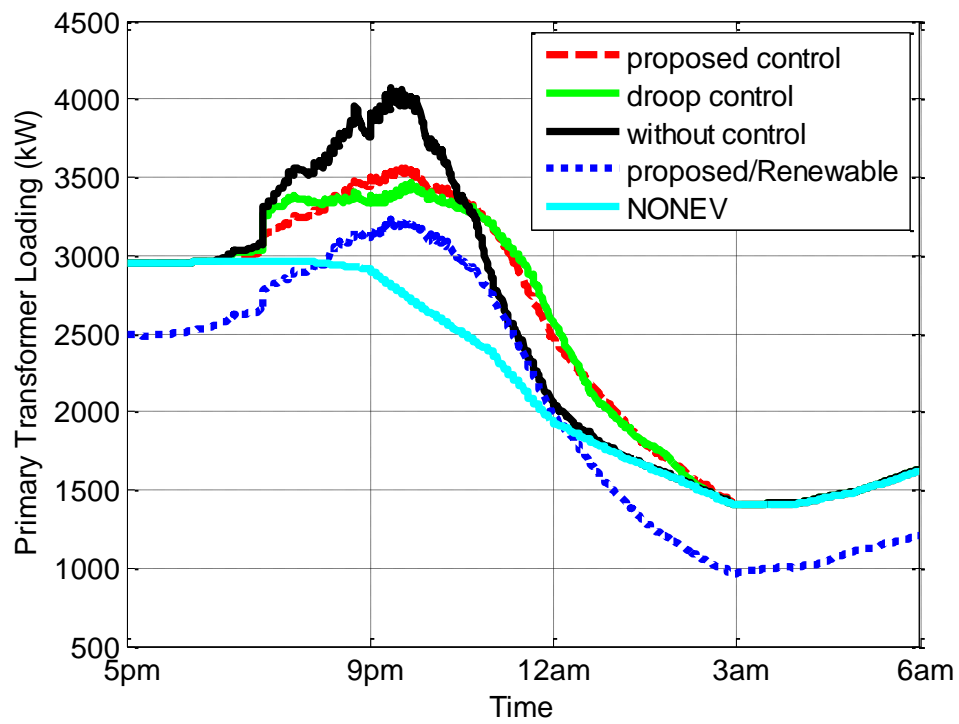
Figure 3.8: Primary transformer loading in the presence of distributed generation
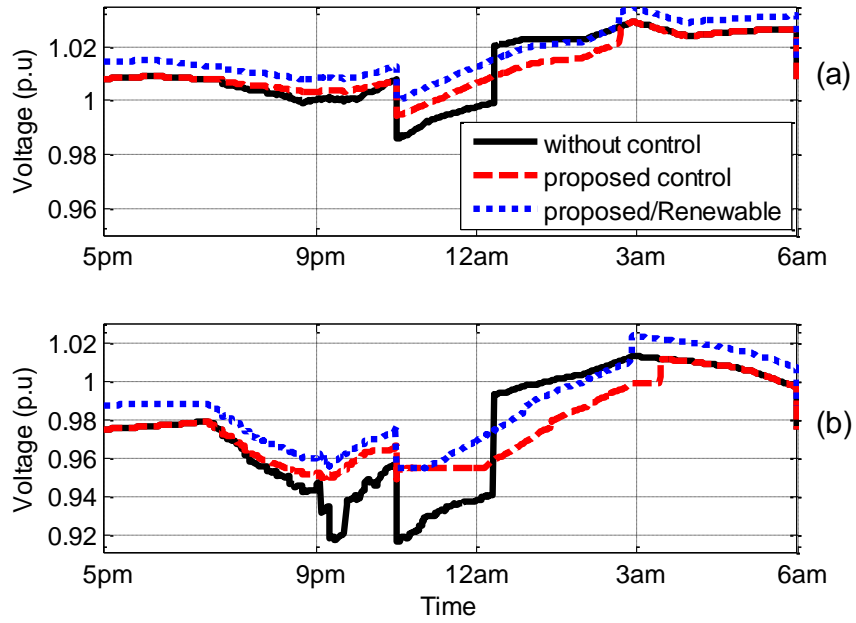
Figure 3.9: Voltages at the secondary distribution transformer in the presence of distributed generation   a) Upstream house.   b) Downstream house
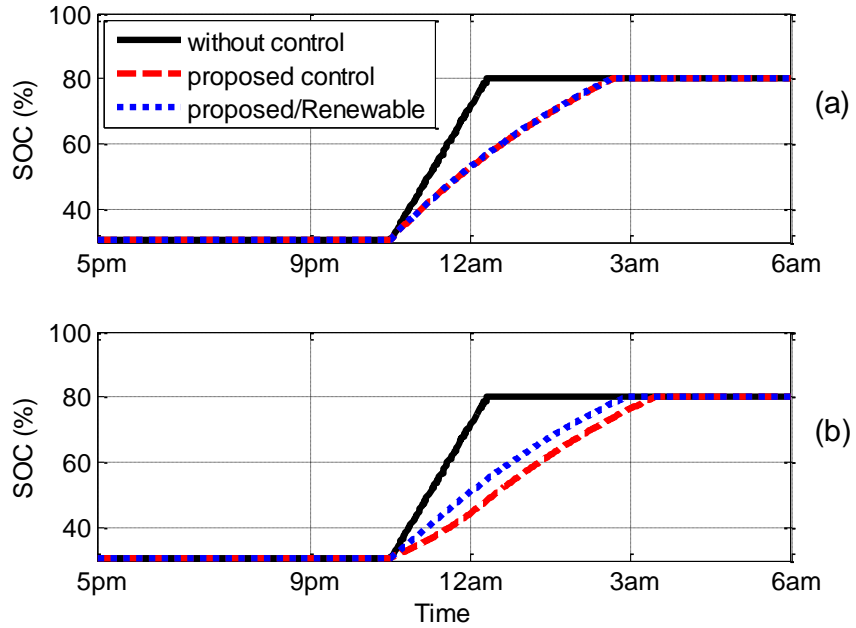
Figure 3.10: SOC in the presence of distributed generation   a) EVup   b) EVdown

3.4.3   Control Performance in the Case of Fast Charging in a Weekend

In this case, the behavior of the controller is investigated when the owners of the EVs want to charge at a faster rate during the morning hours or weekends. A selected full day load profile for a weekend from the same ERCOT system is used. Also, the availability matrix of the EVs was adjusted so that the EVs can be plugged-in at the houses during the morning hours. Before presenting the results, it is worth stating that the final reference current decided by the controller takes into consideration, not only the voltage at the point of connection and the SOC of the battery, but also the customer requirements in terms of how much energy is needed and at what time. According to Equation (3.8), the control scheme includes any possible preferences of the EV owner.

Accommodating the preferences of the owner is done by making the EV current draw dependent on the remaining uncharged battery capacity, if needed. If the owners wanted to reach a certain final $SOC_x(t_{end})$ by a certain departure time dt, the controller will calculate the current that is needed to achieve these requirements$(\frac{SOC_x(t_{end})- SOC_x(t_0)}{dt-st})$. Once the required current is calculated, it will be compared to the one obtained from the controller. Then, the final reference current to the converter will be the maximum of both. This ensures that the requirements of the customers are satisfied. In order to test this case and to be in line with the previously presented results, owner requirements for the EVup are added to charge in the early morning to 80% (maximum capacity chosen in the chapter) in only two hours. Also, a requirement of a maximum three-hour charging is added for the downstream EVs. Other EVs have requirements that range from three to seven hours randomly.
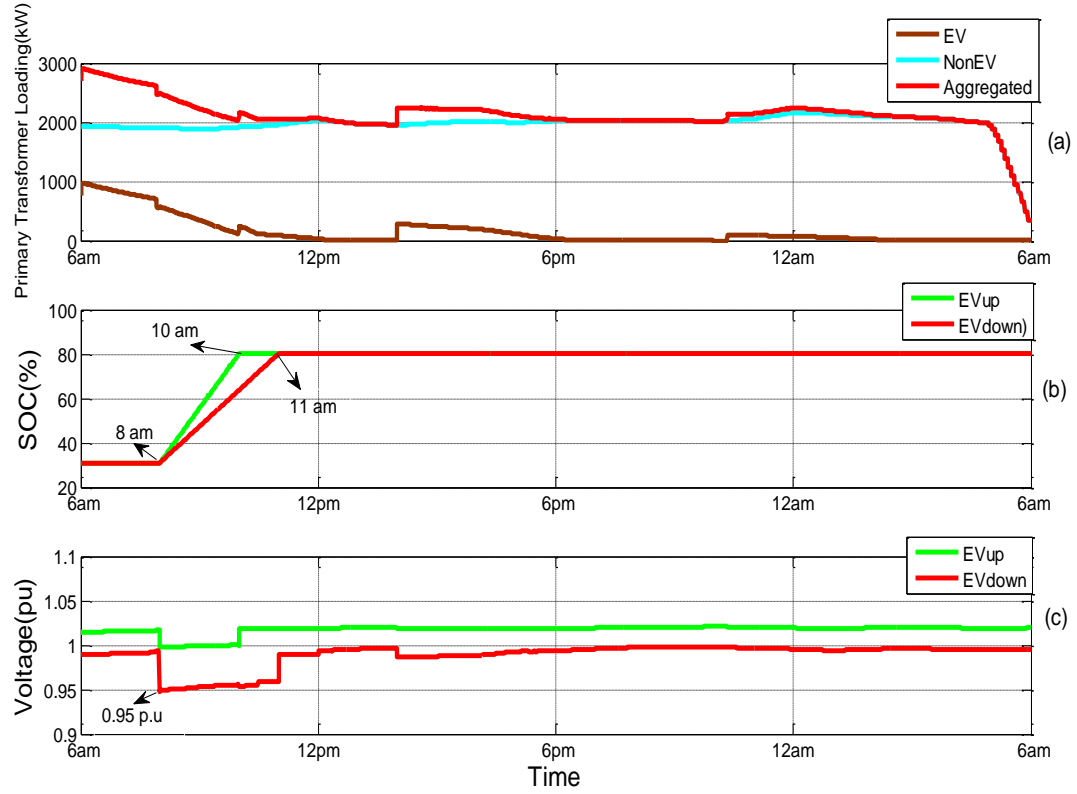
Figure 3.11: a) Primary transformer loading in kW   b) SOCs of the two selected EVs
c) Voltages at the POCs

Figure 3.11 (a) shows the load profile of the primary transformer during a day-time
with the majority of EVs charging during the day-time. Figure 3.11 (b) &(c) show the SOC
accumulation of the two selected EVs (EVup and EVdown), and the voltage profiles at
their points of connection. The figure shows that the controller has the ability to achieve
fast charging if the EV owner wanted to. Figure 3.11 (b) shows that EVup was able to
finish charging within two hours (8-10 am), as the owner requires. The same applies for
EVdown with three-hour charging (from 8-11 am). Figure 3.11 (c) shows that the voltage
profiles are still healthy. This happens regardless of the fast charging required by the EVs

because the system loading during the weekend is less stressful than the weekday. However, if all EVs wanted to charge at very high rates at the same time, the system voltage will be compromised.

3.5   Sensitivity Analysis

In this section, the sensitivity of the proposed controller will be tested. Two cases are evaluated in this section, which are the sensitivity of the controller to changes in the maximum required final state of charge SOC_{max}, and the sensitivity of the controller to design parameters ($\Delta V_c , I_c$).

3.5.1   Sensitivity of the Controller to the Maximum Required Final State of Charge

In this case, different simulations are presented to show if the controller will be affected by the limit SOC_{max}. In all cases, the non-EV loading, availability of the EVs and the parameters of the controller are kept the same. However, the limit SOC_{max} is changed to be the same for all the EVs, with values 80%, 85%, 90%, 95%, and 100% in each simulation case. The results for the different simulations are shown in Figure 3.12 and Figure 3.13. Figure 3.12 shows the voltage profile of one of the phases at the upstream bus 2 and the downstream bus 6, while Figure 3.13 shows the average SOC of all EVs connected to these two buses with different SOC_{max}. The figures show that the control algorithm is not affected by the maximum limit SOC_{max}. This limit only affects how much energy is required from the system. The more the required energy is, the more the stress on the system is, and the longer the charging time is. From the figures, it is clear that as SOC_{max} increases, the voltage at the different buses decreases. Also, the EVs take a longer time to charge.
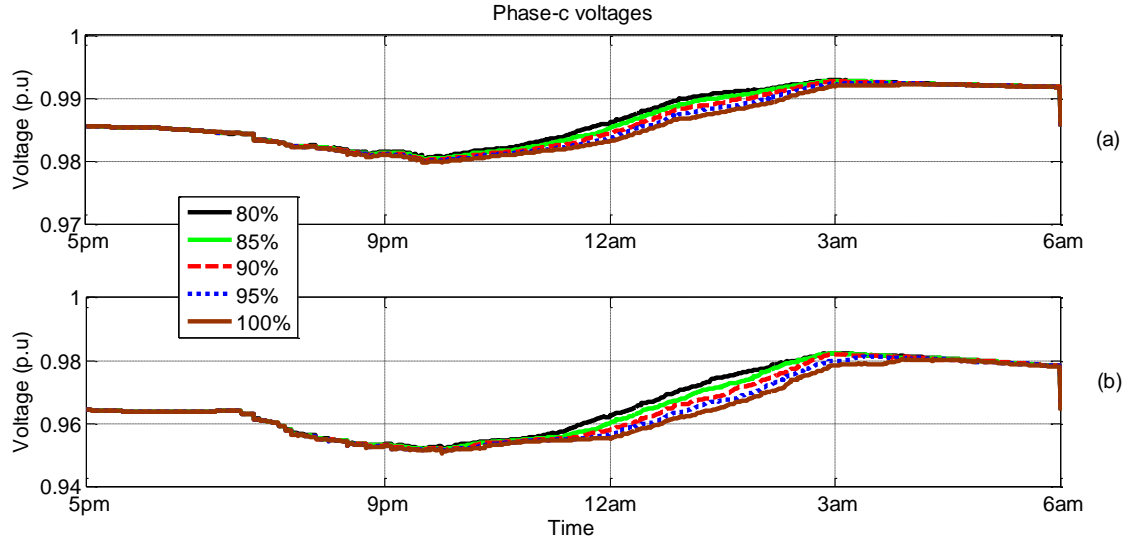
Figure 3.12: Effect of the changes of SOC_{max} on the system voltages
(a) Voltage profile at upstream bus 2   (b) Voltage profile at downstream bus 6
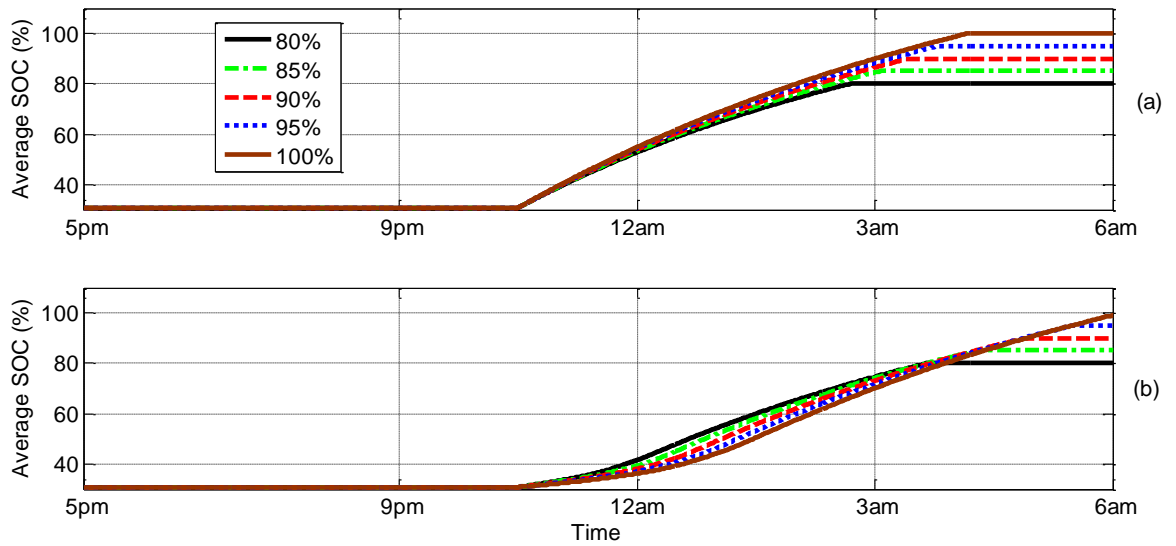
Figure 3.13: Effect of the changes of SOC_{max} on the controller behavior
(a) SOC of EVs at upstream bus 2 (b) SOC of EVs at downstream bus 6

3.5.2 Sensitivity of the controller to design parameters (ΔV_c, I_c)

It was previously mentioned that I_c is the critical charging point at which the voltage at the point of connection is high enough to allow increasing the charging rate of the EV. I_c is basically the current point on the curve that corresponds to ΔV_c ($V_c - V_{ref}$), shown in Figure 3.2 (a) , which is the voltage at which the controller changes from the small slope line of the curve (the blue one) to the large slope one (the red one). Switching between the two slopes is meant to increase the charging rate if the voltage is healthy enough (considered 1.04 p.u in this chapter). The determination of this voltage is important. It represents a compromise between the speed of the charging process and the fairness among the EVs. Since there are variations in the voltages at different buses of the system, where the upstream buses have much higher voltage compared to the downstream ones, it is important to charge the EVs within reasonable times and in a non-discriminatory way as well.

On one hand, if the value of this transition voltage V_c is chosen to be 0.99 p.u, for example, the upstream EVs will be able to charge during a short period of time, but the fairness among the EVs will be worse because the difference in time to full charge among the upstream and downstream EVs will be larger. This happens because the charging rate of the upstream EVs will increase, but the downstream ones will have the same slower charging rate because it is rare that the voltage at the downstream buses have values higher than 0.99 p.u during the charging of the EVs.

On the other hand, if the value of this transition voltage V_c is chosen to be 1.04 p.u, for example, all the EVs will almost charge at the same slow charging rate, which will improve

the fairness but will result in longer charging periods for all the EVs. Therefore, the choice of the V_c (in other words the pairs $(\Delta V_c, I_c)$) is a compromise between the speed of charging and the fairness.

Since the proposed work in this chapter is concerned with EVs at the residential sector, where most of the EVs will charge during the night times, the priority is given to the fairness issue more than the speed of charging. That is why V_c is chosen to be 1.04 p.u. However, it is easy to change that in the design.

Figure 3.14 and Figure 3.15 shown below depict the voltages at the points of connection and the SOCs of the upstream and downstream EVs (EVup and EVdown) for different cases of V_c (1 p.u, 1.01 p.u, 1.02 p.u and 1.03 p.u) for the same non-EV loading condition. All the other operating conditions are kept the same as well. The figures clearly show that most of the changes occur at the upstream EV while almost no changes occur to the downstream ones. The value of V_c has a minor effect on the system voltage, as shown in Figure 3.14.

The most important note from the results is that the choice of the value of V_c has an impact on the fairness. As shown in Figure 3.15, as the value of V_c increases, the EV takes a longer time to charge, where that time is almost equal to the downstream ones. Also, as the value of V_c decreases, the fairness is degraded because the upstream EV will charge faster.
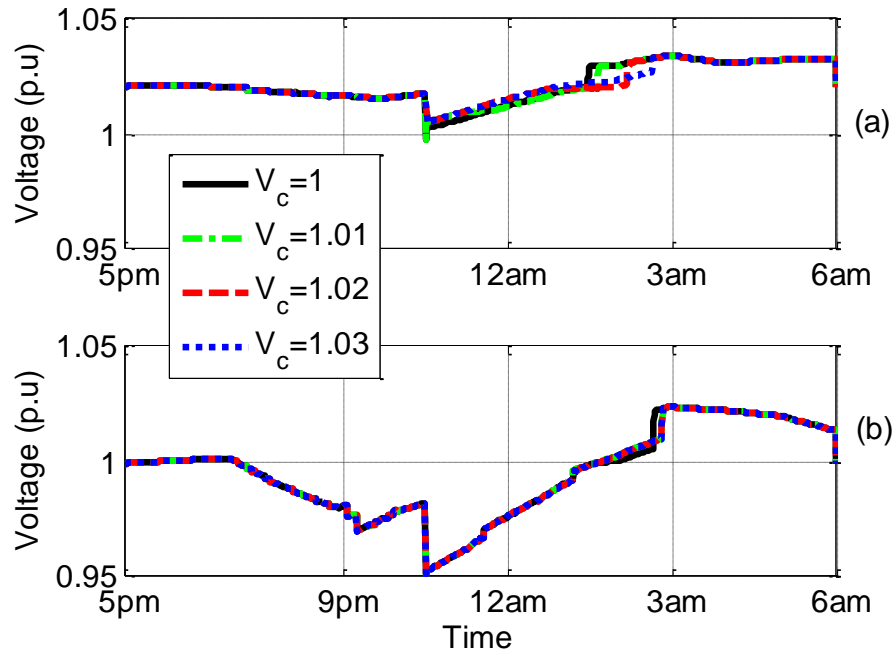
Figure 3.14: Voltage at the secondary distribution transformer with different values of V_c
a) Upstream house.   b) Downstream house
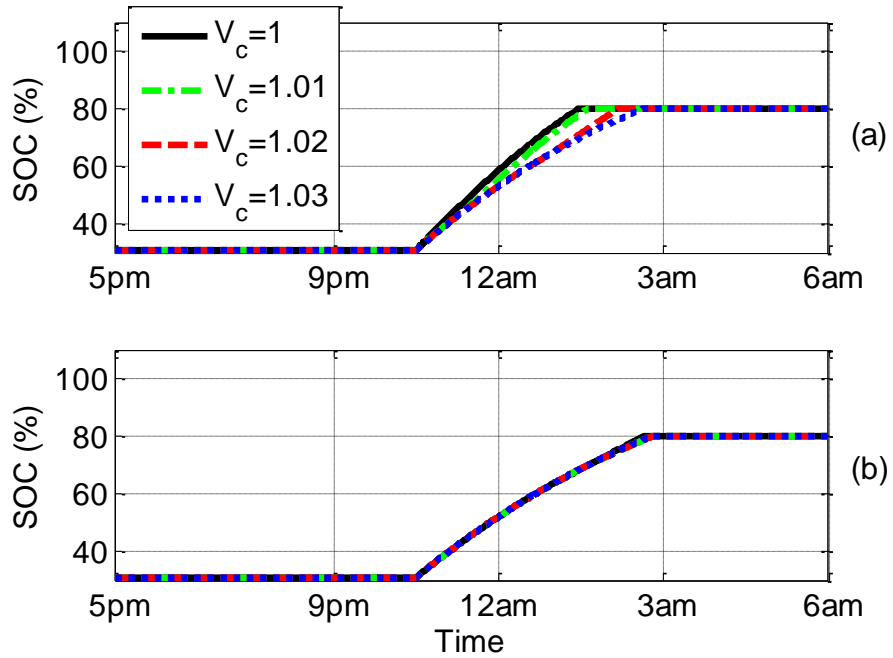
Figure 3.15: SOCs with different values of V_c
a) EVup.   b) EVdown

3.6   Conclusion

This chapter presented an automated controller to allow the adoption of a large number of EVs in the power grid. The chapter showed the negative impacts of opportunistic uncontrolled charging of EVs on the power grid using the simulation. A proposed controller that controls the charging of EVs, taking into consideration the customer requirements, the grid status, and the state of charge of the battery, is validated. The simulation results showed that the controller can successfully charge the EVs without negatively impacting the grid. The controller was also compared to other controllers. The results showed the superiority of the proposed controller in terms of the fair charging among the different EVs, ensuring smooth charging. The proposed controller was also tested in the presence of distributed generation units. The results showed the good performance of the controller and its ability of taking advantage of the presence of local generation to charge the EVs in a faster manner. In addition, the sensitivity of the controller to the design parameters was tested. It was found that the control algorithm is not affected by the maximum limit SOC_{max}. This limit only affects how much energy is required from the system. The more the required energy is, the more the stress on the system is, and the longer the charging time is. The pair $(\Delta V_c, I_{c)}$ represents a compromise between the speed of the charging process and the fairness among the EVs. Since the priority is given to the fairness issue more than the speed of charging. V_c is chosen to be 1.04 p.u. However, it is easy to change that in the design.

Chapter 4   **Experimental Verification and Control of the Impact of Charging of**

Electric Vehicles on Power Grids

The anticipated increase in the number of Electric Vehicles (EVs) will have various impacts on the power system. These impacts include both the system loading conditions and power quality issues. This chapter provides insights on the impacts of EVs charging using a small-scale laboratory distribution system. The chapter shows experimental results about the effect of the charging of EVs on the system loading and voltage levels at different nodes of the distribution system. In addition, an experimental validation of the proposed linear controller, discussed in the previous chapter, is presented. The proposed controller is compared to the conventional droop-based controller experimentally. Moreover, the proposed controller is tested in the presence of an inverter-based distributed generation.

4.1   Introduction

With more adoption of EVs, the number of batteries that need to be charged from the power grid will increase. The load of a single EV that is charged by a level 2 charger can double the peak consumption of a homeowner [131]. Therefore, large-scale deployment of EVs is likely to cause negative impacts on the power grid, if not properly managed. These negative impacts include increasing the system peak load, increasing the system losses, and causing power quality problems, such as voltage sags. Many researchers tried to address the various impacts of EVs on the power grid. A test platform that includes three Li-ion batteries was developed in [132].The aim of the test was to study the impact of smart charging and fast charging on the power system, on the battery state of health and degradation, and to find out the limitation of the batteries for future smart grids. In [133],

the authors assessed the impact of the large-scale adoption of EVs on the Hellenic distribution network. The analysis took into consideration the driving profiles of EVs, their types and road conditions. It was observed that EV charging causes under-voltage problems in rural lines and overloading in urban lines. Also, active power losses were found to significantly increase under opportunistic (dump) charging.

In [134], the authors tried to identify and mitigate the impacts of EV load charging on a residential distribution circuit. The impacts of on-board single-phase charging on a Flemish residential grid was considered in [69], where the authors studied the effect of droop-based charging of EVs. Probabilistic load flow studies were performed in [135] to study the impacts of the charging on the low distribution networks. The primary concern of that approach was to determine the correlation between the different variables. Two autonomous plug-and-play charging scenarios were compared with a standard charging arrangement, and the correlation between the households and the EV charging loads was taken into consideration. So far, the experimental study of the impact of EVs on the distribution systems did not get enough investigation. In [121], an experimental study and control was done on a real-estate feeder capacity during the charging of an EV. However, the impacts of charging the EVs on the system level were not investigated. Therefore, the experimental verification of the impacts of EVs needs more investigation.

4.2 TestBed-Setup

In this section, the experimental set-up that is used to verify the impact of the charging of EVs will be presented. Details about the step by step connections and software can be found in the appendices.

Also, the design of the DC-DC converter that is used to control the charging of the EV is explained in this chapter.

4.2.1   System Description

The system, shown in Figure 4.1, is developed at the Energy Systems Research Laboratory (ESRL) at Florida International University (FIU) [136] to verify the impact of the charging of EVs, and to test the validity of the proposed controller to mitigate these impacts. This small-scale distribution system features controllable dynamic loads, a 3-phase grid connection with the utility, and a controlled grid-tied inverter that emulates renewable energy resources. The configuration of the distribution system and its different components are controlled through solid state switches that are monitored and controlled by a NI LabVIEW data acquisition platform. Figure 4.1 (a) shows the schematic of the system that is used. It consists of a 3-phase 4-bus system, two dynamic loads, two 3-phase rectifiers, two DC-DC converters, two lithium ion (Li-ion) batteries and a grid tied 3-phase inverter. The components of the system are shown in Figure 4.1 (b,c,d). The experimental system emulates a radial distribution system. The EVs are connected at different buses to show how the charging of an EV will be impacted by its location in the system. One EV is connected directly to the utility at bus 1 and the second EV is connected to the down-stream bus 4. The former will be referred to as EVup and the latter as EVdown. The battery of each EV is connected to the system through a 3-phase rectifier and a DC-DC converter. The control and monitoring of the batteries are done through dSPACE 1104, while the dynamic loads are controlled to generate variable load profiles through the LABVIEW platform.
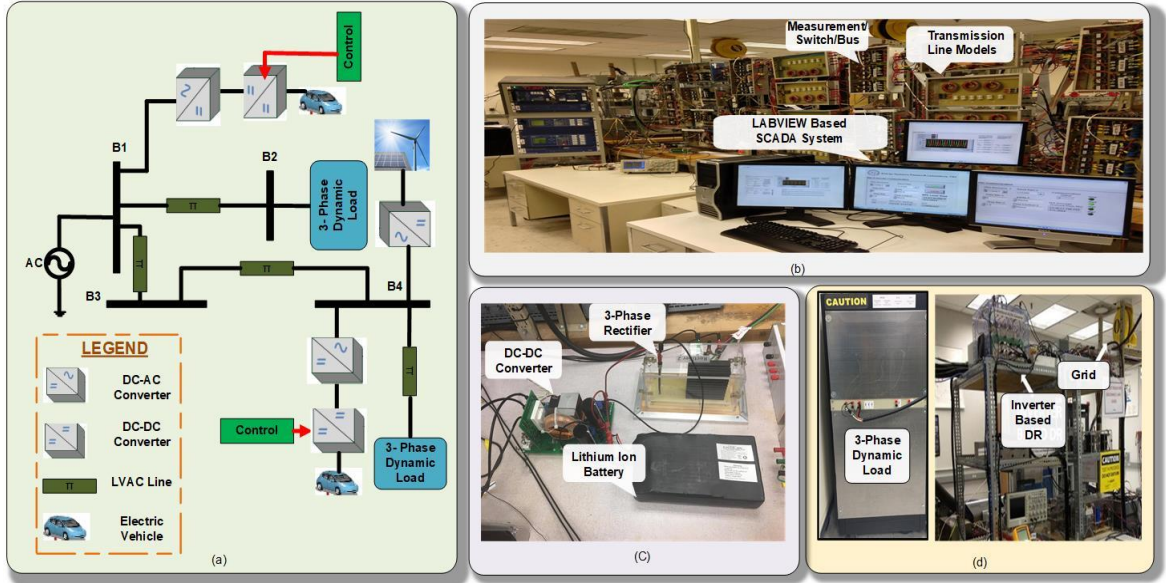
Figure 4.1: Experimental setup
a) Schematic diagram   b) Four bus system with data acquisition   c) Battery charger
d) Loads and sources.

4.2.2   Electric Vehicle Charger

The developed design for the EV charging converter is as shown Figure 4.2. The converter is designed using the buck-boost topology to provide a bi-directional power flow to charge/discharge the battery. However, since this study is focusing on the impacts of the charging of EVs, the converter will be used in the buck mode only and its equivalent circuit in the buck mode is depicted in Figure 4.2 (b). The complete design equations and analysis of the converter can be found in [137]. In this topology, the DC link of the DC-DC converter is interfaced to the AC grid through a six-pulse uncontrolled full wave rectifier. The converter is designed and implemented in a modular manner for ease of assembly, diagnostics, and maintenance. Two fast IGBT modules with anti-parallel diodes are used. The converter is implemented in two main separable parts. The first one is the main board,

which is responsible for carrying the power components (capacitors, switches, heat sink and inductor). The second one has the control, protection and the driving circuits. Different protection functions are provided to disable the IGBT gate signals and protect the system. These functions are over-voltage, over-current and IGBT driver error. A varistor is connected at the low voltage side, which is battery terminals, to protect the battery against over-voltages, where it is known that Li-ion batteries are sensitive to over-voltages. The converter parameters are listed in Table 4.1, where R_{out} and C_{out} are the resistance and capacitance of the output capacitor. Similarly, R_{in} and C_{in} are the resistance and capacitance of the input capacitor and R_l and L are the resistance and inductance of the inductor. F_s is the switching frequency. The rated tested power of the converter is 1250 W.

Table 4.1: DC-DC converter parameters

DC Bus Voltage	300 V
C_{out}	1200 µF
R_{out}	0.008 Ω
L	12.7mH
R_l	0.125 Ω
C_{in}	1200 µF
R_{in}	0.008 Ω
F_s	10kHz
Rated Power	1250 W

(a)

(b)

(c)
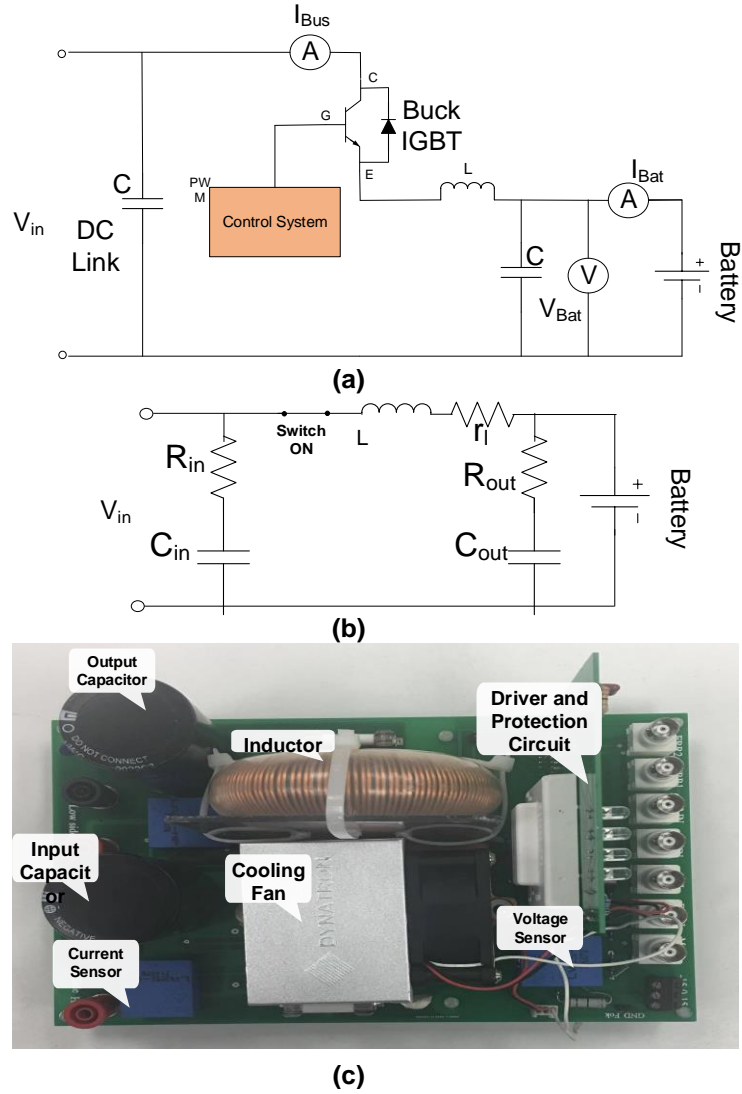
Figure 4.2: DC-DC converter
a) Schematic diagram. b) Equivalent circuit in buck mode during the ON state c)
Hardware implementation.

4.3   Results

This section presents the experimental results. First, the impacts of uncontrolled charging of EVs on the distribution system will be presented and discussed. Second, the ability of the proposed controller, illustrated in the previous chapter, to mitigate these impacts will be demonstrated.

In this experiment, the EVs are emulated using Li-ion batteries with 51.8 nominal voltage and a maximum capacity of 21 Ah, each. The dynamic load patterns are programed using labVIEW to emulate load patterns, such as in [138], in the residential distribution sector during the night hours. A large number of owners might charge their vehicles during the night when the electricity prices are low. The load profiles are shown in Figure 4.3. Since the simulation, in the previous chapter, was for 13 hours from the beginning of the evening to the early morning, the time scale of the experiment is done to be a down-scale of this period, where it is assumed that each minute in the operation of the testbed is equal to 15 minutes of the simulated distribution system. Therefore, the total time of the experiment is designed to be 52 minutes and the batteries are plugged in at t=12 minutes of the operation time. The initial state of charge of the batteries is 52%. Due to hardware limitations of the maximum loading of the testbed, the maximum charging current of the EVs is set to be C/2, which is equivalent to 11.5 A. The charging current of the battery is forced using a PI controller, which is used to generate the reference for the pulse width modulation (PWM) of the DC-DC converter.

4.3.1 Impact of Uncontrolled Charging

Figure 4.4 shows the effect of the charging of EVs on the system active and reactive powers. The figure clearly shows that the system loading has increased, where the peak load increased from 1375 W without EVs to almost 2790 W in the presence of EV charging. It is worth noting that not only the active power has increased, but also the reactive power has increased significantly. In the case of the absence of EVs, the only consumed reactive power is 102 var, which is consumed by the inductances of the transmission lines. In the

presence of EVs, the system reactive power has significantly increased to 1600 var. This is due to the use of uncontrolled rectifiers. This shows the importance of using controlled inverters in the charging process of EVs, to take into consideration the reactive power flow during the charging process. Otherwise, large amounts of reactive power will be consumed from the grid. In other words, future charging stations must follow the standard charging arrangement at unity or 0.95 capacitive power factors [135].

Figure 4.5 shows the voltage profiles at Bus 1 without and with the charging of EVs. The figure shows that the charging of EVs causes voltage drops, where the minimum voltage dropped from 0.984 p.u to 0.966 p.u.
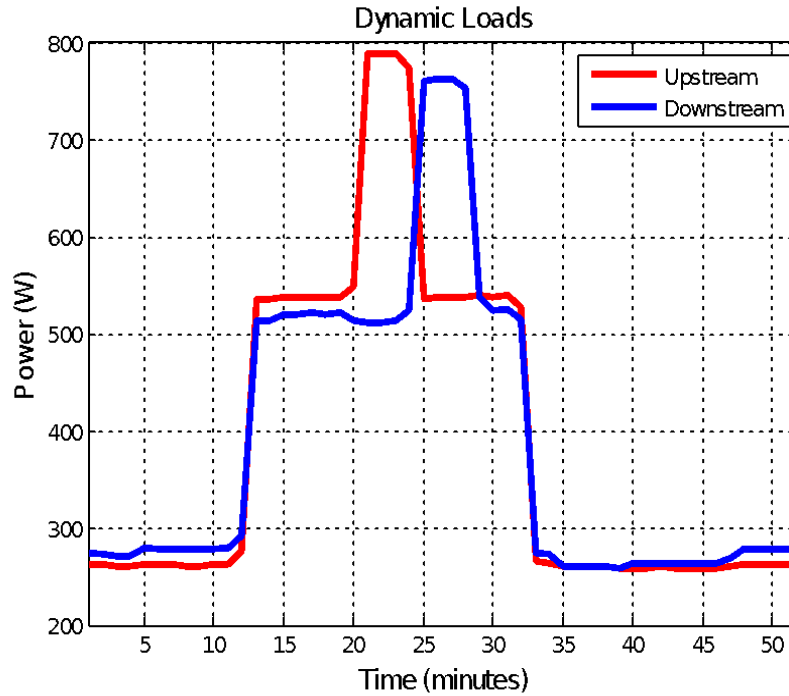
Figure 4.3: Dynamic load patterns

Unlike the upstream Bus 1, Figure 4.6 shows that the voltage sag at the downstream Bus 4 is more severe, where the minimum voltage dropped from 0.952 p.u to 0.908 p.u. This happens due to the voltage drops across the feeders that result in a much lower voltage at Bus 4. This shows the need for more voltage support units in future distribution systems that will accommodate EVs. Otherwise, consumers far from the substation might suffer from severe voltage sags, and the end-user voltages might not satisfy the ANSI standards [126].
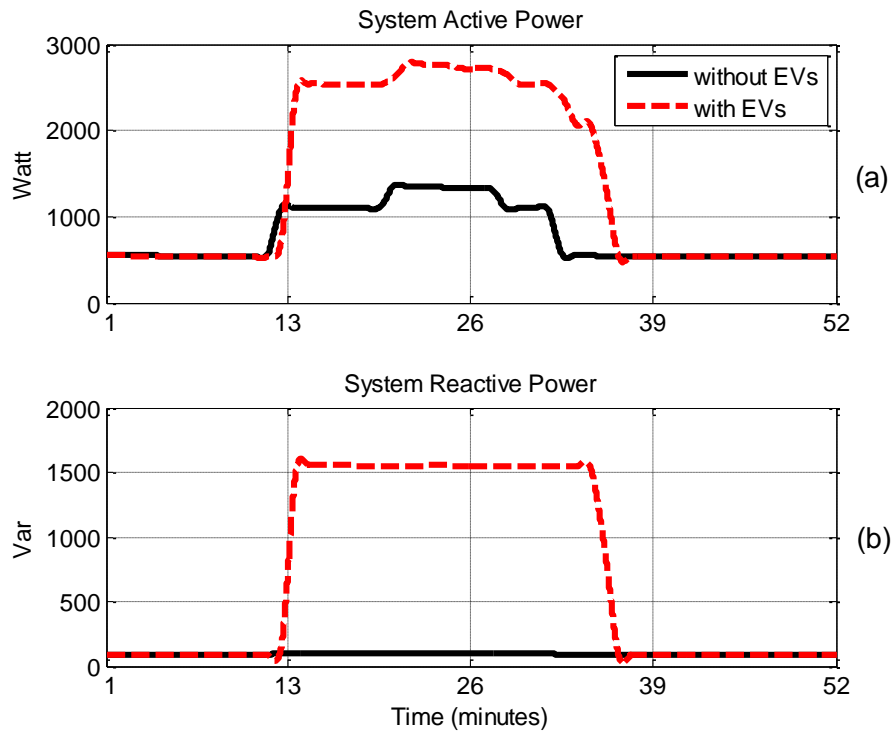
Figure 4.4: a) System active power   b) System reactive power
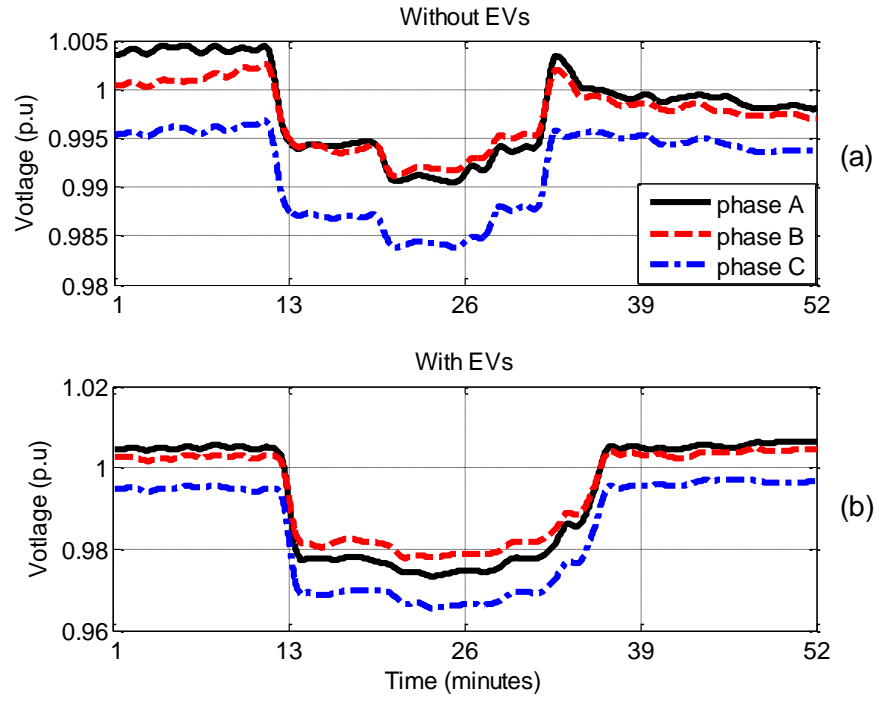
Figure 4.5: Voltage profiles at upstream Bus 1
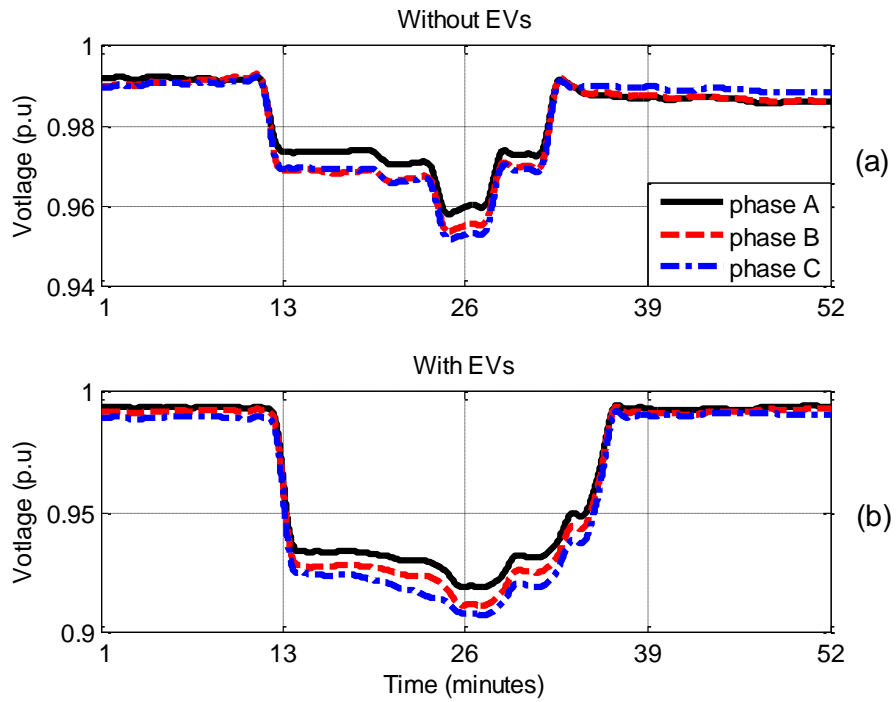
Figure 4.6: Voltage profiles at downstream Bus 4

90

Finally, Figure 4.7 shows the current, voltage and SOC of the battery during the charging process. It shows the uncontrolled dump charging, where the current is high and constant during the charging period. Also, it shows the increase in the battery voltage and SOC during the charging. It is worth mentioning that a maximum of 80% SOC is assumed during the experiment to increase the lifetime of the battery since charging high currents to the batteries at a high SOC degrades the battery and reduces its lifetime [128].
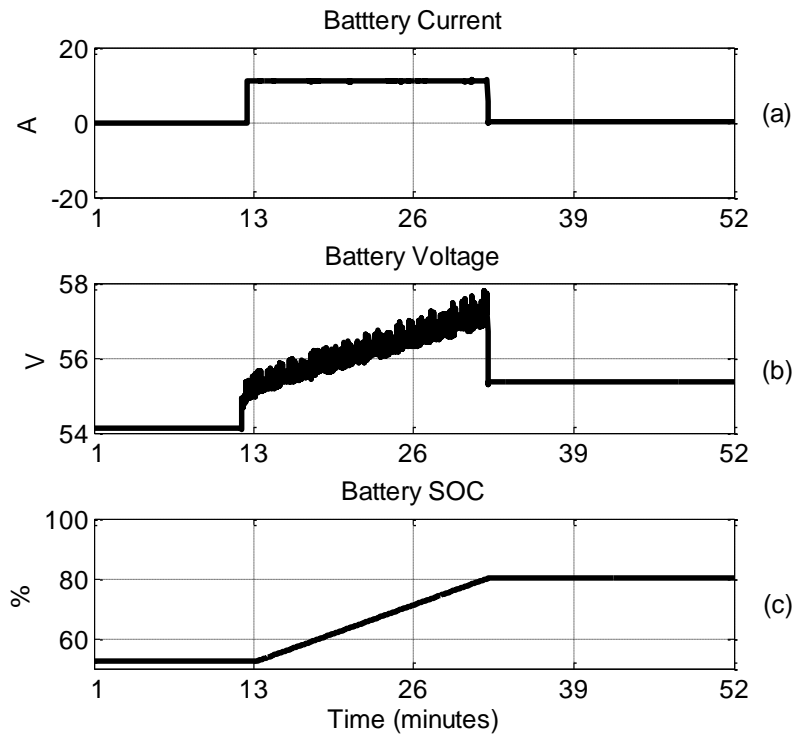
Figure 4.7: Battery performance

4.3.2   Experimental Validation of the Proposed Controller

In this section, the ability of the proposed controller, illustrated chapter 3, to mitigate the negative impacts of the charging of EVs will be demonstrated. Different cases are

validated (conventional droop-based controller and the proposed one), and the performance of the proposed controller is tested without distributed generation and in the presence of distributed renewable generation.

Figure 4.8 shows the grid loading for all the different cases. It is obvious from the figure that, if the EVs are allowed to charge opportunistically at a very high charging rate to finish as soon as possible, there will be high peaking in the system. If the control is applied, the peak load reduces to around 2000 W for both the droop controller and the proposed one. Figure 4.9 (a) and Figure 4.9 (b) show the voltage profiles at the upstream and downstream EVs in the system for phase b, respectively. Figure 4.9 shows that when the EVs are not controlled, the upstream bus was impacted by the EV charging, however the impact is not as drastic as the downstream one, where the voltage goes below 0.92 p.u when the system is at its peak. When the control is applied, the voltage profile is improved and it is limited to 0.95 p.u as a minimum value. If the voltage is going to be lower than the 0.95 standards, the charging rate of the impacted EV reduces to avoid under-voltage problems.

Figure 4.10 (a) and Figure 4.10 (b) show the 3-phase voltages at the upstream bus 1 and the downstream bus 4 for the case of the proposed controller. They show that none of the phases suffer from under-voltage problems, which is desired and follows the ANSI standards.

To have a better understanding of the charging process, in this section, the charging current profile over time will be considered instead of the SOC plots. This will give a closer look at how the different controllers behave.

Figure 4.11 (a) and Figure 4.11 (b) show the charging currents of the two EVs for the different cases. It is obvious from the figure that in the case of uncontrolled charging, both EVs charge at a high current with the same value. This is shown by the black profiles in Figure 4.11. When the droop controller is applied, the upstream EV charges at a higher charging current compared to the downstream one. This is shown in the green dashed profiles in Figure 4.11. For the case of the droop controller, during the period t= 13 to t= 25, the voltages at bus 1, where the upstream EV is connected, and at bus 4, where the downstream EV is connected, are around 0.982 and 0.958, respectively.
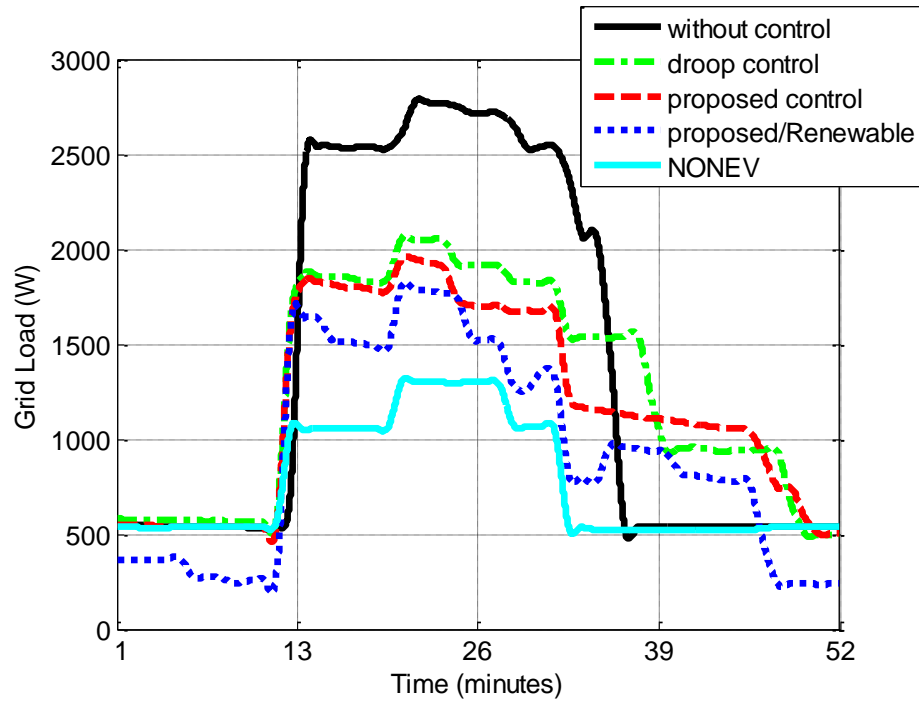
Figure 4.8: Experimental total grid load
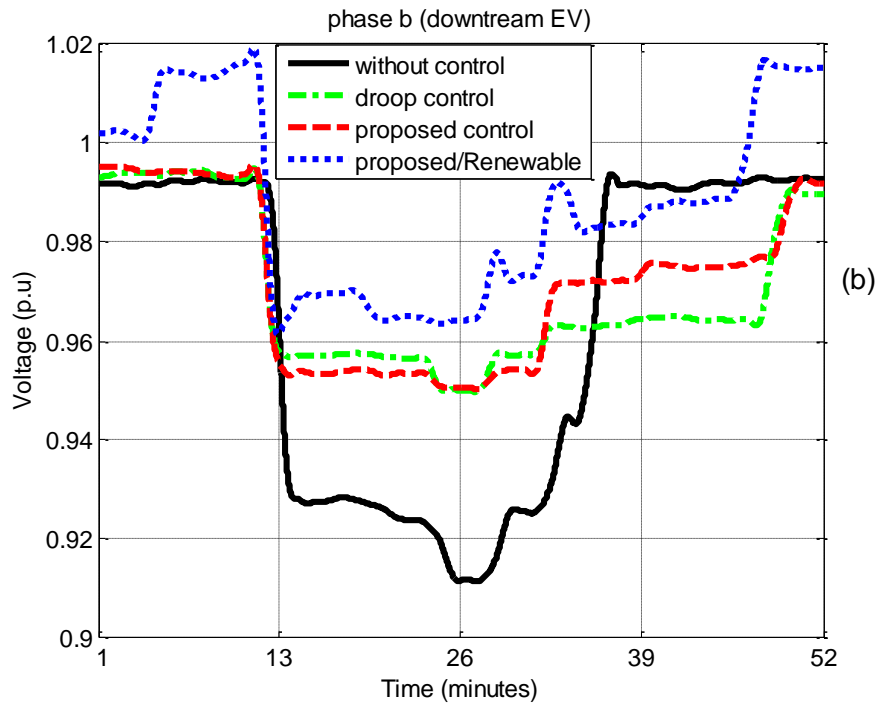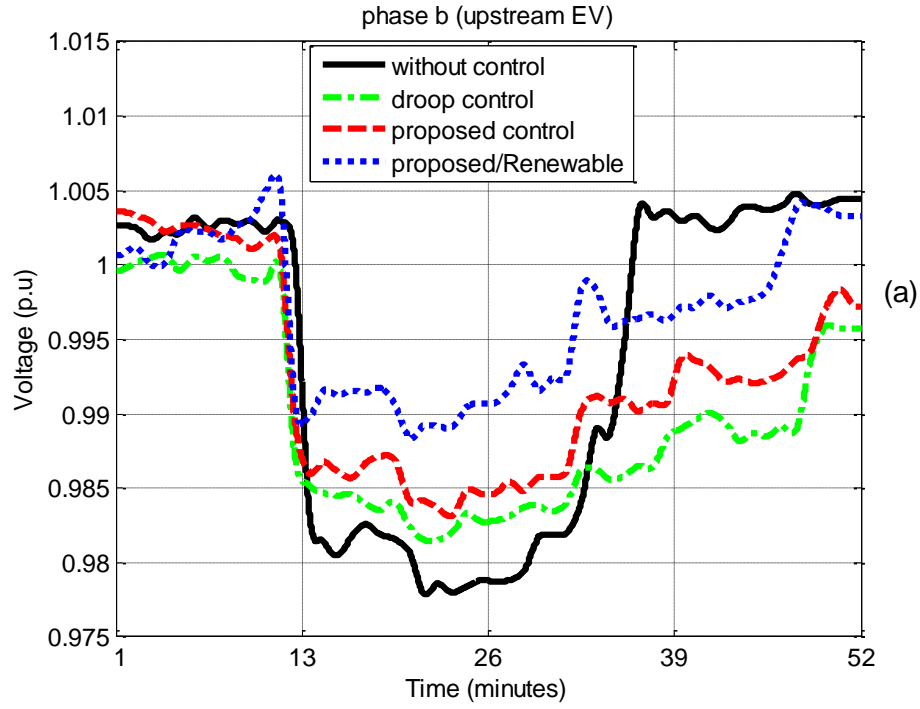
Figure 4.9: a) Phase b voltage profile at the upstream bus 1
b) Phase b voltage profile at the downstream bus 4
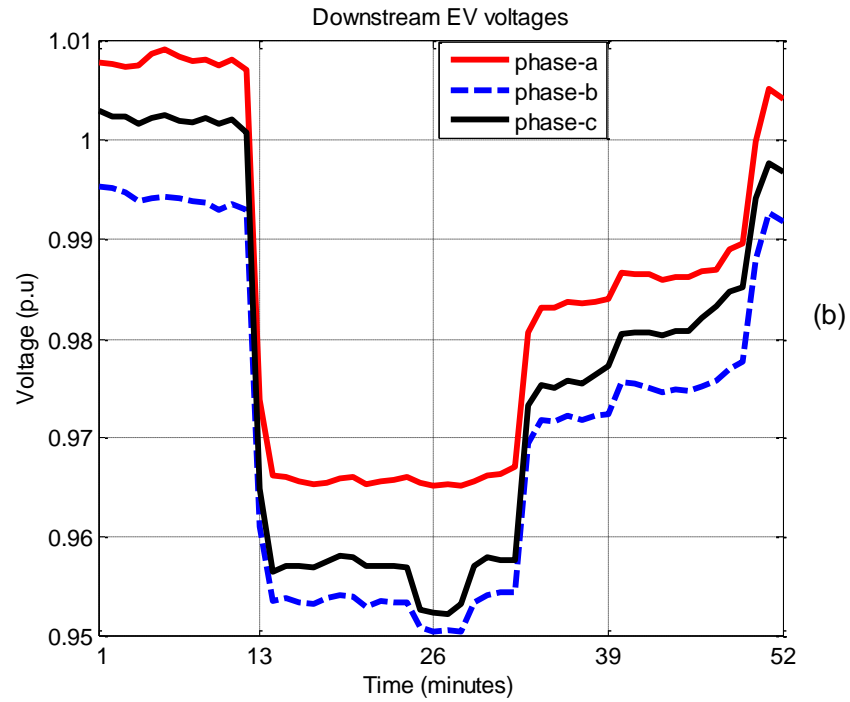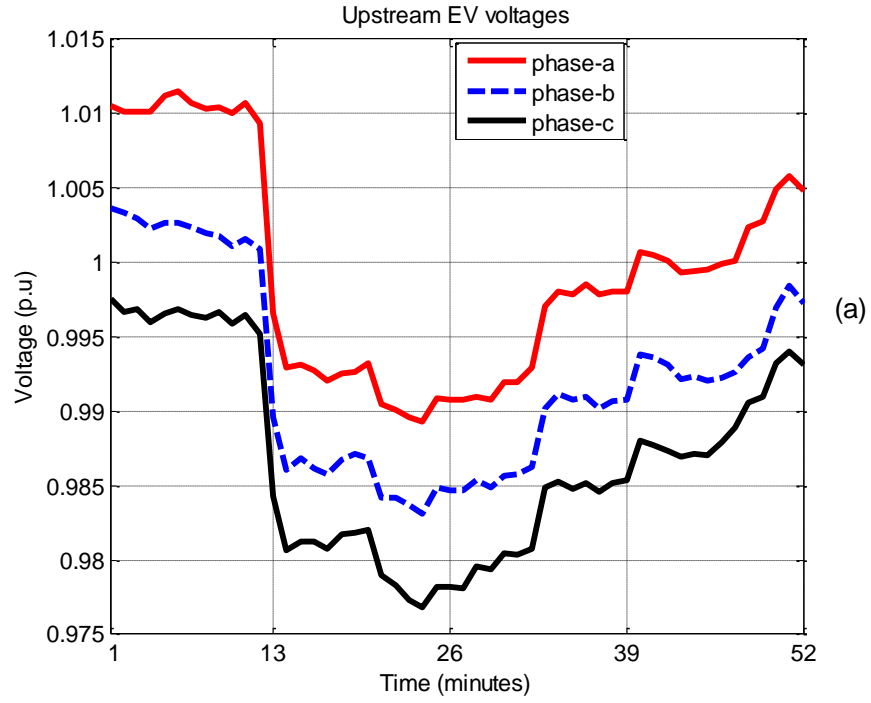
Figure 4.10: a) Voltage profiles at upstream bus 1 for the proposed controller
b) Voltage profiles at downstream bus 4 for the proposed controller
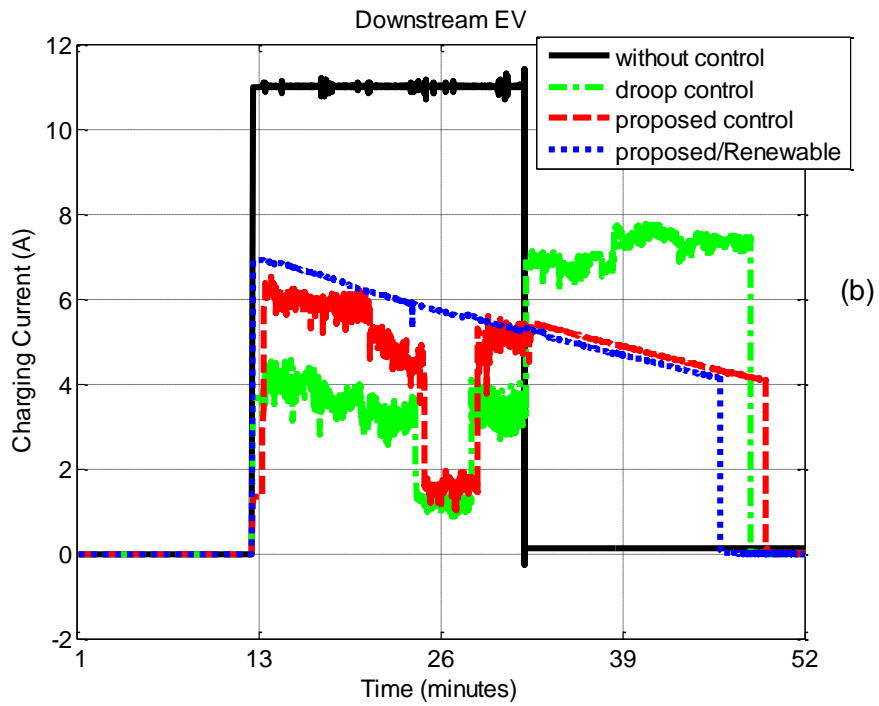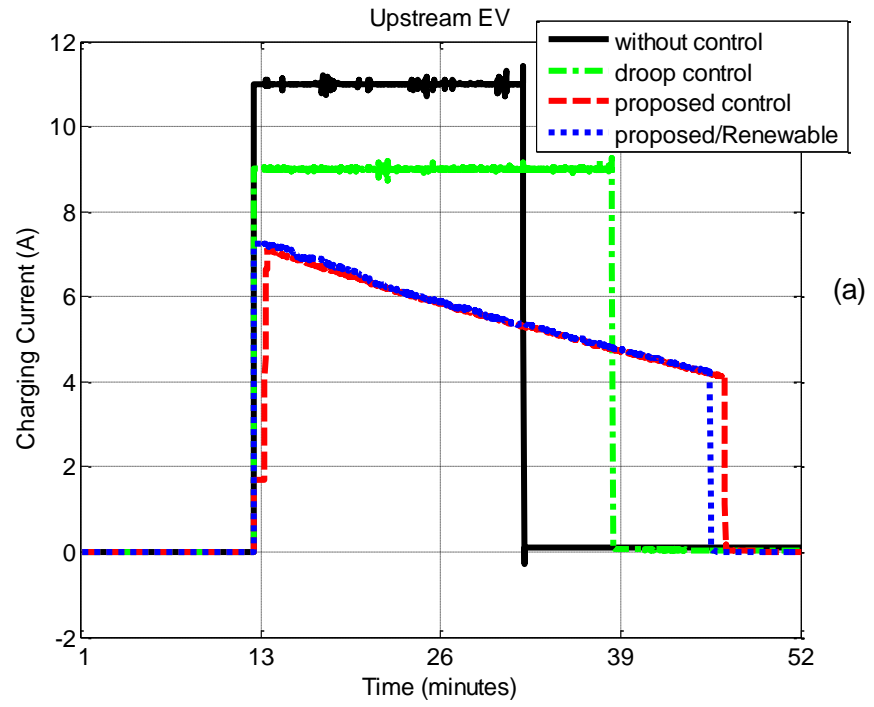
Figure 4.11a) Charging current of the upstream EV
b) Charging current of the downstream EV

96

Although the difference between these two voltages is not very high, it results in a high charging current for the upstream EV compared to the downstream one. The ratio of the charging current is almost two to one. For the same period, the voltages at buses 1 and 4 for the case of the proposed controller are 0.985 p.u and 0.954 p.u, respectively. Although the difference between these two values is almost similar to the case of the droop controller, both EVs charge with a semi-equal charging rate, which is fair and highly desirable. Also, Figure 4.11 shows that the proposed controller takes the SOC of the battery into consideration. It is desirable to decrease the charging current of the battery as the SOC increases. This will increase the lifetime of the battery. This is clear in the red curve in Figure 4.11, where the charging current of the battery decreases over time.

During the period t=25 to 27, the voltage at downstream bus 4 is 0.95 p.u for both the droop controller and the proposed one. Therefore, both controllers reduce the charging rate of the downstream EV to avoid any negative impact on the grid. This is shown in Figure 4.11 (b), where the charging current drops to be around 1.7A for both the droop and the proposed controller.

During the period t=27 till the end, the droop controller abruptly increases the charging current from around 3.8 to 7 A, which is not recommended, especially when the battery is near full charging. This happens because during this period, the non-EV loads have decreased. This resulted in improvements in the voltages. Since the droop controller is highly sensitive to the voltage, it resulted in this abrupt increase in the charging current. This does not happen in the case of the proposed controller where the smooth charging is continued. Table 4.2 shows the time that the EVs take to fully charge. It is obvious from

the table that the proposed controller results in fairer charging among the two EVs. The time difference between them is 2.71 minutes compared to 9.79 minutes in the case of the droop controller.

Finally, the 3-phase inverter is used to emulate the distributed generation unit and inject the power profile shown in Figure 4.12. Since the load at bus 4 is partially fed from the inverter, the voltage drop across the feeders decreases. This results in the voltage improvements shown by the dashed blue curve in Figure 4.9. Due to this voltage improvement, the downstream EV charge at a faster rate, as shown in Figure 4.11 and Table 4.2. The time difference between the two EVs reduces to 0.53 minutes.
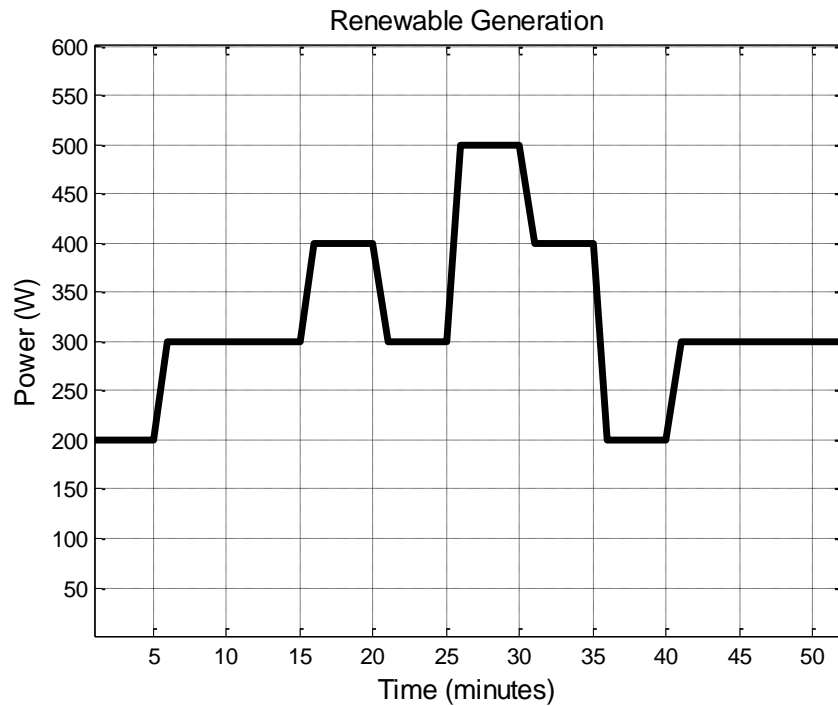
Figure 4.12: Renewable energy power profile

Table 4.2: Time to finish charging for the upstream and downstream EVs in minutes

	EVup	EVdown	Time difference
Uncontrolled case	20	20	0
Droop controller	26.42	36.21	9.79
Proposed controller	34.57	37.28	2.71
Proposed/Renewable	33.49	34.02	0.53

4.4 Conclusion

This chapter presented an experimental validation about the impacts of the uncontrolled charging of EVs on the distribution system. The results showed how the active and reactive powers of the system will be affected by the charging of EVs. A deduction has been reached that future charging stations must follow the standard charging arrangement at unity or 0.95 capacitive power factors. In addition, the results showed that the charging of EVs will cause voltage sags at the different buses, especially the downstream buses, which will have the most drastic voltage drops.

The experimental results demonstrated that the proposed controller can successfully charge the EVs without negatively impacting the grid. The controller was compared to other controllers, and the results showed the superiority of the proposed controller in terms of the fair charging among the different EVs and ensuring smooth charging. Compared to the other conventional controller, the proposed one decreased the charging current of the battery as the SOC increases, which increases the lifetime of the battery.

Moreover, the proposed controller was tested in the presence of distributed generation units. The results showed the good performance of the controller and its ability of taking advantage of the presence of local generation to charge the EVs in a faster manner.

Chapter 5   Automated Distributed Electric Vehicle Controller for Residential

Demand-Side Management

Electric vehicles (EVs) are recently gaining traction in the power sector due to the various challenges and opportunities they provide to utility operators. For electric utilities that incorporate demand-side management (DSM) programs, EVs could become either a burden or an advantage depending on their charging control strategy and the signaling of the DSM program. This chapter introduces a decentralized fuzzy-based controller to successfully integrate and coordinate the charging of EVs. The controller operates in an autonomous mode, which reduces the monetary cost of the communication overhead and preserves bandwidth. The proposed controller takes into consideration the owner requirements in terms of energy needed and time to charge, the voltage at the point of connection with the grid, and the pricing signal coming from the utility. The controller is tested under different DSM programs that exist in the literature. This chapter also proposes a new DSM program that is capable of benefiting from EVs as prosumers that can provide grid services.

5.1   Introduction

In today's dynamic grid, end users have migrated from being passive system elements to becoming active actors playing a major role in the grid operation and control through demand-side management (DSM) programs [139], [140]. With DSM programs, power system operators provide incentives for their customers to force certain energy consumption patterns as much as possible. This can be done by providing changing price signals throughout the day that are intended to guide the power consumption to obtain a

total demand that better matches the power generation. DSM proved its effectiveness in peak shaving and load shifting to non-peak hours, which increases the system reliability and stability. This also defers the investment needed in peaking generation, along with bringing several environmental benefits [141]. Most of the previously used DSM programs focused on industrial large customers to produce significant changes on the system level. The exact terms of the contract are determined a priori, and the system operator performs direct actuations of industrial loads, when needed, upon the contract.

In the recent days, more research has focused on DSM for residential customers [142]–[145]. This was facilitated by the wide adoption of smart metering, introducing time-varying prices, such as time-of-use pricing, and integrating renewables to active distribution networks. However, the successful deployment of DSM programs on residential customers needs more attention because it is not appropriate to perform direct actuation on loads since it will represent an invasion of the user privacy. Moreover, direct load actuation will need large investments to provide the required additional communication infrastructure and control technologies for each user. Therefore, there is a need for a decentralized demand- side management in the residential sector. Decentralized controllers have the ability to make decisions on the local level without the need for extensive communication with other entities.

In the residential sector, EVs are going to represent large loads that are added at the house level compared with other appliances. Therefore, there is a need to carefully control the charging of EVs. Also, unlike other loads at the house level, an EV has the ability to feed power back to the grid, which makes it a unique appliance that should be taken care

of at the residential sector, where most of the EVs will be charging during the nights when the owners of the EVs come back home.

In [146], the residential sector participation in DSM was incentivized in a non-discriminatory way by providing different individualized DSM prices for each user based on the history of his/her behavior and convenience. To achieve these objectives, heavy communication and data analysis are required from the SCADA system. In [147], the authors considered using a retired EV battery as an energy storage for DSM; however, only a single house was considered in that study. In [37], a multi-objective optimization is used to coordinate the charging of the plug-in EVs in a way that satisfies the network technical constraints, as well as the customer convenience. Heavy communication between the EV customers, vehicle coordinator and the Energy hub operator at the distribution system company is required. The former also requires the knowledge of the load profiles.

In [148], [149], the economic feasibility of demand management pricing schemes was investigated. In [150], dynamic energy management in a decentralized way was introduced. The authors aimed at testing the different time-of-use policies and to avoid the rebound effect. They introduced a new policy that uses multi time-of-use tariffs (MTOU), where each group of residential customers receives the time-of-use tariff with a one-hour delay from the previous group. In [15], the authors addressed the problems of centralized EV charging algorithms under a realistic communication infrastructure, where the number of messages to be exchanged is limited. This was done using a two-stage dual coordination using multi-agents. In [56], an optimal DSM is achieved using a model derived from game-theory. Each consumer's scheduler is required to broadcast its consumption schedule to all

other participants in the DSM program. Electric vehicles for charging and discharging in the households were considered in [48]. In this study, the impact of price-based demand response strategies on smart household load pattern variations was assessed. The household load datasets were acquired to perform optimal appliance scheduling considering an hourly varying price tariff scheme.

In this chapter, a decentralized controller is proposed to make the best use of the EVs under DSM programs. The contribution of the chapter is twofold. First, the proposed controller is a decentralized one. That is, the controller will make all the decisions at the local level, which minimizes the cost of the communication infrastructure and in a way that is compatible with the current demand-side infrastructure. It also takes into consideration the customer satisfaction in a fair manner, and the grid voltage standards that are defined by the ANSI C84.1-2006 code [126]. The proposed decentralized controller is tested and analyzed under different DSM programs presented in the literature. It is also tested in the presence of voltage control units and in the presence of distributed generations as well. Second, a new DSM program is proposed that is capable of benefiting from the fact that EVs can act as a controllable continuous energy consumer (load) or producer (source) without significant changes to the current DSM infrastructure.

5.2 Proposed Decentralized Controller

In this section, the different parts of the proposed controller will be explained.

5.2.1 Controllers Inputs and Outputs

The success of any demand-side management program in the residential sector is contributed to its ease of use by the customers without any invasion to their privacy,

fairness to all the customers connected to the system, its infrastructure cost, and its ability

to bring benefits to the system operator. In that paradigm, with the proper control algorithm

and DSM program, EVs can be effective in reducing the electricity bills for the customers,

and to provide flexibility to the distribution system operators. To do so, the direct

objectives of the EV battery controller are to satisfy the requirements of the owner of the

EV, try to minimize its negative impact on the system voltage, and to minimize the cost of

the charging by following the price signals that are coming from the grid operator.

Therefore, the inputs to the controller will be the customer requirements, the voltage at the

point of connection (POC), and the price signal coming from the grid, as shown in Figure

5.1. These three values with a voltage set-point (V_{ref}) will be the inputs to a fuzzy controller

that will decide on the charging/discharging rate based on the coming inputs. The fuzzy

logic controller is used in this chapter because it can be designed without the need for

training data, as long as we know the domain we are modelling and its reaction or rules.
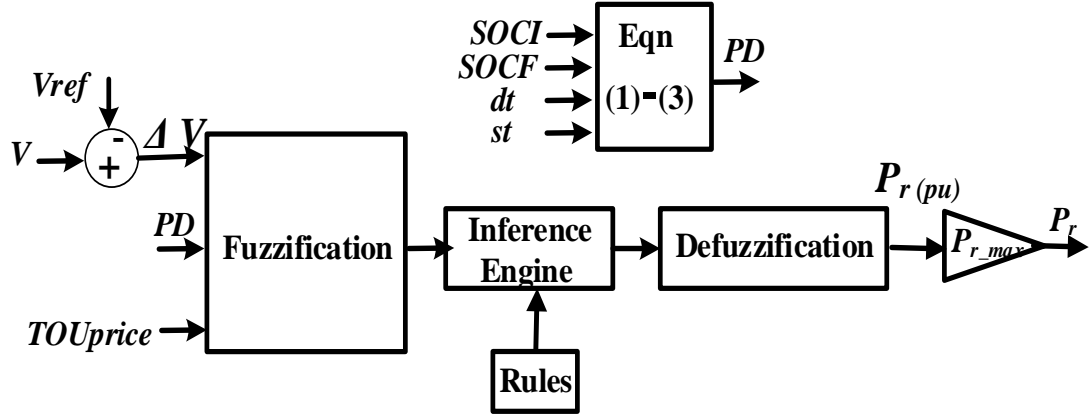
Figure 5.1: Decentralized controller block diagram

It has the advantage of its interpretability and simplicity since it allows modelling using near natural language rules and can handle the different circumstances that might arise in real systems.

The first input to the fuzzy controller is the requirements of the EV owner, which will be given by the two different inputs. These two inputs are the required final state of charge and the required departure time. Based on these data, the required power draw (PDr_i) by the EV to satisfy the owner's desire is defined by the following equation:

$$PDr_i = \frac{SOCF_i - SOCI_i}{hr_i} \tag{5.1}$$

where *SOCF* and *SOCI* are the required final and initial state of charge, respectively. *hr* is the number of hours before the departure time of the EV. It is the difference between the required departure time and the time the EV started parking, as shown by relation (5.2), where *dt* and *st* are the departure and start times, respectively.

$$hr_i = dt_i - st_i \tag{5.2}$$

The value of the power draw should be modified, as given in equation (5.3), to ensure that the customer requirement is within the acceptable value of the EV battery characteristics.

$$PD_i = \min(PDr_i, Pr_{maxi}) \tag{5.3}$$

where Pr_{maxi} is the maximum charging rate of the ith EV battery. PD_i is the safest power draw of the ith EV that can satisfy the requirements of the owner. It is the minimum of the power required by the owner and the maximum charging rate of the battery. This is to ensure that the power required at each hour does not exceed the maximum charging rate of

the battery. It is assumed that the charger can handle this power. This PD_i is normalized before entering the controller. The fuzzy controller will decide on the priority of charging of the different EVs based on that normalized value. As a general rule, the higher the value of PD_i is, the higher priority the EV owner should have. Higher values of PD_i means either the EV owner wants to charge as soon as possible or the amount of energy required to be charged in the battery is large, and vice versa. The value of PD_i will help prioritize the EV flexibility in contributing to the DSM.

The second input to the fuzzy controller is ΔV, which is:

$$\Delta V_i = V_i - V_{ref,i} \tag{5.4}$$

Where V_i is the measured voltage at the point of connection (POC) in p.u. $V_{ref i}$ is a reference set-point that will be sent by the system operator. This value can be kept constant all the year or changed seasonally depending on the system behavior.

The basis for selecting the voltage set-points is that, EVs connected across the distribution system contribute almost equally in the DSM, irrespective of their charging point location. If all voltage set-points are set identically, the EVs connected to downstream POCs (or those connected to the primary buses through long secondary wiring) will generally be at a disadvantage compared with those connected to upstream POCs (or have short secondary wiring). Therefore, as a rule of thumb, the more downstream the POC is, the lower the voltage set-point should be. To select these voltage set-points to achieve that goal, the historical value of the daily minimum voltage $V_{min,d,i}$ is tracked. This typically is associated with the daily peak period. These minimum voltage values are averaged out for several days. This average value is then used as a voltage set-point, or a voltage reference,

$V_{ref,i}$. This reference voltage needs to be constrained by the minimum permissible voltage level 0.95 p.u. That is,

$$V_{ref,i} = \max(\frac{1}{D}\sum_{d=1}^{D} V_{min,d,i}, 0.952)$$ (5.5)

where *D* is the number of days. A value of 0.002 p.u is added to the minimum permissible voltage level as a safety margin. The advantage of this method is that it is simple and systematic.

The third input to the fuzzy controller will be the time-of-use tariff (TOU) coming from the system operator, which will be a signal with a certain value for on-peak periods and another one for off-peak periods [151]. In some cases, a third signal that represents critical peaking pricing (CPP) can be sent. The output from the controller will be the charging/ discharging rate of the EVs.

5.2.2   Fuzzy Controller Design

The fuzzy controller has three inputs and one output. Each of the controller inputs and the output will have its membership functions. The power draw input, which represents the owner requirement, will have a membership function, as shown in Figure 5.2. The EV owners' requirements are divided into five different priorities. Extra Low (EL) represents that the EV owner is not in a hurry or does not need a large amount of energy. This type of customer shows a great desire to participate in the DSM to charge his/her battery with the lowest cost. Extra High (EH) represents a customer with extremely high demand who does not care about the cost. His priority is to charge the EV as soon as possible. The other three memberships are in the middle of the two extreme cases. Based on their energy requirement, they will be divided to Low (L), Medium (M) and High (H).

The voltage memberships are depicted in Figure 5.3. The Zero (Z) membership function represents operating close to the normal operating conditions. Positive Low (PL) represents that the voltage is in a very good condition within the acceptable limits, while Positive High (PH) represents the case of over-voltage (above 1.05 p.u). Similarly, Negative Low (NL) represents that the voltage is near a bad condition, while Negative High (NH) represents the case of under-voltage (below 0.95 p.u).

The time of use tariff is almost a certain signal that has a certain meaning. It can mean either connection in the off-peak period or disconnection in the on-peak period and sometimes it can refer to a critical peak or emergency, as shown in Figure 5.4. In this work, these signals are translated to the fuzzy controller as Charging (CH) for the off-peak period, No Charging (NC) for the on-peak period and Discharging (DS) for the critical peak.
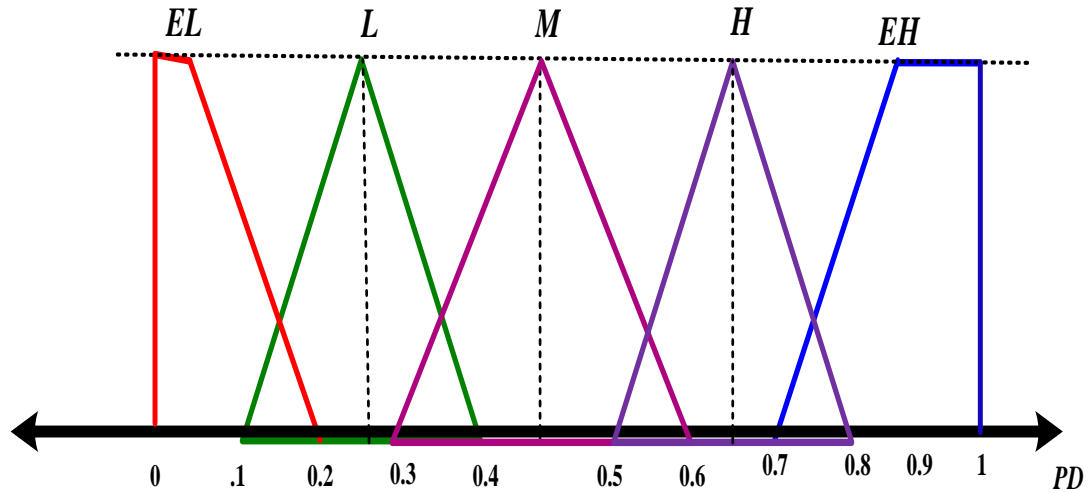
Figure 5.2: Fuzzy membership function of power draw (*PD*)
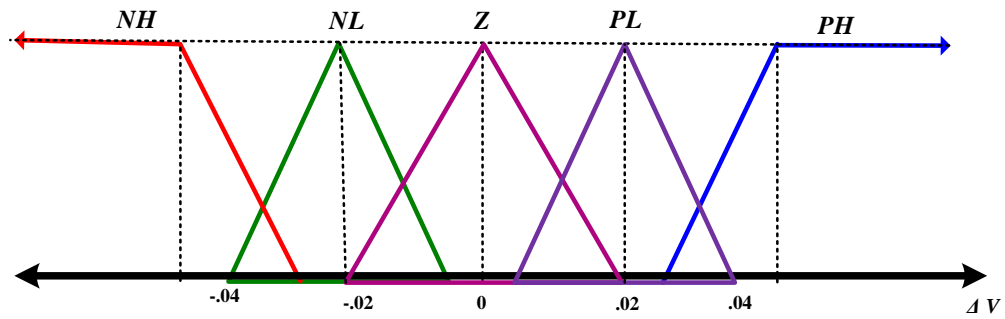
Figure 5.3: Fuzzy membership function of power draw (ΔV)
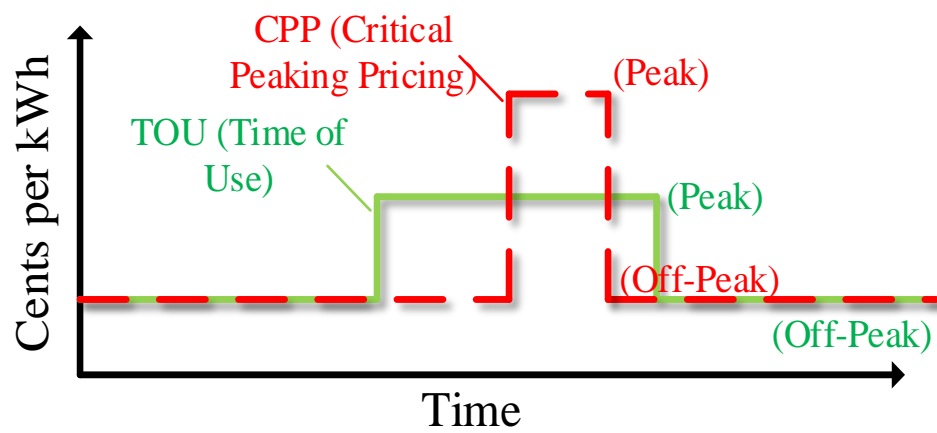
Figure 5.4: TOU signals
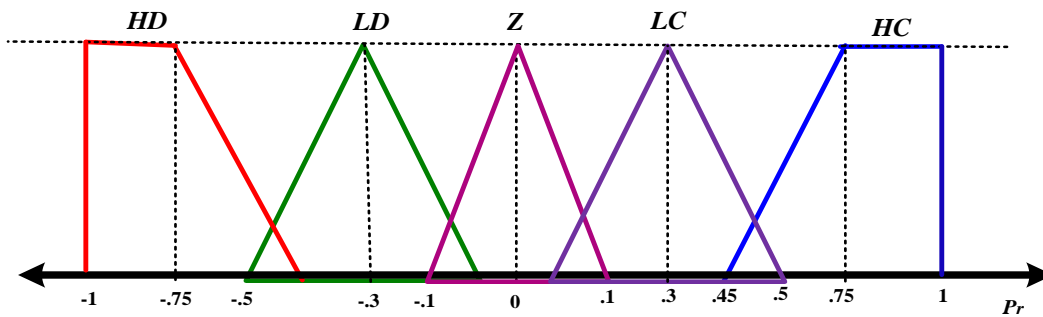
Figure 5.5: Fuzzy membership function of the charging rate (P_r)

Table 5.1: Rules when TOU is (CH) on left and when TOU is (DS) on the right

ΔV / PD	Z	PL	PH
EL	LC	LC	HC
L	LC	LC	HC
M	LC	HC	HC
H	HC	HC	HC
EH	HC	HC	HC

ΔV / PD	NH	NL	Z
EL	HD	HD	LD
L	HD	HD	LD
M	HD	HD	LD
H	LD	Z	Z
EH	Z	Z	Z

Table 5.2: Rules when TOU is (NC)

ΔV / PD	NH	NL	Z	PL	PH
EL	Z	Z	Z	Z	Z
L	Z	Z	Z	Z	Z
M	Z	Z	Z	Z	Z
H	Z	Z	LC	HC	HC
EH	LC	HC	HC	HC	HC

Finally, the output membership functions are divided into five memberships that range from the maximum charging rate (HC) to the maximum discharging rates (HD), as shown in Figure 5.5. The value of the charging/discharging rate P_r at the output will be decided based on the inputs and the rules in Table 5.1 and Table 5.2. It should be mentioned that it is unexpected that the system operator will send a TOU signal that means off-peak (charging) while the system is in a bad voltage condition (NL) or suffering from under

110

voltage (NH). Similarly, it is not expected that the TOU signal will be on-peak or critical peaking while the system is in a good voltage condition or in an over-voltage condition.

Table 5.1 shows the rules for the incoming TOU (CH) on the left and for the incoming TOU (DS) on the right. When the TOU signal is (CH), it shows that EV owners with priorities (H) and (EH) will always charge at a very high charge rate (HC) while other priorities will charge at moderate levels depending on the voltage status. When the TOU signal is (DS), EVs with priorities (EL) and (L) will participate the most in the discharging process since they are flexible, while EVs with priorities (H) and (EH) will not participate in the discharging process. Other statuses will be defined based on the voltage difference value. When the incoming TOU signal is (NC), rules in Table 5.2 will be applied. It shows that almost all the EVs will take no action except that the EVs with priorities (EH) will charge regardless of the signal.

It is worth mentioning that the controller will try to satisfy the time and energy constraints of EVs with priorities (H) and (EH) since they are willing to pay more money to finish. However, for other priorities (EL, L, M), the controller will satisfy their energy requirement, but may deviate the required finishing time since those owners are more interested in reducing their bills.

The output of the fuzzy system will be in per unit. Therefore, it will be multiplied by the maximum charging rate (Pr_{maxi}), as shown in Figure 5.1, to obtain the actual value.

5.3 Description of Test System

The configuration of the distribution test system is shown in Figure 5.6 and Figure 5.7. It is the same system that was adopted in the previous chapters. More details about the system voltage level and parameters can be found in chapter 3.
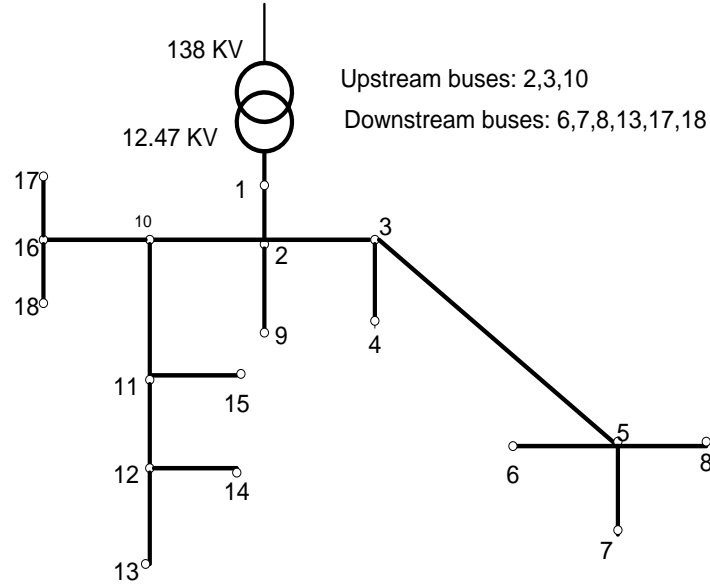
Figure 5.6: Primary distribution system
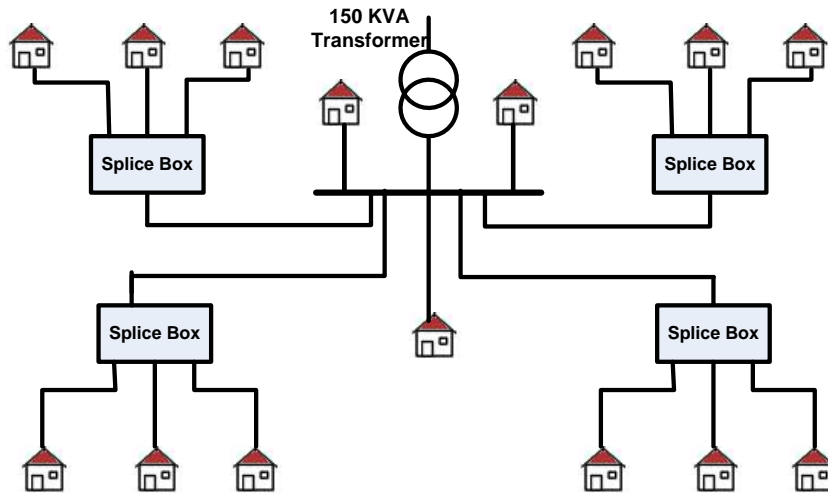
Figure 5.7: Secondary distribution network topology

5.4 Results

The proposed controller is validated through simulations using Matlab/Simulink, where several simulations are conducted. In this study, the only assumed controllable loads are the EVs and the time span of the simulation is for one day starting at 6 a.m. till 6 a.m. of the next day. The initial SOC is assumed to be a random value between (30-60%) while the final SOC is assumed to be a random value between (70-100%). The required number of hours to charge the EV to the final SOC is assumed to be a random number between three and seven hours. Only some of the results corresponding to buses 2 and 6 are presented. The former is the most upstream primary load bus with the highest voltage, where the selected EVup is connected, while the latter is a downstream bus, where the selected EVdown is connected. The minimum voltages at the different buses for the simulation period will be given as well. To validate the controller, six different cases are simulated:

A. Uncontrolled charging to show the effect of integrating a large number of EVs to the distribution system.

B. Conventional TOU tariff to show what was reported by many researchers that conventional TOU will result in a "rebound effect."

C. Multi-group TOU tariff to introduce flexibility to the system and at the same time avoid the rebound effect.

D. A new suggested DSM program to show how the EVs, as prosumers, can increase the system flexibility, support the grid in case of peak periods, and avoid the rebound effect. It will be referred to as multi-group TOU with critical peaking (MTOUCP).

E. In the presence of voltage control units such as capacitor banks to see the controller performance when the voltage is controlled by the operator.

F. In the presence of distributed generation units such photovoltaic (PV) units to see the performance of the controller when there is a local generation at the house.

5.4.1 Uncontrolled Charging

In this test, the EVs will be allowed to charge at the maximum charging rate to finish charging as soon as possible. The impact of uncontrolled charging of EVs on the system is depicted in Figure 5.8 and Figure 5.9. The left-hand side of Figure 5.8 shows how severely the voltage drops at a downstream house in the system, where the voltage goes far below the 0.95 p.u. Without EVs, the voltage is in a good condition, as shown in the right-hand side of Figure 5.8. This is also shown by comparing the primary buses voltages in the second and third columns of Table 5.3. This is also confirmed in Figure 5.9, where it is obvious that the total system load has increased due to the EV loading. This increase in loading leads to severe voltage drops, more line losses, and the need to run expensive peak generating units.
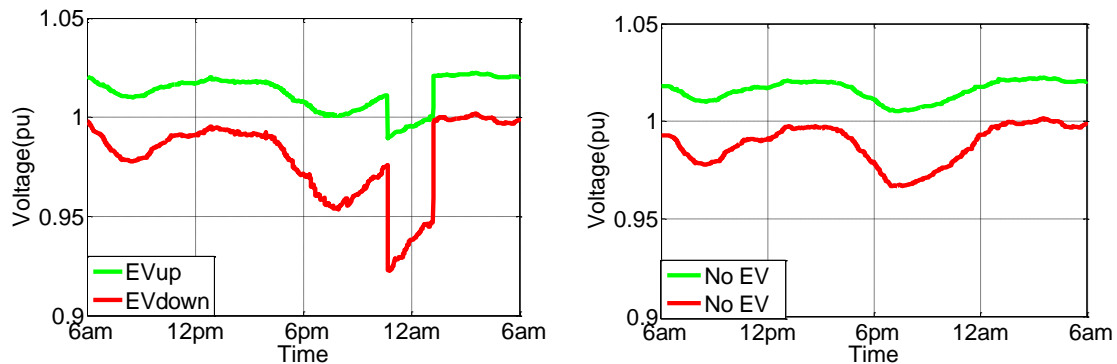
Figure 5.8: Voltage profiles at the secondary selected POC. Left: in the presence of EVs. Right: without EVs

114
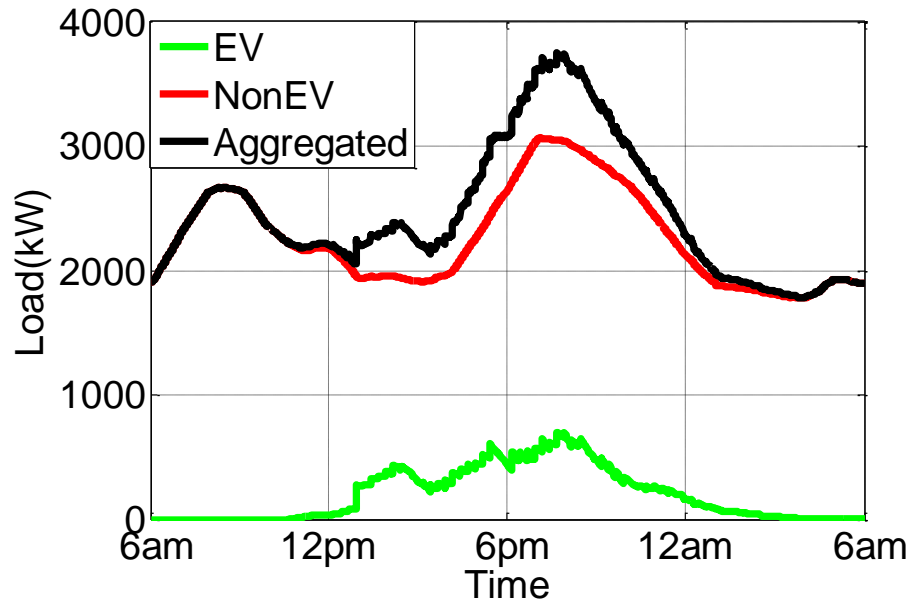
Figure 5.9: Total system loading in case of uncontrolled charging

5.4.2 Controller Performance under Conventional TOU Tariff

In this test, the proposed controller is used under the conventional time of use tariff, shown in Figure 5.10, where a peak time is assumed from (6 a.m to 10 a.m) and another peak from (6 p.m to 10 p.m) [151]. It is assumed that the EVs will not play any role in the morning peaking since all the EVs are assumed to be fully charged before people go to their work, and there is no desire to discharge the vehicles. However, it will have a great impact in the evening periods [150].

Figure 5.11 shows the EV loading, Non EV loading and the total system loading. It is obvious that the TOU signal defers the EVs' charging away from the system peak time. However, another peak is introduced in the next few hours due to the large loading that is connected to the system (the newly coming EVs and the deferred ones) at the same time.

This is what is called the "rebound effect," and it is confirmed by many researchers [146], [150]. It is worth mentioning that if the conventional critical peaking pricing tariff known as CPP, where a signal is sent for a half or an hour that matches the system peak or in case of emergencies to alert customers to turn off the loads or to support the system is applied, the rebound effect will exist as well. Figure 5.12 shows the voltage profiles at the secondary sides of the two selected POCs (EVup and EVdown). It shows that the controller in the presence of the time of use tariff keeps the voltage within the standards. This is also shown by comparing the fourth column of Table 5.3 with the case of uncontrolled charging in the third column. The rate of charge in terms of the SOC is depicted in Figure 5.13. It shows that the EVs almost stop charging during the peak time, as shown on right hand side of Figure 5.13. It also shows that both the EVup and EVdown charge at the same rate regardless of their location, which is highly desired and fair.
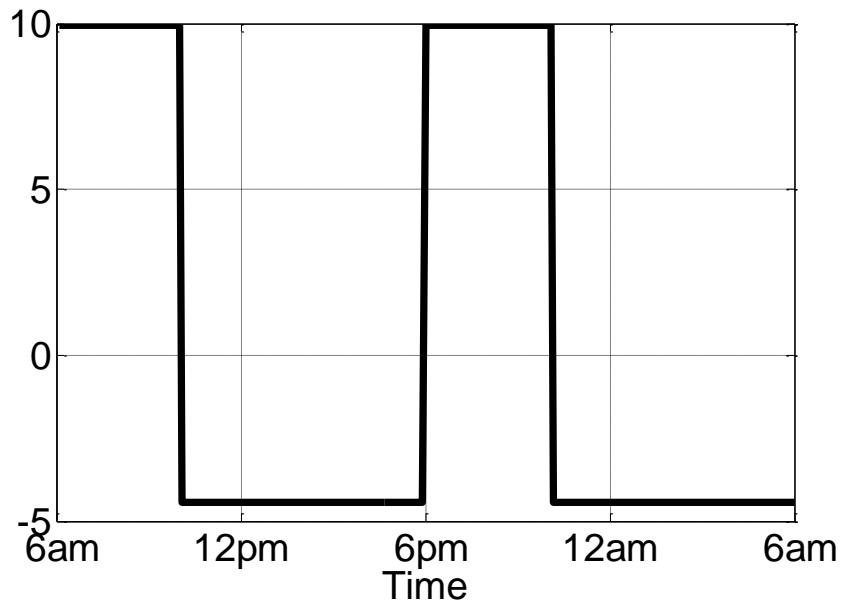
Figure 5.10: Conventional TOU tariff
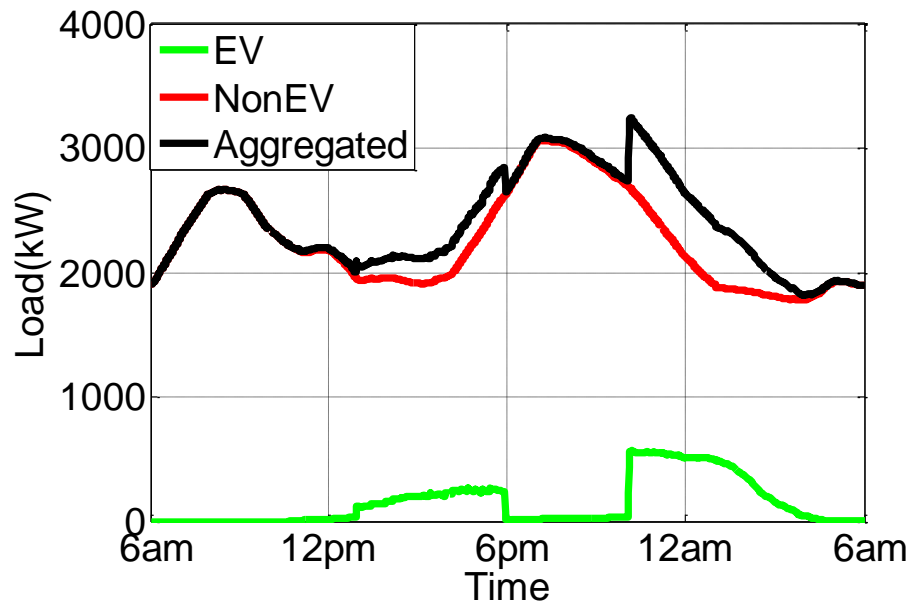
Figure 5.11: Total system loading under conventional TOU tariff
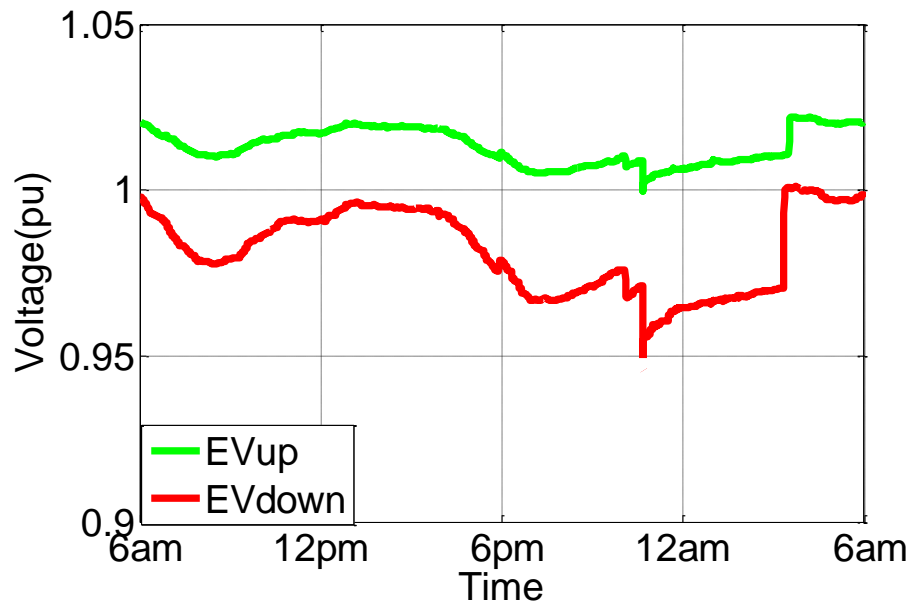
Figure 5.12: Voltage profiles at the selected POCs under conventional TOU tariff

Table 5.3: Minimum voltages at the primary buses under different cases

Bus number	Without EVs	Uncontrolled charging	conventional TOU	Multi-group TOU	MTOUCP
2	0.9839	0.9794	0.9826	0.9838	0.9842
3	0.9741	0.9661	0.9718	0.9739	0.9745
4	0.9736	0.9654	0.9713	0.9735	0.9741
5	0.9612	0.9493	0.9575	0.9609	0.9616
6	0.9591	0.9463	0.95515	0.9586	0.9595
7	0.9587	0.9460	0.9546	0.9583	0.9590
8	0.9585	0.9453	0.9545	0.9579	0.9589
9	0.9834	0.9789	0.9821	0.9833	0.9837
10	0.9746	0.9672	0.9723	0.9744	0.9750
11	0.9708	0.9622	0.96804	0.9705	0.9712
12	0.9692	0.9599	0.9664	0.9690	0.9696
13	0.9682	0.9584	0.9653	0.9680	0.9686
14	0.9691	0.9597	0.9662	0.9688	0.9694
15	0.9705	0.9618	0.9677	0.9703	0.9709
16	0.9710	0.9624	0.9686	0.9709	0.9715
17	0.9709	0.9622	0.9684	0.9707	0.9713
18	0.9708	0.9621	0.9683	0.9706	0.9713
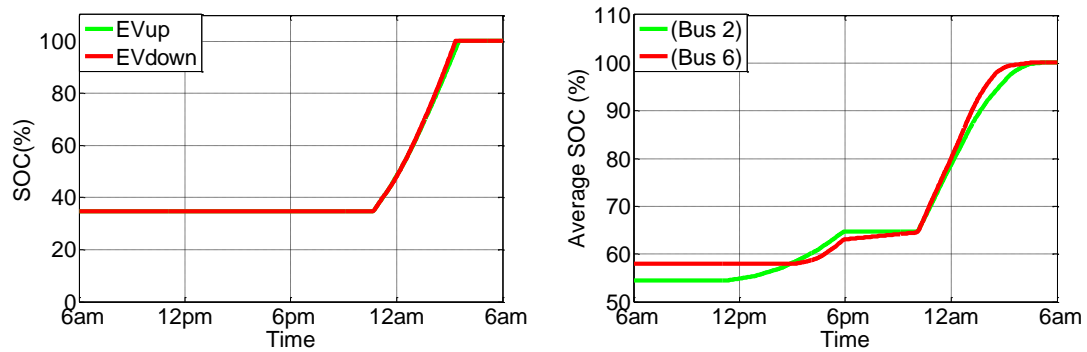
Figure 5.13: Left: SOC of the two selected EVs. Right: the average SOC of all EVs connected to bus 2 and 6 under conventional TOU tariff

5.4.3   Controller Performance under Multi-group TOU Tariff

The main purpose of demand-side management programs is to smooth the consumption

and reduce the total "peakiness" of the demand, which increase the system reliability and

reduce the peak demand feeding costs. The introduction of conventional TOU or CPP rates in the network, where each consumer automatically decides on the demand according to his/her needs by responding to the same signal may actually exacerbate the basic issue that the demand-side management program was supposed to address.

To avoid the rebound effect, the idea of a multi-group time of use tariff was developed in [150]. It is a mean to smooth the aggregated demand and avoid the rebound effect in a way that is compatible with the current infrastructure of the DSM.

The idea of Multi-group TOU depends on introducing a delay for the off-peak signal that is sent. For example, the customers of the system will be divided to several groups. The first group will receive the off-peak TOU signal and after an hour, the second group will have the signal, followed by the third group after two hours. It should be mentioned that when the second and third groups have the off-peak signal, the first group is still having it. Multi-group TOU is done to avoid having the whole controllable loads connected to the system at the same time. To be completely fair with all customers, the groups can be exchanged on a periodic basis. For example, after four months, the second group can receive the first TOU signal instead of the first group, and so on. The multi-group TOU that is used here is shown in Figure 5.14, where there is an hour time delay in receiving the off-peak TOU signals between the three groups. The three groups to which the system was divided are given in Table 5.4. The upstream bus 2 and the downstream bus 6 were put in the same group to ensure that they will receive the same TOU signal. Hence, the comparison of the SOC of the EVup and EVdown will be fair.

119

Figure 5.15 shows the EV loading, Non EV loading and the total system loading. It is clearly obvious that the controller stopped charging during the system peak period and at the same time, with multi-group TOU structure, the rebound effect does not exist anymore. The EVs' loading comes on different stages, which helps avoid overloading the system and, at the same time, behaves in a better way for valley filling.

Figure 5.16 presents the effect of the multi-group TOU on the two-selected extreme POCs, where it shows that the voltage has a further improvement compared to Figure 5.12. This is confirmed by the primary buses' voltages in column 5 in Table 5.3. Figure 5.17 presents the SOC of the EVs. It is almost the same as Figure 5.13. It means that the system operator will get the benefits of multi-group TOU without negative impacts on the customers.

So far, most of the demand-side management programs used to deal with the residential customers as loads that consume power (whether it is controllable or not). However, with more EVs in the distribution system, the current programs should consider the presence of small distributed prosumers, such as EVs that can help the system operator during the peak hours.

This can be done using the current infrastructure by the new proposed method, multi-group TOU with critical peaking (MTOUCP). To convince the EV owners to support the grid during the peak times or emergencies, more incentives should be given to them (i.e reducing the cost of electricity prices even more during the off-peak hours for registered houses with EVs in the DSM program).

Table 5.4: Different TOU groups

| Group number	Buses numbers
1	2,6,10,16,17,18
2	3,4,5,7,8,9
3	11,12,13,14,15
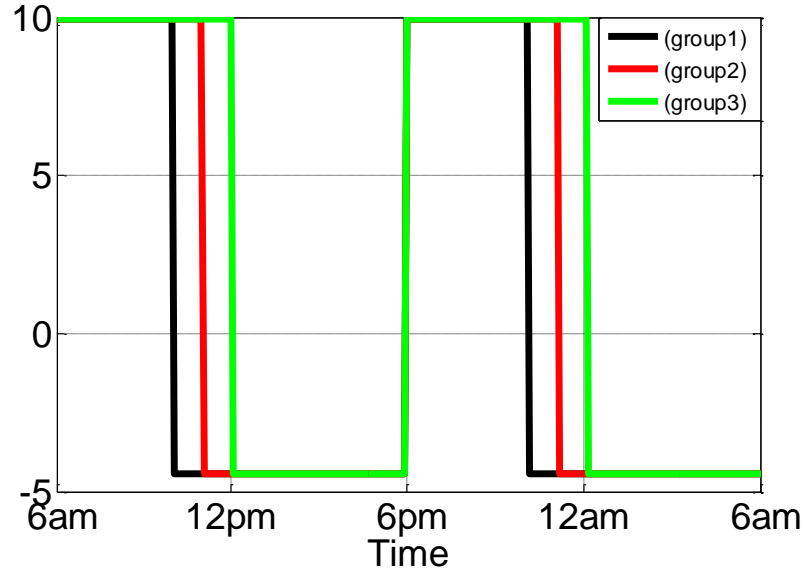
Figure 5.14: Multi-group TOU tariff
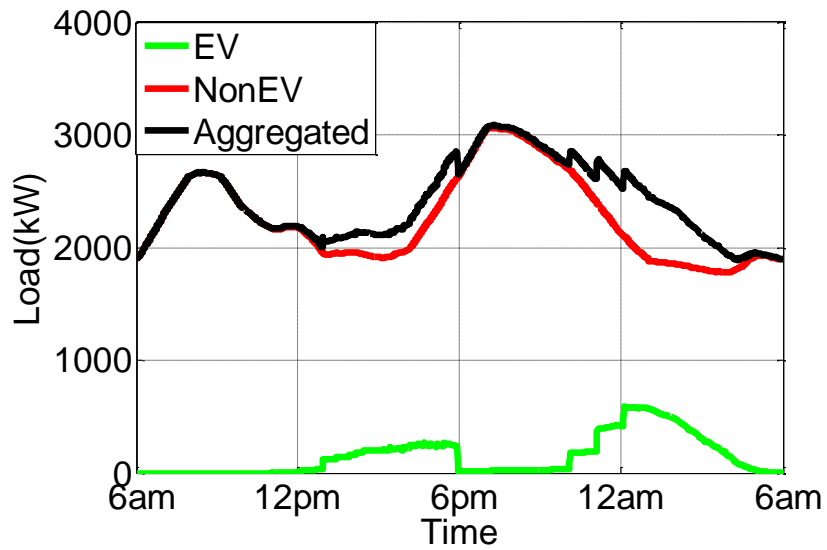
Figure 5.15: Total system loading under Multi-group TOU tariff
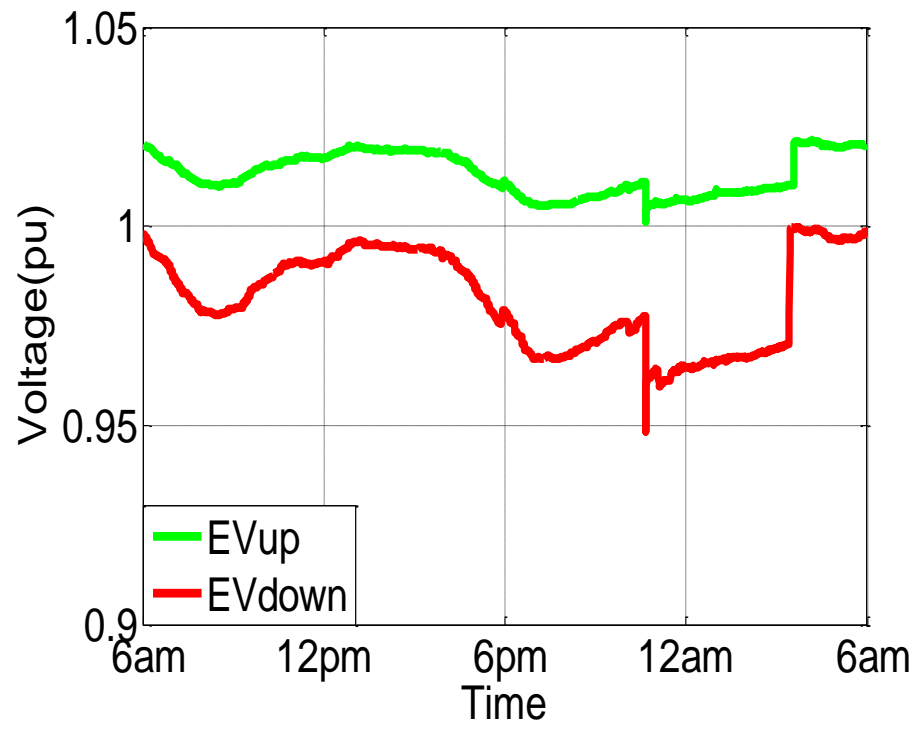
Figure 5.16: Voltage profiles at the selected POCs under Multi-group TOU tariff
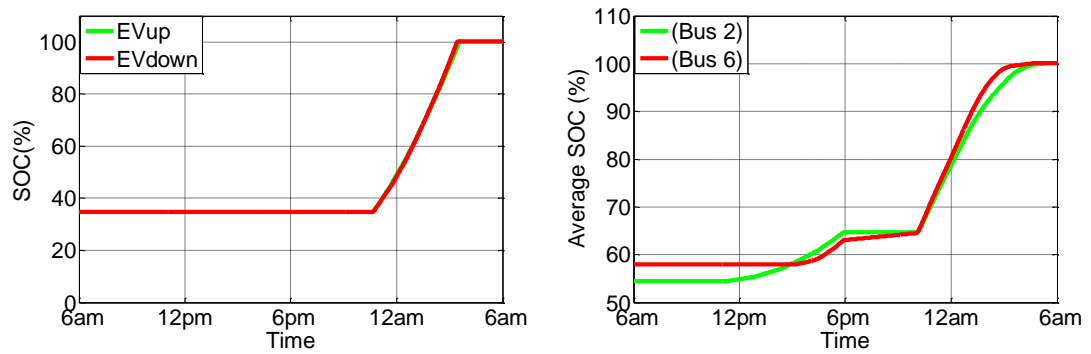
Figure 5.17: Left: SOC of the two selected EVs. Right: the average SOC of all EVs connected to bus 2 and 6 under Multi-group TOU tariff

5.4.4 Controller Performance under Multi-Group TOU with Critical Peaking (MTOUCP)

The multi-group TOU with critical peaking (MTOUCP) is a combination of the critical peaking pricing tariff (CPP) and the multi-group TOU presented in the previous section. It combines the virtues of the two programs.

A critical TOU is sent during the peak period of the system to alert the customers to turn off some of their devices or use the EV to support the grid. Multi-group is used to distribute the burden among the different groups during the on-peak time and to defer the signal during the off-peak time to avoid the rebound effect. Figure 5.18 shows the TOU rates that are used in this section, where a half an hour delay between the different groups is used during the critical-peak period and an hour delay during the off-peak period. These delays can vary from a system to another, depending on the system loading behavior. Figure 5.19 shows that the system peak loading is shaved due to the CPP signal and the rebound effect is avoided due to the multi-group TOU. The load peaking is reduced by 100 kW. However, more reduction can be obtained by synchronizing the critical-peak TOU signal to be at the same time for the three groups, if needed. Figure 5.20 shows the voltage improvement due to the use of MTOUCP. A voltage improvement can also be noticed in last column of Table 5.3. Figure 5.21 depicts the SOC profile under the MTOUCP. It shows that the SOC decreases during the peak period due to discharging the EVs. Therefore, there will be a small-time delay till the EVs finish charging. However, the rate of charge for the EVs connected to the up and down-steam of the system is almost the same.
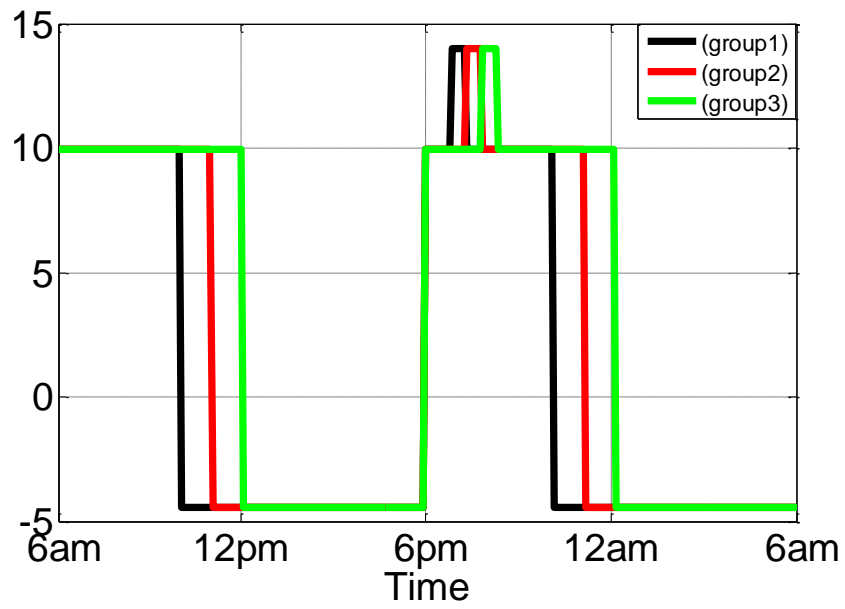
Figure 5.18: Multi-group with critical peak TOU tariff
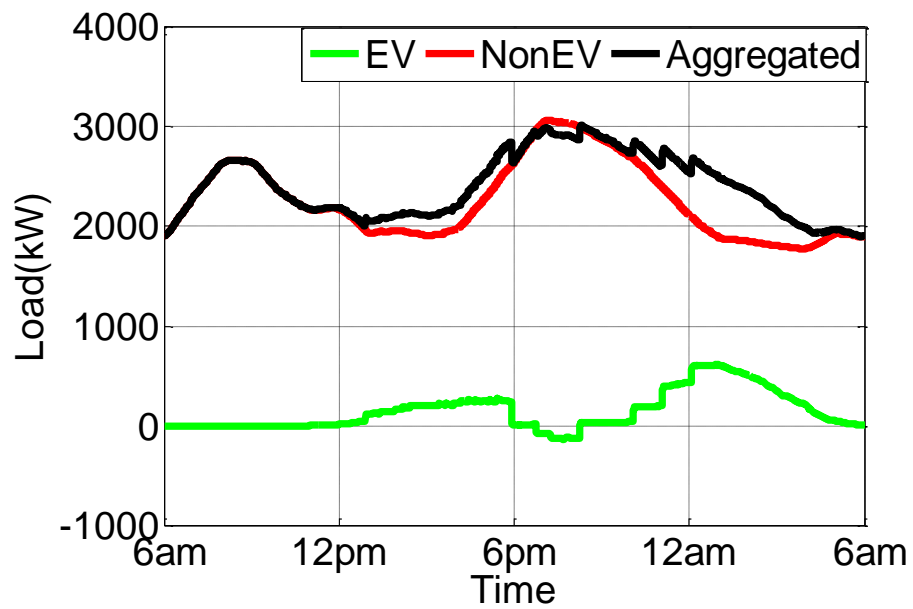
Figure 5.19: Total system loading under Multi-group with critical peak TOU tariff

124
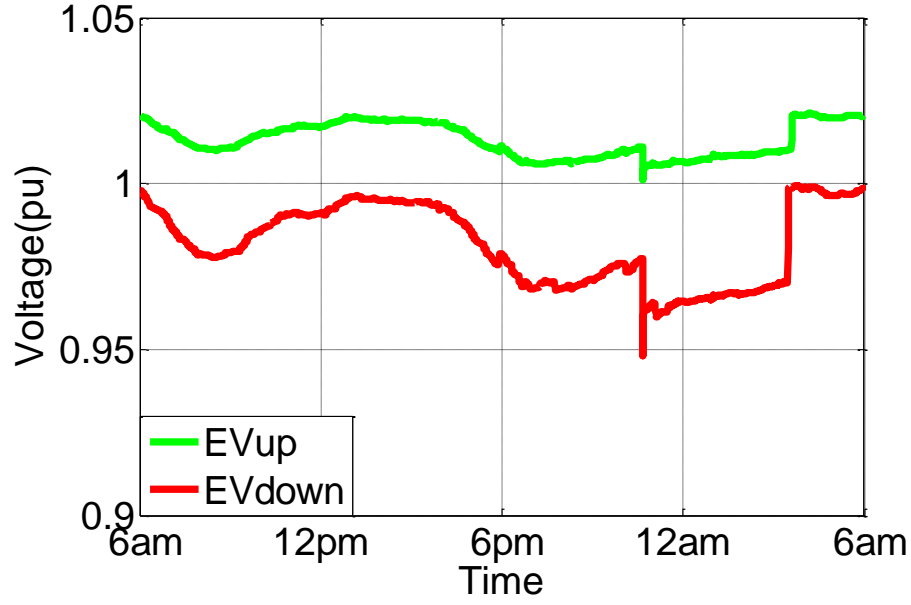
Figure 5.20: Voltage profiles at the selected POCs under Multi-group with critical peak TOU tariff
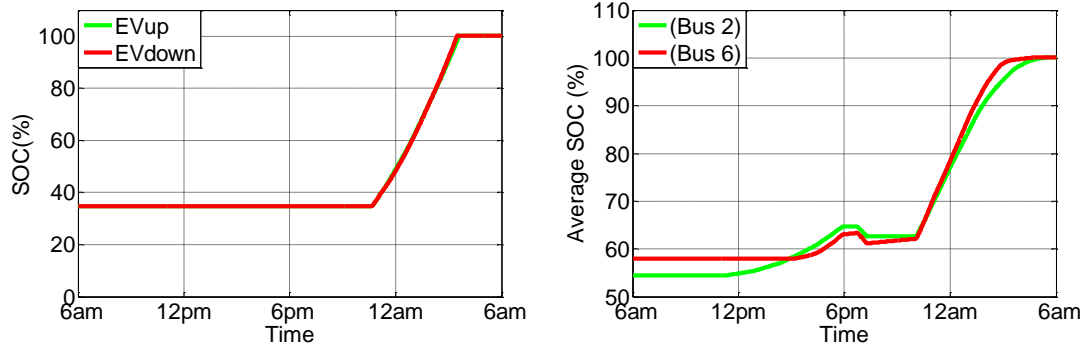
Figure 5.21: Left: SOC of the two selected EVs. Right: the average SOC of all EVs connected to bus 2 and 6 under Multi-group with critical peak TOU tariff

5.4.5 Controller Performance in the Presence of Voltage Control Units

In this section, the controller performance under the MTOUCP demand-side management is tested in the presence of voltage control units. It is the responsibility of the utility to maintain the voltage at the household levels within the specified standards by

installing voltage control units. In this chapter, shunt capacitors are considered to be connected at bus 5. This bus is a downstream bus and supporting the voltage at this bus will improve the voltage not only at this bus but also at buses 6, 7, and 8, which suffer from low voltages due to the voltage drop across the feeder. The total available capacity of the capacitors is assumed to be 1 MVAR. The capacitor variation step is equivalent to 0.1 MVAR, which causes an increase/decrease of about 0.007 per unit voltage [75]. The capacitor bank is assumed to be controlled by an autonomous feedback controller whose voltage set point is 0.99 p.u and bandwidth is 0.007 p.u. Figure 5.22 depicts the voltage profiles at the upstream and downstream houses. Comparing Figure 5.22 to Figure 5.20, it is noted that the voltage at the downstream house has improved due to the presence of the shunt capacitor. The corresponding steps of the three-phase shunt capacitor are shown in Figure 5.23. Due to the voltage improvement at the point of connection at the downstream house that is connected to bus 6, the charging rate will increase according to the controller logic. A comparison between the charging of the downstream EV without and with the connection of the shunt capacitor is shown in Figure 5.24. It is obvious from the figure that the charging rate has increased and the EV finishes charging in less time without mitigating the system voltage.

5.4.6 Controller Performance in the Presence of Distributed Generation Units

To take into consideration the presence of the distributed generation units in the distribution system, the controller performance is tested in the presence of the rooftop PV system. The PV penetration is assumed to be 5%, which is more than double the current

penetration depth of the PVs in the northwestern energy, where the load profiles, in this study, are based on [152].
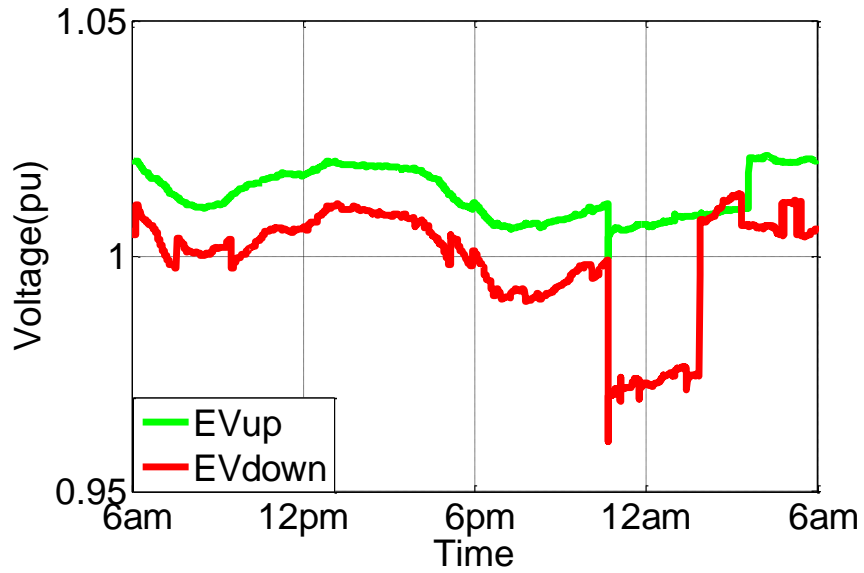
Figure 5.22: Voltage profiles at the selected POCs under Multi-group with critical peak TOU tariff in the presence of shunt capacitors
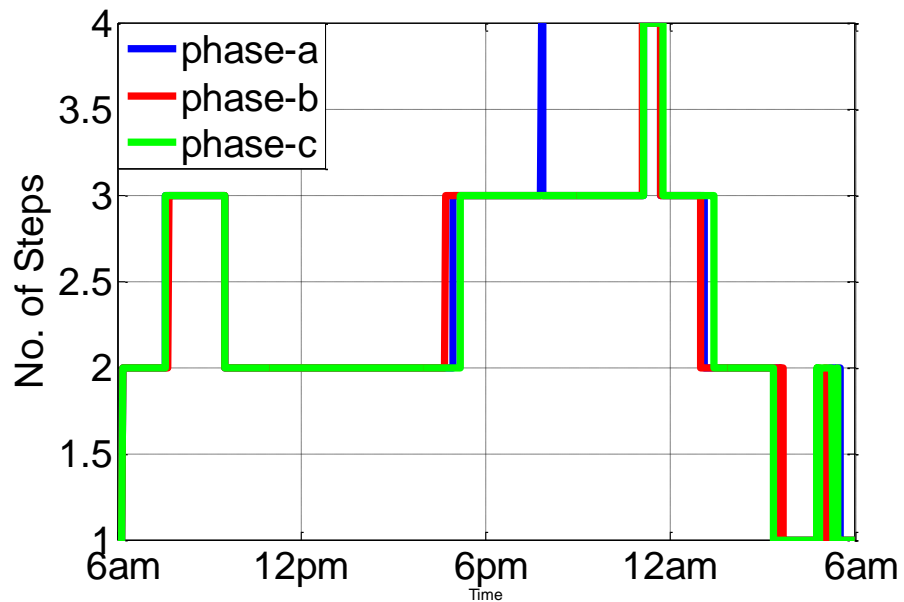
Figure 5.23: Steps of the shunt capacitor at bus 5
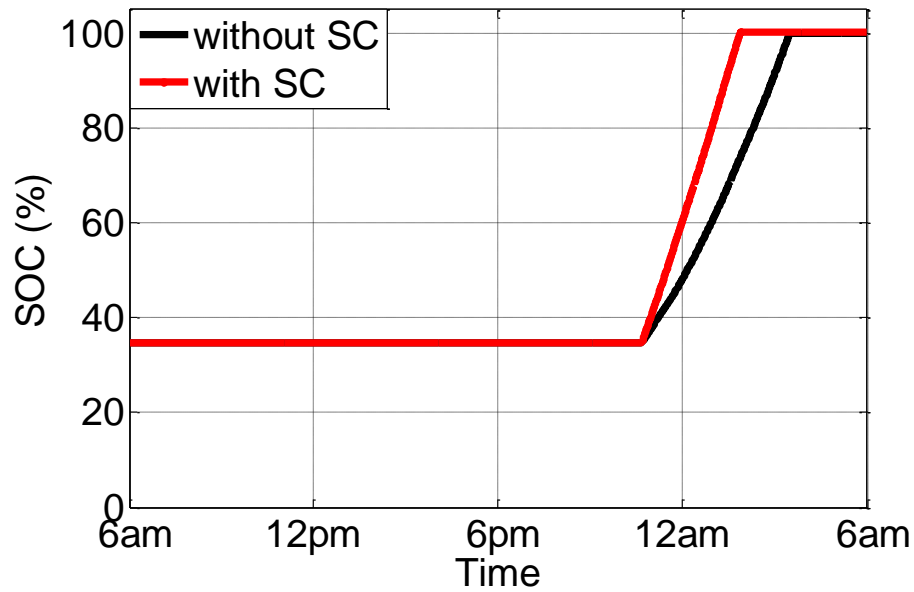
Figure 5.24: SOC of the downstream EV (EV down) without and with shunt capacitor (SC) at bus 5

Figure 5.25 shows a scaled solar energy profile for a sample summer day in this region [153]. The solar PVs are scattered among the different houses in the system, and their energy represents 5% of the total energy. Since solar energy will feed some of the loads during the morning hours, the power supplied through the primary distribution transformer will be reduced. This is illustrated in Figure 5.26, where it is obvious that the transformer morning peak is less in the presence of rooftop PV. However, this does not greatly impact the night peak when most of the EVs are charging because there is no power coming from the solar PVs during the night. Due to the local generation coming from the PVs during the morning hours, there will be a voltage improvement. This is depicted in Figure 5.27. This voltage improvement is due to the fact that local PV generation helps reduce voltage drops across the feeders. Since most of the EVs at the residential sector charge during the night

hours when the owners of the EVs come home, the charging process of the EVs will not be highly impacted by the presence of the PVs, which generate power during the morning hours only. This is shown in Figure 5.28, where the average rate of SOC is almost the same with and without PV systems.
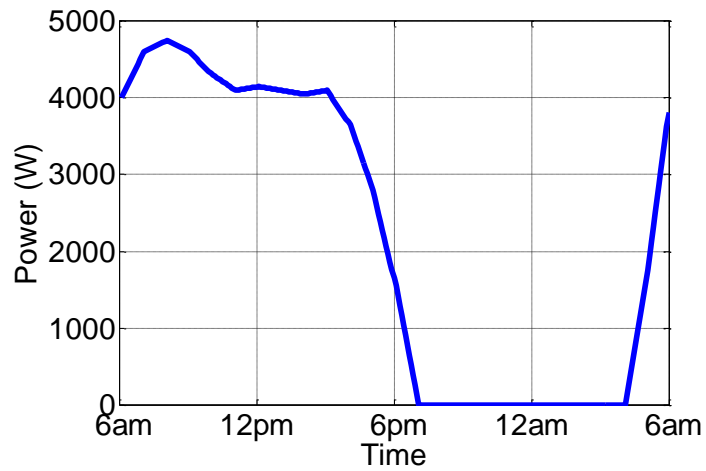
Figure 5.25: Solar power profile
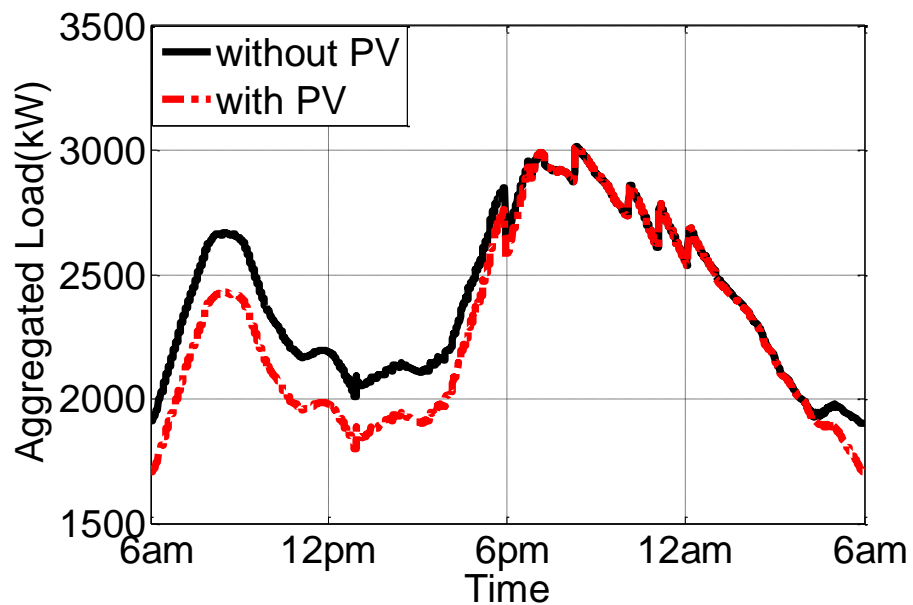
Figure 5.26: Aggregated load at the primary distribution transformer
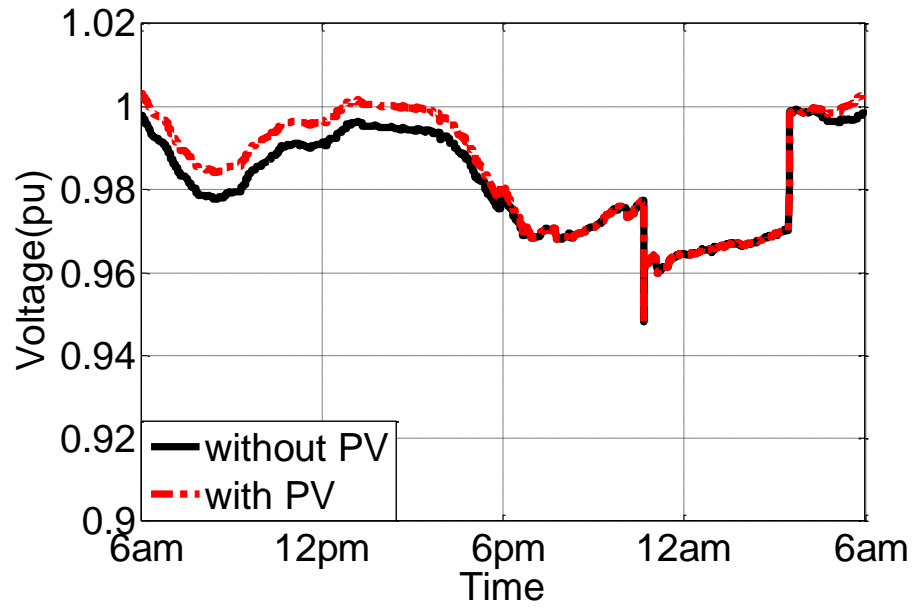
Figure 5.27: Voltage profile at the downstream EVdown
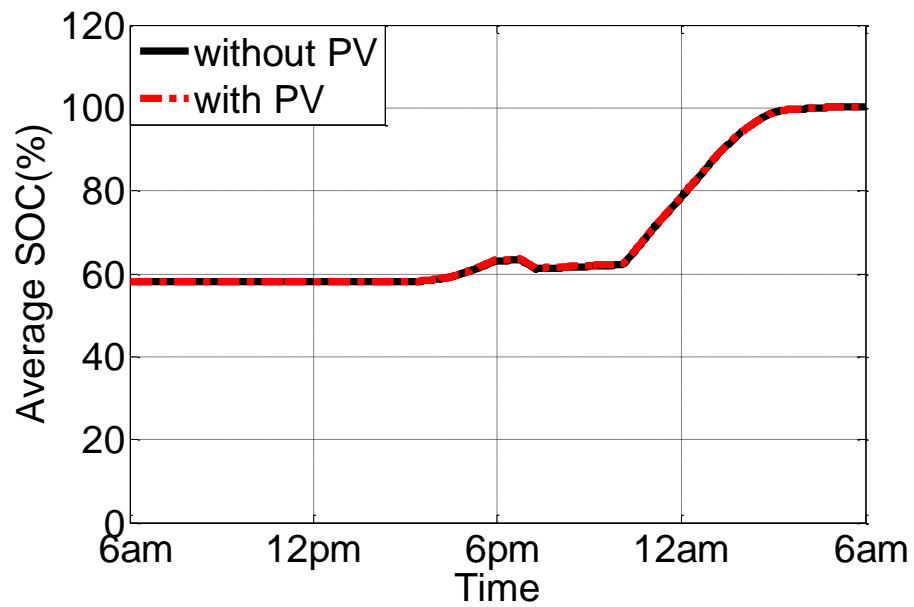
Figure 5.28: Average SOC of the downstream EVs at bus 6

5.5 Conclusion

An effective decentralized fuzzy-based controller for electric vehicle charging is proposed in this chapter. The proposed controller, while requiring minimum real-time communication that already exists in the current DSM infrastructure, effectively coordinates the charging process among the different EVs connected to the system in a fair manner. It takes into consideration the customer charging requirements, the system voltage, and the cost of customer bills, depending on the coming price signal from the system. The results proved that a better valley filling can be obtained, and the voltage can be maintained within the standard limits. The controller was analyzed under different DSM schemes and showed how the different DSM schemes can affect the system loading and voltage.

From these analyses, a new scheme that is called a multi-group TOU with critical peaking (MTOUCP) is proposed. The new scheme can effectively help mitigate the system peaking and avoid introducing new peaks "the rebound effect." The new scheme is compatible with the current DSM infrastructure and does not need any further investments. The proposed scheme brings some benefits to the utility operators by allowing the EVs to discharge some of the energy to support the power grid during high-peak periods. However, proper incentives should be given to convince the owners of the EVs to use their batteries to provide ancillary reserve services to the system.

The controller performance was also tested in the presence of voltage control units, such as capacitor banks, and in the presence of distributed generation units, such as photovoltaic systems. The proposed controller gave satisfactory results in both cases.

Chapter 6   Bi-Layer Multi-Objective Optimal Allocation and Sizing of Electric Vehicle Parking Garage

The anticipated increase in Electric vehicles' (EVs) adoption necessitates the need for electrified transportation infrastructure to charge these vehicles. Although the EV parking garage can represent a good investment opportunity, it brings more challenges to the distribution system operator. Therefore, the allocation and sizing of the parking garage should be carefully planned. The planning process should take into consideration the economic aspects of the investor, as well as the technical aspects of the distribution system. In this chapter, a bi-layer multi-objective optimization problem is formulated to optimally allocate and size an EV parking garage. The optimization formulation tries to maximize the profits of the investor of the EV parking garage, as well as minimize the losses and voltage deviations for the distribution system operator. Dealing with these contradicting objectives simultaneously will results in a set of Pareto solutions. A decision-making criterion based on statistics is used to decide on the optimal location and size of the parking garage. Sensitivity analysis to show the effect of the different objectives on the selection of the optimal size and location is also performed.

6.1   Introduction

With the increase of the penetration level of electric vehicles (EVs), there will be a great need for charging stations' infrastructure to provide power to those vehicles [154]–[156]. The EV owners will primarily prefer to charge their vehicles at homes. However, many EV owners do not have a private parking space. Therefore, there will be a need for non-residential charging stations in other places, such as work, business districts, near

bulky public transportation stations, and other public facilities. While the EV parking lot (PL) may represent a promising investment in the near future, it might bring some challenges to the distribution system designer/operator due to the large loading that can be added to the system. Therefore, the optimal sizing and allocation of an EV public PL will be a problem of great interest. Allocation and sizing of energy storage was widely investigated in the literature [157]–[159]. Optimal sizing for large energy storage as a price maker that can play a role in the electricity market was also considered in [160]. In [161], a second-order cone programming (SOCP) was used to optimally plan and operate the energy storage system in a localized isolated distribution network. In [162], a fuzzy particle swarm optimization (FPSO) algorithm was used to optimally operate the energy storage system to mitigate the risks faced by the distribution companies in electricity markets.

While it seems that EV PL is more or less a conventional energy storage unit, it has many additional aspects that should be considered. These aspects include: 1) the different preferences of the EV owners that the PL operator should satisfy, 2) having a heterogeneous mix of batteries with different capacities and maximum charging rates and, 3) the uncertainty associated with the vehicles' availability. In addition, PLs are expected to be close to the load centers, which mean they will have diverse impacts on the distribution system. Therefore, more attention should be paid to the optimal sizing and allocation of PLs. Some researchers tried to consider that problem in the literature. Optimal coordination for operational planning of EVs in the microgrid was considered in [163]. The authors used an economic method called Sortino ratio to maximize the profits per unit risk, while the size and location of the EVs were assumed as a priori. In [164], an Analytic

Hierarchy Process (AHP) was used to determine the optimal weighting coefficient for each objective in a mutli-objective problem to determine the optimal site and size of PLs. In [165], the authors developed a two stage multi-objective formulation to optimally allocate a PL, taking network constraints into consideration. However, the optimal profit of the PL was obtained in the first stage, then optimal allocation and sizing were done in the second stage. This neglects the mutual effect that the optimal sizing and allocation might have on the profits in the first stage. The authors in [166] investigated the allocation problem of EV PLs in a distribution network, but they just addressed the technical aspect of the problem, and no economic aspects were considered.

In this chapter, a bi-layer multi objective optimization for optimal sizing and allocation of a commercial PL is considered. The problem formulation takes into consideration multiple EVs with different characteristics (battery capacities and maximum charging rates) and customer preferences (energy and departure times). The formulation looks at both the economic aspects trying to maximize the PL profits, as well as the technical aspects trying to minimize the losses and voltage deviations in the distribution system at the same time. In addition, sensitivity analysis to show the effect of the different objectives on the selection of the optimal size and allocation is performed.

6.2 Methodology

Due to the growth in the number of electric vehicles, more electrified PLs will be needed soon. Therefore, the problem of optimally allocating an electric vehicle PL will be of special interest. From one side, the PL might represent a large load to the system since it is preferred from the PL investor's point of view to charge the maximum possible number of

EVs in the shortest possible time to increase the revenues. From the other side, the distribution system operator would like to minimize the system losses and voltage deviations. This necessitates the need to optimally size and allocate the PL during the planning stage to achieve these contradictory objectives. This represents a reasonable potential for using the Pareto-based method, as it gives a set of optimal solutions (Pareto front), which helps realize the different trade-offs between the considered objectives [167].

In the near future, where the market environment of ancillary services is not fully developed in most of the places, it is expected that the EV PL will operate like the conventional diesel charging station, where the PL purchases its energy from the wholesale market, and then sells this energy to the EVs at a pre-defined charging tariff. Therefore, in this chapter, the PL is assumed to do only energy arbitrage, where a unidirectional power flow is assumed.

The case of an EV PL is more complicated than conventional charging stations because electricity is a commodity that will not be stored (the PL is not expected to have dedicated energy storage), and the PL operator needs to satisfy multiple charging requests from different EVs with different preferences. In addition, the EVs are expected to be parking for longer time periods. Therefore, the PL is anticipated to try to optimally schedule the charging of the EVs, taking the electricity market prices and the preferences of the EV owners into consideration.

The first step in the planning of the EV PL is to model the PL behavior and calculate its expected revenues. However, some of the parameters of the PL model like the maximum power (power size) of the PL will be determined by the distribution system operator who

will try to minimize the system losses and voltage deviations. The optimization procedure that will be used is shown in Figure 6.1, where a bi-layer optimization method is introduced. The proposed method aims at maximizing the PL profits, as well as minimizing the losses and voltage deviation of the distribution system simultaneously.
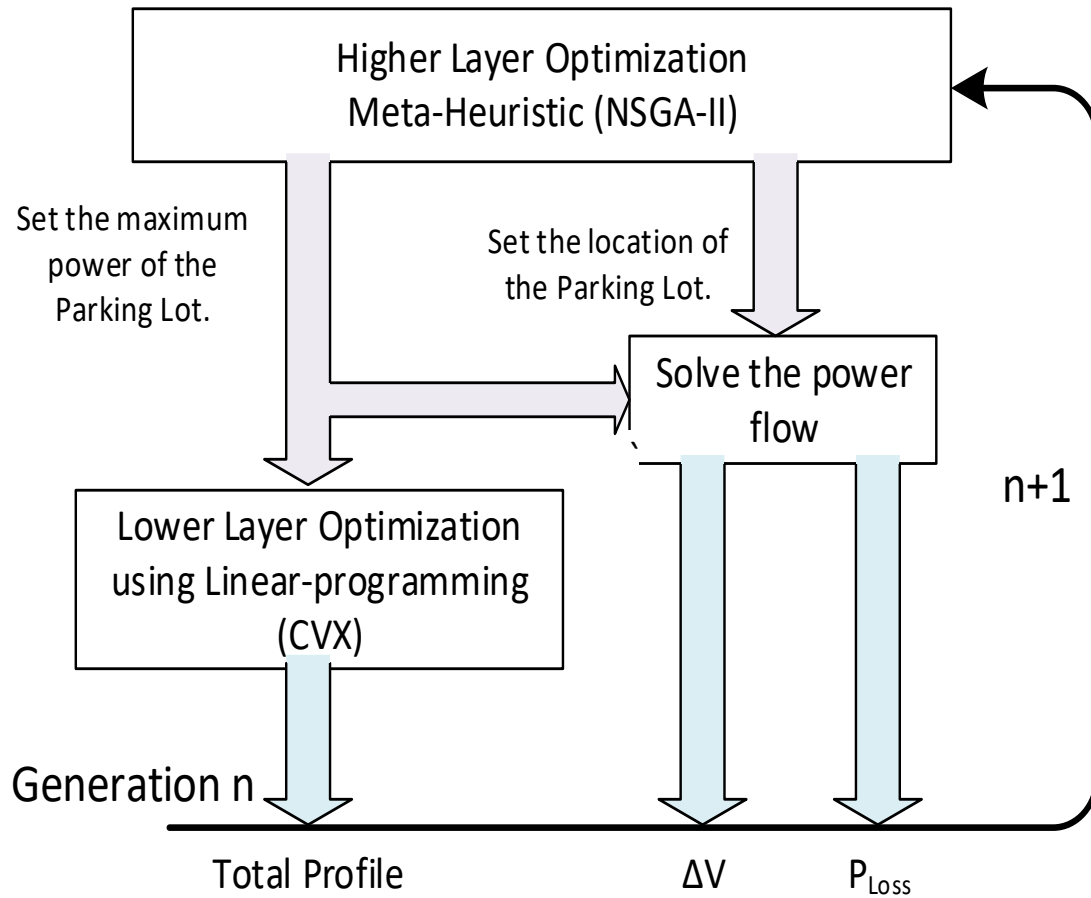
Figure 6.1: A flow chart for the proposed bi-layer optimal planning procedure

The optimization procedure will first start with a random size and candidate location and pass these values to the second layer, where the PL scheduling problem will be solved and give the expected profit. At the same time, using the given size and location, the power

flow problem will be solved, and the voltage deviations and line losses will be obtained. The three calculated values: profits, voltage deviations, and line losses will be passed to the first stage, which will evaluate and sort the different solutions and decide whether to go to the next iteration process or not, and what will be the new size and location for the next iteration step. The process will be continued until a maximum number of iterations is reached.

The presented problem in this chapter is a multi-objective optimization problem (MOOP) with three objective functions; maximizing the PL profit, minimizing the voltage deviations, and minimizing the power losses in the distribution system accommodating the PL. In many studies, the aggregate weight functions method is used to solve the MOOP. In this method, the MOOP is relaxed to be a single objective through assigning a weight vector to the objectives and adding them altogether. Then, the problem is solved using any of the single objective techniques. Despite the simplicity of this method, it suffers from major drawbacks including, but not limited to: 1) the difficulty of the appropriate assignment of the weights, 2) the solution is changed by changing the weight vector, and 3) its failure to generate feasible solutions on the nonconvex portions of the optimum solution front [168], [169]. Furthermore, it generates only one solution, which significantly limits the options in the decision making process [170]. Whereas in the Pareto optimality (PO) based methods, a set of points that all fulfill the definition of an optimal solution and meet the problem constraints are obtained. This set of optimal solutions is known as the Pareto Front (PF).

Different methods were proposed in the literature to generate the PF, among these methods, Non-dominated Sorting Genetic Algorithm II (NSGA-II) has been one of the most successful techniques. The NSGA-II is an extension of the GA and uses an elitism approach and sorting algorithm to determine the Pareto Front (PF) [171]. Following the determination of the PF, a decision-making criterion is utilized to select a single solution between the different obtained trade-offs.

6.3 Problem Formulation

6.3.1 Objective Function of the Parking Lot

For the case of an EV PL, the expected operational income for a certain day (*INC*) comes from charging the EVs at a pre-defined tariff, which will depend on the required departure and start times. This is shown in equation (6.1).

$$INC(d) = \sum_i \sum_t \delta_i \cdot AV_{it} \cdot PR_{it} \cdot EVPer_t \qquad (6.1)$$

where *i* is the EV index, *t* is the time period, and *d* is the day index. *INC* is the operational income of the PL, δ is the charging tariff, AV is a binary factor indicating the vehicle availability (0 is unavailable and 1 is available), PR is the charging rate and $EVPer$ is the percentage of the remaining EVs after unexpected departure.

The operational cost of the PL, shown in equation (6.2), comes from purchasing the required energy from the market to charge the EVs.

$$CO(d) = \sum_i \sum_t AV_{it} \cdot PR_{it} \cdot \pi_t \cdot EVPer_t \qquad (6.2)$$

where CO is the operational costs of the PL and π is the market energy price. The availability index AV_{it} is used to ensure that the charging of the EV will represent a revenue

or a cost only if the EV is available. $EVPer_t$ is a parameter used to take into consideration the possibility of unexpected departure of the EVs [80]. It can be estimated by considering the percentage of the EVs that is remained for charging as represented by equation (6.3), which is a function of the accumulated probability of the unexpected departure of the EVs at a certain hour (Dep_{it}). The value of Dep_{it} is a function of the time of the scheduled trip for each EV during the day, as depicted in equation (6.4).

$$EVPer_t = 1 - \frac{1}{NEV}\sum_{i=1}^{NEV} Dep_{it} \qquad\qquad \forall\, t \qquad\qquad (6.3)$$

$$Dep_{it} = \sum_{h=1}^{t} Dep_i(h)\,, \qquad\qquad \forall\, i,\ st \le t \le dt \qquad (6.4)$$

where *st* and *dt* are the starting and departure times of the EVs. *NEV* is the number of the charging stations in the lot. The total revenue for a certain day is the difference between the income and the cost, as illustrated in (6.5).

$$revenue\ (d) = INC(d) - CO(d) \qquad\qquad (6.5)$$

In order to estimate the annual revenue, weighted representative days are used [172]. Each representative day is weighted by a factor K_d, and the sum of all factors is equal to the total number of days in the year (which is 365). The days are chosen in such a way to represent the weekdays and weekends in the different seasons. For a number of representative days *(DY)*, the one-year revenue is given in (6.6).

The PL investment cost includes the costs of charging stations and the laboring for installation, some auxiliary materials, and permits, as given in (6.7). Hence, the total profit from investing in an EV PL for the project time span is given by (6.8).

$$Yearly\_revenue = \sum_{d=1}^{DY} K_d \cdot revenue\ (d) \tag{6.6}$$

$$INV = (HD + INS) \cdot NEV \tag{6.7}$$

$$Total_{profit} = \left(\sum_{y=1}^{yrs}(1 + dr)^{-y} \cdot (Yearly_{revenue})\right) - (INV + MTC) \tag{6.8}$$

where *INV*, *HD* and *MTC* are the investment, hardware of the charging station, and maintenance costs, respectively. *NEV* is the number of the charging stations in the lot. *INS* represents the installation and permit costs. *dr* is the discount rate and *yrs* is the number of operational years and *y* is the year index. Finally, the PL objective function can be formulated as:

$$Maximize\ (Total\_profit) \tag{6.9}$$

6.3.2   Objective Functions of Distribution System Operator

6.3.2.1   First Objective:

Connecting the PL to the distribution system can cause severe voltage drops not only on the bus where it is connected, but also on other busses depending on the power flow in the network. This occurs especially at the peak hours, either when the PL is full (many cars are charging), or when the other loads in the distribution system are at their peaks. Therefore, it is required to optimize the PL location and the size to minimize this voltage deviations upon energizing the loads. The reference value for the bus voltage is taken as 1 p.u and the objective function for voltage deviation is given in (6.10), where V_j is the voltage at bus j and V^{ref} is the reference voltage. N_b is the total number of buses in the system.

$$Minimize\ \sum_{i=1}^{N_b}\left(V_i - V^{ref}\right)^2 \tag{6.10}$$

6.3.2.2 Second Objective:

In the second objective function, it is required to minimize the total active power losses in the systems, as given in (6.11).

$$Minimize \sum_{m=1}^{N_l} 3 . I_m^2 . R_m \qquad (6.11)$$

where m is the distribution line index, I_m, R_m is the current flowing through and the resistance of distribution line m, respectively. N_L is the number of the distribution lines

6.3.3 Decision Variables

The decision variables in this problem are:

- Location of the PL in the distribution network: A decision variable x_{PL} is assigned to control the location of the PL, where $x_{PL} \in \{N_b\}$.

- Maximum power of the PL: A decision variable P_{PL}^{max} is assigned to control the maximum size of the PL.

6.3.4 Constraints

6.3.4.1 Parking Lot Constraints

The PL is subjected to some operational constraints as follows:

$$AV_{it} \cdot PR_{it} \geq 0 \qquad \forall i, t \qquad (6.12)$$

$$AV_{it} \cdot PR_{it} \leq PR_{max} \qquad \forall i, t \qquad (6.13)$$

$$\sum_t (AV_{it} \cdot PR_{it} \cdot \eta) \Delta t + init\_soc_i = \min(fin\_soc, BC_i) \qquad \forall i \qquad (6.14)$$

$$\sum_i AV_{it} \cdot PR_{it} \leq P_{PL}^{max} \qquad \forall t \qquad (6.15)$$

where $init\_soc_i$ is the initial state of charge, η is the charging efficiency and Δt is the charging duration.

Constraint (6.12) is imposed to force unidirectional charging of the EVs since the PL is assumed to do unidirectional flow only. Constraint (6.13) is to limit the charging rate of any EV to its maximum charging rate PR_{max}. Equation (6.14) is meant to satisfy the EV owner's preference. It means that the EV should be charged to the required final state of charge *(fin_soc)* at the required time, where the summation over *t* means charging over the required period *(dt-st)*. If the EV owner does not have any energy requirements, the maximum battery capacity (BC_i) is assumed.

Finally, the summation of the charging power for all EVs at any hour should not exceed the maximum capacity of the parking lot P_{PL}^{max}, as given in (6.15). This maximum size of the PL will be determined in a way that maximizes the investor's profits and minimizes the losses and voltage deviations of the distribution system.

6.3.4.2 Distribution System Constraints

Constraints (6.16) and (6.17) are the power balance equations in the system, where P_{Gj} and P_{Dj} are the active powers into bus *j* from generator *g* and load *d*, respectively. The same notation holds for the reactive power constraints in (6.17). *G* and *B* is the distribution line conductance and suceptance, respectively.

$$\sum_{G=1}^{N_G} P_{Gj} - \sum_{D=1}^{N_D} P_{Dj} - P_{PL}^{max} = V_j \sum_{j'=1}^{N_b} V_{j'} . \left[G_{jj'} \cos(\theta_j - \theta_{j'}) + B_{jj'} \sin(\theta_j - \theta_{j'}) \right] \tag{6.16}$$

$$\sum_{G=1}^{N_G} Q_{Gj} - \sum_{D=1}^{N_D} Q_{Dj} = V_j \sum_{j'=1}^{N_b} V_{j'} . \left[G_{jj'} \sin(\theta_j - \theta_{j'}) - B_{jj'} \cos(\theta_j - \theta_{j'}) \right] \tag{6.17}$$

Since the system understudy in the chapter is a primary distribution system, the allowed voltage variations are set from $V_{min} = 0.9$ p.u. to $V_{max} = 1.1$ p.u as follows:

$$V_{min} \leq V_j \leq V_{max} \tag{6.18}$$

Constraint (6.19) is limiting the apparent power flow in the distribution lines S_m to be below the allowed limits S_m^{max} to avoid any thermal issues.

$$|S_m| \leq S_m^{max} \qquad \forall m \in N_l \tag{6.19}$$

Constraints (6.20) and (6.21) are assuring that the operation point of the generator is within its safe operating region.

$$P_G^{min} \leq P_G \leq P_G^{max} \qquad \forall G \in N_G \tag{6.20}$$

$$Q_G^{min} \leq Q_G \leq Q_G^{max} \qquad \forall G \in N_G \tag{6.21}$$

6.4 Case Study and Results

The PL is assumed to have a maximum of 500 charging stations, where the charging stations are assumed to be the commercial level 2 stations given in Table 6.1 and can supply three different levels of power. Details about level 2 charging stations for commercial purposes can be found in [154]. The different costs associated with level 2 charging stations can also be found in [154]. It is assumed that the PL is located in Texas, where grants from the Alternative Fueling Facilities Program to provide 50% of the cost of alternative fuel facilities is applied [154] . In addition, the PL is assumed to be in a city center near work areas and shopping malls. Therefore, the EVs are expected to be parking for long time periods.

It is also assumed that the EV fleet that is using the PL consists of three different types of EVs, which are Tesla Model S, Mitsubishi i-MiEV and Nissan leaf with percentages of 30%, 20% and 50%, respectively. The technical specifications for the batteries of those vehicles are given in Table 6.2. To generate different profiles (Availability, initial and required final state of charge, required departure time) for the different EVs, Monte Carlo Simulation was used. The probabilistic model found in [173] for the arrival of the EVs in a business district is used to generate the availability matrix for the EVs in the PL. It is based on a truncated normal distribution, which was validated using a historical data of a parking deck. The initial state of charge is modeled as a random variable under log normal distribution found in the same reference [173], while the final state of charge was assumed to be between (70-100%). It is assumed that the PL will charge the EVs with a tariff based on how fast they want to charge their required energy according to Table 6.3.

Historical hourly market prices from ERCOT, Texas [174] are used, where the PL is assumed to be. The discount rate over the planning horizon is assumed to be 5%, and the planning span is assumed to be 15 years. The PL scheduling problem is solved using the CVX toolbox, which is a MATLAB based modelling system for convex optimization [175]. The parameters of the NSGA-II is set as follows: the maximum number of generations is 50 and the number of individuals in each generation is 50. The IEEE 30 bus system [176], shown in Figure 6.2, is used as the primary distribution system.

Table 6.1: Description of level 2 charging station power and charging times

Charging level	Vehicle Range added	Supply power
AC level 2	10 miles/hour @ 3.4kW	208/240VAC/20-100 A
	20 miles/hour @ 6.6kW	
	60 miles/hour @ 19.2 kW	(16-80) A continuous

Table 6.2: EVs characteristics

	Maximum Charging Rate (kW)	Maximum Capacity (kWh)
Tesla Model S	20	85
Mitsubishi i-MiEV	3.3	16
Nissan leaf	3.3	24

Table 6.3: charging tariff

δ ($\text{¢}/kWh$)	Time to finish (hours)
15	$t \geq 8$
20	$4 < t < 8$
25	$t \leq 4$
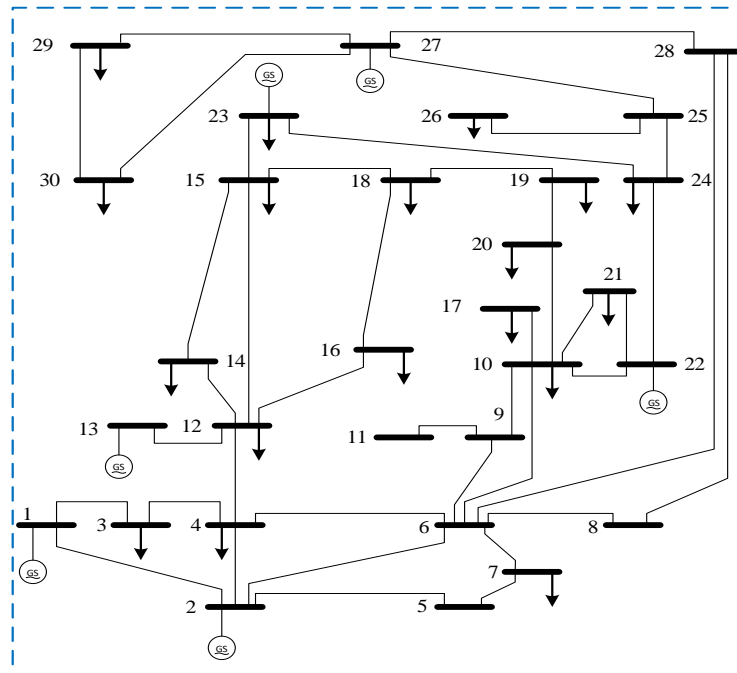
Figure 6.2: IEEE 30 bus test case

The power flow problem is solved using MATPOWER toolbox [177]. In order to obtain the solution in a reasonable time, the optimization problem is solved on eight representative days, two days are selected to represent each of the four climate seasons. One day is representing the weekend and the other day is representing the weekday. In order to have an accurate representation for a real-world case, a real hourly load profile for the same days of the market price mentioned before is obtained from [178], and added to the system. The addition of this load profile helps in capturing the variable loading conditions of the distribution system to be considered in the optimization process. In this specific problem, the candidate buses to allocate the PL in the optimization problem is limited to the load buses. The problem is a mixed integer with non-linear constraints. To have a comprehensive understanding of the effect of the three different objectives on the optimum size and location, multiple cases will be processed. First, the problem will be solved as a multi-objective problem using Pareto optimization. Then, sensitivity analysis will be performed, where the conventional genetic algorithm (GA) will be used. In this sensitivity analysis, only one objective will be considered at each time to see its effect on the optimal size and location decision.

6.4.1 Pareto Multi-Objective Optimization

In this case, the three objectives will be used simultaneously, and the different trade-offs will be obtained and sorted using the NSGA-II. The optimization problem resulted in obtaining eight Pareto fronts (PFs). The eight PFs are depicted in Figure 6.3 (a) through (h). Each PF is a set of optimal solutions of a single representative day.
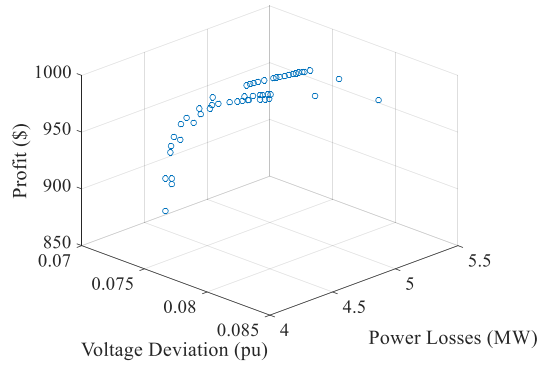
(a)
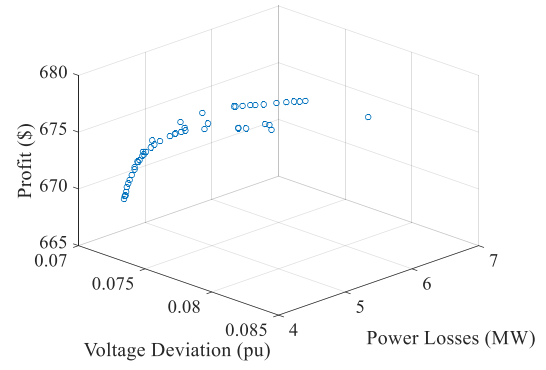
(b)
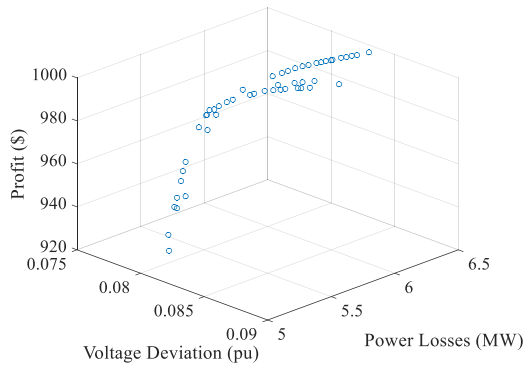
(c)
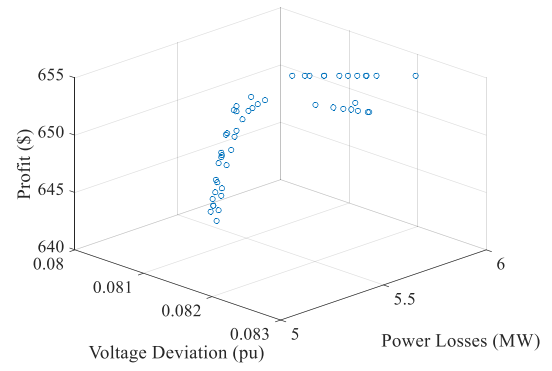
(d)
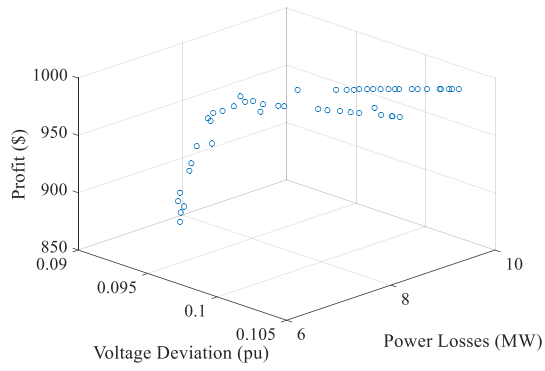
(e)
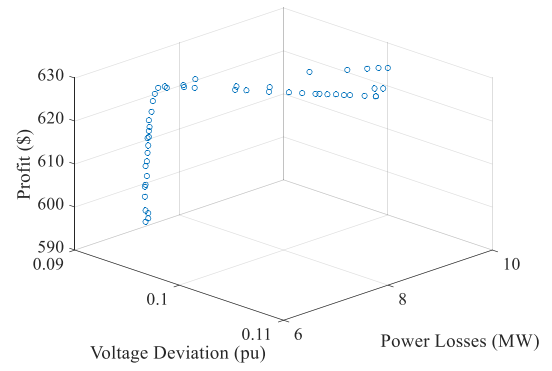
(f)
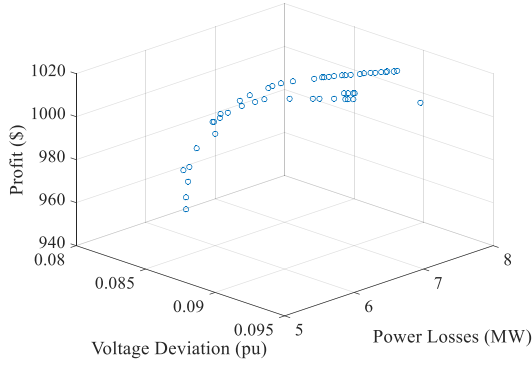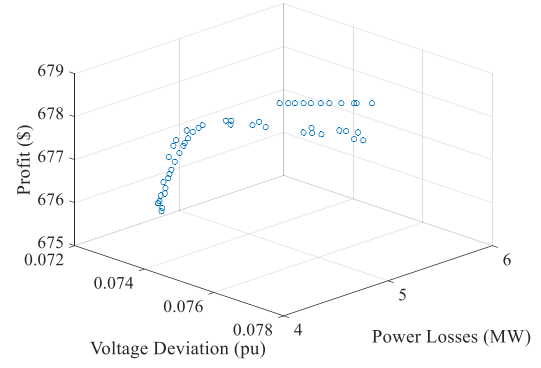
(g)   (h)

Figure 6.3: 3D Pareto fronts for PL allocation and sizing problem, (a) day one (winter-weekday), (b) day two (winter-weekend), (c) day three (spring-weekday), (d) day four (spring-weekend), (e) day five (summer-weekday), (f) day six (summer-weekend), (g) day seven (fall-weekday), (h) day eight (fall-weekend).
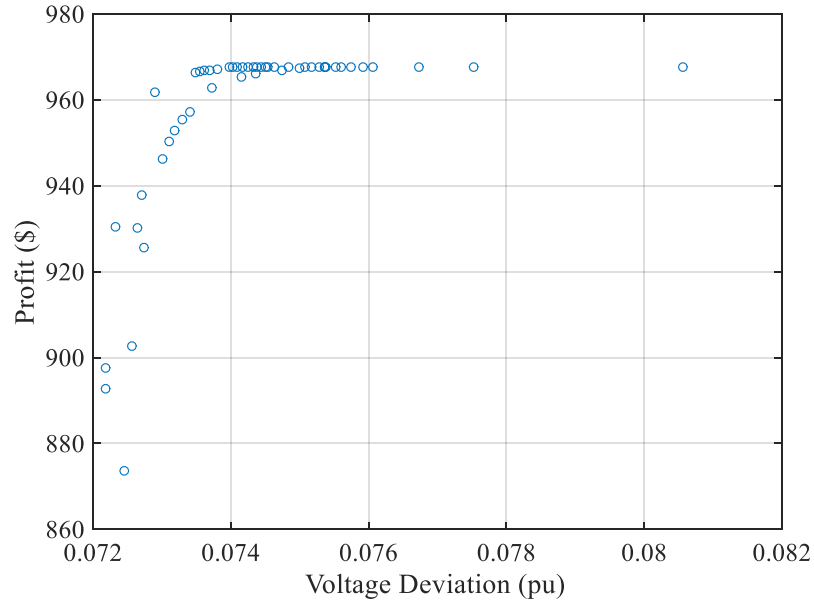
Figure 6.4: Side projection for the 3D Pareto front for day one showing the relation between two of the objectives

Figure 6.3 (a) shows the PF obtained for day one, which represents a typical working day in the winter season. It can be seen that the PL profit is varying between 873.5 $/day

148

and 967.7 $/day. It can also be realized from the 3D figure that increasing the PL profit is associated with an increase in the voltage deviation and the power losses of the distribution system. This is well justified because the objective of the optimization algorithm is increasing the revenues through increasing the maximum power allocated for the PL, which represents an additional load to the system. Therefore, improving one objective in the design process (monetary profit) worsens the other two objectives (voltage deviations from the nominal values and the power losses). This leads to realizing the different trade-offs in the design process using the proposed Pareto-based framework. It should be noted that the obtained PFs yield a different shape (flipped shape). This is due to the fact that, in this specific problem, one objective is maximized whereas the other two are minimized. Furthermore, the objectives are explicitly contradicting.

By comparing the obtained PFs to each other, certain differences can be identified. These differences are due to:

1) The difference in the number of EVs using the PL from a weekday to a weekend, where Figure 6.3 (a, c, e, g) represent weekdays while Figure 6.3 (b, d, f, h) represent weekends.

2) The difference in the loading profile of the distribution system from season to season.

For example, on one hand, comparing Figure 6.3 (a) and Figure 6.3 (b) show that the profit is less during the weekend because the number of cars is less. On the other hand, comparing Figure 6.3 (a) with Figure 6.3 (e) shows that the power losses in the summer day, Figure 6.3 (e), is much higher. This is because, the overall loading of the distribution

system is higher during the summer in the area under study. This yields higher losses in the system. Figure 6.4 depicts a 2D projection for the PF shown in Figure 6.3 (a). The figure shows the relation between two objectives, which are the voltage deviation and the profit. The presented set of fronts emphasizes the integrity of the presented design method, as it incorporates several factors and targets different objectives simultaneously.

At this point of the planning stage, several solutions are obtained. However, only one solution is required by the decision maker to be implemented. This requires a decision-making criterion to select a single solution among the obtained PFs.

In this chapter, a decision-making criterion that is based on a histogram of the most appearing solution in the PFs, obtained over the year, is utilized. Figure 6.5 and Figure 6.6 show histograms for the chosen candidate buses and optimal sizes obtained from the different Pareto front trade-offs. From Figure 6.5, it is obvious that bus 3 and bus 21 are the most frequent selections to allocate the PL. Figure 6.6 shows that sizes of 0.5 MW, 1 MW, and 2 MW are the most frequent optimal sizes.

Further analysis for the power flow and the optimal scheduling of PL is done using these optimal candidate locations and sizes. It is found that although the 0.5 MW is the most frequent size, it will result in a huge reduction in the profits. This is mainly due to the small size of the PL, which will reduce the PL ability to charge a large number of vehicles at the same time. This 0.5 MW size is frequent because it is the best fit for the weekends, where the number of electric vehicles is less, hence the maximum load is less. However, for weekdays it will fit for some of the individuals in the solutions, which minimizes the

150

losses and deviation and greatly sacrifices the profits. Therefore, this optimal size will be discarded, as it will greatly reduce the profits.

The second two optimal sizes of 1 MW and 2 MW is then tested. It is found that the 2 MW size will result in higher profits, however the increase in profits is not high enough to justify the associated increase in power losses and voltage deviation. The yearly and the total profits over the project planning span is given in Table 6.4.

Load flow studies are performed to obtain the losses and voltage deviations for the two optimal sizes (1 and 2 MW), and the two optimal locations (bus 3 and bus 21). It is found that bus 21 results in higher losses and voltage deviation, which means that bus 3 is the optimal site, where the PL can be located.

The profits and the maximum voltage deviations at bus 3 is given in Table 6.5 for the 1 and 2 MW sizes. Figure 6.7 shows a comparison of the distribution system losses for the 1 and 2 MW sizes when the PL is connected at the optimal location at bus 3. It is obvious from Table 6.5 that the 2 MW size results in higher profits than the 1 MW size, but from Figure 6.7, it also results in higher losses over the course of different days.

Table 6.4: Profits for the one and two MW optimal sizes

	1 MW	2 MW	Difference
Yearly Profit	323469.9	327163	3693.072
Total Profit	1615107	1653440	38332.83
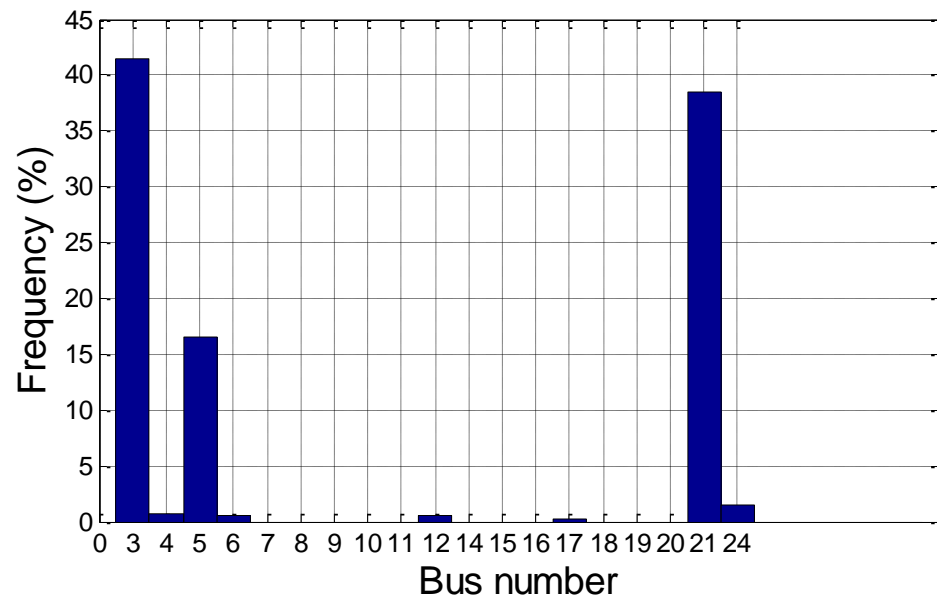
Figure 6.5: Histogram of the obtained optimal candidate buses
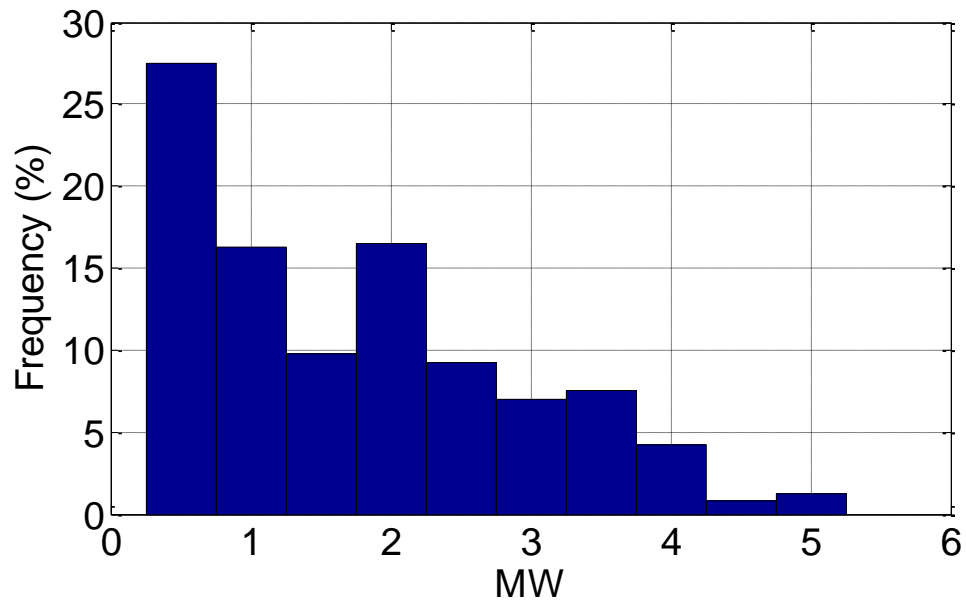
Figure 6.6: Histogram of the obtained optimal sizes

Table 6.5: Profits and maximum voltage deviations for optimal sizes at bus 3

	1 MW			2 MW	
	Profit ($)	ΔV (p.u)		Profit ($)	ΔV (p.u)
day 1	960.729	0.072		967.725	0.072
day 2	673.505	0.071		675.779	0.071
day 3	985.665	0.079		997.308	0.079
day 4	653.968	0.080		653.974	0.080
day 5	964.647	0.093		988.309	0.093
day 6	627.756	0.092		628.026	0.092
day 7	998.801	0.083		1012.100	0.084
day 8	677.911	0.072		678.021	0.073
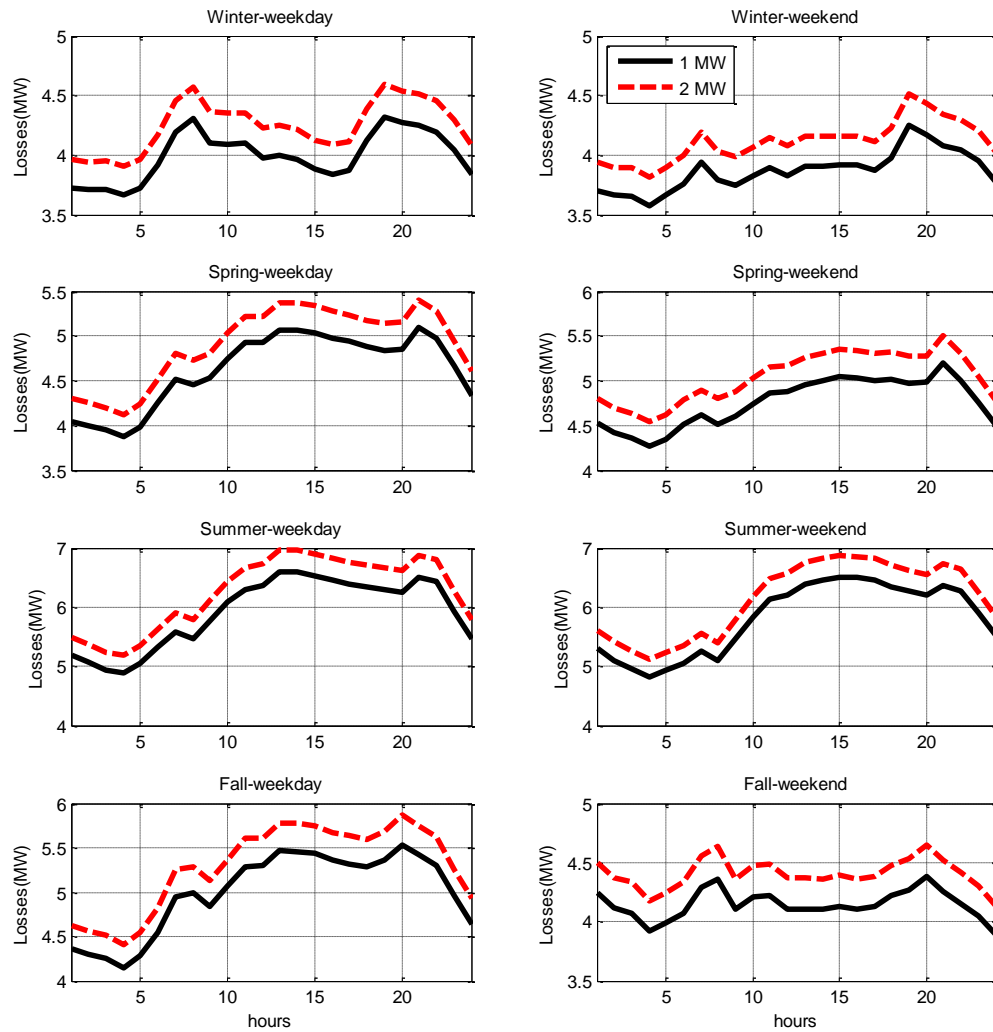
Figure 6.7: Distribution system losses for the 1 and 2 MW sizes at bus 3

6.4.2 Sensitivity Analysis Using Single Objective Optimization

In this section, the effect of the three different objectives on the selection of the optimal size and location is tested. These three objectives are the minimization of the voltage deviations, minimization of the power losses, and the maximization of the profits. The problem here is solved as a single objective optimization problem using the genetic algorithm, where only one objective is selected each time. The obtained results from the three cases is shown in Table 6.6.

From the table, it is obvious that for the cases of minimization of voltage deviations or losses minimization, the optimal size will be the same, which is 0.6 MW. This size will yield a feasible solution for the PL profit maximization problem for all days. It will also result in the lowest voltage deviations and losses. This is well justified since selecting the lowest feasible size (for the PL operator to make profits) will be preferred for the sake of voltage deviations and losses minimization.

Also, the table shows that while the voltage deviations and losses minimization have the same preference toward the size, they have a different preference toward the optimal location. While voltage deviations minimization results in bus 21 as an optimal location, the loss minimization problem results in bus 3 as the best location. It is worth mentioning that both the optimal sizes and locations appear as potential candidates in the multi-objective problem in the previous section. From the point of view of profit maximization as a single objective problem, Table 6.6 shows that the 2.5 MW size will be the optimal size for the PL owner. This is justified since increasing the PL size will result in a higher

profit. The table also shows that the profit maximization has the same preferred optimal location as the losses' minimization problem.

Table 6.6: Optimal size, location, and profits obtained from the single objective problem

	Size (MW)	Bus location	Total profits
Voltage	0.6	21	1503700
Losses	0.6	3	1503700
Profit	2.5	3	1663000

From the analysis mentioned before, a main observation can be made as follows:

The multi-objective Pareto optimization problem almost gave all the solutions obtained using the single objective problems shown in the sensitivity analysis. This proves the superiority of the proposed algorithm and problem formulation in giving all the possible trade-offs compared to the single objective problem, which gives limited options. This is because in the single objective problem, only one solution is obtained. This solution performs well in favor of one of the participating parties while causing a negative impact on the other party. This was obvious from Table 6.6, where the first two cases (voltage deviations and losses minimization) selected the 0.6 MW size, as the optimal size. This size satisfies the system operator requirements, while it badly impacts the PL investor. The same applies for the third case, where the profits were maximized by increasing the size, neglecting the negative effects of this size on the distribution system. Unlike the single objective problem that gives one solution, the Pareto multi-objective problem gives all the possible trade-offs, allowing the different parties to see all the options and apply further analysis to choose the best compromise.

6.5 Conclusion

In this chapter, a bi-layer multi-objective optimization problem is presented to allocate and size an EV PL while considering its impacts on the distribution system. The optimization problem is solved to maximize the profits of the PL investor, as well as minimize the losses and voltage deviations for the distribution system. Therefore, the benefits of all the parties are fulfilled in this study. The proposed method, to solve the problem, is based on the Pareto concept, in which a set of optimal solutions is obtained. The results showed the different trade-offs that might be induced while dealing with the contradictory objectives. A solution that achieves the best profit while keeping the voltage deviations and power losses minimum is selected based on a statistical decision-making criterion.

Also, sensitivity analysis to show the effect of the different objectives on selecting the optimal size and location was performed. The results showed that each objective will result in the optimal size and allocation from one perspective for one of the participating parties, neglecting the negative impact on the other party.

The results showed that the multi-objective Pareto optimization problem almost gave all the solutions obtained using the single objective problems shown in the sensitivity analysis. This proves the superiority of the proposed algorithm and problem formulation in giving all the possible trade-offs compared to the single objective problem, which gives limited options.

Chapter 7   Co-Simulation of Improved AIMD Algorithm for Decentralized

Charging of Electric Vehicles

Mass adoption of Electric Vehicles (EVs) will bring some challenges to the operators of electric utilities. This chapter proposes a decentralized control algorithm to manage the charging of distributed EVs. The proposed algorithm is inspired by the Additive Increase - Multiplicative Decrease (AIMD) algorithm, which is commonly used for the management of communication network congestions. The improved algorithm takes into consideration the preferences of the owners of the EVs. Also, it eliminates the overloading and the under-voltage problems that might be associated with the charging of EVs. The proposed algorithm is validated using a co-simulation platform, where the power components are simulated using MATLAB/Simulink and is linked to embedded microcontrollers over a real-time communication network via the Data Distribution Service (DDS) middleware.

7.1   Introduction

As mentioned in previous chapters, decentralized control algorithms of EV charging can be divided into two categories: 1) Decentralized autonomous control, which is fully independent of any communication [179]. In this type of control, the decisions are made locally based on local measurements of the controlled process or system. 2) Communication-assisted decentralized control, which depends on information exchange, over communication channels, between the system operator/aggregator and the charging stations [180], in addition to the local measurements. While the first type is suitable for utilities that do not have any communication infrastructure, it does not result in the most efficient use of the system resources. Unlike the first type, the second type requires a

communication link, which gives the system operator more observability, and results in a better utilization of the system resources.

Most of the autonomous control algorithms reported in the literature are based on droop control [181], [182]. In [181], the authors proposed a power/frequency droop control algorithm, where the EV autonomously adapts its output power based on the frequency of the microgrid. In [182], a voltage-feedback control for charging the EVs was suggested. However, the issue of fair charging among the EVs connected to the different buses in the system was not addressed.

In addition to the autonomous controllers, many researchers developed decentralized control algorithms that use low bandwidth communication [48]. One of the algorithms that is suggested for communication-assisted decentralized control is the Additive Increase - Multiplicative Decrease (AIMD) algorithm. The AIMD ensures fair distribution and efficient usage of the power. The AIMD algorithm is originally used for congestion management in computer networks [183]. It was first applied to manage the charging of EVs sharing a limited resource in [180], [184]. In [180], the authors considered the problem of adjusting the charging of the EVs to achieve fair charging among them without exceeding a total capacity constraint, and with a unidirectional communication from the system operator to the EVs. They used the AIMD algorithm as a decentralized control algorithm, which requires minimal communication. In [184], the authors extended the work presented in [180] in different charging scenarios, while considering time-varying resources. The performance of the AIMD-based EV charging over a communication

network was considered in [185], where the authors used a co-simulation model using OPNET to test the real-time application of the AIMD over a wireless network.

The control of the connection/disconnection rate of the EVs was suggested in [186]. Instead of controlling the charging rate of the EVs, the authors in [186] increase the connection rate of the EVs by one, as long as the total power demand is less than a certain value. Once the power limit is exceeded, the controller disconnects the EVs, one by one, till the system restores its healthy state.

None of the aforementioned works, that used the AIMD algorithm, considered the network dynamics and the under-voltage problems that might occur in the grid. To take the grid voltage-constraints into consideration in addition to the power limit constraint, the authors in [187], [188] proposed an enhanced AIMD that charges the EVs in a fair manner, taking into consideration the grid voltage and transformer power constraints. Although, the authors have described the functionality of the proposed algorithm, they did not describe the physical implementation of the communication infrastructure, which is needed to support the proposed algorithm. Also, they did not consider the customer's preference. Similar concepts of the AIMD that take the local voltages into consideration were used for the management of battery storage devices that support the grid in [189]. Due to the scope of the work, the effects of the owner preference were not considered.

Accordingly, this chapter proposes an AIMD-based decentralized control algorithm for charging the EVs, taking the grid voltage and capacity constraints into account. The proposed algorithm also considers the preferences of the owner of the EVs in terms of the energy and time required to finish the charging. The proposed algorithm is validated using

a co-simulation platform, using the Data Distribution Service (DDS) as a link between the simulated power system and the embedded microcontrollers, to study the performance of the algorithm over a real communication network. The dynamics of the power network are considered in the model as well.

7.2   Controller Description

The AIMD algorithm was originally used for managing the congestion in the communication networks to guarantee efficient use of the available bandwidth and ensure fair distribution among the users [183]. The AIMD algorithm has its own advantages, such as the decentralized actions, eliminating the need for a heavy communication infrastructure, low computation burden, since each entity decides on its own control action locally, and scalability, which provides great flexibility to system operators.

Similar to the fair distribution of the communication bandwidth, large-scale penetration of EVs into the power grid with limited generation resources will require fair EV charging and addressing the grid constraints. Therefore, the AIMD was adapted and applied to manage the charging of EVs by Studli in 2012 [180]. The basic idea of the AIMD algorithm in charging the EVs was to ensure that the maximum capacity of the transformer, or the power allocated to a certain area, will not be exceeded, and at the same time this power is used in the most efficient way. The algorithm was used in a decentralized way to ensure fair distribution of the available power among the EVs.

The original idea of the AIMD algorithm is to increase the charging rates of the connected EVs, gradually, with an additive constant (α), in kW/s. When the maximum

capacity of the system is reached, the EVs decrease their charging rates by a multiplicative factor (β).

Once the system is not overloaded, the algorithm starts increasing the charging rates again using the additive constant, and so on. The change from the increase to the decrease phase is based on an event trigger, which will be sent to all the EVs by the system operator, when the total power consumed by the EVs exceeds the system's capacity. This event is called capacity or power event.

The algorithm in its original form is fully decentralized, where the charging rates are decided upon locally based on the additive and multiplicative constants that are the same for all the EVs in the system, to ensure fair distribution of power. The communication is only used when an event is triggered, and it is a unidirectional and low bandwidth communication.

It was shown in previous studies that the algorithm was able to ensure that the system is not overloaded and the allocated power to the different EVs is almost the same. However, the algorithm in its original form cannot ensure that the voltages at the different buses in the system are within the standards.

To consider the system voltages and the capacity, other authors [187] suggested that the EVs can send their voltages at the point of charging to the system operator, and these values will be compared to the standards. An event will be triggered if the total charging power exceeds the system capacity or if there is an under-voltage at any of the buses. The event will be triggered even if there is under-voltage at only one bus in the system. This is done

to distribute the burden of the under-voltage problem among all the EVs. Otherwise, the EVs at the far end of the feeder, away from the generation station or the substation, will always lack behind other EVs, because of the voltage drops across the feeders.

To improve the algorithm and ensure its validity, this chapter proposes that the algorithm could be improved by ensuring that overloading and under-voltages are avoided, and the owners' preferences are taken into consideration, simultaneously. The proposed improved algorithm is shown in Figure 7.1. Its communication implementation will be discussed in the next section. The controller first checks if there is an event or not. The event can occur due to exceeding the power or the voltage limits. If no event trigger is received from the system operator, the controller checks the state of charge (SoC) of the battery. If the battery is not fully charged (SoC <80%), the controller will start charging and increases the charging rate gradually with an additive factor (α).

To consider the owner's preferences, the additive parameter (α) will be tuned to be linearly proportional to the desired charging rate CR^*, as shown in Figure 7.2. This reflects the required energy and the time desired by the owner. Therefore, each EV will have its own (α), based on the owner's requirements.

If an event is received, the controller will enter the decreasing phase. To avoid undercharging problems, and to increase the lifetime of the battery, the controller will first check the SoC of the battery. If the battery is under-charged (SoC <20%), it will be excluded from the decreasing phase, and it will continue charging with the same rate.
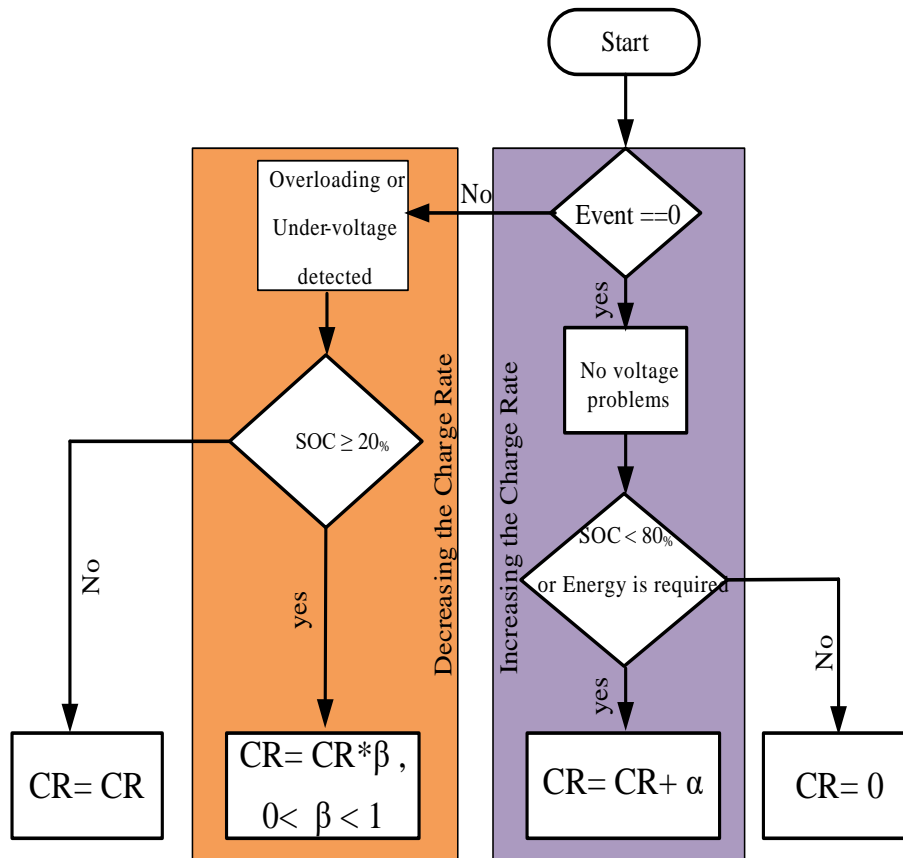
Figure 7.1: A flow chart for the improved AIMD algorithm
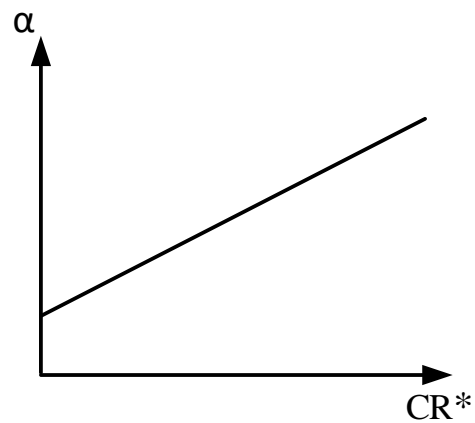
Figure 7.2: The relation between the required charging rate and the addition factor

Otherwise, it will decrease its charging rate by a multiplicative factor (β). The loop will continue as long as the battery does not reach the energy level required by the EV owner.

7.3 Co-Simulation System Description

A co-simulation setup was developed to evaluate the developed controller over a real communication network. As seen in Figure 7.3, the power system components are simulated on MATLAB/Simulink. The adopted system is composed of 4 busses. To accommodate the anticipated large-scale penetration of EVs, it is assumed that there is an EV on every bus in the system. The system has a detailed model of the power electronics, such as the DC-DC converters and rectifiers that are connected to the batteries of the EVs. An EV Agent is assigned to each EV to control its charging process, based on the proposed control strategy in this chapter. The Agents of the EVs are interfaced with the FIU Testbed's communication network through the MATLAB DDS Toolbox [190]. The Agents in this work exchange information with the system operator, which is an embedded microcontroller running on a Linux Kernel, over the Testbed's communication network.

In practice, there are two main different types of communication network architectures for industrial control systems. The first one is the client-server-type network, which is commonly used in Supervisory Control and Data Acquisition (SCADA) systems. For data to be transferred in such networks, clients need to initiate requests to a server, reducing the flexibility and reliability of the decentralized controllers [191]. The server in the SCADA system is a bottle-neck from the communication perspective, and makes the network prone to a single-point-of-failure. Contrary to that, the peer-to-peer-type networks, that are the second type of industrial control networks, create direct connections between the network

nodes, eliminating the need for a server. Therefore, to meet the requirements for the proposed decentralized controller, the communication infrastructure is built based on the Data Distribution Service (DDS) standard.

In the proposed communication infrastructure, the Agents in the simulation environment and the system operator exchange messages via the DDS middleware. DDS is a data-centric middleware that utilizes the publisher/subscriber model for decentralized and distributed control applications. As depicted in Figure 7.3, DDS gives communicating nodes an abstraction level by providing a relational data model in a decentralized data space, which decouples applications in both time and space. In other words, for a given network, a global data space, which includes different data topics, is introduced. Each data topic in the global data space has a predefined set of data types.

In this chapter, three data topics were created. The EV Topic holds a data structure containing the EV ID and the voltage at the point of connection in per unit. The Power Topic and the Events Topic hold data structures with total power and events, respectively.

All the EV Agents publish the voltage in per unit at their points of connection and the EV IDs to the EV Topic. The power Agent publishes the total consumed power to the Power Topic. On the other hand, the system operator subscribes to the EV Topic and Power Topic and publishes its decision to the Events Topic. Finally, the EV Agents subscribe to the Events Topic and take the appropriate control actions on the simulated power system.
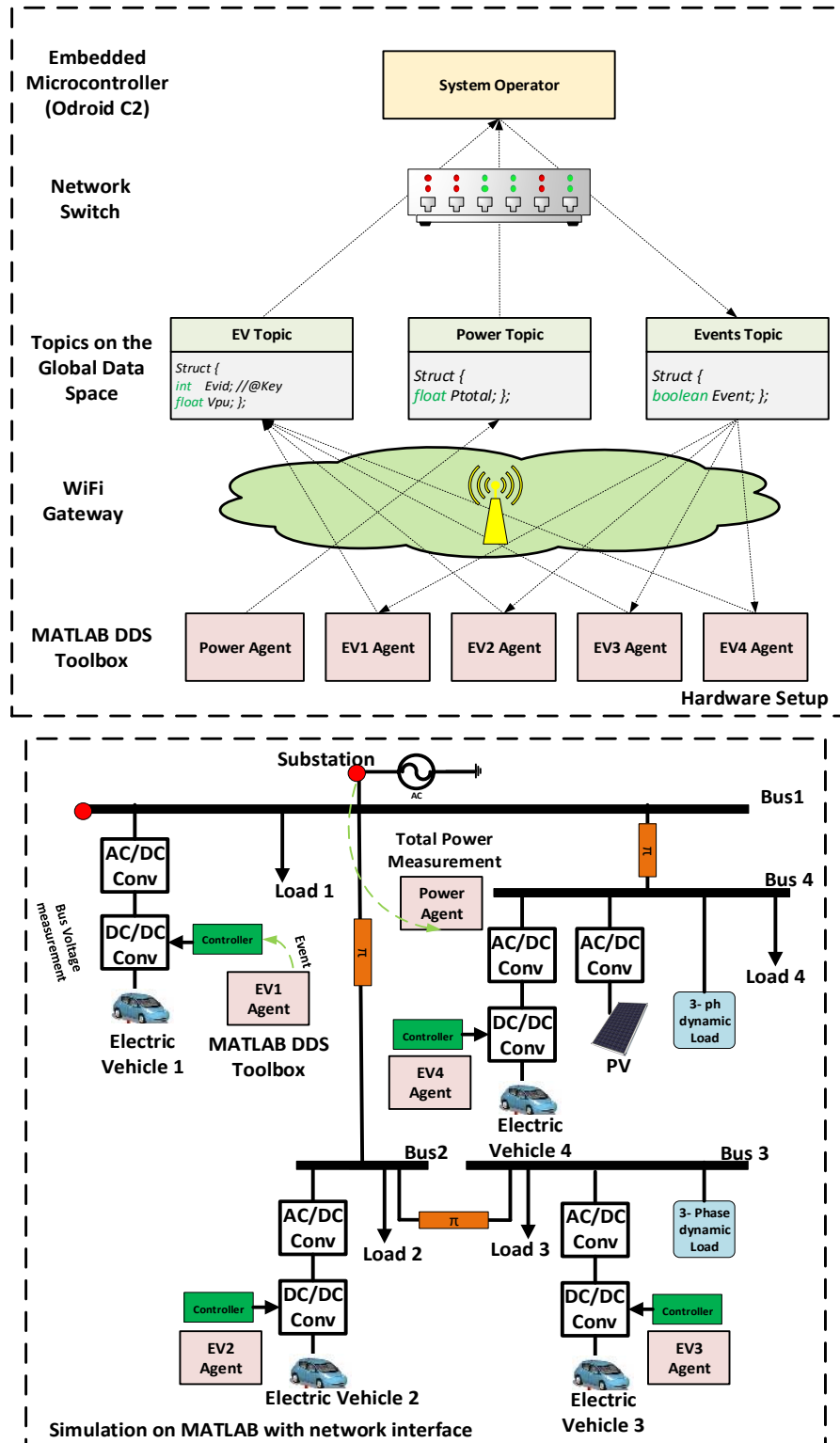
Figure 7.3: Co-simulation setup

7.4   Results

To validate the proposed control algorithm, it was implemented and tested in the co-simulation platform shown in in Figure 7.3. The validation is performed under different loading conditions and in the presence of renewable generation units. To test the ability of the controller in avoiding overloading and under-voltage problems, and ensuring fair distribution of power, four different cases are presented:

1. The effect of uncontrolled charging of EVs.

2. The controller performance when considering power events only.

3. The controller performance when considering power and voltage events.

4. The controller performance when considering power and voltage events, taking into consideration the EV owner preferences.

In this section, it is assumed that the minimum allowed voltage at the different buses is 0.955 p.u. This voltage limit satisfies the ANSI C84.1-2006 standards. The maximum allowed total power is chosen to be a normalized value of 100%.

7.4.1   Effect of Uncontrolled Charging of EVs

To show the effect of opportunistic charging on the adopted system in this chapter, the EVs are allowed to charge at high rates to finish as soon as possible. As depicted in Figure 7.4 (a), the uncontrolled opportunistic charging results in under-voltage problems, especially at the downstream busses, such as Bus 3, where the voltage goes as low as 0.94 p.u. The under-voltage problem is best witnessed at the downstream bus because of the voltage drops across the feeders, which result in low voltages at the end users downstream.

Also, Figure 7.4 (b) shows that the main substation, feeding the different loads in the system, is heavily overloaded due to the uncontrolled charging of the EVs. This highly degrades the system lifetime and may result in related thermal disconnection issues at the substation. Figure 7.5 shows the charging currents of the different EVs and their SoCs. The figure shows that the EVs charge at high rates to finish as soon as possible. The minor changes in the charging currents among the EVs are contributed to the different voltages at the different buses that produce different rectified DC voltages at the inputs of the DC-DC converters.

7.4.2 Controller Performance When Considering Power Events Only

In this section, the proposed AIMD algorithm is used. The only variable that will generate event triggers is the power. It is assumed that the system operator will try to maintain the total power of the system to be equal to or less than 100% of the total capacity of the substation. Figure 7.6 (a, b) show that although the voltage at the downstream bus goes below 0.955 p.u for some periods of time, the total power is always maintained to be less than 100%, which ensures that the system is not overloaded. Figure 7.6 (c) shows the event triggering signals that are sent from the system operator to all the EVs connected to the system over the communication network. The event triggering is aligned with the power events when the total power hits the 100% limit.

Figure 7.7 shows the complete fairness of the proposed algorithm, where all the EVs charge by the same charging rate and finish at the same time.

Although the AIMD algorithm in its original form eliminates overloading the system and ensures fair distribution of power, it does eliminate the under-voltage problems and is not able to take the customer's preferences into account.
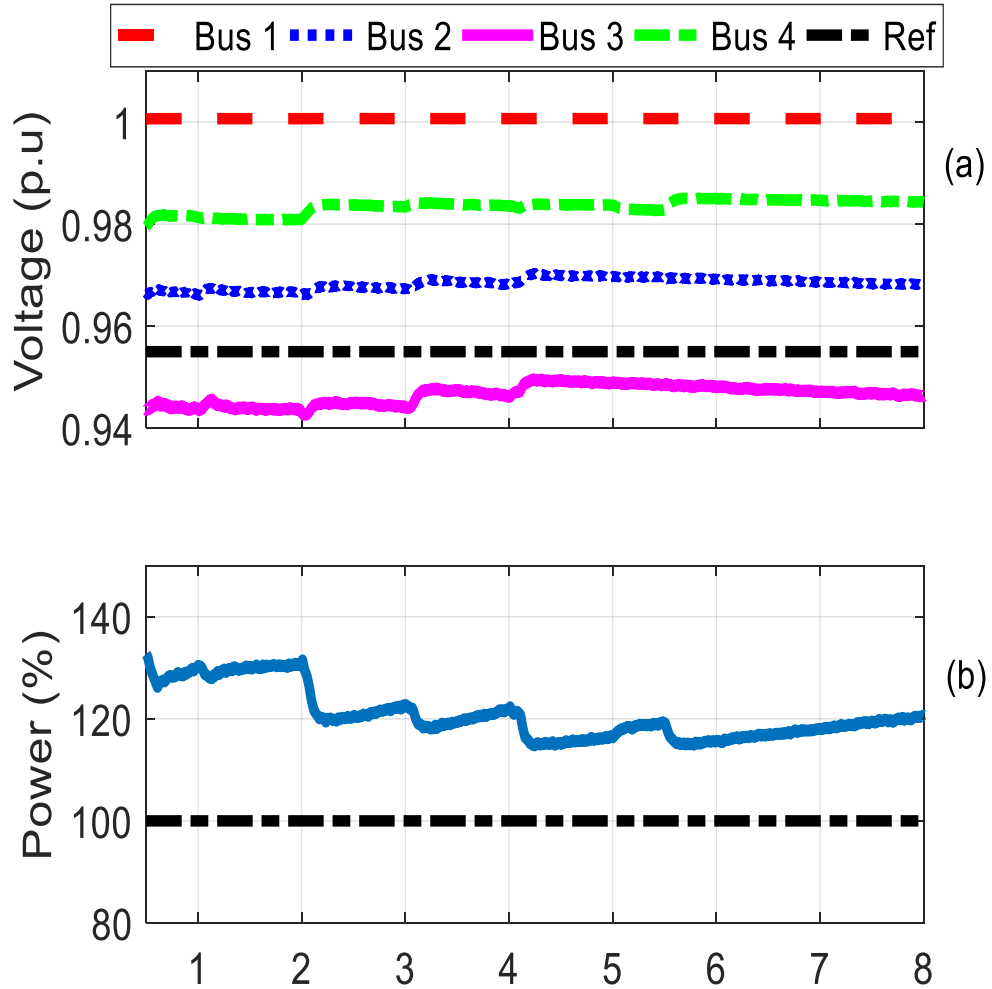
Figure 7.4: a) Voltages at the different buses. b) System loading in case of opportunistic charging (Limits: Black-Dashed Line)
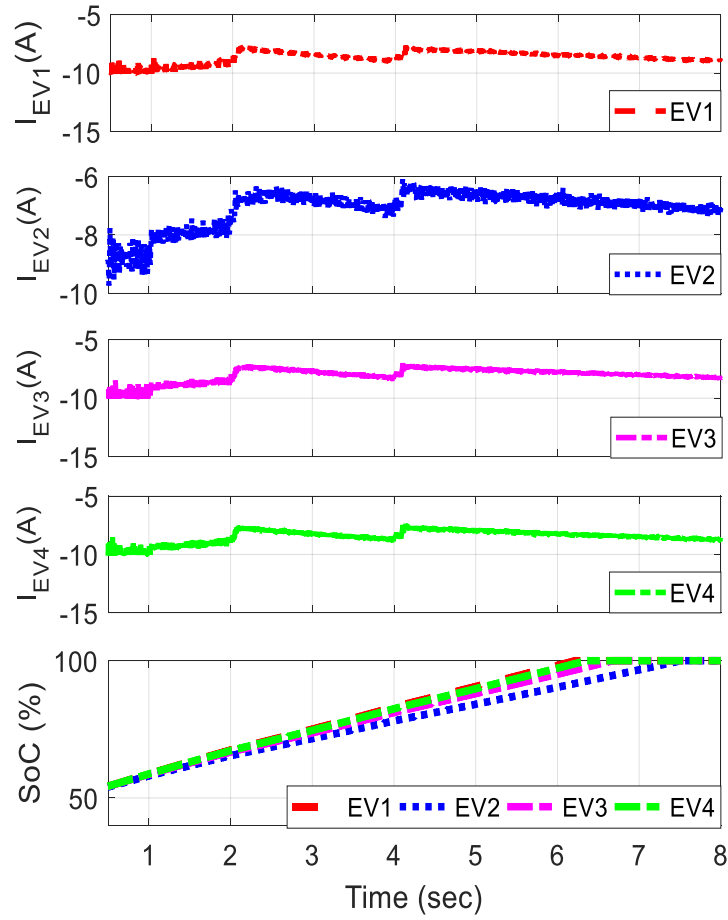
Figure 7.5: Currents and SoCs of the different EVs in case of opportunistic charging

7.4.3 Controller Performance When Considering Power and Voltage Events Only

In this case, the system operator will trigger an event whenever there is a power overloading or under-voltage problems at any of the buses. Figure 7.8 shows that the overloading problem is avoided, and all the voltages are higher than 0.955 p.u., as set in the design. Figure 7.8 (c) shows that all the events are triggered whenever the voltage at the downstream bus touches the 0.955 boundary. This illustrates that the under-voltage problem can be a tighter constraint in some cases and it cannot be captured by power events designs

only. Figure 7.9 also shows that the fair distribution of power is ensured and all the EVs finish charging at the same time.

Comparing Figure 7.8 (b) to Figure 7.6 (b) shows that taking the voltage constraint into account results in less utilization of power. Less utilization of the available power produces delays in the end of charge time of the EVs, as shown in the SoC plot of Figure 7.9 compared to Figure 7.7.
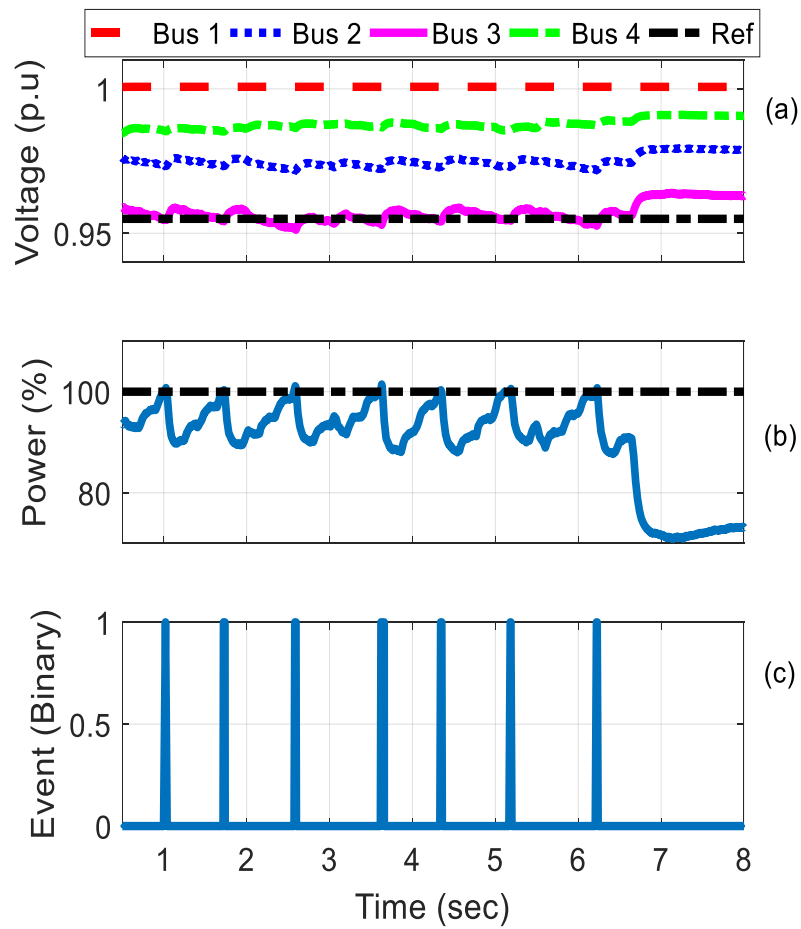
Figure 7.6: a) Voltages at the different buses. b) System loading c) Events in case of AIMD with power event (Limits: Black-Dashed Line)
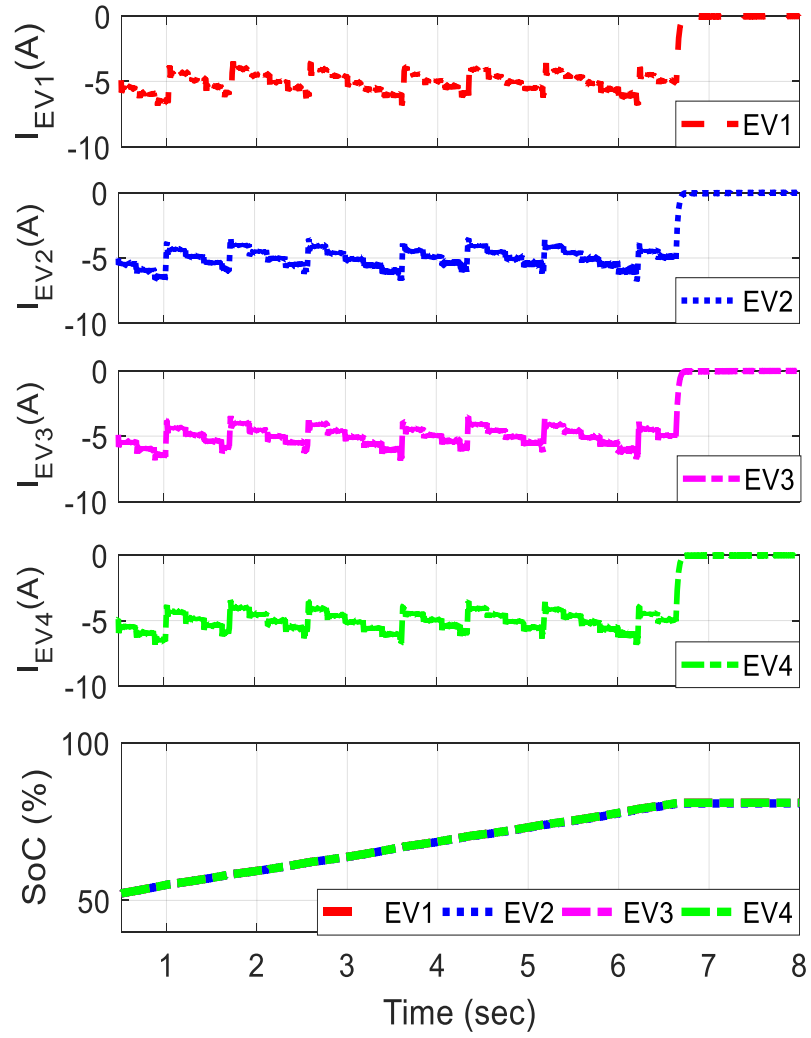
Figure 7.7: Currents and SoCs of the different EVs in case of AIMD with power event

Therefore, it seems that ensuring the voltage limits in the power system using the AIMD algorithm might compromise the end of charge time of the EVs. Therefore, the case of taking the customer's preferences into account is of great importance for the practical validation of the AIMD algorithm.

7.4.4 Controller Performance While Considering the Preferences of the EV Owner

In this section, the owners of the EVs are assumed to have certain charging preferences. It is assumed that two EVs (EV2 and EV3) would like to finish charging by the end of the simulation time and the other two EVs (EV1 and EV4) would like to finish within 5 and 6 simulation seconds, respectively. Figure 7.10 (a, b) illustrates that there are no system overloading or under-voltage problems regardless of the fact that some of the EVs consume higher power at the beginning to finish faster. The event triggering in Figure 7.10 (c) is contributed to both power and voltage events. During the first 5 seconds, the events occur due to power triggering, where the power limit was reached multiple times due to the high-power consumption of the EVs. During the remaining period, the event triggering occurs due to voltage problems.
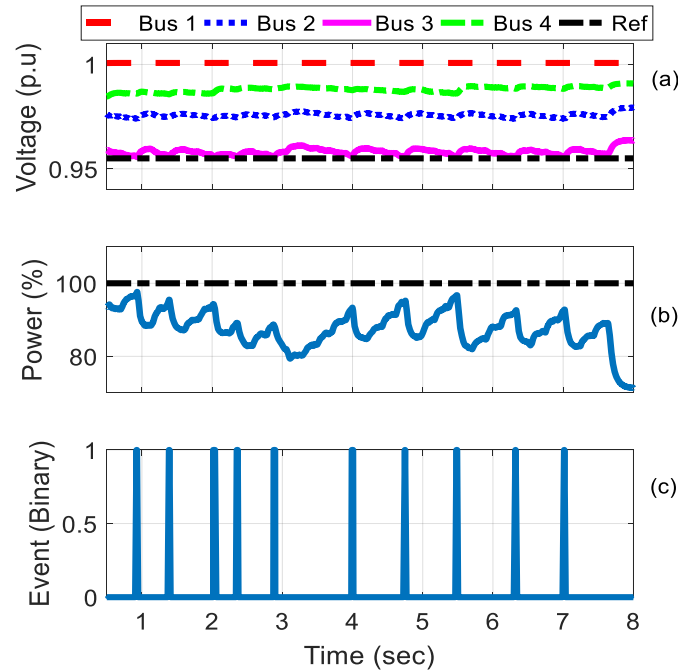
Figure 7.8: a) Voltages at the different buses. b) System loading c) Events in case of AIMD with power and voltage events (Limits: Black-Dashed Line)

173

Unlike the previous case, taking the customer's preferences into account pushes the system to better utilization of the available power to satisfy the customer preferences, while avoiding the overloading and under-voltage problems, simultaneously. The charge currents and SoCs of the different EVs are shown in Figure 7.11. From the figure, it is obvious that the EVs are able to charge within the required time frames.
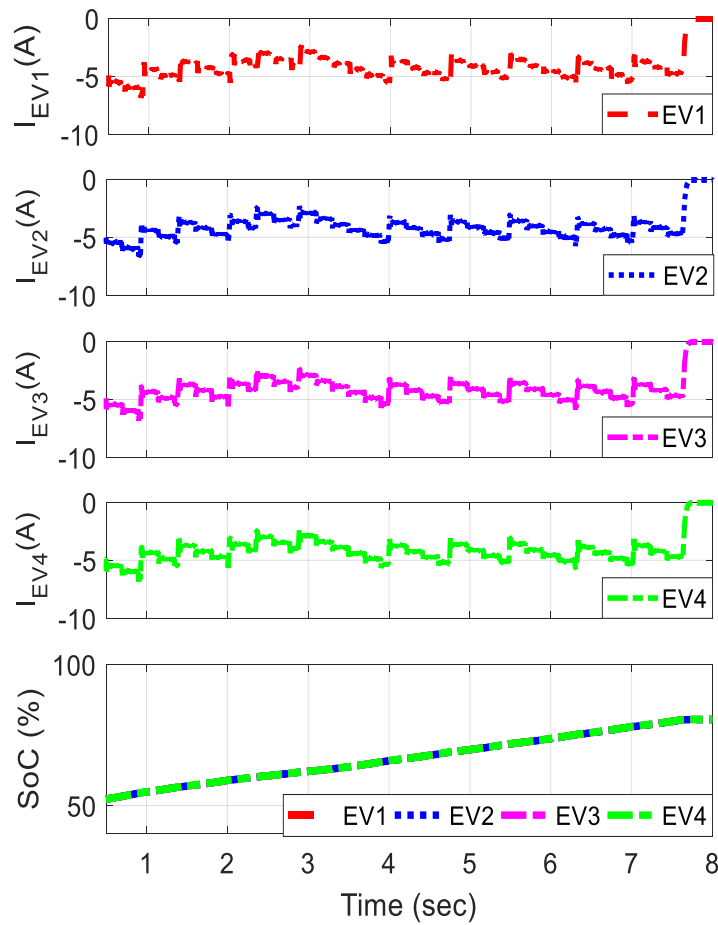
Figure 7.9: Currents and SoCs of the different EVs in case of AIMD with power and voltage events
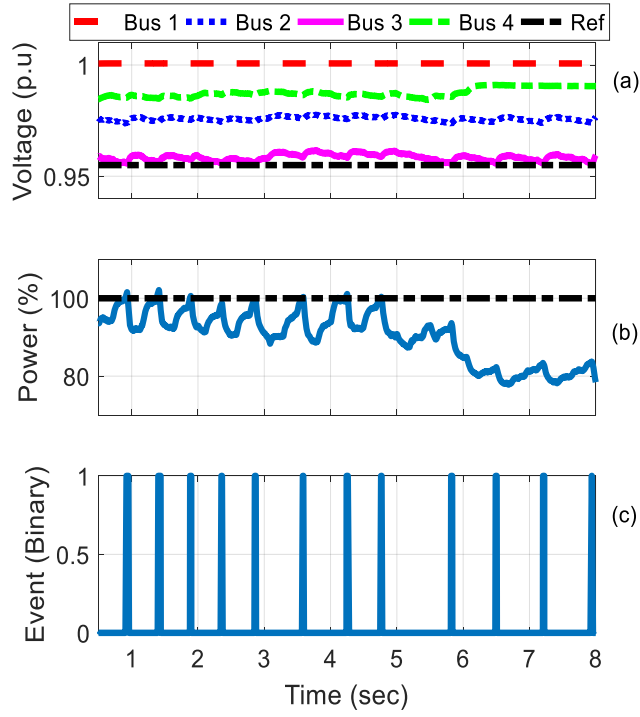
Figure 7.10: a) Voltages at the different buses. b) System loading c) Events in case of AIMD with power and voltage events with owner preferences
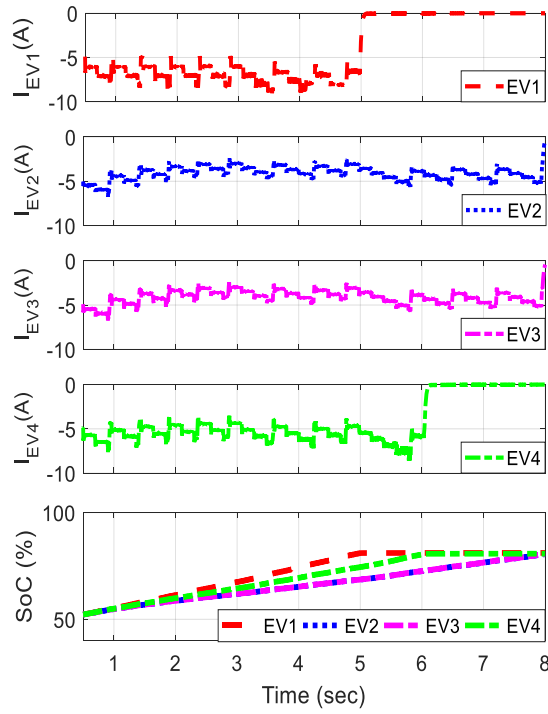
Figure 7.11: Currents and SoCs of the different EVs in case of AIMD with power and voltage events with owner preferences

175

7.5   Conclusion

In this chapter, a decentralized control algorithm for managing the charging of distributed EVs is proposed. The proposed AIMD algorithm is validated using a co-simulation platform that uses a real communication network based on the DDS standard. Unlike the work that is reported in the literature, the proposed AIMD algorithm in this work is able to ensure that overloading and under-voltage problems are avoided. The proposed algorithm was tested under different cases. It was first tested in the case of considering only power events. This case showed that the original AIMD algorithm can avoid overloading the system, but it fails in ensuring the healthy states of the voltages at the different buses in the system.

Then, the controller is test while considering both power and voltage events in the system. It was found that the voltage event can be a limiting factor as it imposes a stricter constraint than the power, and it results in more multiplicative decrease events.

Finally, the proposed controller was tested to see its ability to take the preferences of the owners of the EVs into account, in terms of the needed energy and required time, without mitigating the system loading or voltages. It was found that taking the customer's preferences into account, using the proposed algorithm, pushes the system to better utilization of the available power to satisfy the customers' preferences.

Also, the algorithm is able to fairly distribute the available power among the users. Due to its simplicity and decentralization, the proposed algorithm can be easily scaled to accommodate any number of EVs in the system.

Chapter 8 Medium Voltage Direct Current Shipboard Power Systems

Medium voltage direct current (MVDC) systems are gaining more interest in maritime ship power systems. This is due to the nature and the amount of the onboard electrical demand. Therefore, a proper modelling and control of the different components of the shipboard power system should be carefully addressed. This chapter provides an overview on the MVDC all electric ship (AES), describing differences of the maritime MVDC systems compared to their counterparts of terrestrial MVAC systems. Also, a brief description of the different components of the AES power system is presented. To show the challenge of controlling and maintaining the voltage of the MVDC bus of the onboard power system, in the presence of the highly power consuming pulsed loads, a case study on the control of the onboard storage system is performed.

A benchmark of a MVDC power system is developed and used to test the control algorithm. The purpose of the controller is to ensure the load-generation balance, maintain the MVDC bus constant, and ensure proper power sharing among the storage devices. To reduce the complexity of the control algorithm and ensure proper illustration of the challenge and the solution, this chapter focuses only on the control of battery storage devices. Hybrid types of storage systems will be considered in the following chapters.

8.1 Introduction

The next generation of ship power system is adopting more electrical energy that increases complexity of the supply and the control process of the isolated marine power system. This is mainly driven by the increasing electrical demand and the nature of anticipated new types of loads, such as electromagnetic aircraft launch system (EMALS).

These kinds of loads draw intermittent pulses of power from the system [192]. Due to the need of high power supply and flexibility in All Electric Ship (AES) power system, medium voltage direct current (MVDC) systems are going to be viable options [7]. The MVDC power system has multiple advantages against the MVAC system. These advantages include:

1. The replacement of bulky transformers with the compact power electronics.

2. Increased fuel efficiency and elimination of the synchronization problems.

3. Reducing the risk of systematic disintegration while supporting the emerging pulsed loads.

4. Easier parallel connection or disconnection for dc power sources.

In terms of the differences between the onboard ship power systems and the terrestrial MVAC systems, there are distinct differences among them. Changes in loads (per unit magnitude of step loads) on shipboard systems represent a larger percentage of available stored energy than in terrestrial systems. Additionally, a MVDC system utilizes high speed switches and power electronic converters in the majority of its power transmission paths. This is in contrast to the terrestrial power grid, where relatively few of the transmission paths have power electronic devices [192]. The power electronic switching changes the dynamic nature of the power system significantly and leads to states whose derivatives vary continuously. Moreover, there are differences in the physical nature of the instabilities. For example, the electrical frequencies of the generators in a MVDC system are well decoupled from the MVDC bus, which eliminates the problem of rotor angle and frequency instability inherent in the terrestrial.

178

8.2   Components of MVDC Ship Power System

A notional functional block of a ship MVDC power system is presented in Figure 8.1. The functional blocks are defined as follows [192]:

- Shore power interface, which is primarily a power source that adapts electric energy from the utility system on shore to MVDC (e.g., interface transformer + rectifier).

- Power generation that is primarily a power source that converts prime energy from fuel into MVDC (e.g., gas turbine + PM generator + rectifier).

- Energy storage that is a stand-alone power source that primarily provides power to the system when needed but also draws power from the system to recharge (e.g., a battery with a bidirectional DC/DC converter).

- Pulsed load is a stand-alone load center that primarily draws intermittent pulses of power from the system [such as electromagnetic aircraft launch system (EMALS)].

- Propulsion system, which is a load center that draws power from the system for propulsion of the vessel. It may also provide power during certain maneuvers, such as crash back (e.g., a motor drive inverter + propulsion motor).

- Ship service that is a load center that draws power from the system to power ship services within zones (e.g., DC/DC converter for in-zone distribution of LVDC, DC/AC inverter for in-zone distribution of LVAC). Note that "ship service" modules may take power from either the MVDC bus or from in-zonal energy storage systems, as shown in Figure 8.2.

- Dedicated high-power load, which is a stand-alone load center that draws 1 MW or more of power in steady-state operation (e.g., 3 MW radar sensor array).

- MVDC bus that is a functional block that allows interrupting and isolating sections of the MVDC system (e.g., mechanical disconnect, solid-state DC breaker). In addition, each functional block in the system can connect, disconnect, and isolate itself from the system through its own means (e.g., a "power generation" module should have at least a disconnect switch at its DC output).
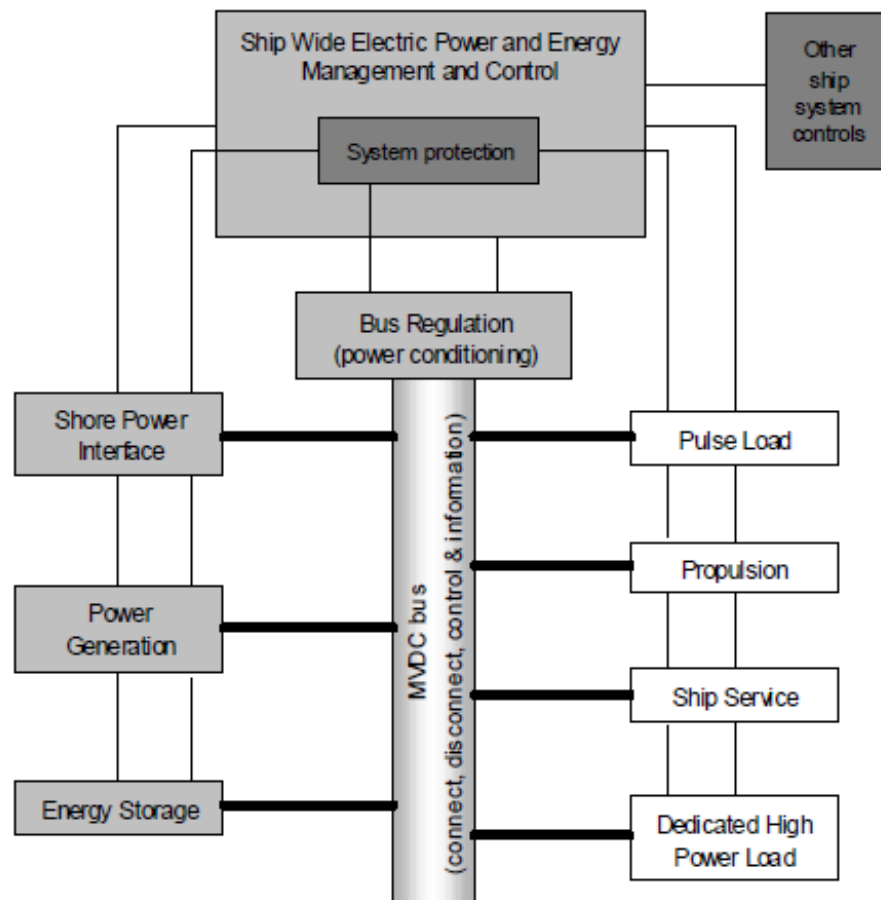
Figure 8.1: Functional diagram of MVDC shipboard power system [192]

In the case of maritime applications, the onboard energy storage systems (ESS) are taking on a pivotal role in the next-generation AES. For U.S. navy surface combatants, the main reasons for an ESS are twofold: 1) to enhance survivability and 2) to enable high-

energy pulsed loads [7]. The second reason is mainly driven by the nature of the response time of the generator sets to power fluctuations, which is low to moderate. Sudden demands or rejections in DC bus power caused by step-loads from pulsed load devices or the loss of a generator set are met through the use of quick response energy storage devices. Furthermore, energy storage devices may be used to enable a dark ship system restart. All energy storage devices, such as capacitor banks or batteries, charge from, and discharge to, the MVDC distribution bus via bi-directional DC/DC converters.
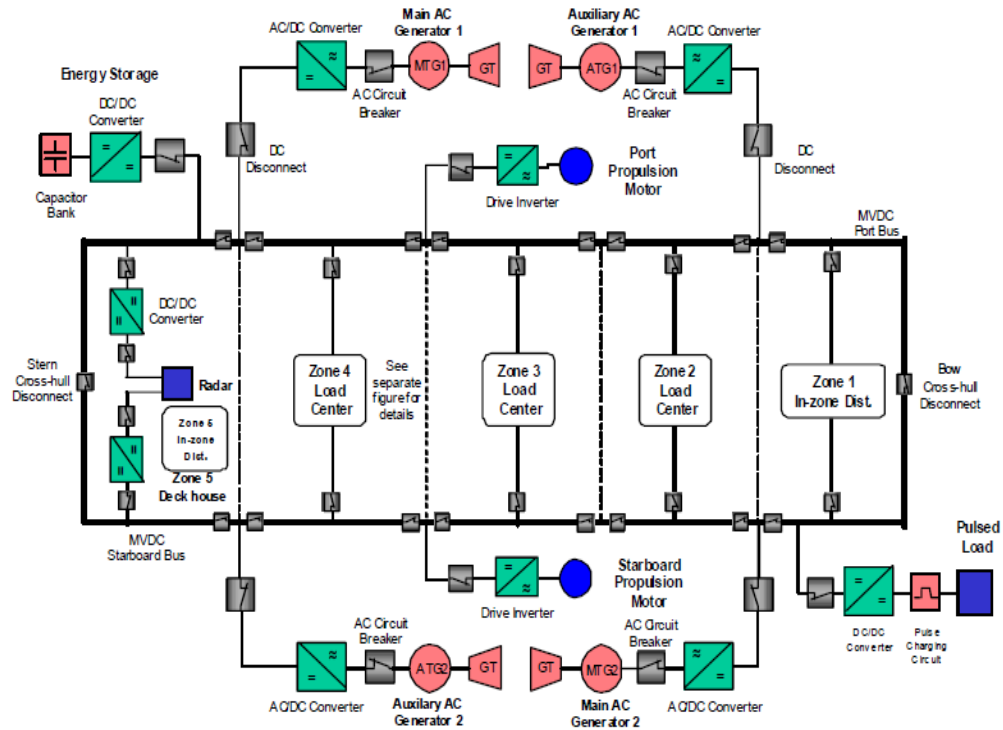
Figure 8.2: Architecture of a MVDC system with different zones [192]

8.3 Control of Batteries on MVDC Shipboard Power System

Due to the anticipated use of new types of pulsed loads on AES, and the limited capabilities of the onboard gas-driven generators, in terms or ramp rates, there is a need for

automatic control algorithms that should provide smooth insertion and removal of power sources and sharing of loads, as desired.

In this chapter, an automatic decentralized controller for fair power sharing among batteries on the MVDC ship power system is illustrated and tested. The controller requires no communication or knowledge of the generator and load currents. It can ensure load-generation balance for normal operating conditions and during feeding the pulsed loads. It also ensures that the MVDC bus voltage is within the IEC 60092-101 standards [192]. The controller is based on a two-function controller that uses the concept of virtual impedance controller [193], and the exponential SOC controller [76]. To avoid unnecessary discharging of the batteries, the controller uses state machine logic to ensure efficient use of the energy storage units. In the next section, a benchmark MVDC system will be presented and followed by the proposed controller description.

8.4   Notional MVDC Test-Bench Description

The test-bench MVDC ship power system is shown in Figure 8.3. To meet the total installed demand of the loads, two large capacity "main" generator sets (36 MW) can be supplemented with two or more small capacity "auxiliary" generator sets (4 MW) [192]. The generators are connected to a controlled rectifier. This allows more fuel efficiency since the generators are not obligated to operate at a fixed speed anymore. The ship is driven using a propulsion system that uses induction motors. The propulsion system represents 80% of the total ship power system loads [194]. The radar system represents a standalone load that draws around 3 MW in its steady state operation. Ship service loads are supplied from the MVDC through DC/DC or DC/AC converters. Pulsed loads represent

a load center that draws intermittent pulses from the system. It draws power in the range of 2 MW within one second.

The generators on the ship power systems are designed to supply the continuous loads that are connected to the system. Also, the response time of the gas-driven generators is slow. Therefore, sudden load additions or rejections to the MVDC bus, caused by step changes coming from the pulsed loads, are met by the batteries. It is worth mentioning that in this chapter, the batteries connected to the system are oversized to be able to provide the required high power density during the transient period.
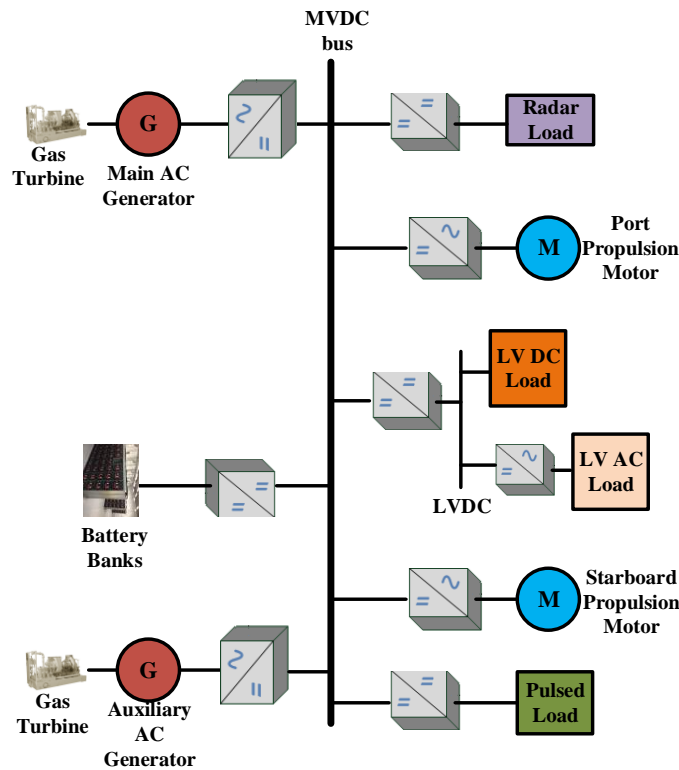
Figure 8.3: Notional MVDC test bench

To maintain the MVDC bus voltage within the standards and to increase the lifetime of the batteries, proper energy management and control of the batteries are required. Therefore, the next section will provide an illustration for the proposed controller.

8.5 Controller Design

To ensure adequate operation of the MVDC AES in the presence of large pulsed loads, there is a need for proper control of the batteries. The battery storage system needs to be fast and reliable to meet the system needs, and its controller needs to achieve certain objectives that ensure the proper operation of the overall system.

The controller should ensure load-generation balance and avoid unnecessary discharging/charging of the batteries to increase the lifetime of the system. Therefore, there is a need for an automatic decentralized algorithm that should provide smooth insertion and removal of the batteries [192]. Decentralized control algorithms usually have the ability to provide a fast response and they are less expensive than the centralized ones.

Due to the nature of the decentralized controller, it does not know about the capability of the connected generators. For example, when a large load is added to the system, it will cause a momentary voltage drop on the MVDC bus. This may prompt the batteries to start discharging regardless of the fact that the generators can supply this added load. Therefore, the control algorithm should satisfy the following objectives:

- Ensures load-generation balance.

- Ensures proper power sharing among the batteries.

- Avoids unnecessary discharging/charging of the batteries. It is only when there is a deficit/surplus, the batteries will be used.

The proposed controller that satisfies these requirements is shown in Figure 8.4. It consists of an outer droop-exponential controller that tries to ensure load-generation balance and equal power sharing among the batteries. The droop-exponential controller is followed by a state machine logic that takes the reference current from the controller I_{DE}

184

and decides if this value will be passed to the PI controller or it will be manipulated to avoid unnecessary discharging/ charging. Once the final reference current I_{ref} is obtained, it will be compared to the converter current and the error will be passed to a PI controller that will force the converter to follow the reference value of the current. The details of the various parts of the controller are as follows:

8.5.1 Droop Exponential Controller

This part of the controller is a combination of the virtual resistance droop controller that is used for equal power sharing in the DC micro-grids and the exponential controller that tries to take into consideration the state of charge of the battery when deciding on the current reference value of the controller. The droop exponential part of the controller is shown in Figure 8.5. The current reference value of the controller I_{DE} is coming from two parts: The first one is based on the value coming from the droop part, shown in Figure 8.6 (a), while the second part is coming from the exponential part, shown in Figure 8.6 (b). The multiplication by the base current Ir_{base}, shown in Figure 8.5, is meant to change from the p.u unit value, coming from the controller into an actual value in Ampere. The base current value is equal to the maximum allowed current that can be charged/discharged into/from the battery.
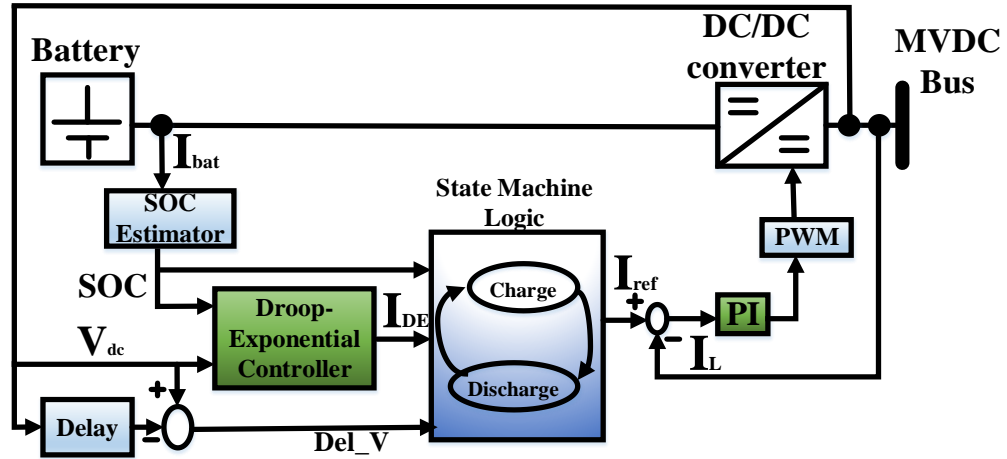
Figure 8.4: Schematic diagram of the proposed controller
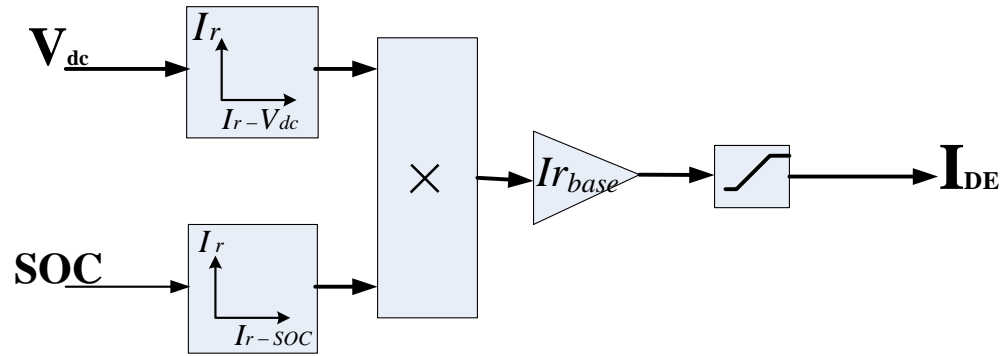
Figure 8.5: Droop exponential controller
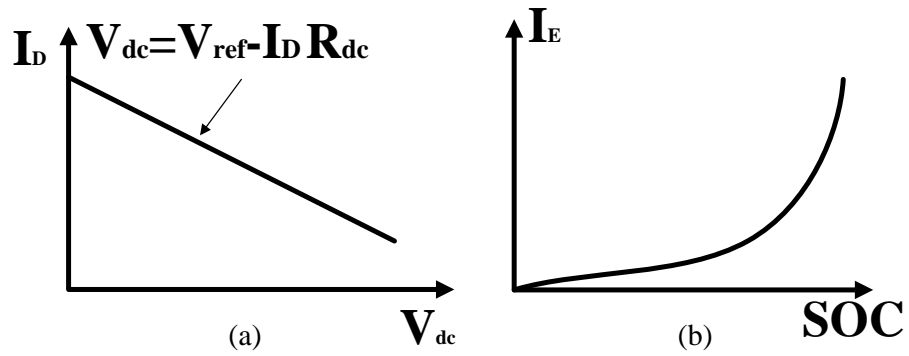
Figure 8.6: (a) Virtual impedance droop controller (b) Exponential controller

During the discharging of the batteries, the reference current will be managed partially by

the droop controller. Therefore, the MVDC bus voltage is given by relation (8.1), where

R_{dc} is the virtual resistance of each droop control loop, I_D is the portion of the output current that is coming from the droop control part. V_{dc} is the voltage at the common MVDC bus and V_{ref} is the voltage reference for the MVDC bus.

$$V_{dc} = V_{ref} - I_D R_{dc} \qquad (8.1)$$

To take into consideration the state of charge of the battery, the battery current is measured and the state of charge (SOC) of the battery is estimated according to relation (8.2):

$$SOC = SOC(0) - \int_0^t \frac{I_{bat}}{C_{bat}} \, dt \qquad (8.2)$$

where $SOC(0)$ is the initial state of charge of the battery, I_{bat} is the battery current and C_{bat} is the battery capacity. Once the SOC is estimated, it will be used in the second exponential part of the controller.

It is desired that the battery with the highest SOC should discharge faster than the others to ensure the balance among the batteries and increase the lifetime of the overall storage system. In case of charging, it is required that the battery with the lowest SOC be charged faster than the others. Therefore, the controller will decide on part of the I_{DE} current based on the SOC based on the following equation:

$$I_E = exp^{\alpha \cdot SOC_{p.u}} \qquad (8.3)$$

where exp(.) stands for the exponential function and $SOC_{pu,i} = SOC_i/Cbat$. This relation is depicted in Figure 8.6 (b). This relation will bias the effective discharging rate toward the highest charged battery.

It is worth noticing that in this chapter, the droop controller is designed in a unidirectional way, where it is designed to support the grid during the voltage drops (i.e: to manage the discharging of the batteries). The bidirectional case will be considered in the next chapter.

In the case of battery charging in this chapter, the charging current will be manipulated by the state machine logic.

The final reference current coming from the droop-exponential controller is as illustrated in relation (8.4):

$$I_{DE} = K \cdot I_D \cdot I_E \cdot Ir_{rbase} \tag{8.4}$$

where K is a constant value that increases/decreases the reference value based on the battery type and rating. I_D is the part of the controller current that is coming from the droop relation and I_E is the part of the controller current that is coming from the exponential relation. Ir_{base} is equal to the maximum allowable current of the battery.

Once the reference current I_{DE} is obtained, this value will be passed to the state machine logic that will generate the final reference value I_{ref} to the PI controller.

8.5.2   State Machine Logic

The state machine logic is responsible for generating the final charge/discharge reference current I_{ref} to the PI controller. It is shown in Figure 8.7. The inputs to the state machine logic are the discharge reference from the droop-exponential controller, the change in the voltage of the MVDC bus (V_t - V_{t-1}) and the SOC of the battery.

188
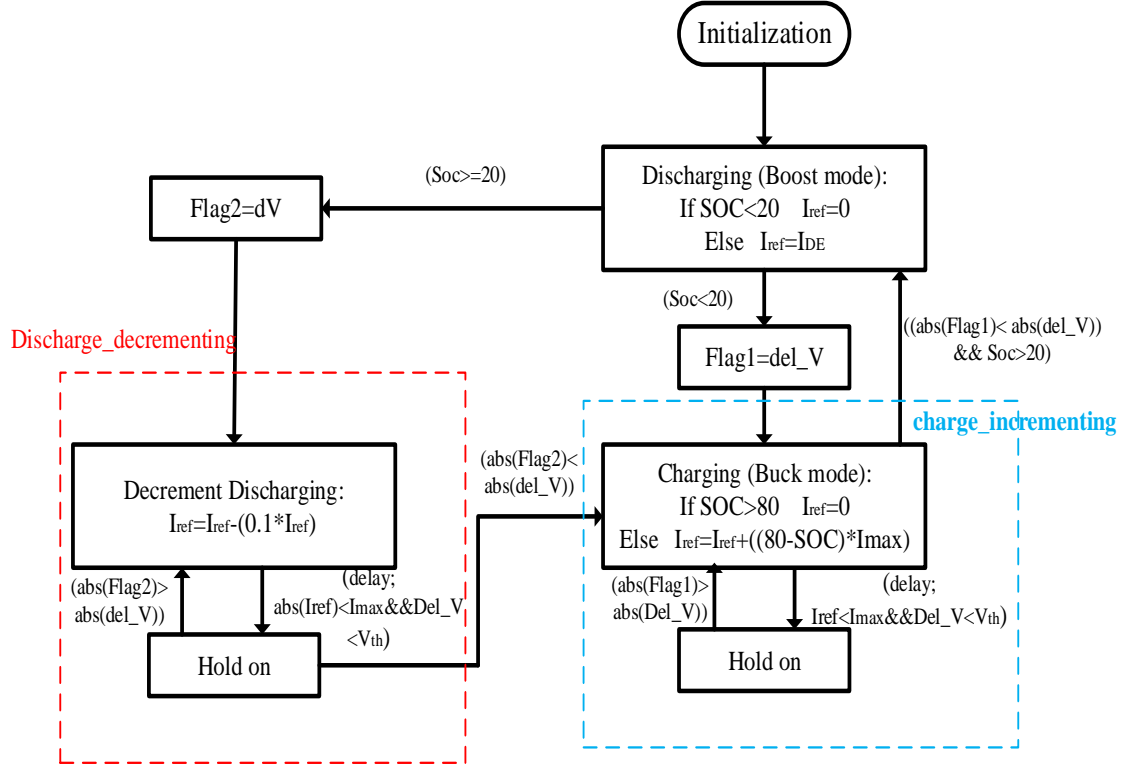
Figure 8.7: State machine Logic

The main function of the energy storage is to maintain the MVDC bus constant and to ensure load-generation balance. Mainly, the energy storage system will be used when there is a deficit in the generation, especially while feeding the intermittent pulsed loads. The charging of the batteries will occur when there is a surplus of energy that will be detected by the change of the bus voltage.

Once there is a change in the MVDC bus voltage, the state machine logic will be activated and receive the discharge reference current I_{DE}. To avoid unnecessary discharging of the batteries, the reference current I_{DE} will go to the discharge decrementing block, which will reduce the reference current and wait for a few microseconds. The change in

voltage will be detected after that waiting time (the delay). If the voltage has decreased by reducing the discharge reference current, this indicates that the system needs the support from the batteries. Therefore, the controller will stop decrementing the discharging current.

If the voltage did not change or it increased, this means that the generators are supporting this extra load. Therefore, the discharging current will be decremented till it reaches zero.

In the case of the increase in the MVDC voltage, the state machine will switch to the charging mode, where it will increase the charging reference current through the charge incrementing block. This block will increase the charging current, based on a pre-designed relation inside the state machine, then it will check the change of the MVDC voltage after each increment to ensure that the charging of the batteries does not negatively impact the voltage of the MVDC bus. If the *SOC* of any battery is below 20%, this battery will not participate in the discharge process. Similarly, if the *SOC* of the battery is higher than 80%, this battery will not participate in the charging process.

8.6   Testing of the Proposed Control Algorithm

To validate the proposed controller, it was implemented and tested in the notional MVDC system given in Figure 8.3. To test the ability of the controller for proper power sharing, it is assumed that the storage system consists of two large batteries. Each one of them has a rated capacity of 800 Ah and a nominal voltage of 800 V. The batteries are assumed to have a maximum current of 2400 A. The validation is performed under different loading conditions and different state of charges of the batteries.

8.6.1 Controller Performance with Equal SOCs of the Batteries

First the controller performance is tested when the two batteries have equal state of charge of 50% of their capacities. Figure 8.8 shows the loading connection/disconnection process, where there is a propulsion system load of 6400 A connected to the system at the beginning. The system continues to start operation. At t=0.7 sec, service loads of 1000 A are added to the system. It is worth mentioning that the generators can feed loads up to 8000 A when the generators reach their maximum capacities. Therefore, as long as the current is less than 8000 A, the batteries should not supply any current.

At t=1.5 sec, a radar system load of 600 A is added to the system. From 1.5 to 2 seconds, the generators are working at their rated power. Figure 8.9 and Figure 8.10 show that during this period (0-2 seconds), the batteries are idle. At t=2 sec, a pulsed load of (400 A) is added for one second. Since the generators are already running at their rated capacities, the batteries should supply the extra load to ensure load-generation balance. This is shown in Figure 8.9 (a), where the two batteries start to discharge. This is also verified by the decrease in the SOCs in Figure 8.10. Since both batteries have the same initial SOC, Figure 8.9 (a) shows that both batteries feed the same amount of current. This ensures equal load sharing among the batteries and increases the lifetime of the system.

It is worth mentioning that a high current of 1000 A is drawn from the batteries because they are connected at the low-voltage side of the converter, and the discharge of the battery is associated by a decrease in the battery voltage, as shown in Figure 8.9 (b). After the pulsed load is disconnected at t=3 sec, the batteries are smoothly disconnected as well since the generators can feed the existing loads. At t=3.5 sec, another load is disconnected, which means that there is a surplus of energy that can be used to charge the batteries. Therefore,

the batteries are smoothly connected again but in the charging mode in this case. Figure 8.9 (a) shows that the currents of the batteries become negative (which means charging) after t =3.5 sec. Both batteries charge with the same current, which is desirable. Figure 8.9 (b) shows that the voltages of the batteries increase after t= 3.5 sec. The charging process is also confirmed by the increase in the SOC, as depicted in Figure 8.10. Finally, Figure 8.8 (a) shows that regardless of the different loading condition on the ship power system, the MVDC bus voltage is kept constant and within the standards.
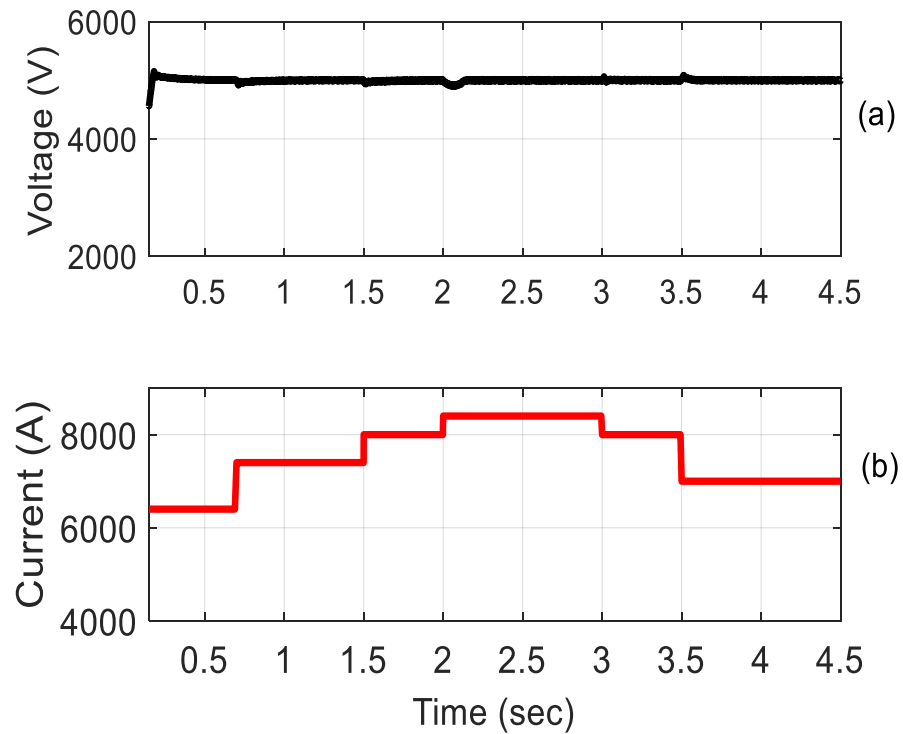
Figure 8.8: Case of equal SOCs a) The MVDC bus voltage. b) Total load current.
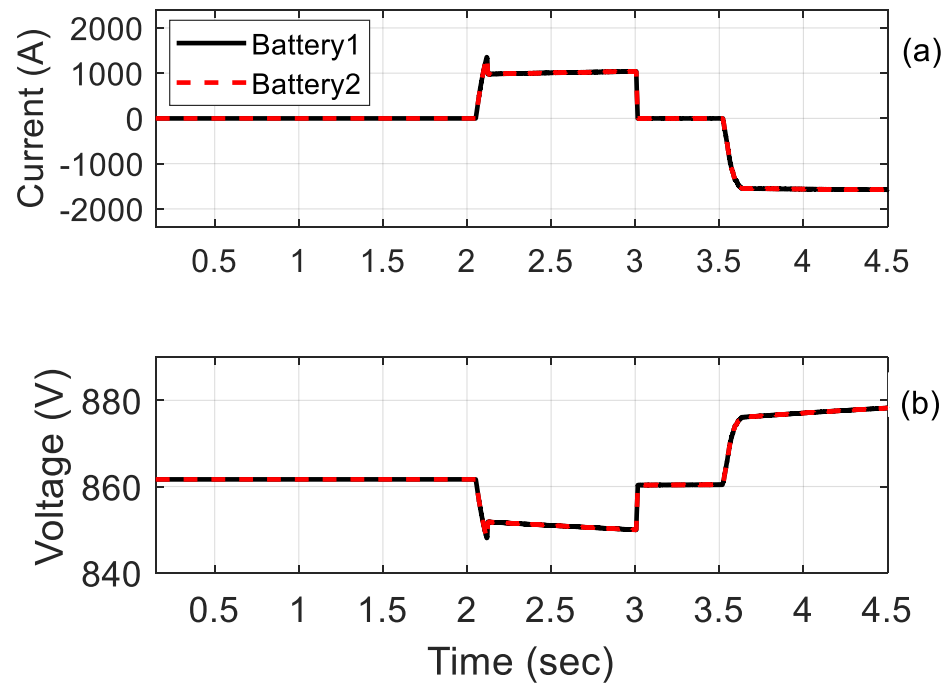
Figure 8.9: Case of equal SOCs a) Battery current. b) Battery voltage.
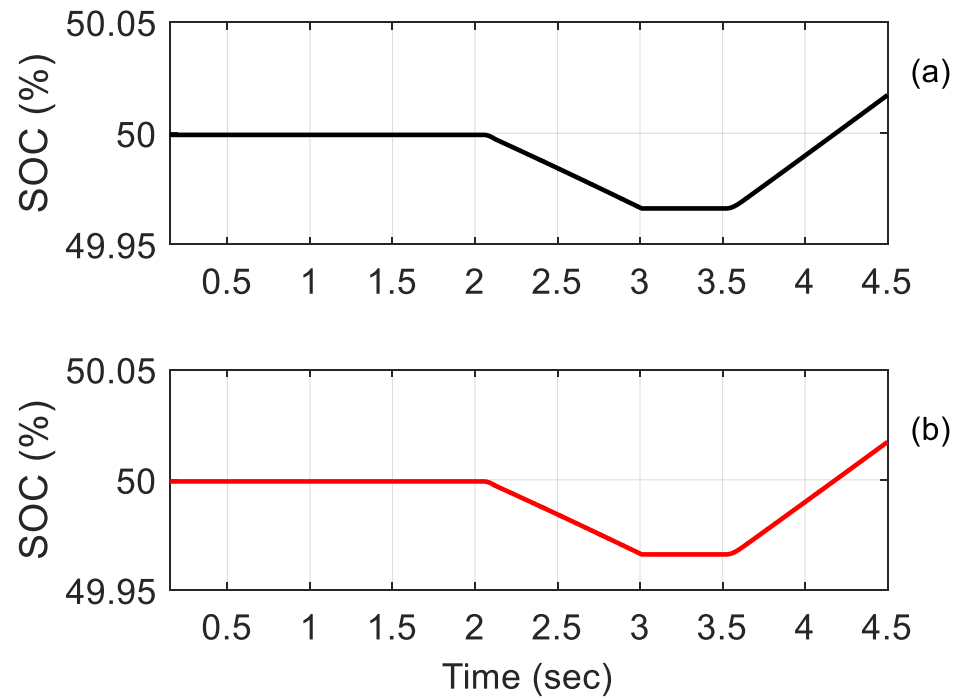
Figure 8.10: Case of equal SOCs a) SOC of battery 1. b) SOC of battery 2.

193

8.6.2 Controller Performance with Different SOCs of the Batteries

In this test, the same loading conditions are applied but the initial SOC of the two batteries are different, where the first battery has a higher initial SOC of 75% of its capacity while the second battery has only 45% of its capacity. The same loading conditions of the previous section are applied. Figure 8.11 (a) shows that the MVDC bus voltage remains constant with the different loading conditions, which confirms the good performance of the controller in the case of different SOC of the batteries.

At t= 2 sec, when the pulsed load is connected and the generators can no longer support this extra load, the two batteries start to discharge to maintain the load-generation balance. Since the first battery has a higher SOC, its contribution in supporting the system is higher, as shown in Figure 8.12 (a), where the discharge current of battery 1 is 1500 A while the discharge current of battery 2 is 400 A. This is also shown by the difference in the drop of the battery voltage in Figure 8.12 (b), where the drop in the voltage is higher for battery 1 compared to battery 2.

The decrease in the SOC of the batteries during the period 2-3 seconds is shown in Figure 8.13. At t=3 sec, the pulsed load is disconnected. Therefore, the batteries are disconnected as well. At t=3.5 sec, when another load is disconnected, both batteries start to charge. However, since battery 2 has lower SOC, its charging current is higher than that of battery 1, which is desirable. Figure 8.13 depicts the increase of the SOC of the batteries after t=3.5 sec. It illustrates that the rate of the increase in the SOC is higher for battery 2 compared to battery 1. This is due to the higher charging rate of battery 2.
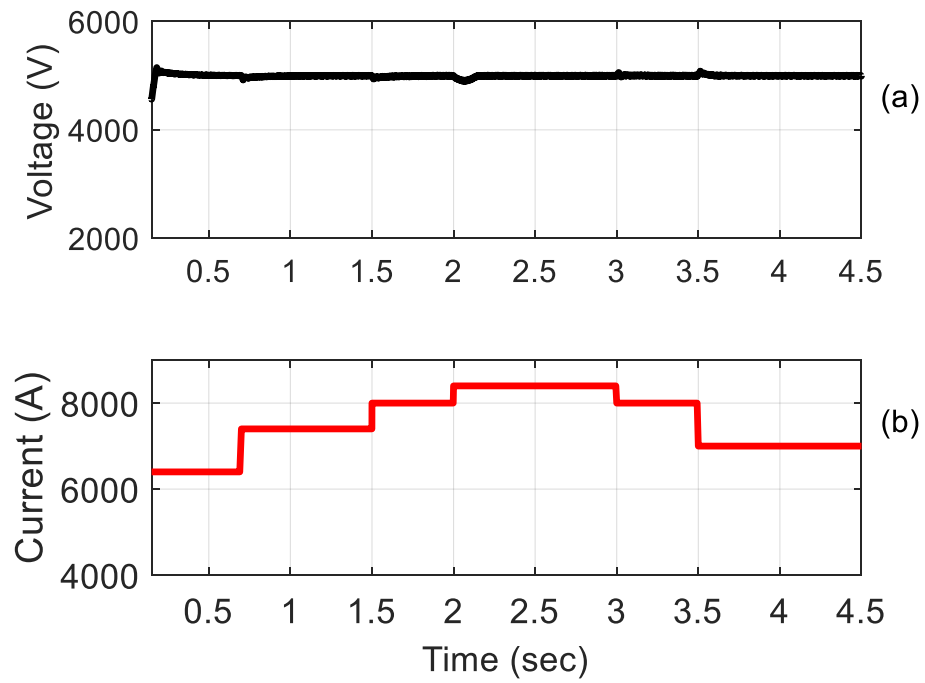
Figure 8.11: Case of different SOCs a) The MVDC bus voltage. b) Total load current.
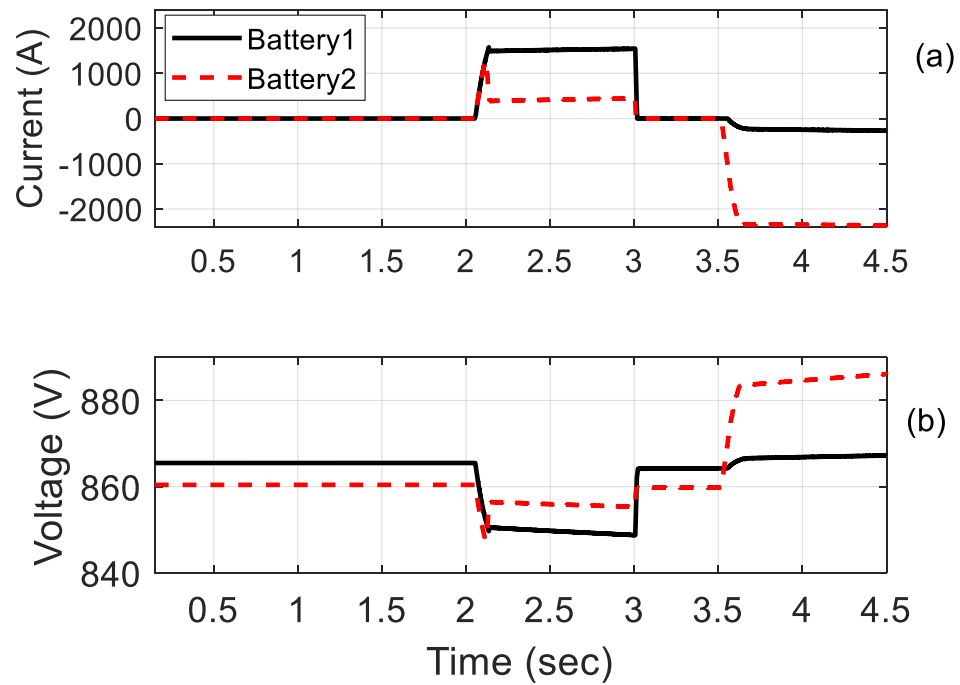
Figure 8.12: Case of different SOCs a) Battery current. b) Battery voltage.
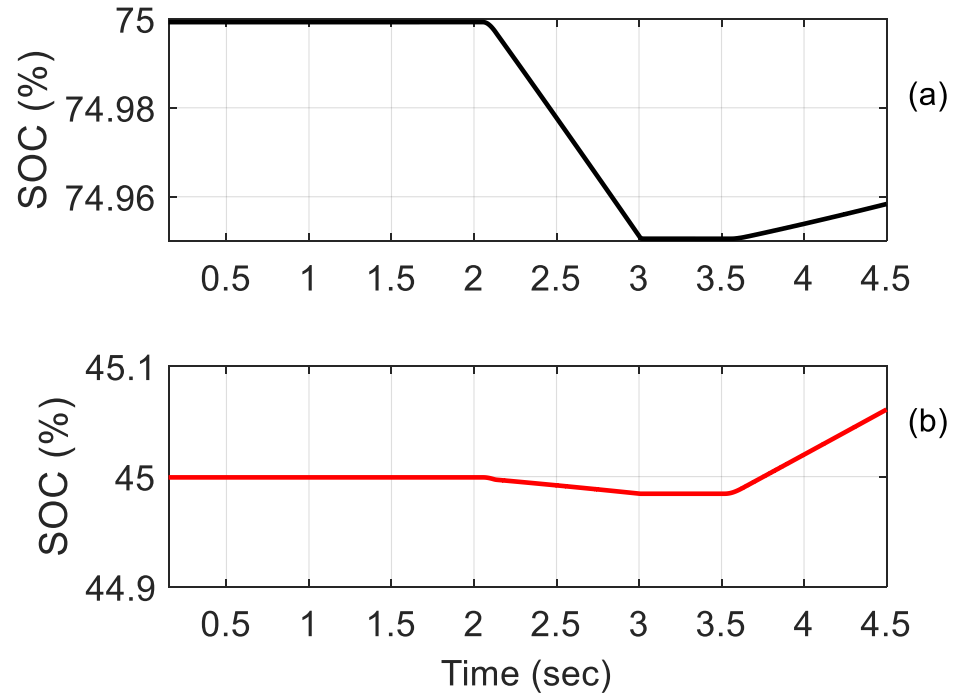
Figure 8.13: Case of different SOCs a) SOC of battery 1. b) SOC of battery 2.

8.7 Conclusions

In this chapter, an overview of the advantages and the components of a maritime MVDC ship power system is presented. Also, an initial validation of an automated decentralized controller for the onboard battery storage in the presence of pulsed loads is proposed. The controller is based on a combination of virtual impedance droop control and SOC exponential control to support the system and ensure proper power sharing. State machine logic was used to avoid unnecessary discharging of the batteries. The results showed that the controller ensures load-generation balance, and the voltage of the MVDC is kept constant. It also ensures proper power sharing among the batteries, which increases the system lifetime. This is also important for the reliable and economic operation of the ship board power system.

196

Chapter 9   Decentralized Control Algorithm for the Hybrid Energy Storage of

Shipboard Power Systems

This chapter proposes a decentralized control algorithm for the future MVDC shipboard storage system to enhance the onboard survivability. This chapter provides a more comprehensive control strategy that aims at coordinating the charging of a hybrid energy storage, consisting of multiple batteries and supercapacitors.

The control algorithm takes decisions based on local measurements, which makes it robust against cyber-attacks and able to provide fast response. The voltage profile of the MVDC bus has sufficient information about the system status, which is utilized for managing the hybrid energy storage system. Insertion/removal of the storage devices, such as batteries and supercapacitors, is made according to the mathematical morphology-based voltage processing and state-machine logic algorithms. To ensure proper power sharing, an adaptive droop control is used, taking into consideration the state-of-charge of the storage units. FPGA in the loop validation results confirm the ability of the proposed controller to maintain the MVDC bus voltage and the adequate operation of the storage entities simultaneously.

9.1   Introduction

As mentioned in the previous chapter, the MVDC power system has become the preferred solution for future all electric ships (AES). This stems from the fact that future AES will have new types of emerging loads that are mostly DC loads. Also, it allows efficient operation of the generators, since it eliminates the need for synchronization among the different generators [195]. Due to the high ramping rate of the emerging pulsed loads

on the AES, currently used diesel or gas-driven generators do not have the capabilities to feed them [196]. Although the ramp-rate of these generators can be relaxed to follow the behavior of the pulsed loads, the lifetime of these generators will be severely reduced due to the wear and tear [197], [198]. Therefore, storage devices on a MVDC shipboard are going to play a vital role in the successful operation of the MVDC ship power system. To study, control and analyze future MVDC systems, authors started to develop models and designs of future AES. Designing and modelling of a MVDC AES was considered in [196], [199]. In [199], for example, a model for the shipboard MVDC power system for dynamic analysis was proposed. The authors suggested an analytical time domain modelling technique to facilitate the analysis of the generator transient.

Also, several types of controllers have been proposed to ensure load-generation balance on the MVDC power system. The MVDC ship power system with energy storage devices and pulsed loads was considered in [200], [201], where centralized controllers were proposed to manage the charging/discharging of the hybrid energy storage system. Using the information about the currents of the generators and loads, the controller decides on reference values for the hybrid storage system. In [202], [203], the authors proposed a model predictive centralized controller to coordinate the operation of the energy storage devices. The main purpose of the controller was to mitigate the fluctuations in the propulsion system. In [204], a centralized controller was proposed to manage the fault ride through-capability of the converters connected to the storage system. In [205], the author proposed a master-slave control technique to ensure proper power sharing among the interconnected converters. Nonetheless, the slave controllers cannot operate independently without the master controller, and they cannot react to the load power variation, which

reduces the reliability. Hierarchical control algorithms were proposed in [206]–[208] to manage the power flow. In [206], a hierarchical optimization technique was used to control the power flow in the presence of pulsed loads. However, the issue of managing hybrid energy storage devices with different characteristics was not considered. In [207], a cooperative asymmetrical droop controller was used to allow the gensets of the MVDC power system to work in their most efficient operational points, while the hybrid energy storage system was used to absorb the fluctuations. No pulsed loads were considered, and the power sharing among storage devices of the same type was not considered as well. In [208], the authors focused on the higher layer of a hierarchical control architecture for managing the energy allocation to meet the ramp rate of load devices. It collects data from the generators and the loads to decide on the participation of the storage system. In [209], the authors investigated the mutual interactions of the LVAC and MVDC networks, taking into consideration the effect of distributed control actions where information is exchanged among neighbors in the control network. Energy storage was not considered.

Generally, centralized and hierarchical controllers ensure the optimal use of resources on the ship. However, the cost and the complexity of the controller increase nonlinearly as the number of system components increases. Also, there is always the risk of communication failure with the higher-level controller. This is of significant importance in mission-oriented applications, especially in the presence of the current issues of cyber-attacks. Therefore, decentralized controllers have become a potential solution for these issues. Due to the need for an automatic control algorithm [192] that ensures smooth insertion/ removal of loads, this chapter proposes a decentralized controller to manage the charging/discharging of multiple hybrid energy storage systems. The proposed controller

aims at ensuring load-generation balance and proper operation and power sharing among

the different storage devices. To be able to decide on the proper use of the storage devices,

the controller does fast signal processing of the voltage signature of the MVDC bus, and

to ensure adequate power sharing, the controller uses an adaptive droop controller to decide

on the current reference of the different storage devices. The controller was validated using

FPGA in the loop to ensure its effectiveness.

9.2   Test-Bench System

In this chapter, the previously used notional MVDC system is expanded to include the

batteries, as well as the supercapacitors. The expanded system is shown in Figure 9.1, and

details about the rated power of the different components are given in Table 9.1. A

simplified circuit diagram of the system is also shown in Figure 9.2. The parameters of the

circuit are depicted in Table 9.2.

Table 9.1: MVDC system parameters

Type	*Quantity*	*Power (MW)*	*Maximum Current*
Main Generators	2	36	7200
Auxiliary	2	4	800
Propulsion Motors	4	32	6400
Radar System	1	3	600
Service Loads	-	5	1000
Pulsed Loads	1	2	400
Batteries	2	-	±1600
Supercapacitor	2	-	±2400
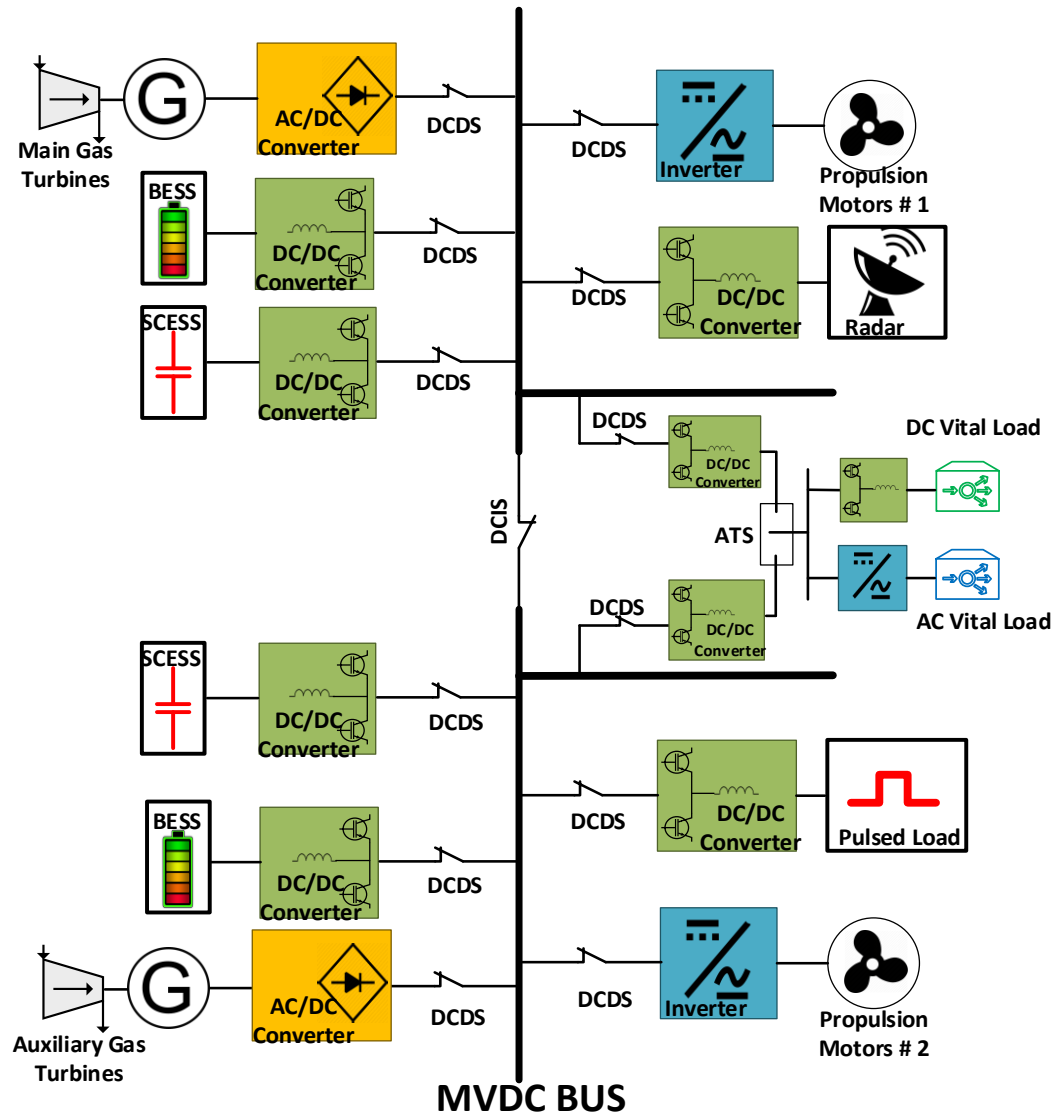
Figure 9.1: Expanded notional MVDC ship power system
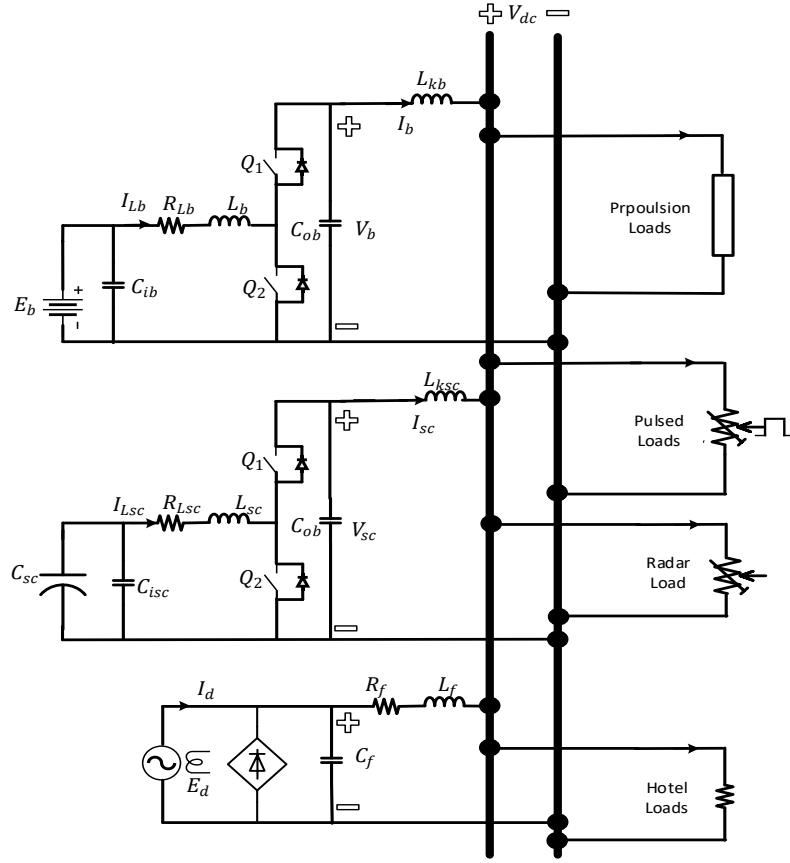
Figure 9.2: Simplified circuit of the system

Table 9.2: MVDC circuit parameters

E_b	800 V
C_{ib}	6000 μF
R_{Lb}	0.125 Ω
L_b	6.35 mH
C_{ob}	1200 μF
L_{kb}	30 μH
C_{SC}	100 F
C_{iSC}	6000 μF
R_{LSC}	0.125 Ω
L_{SC}	1.5875 mH
C_{oSC}	1200 μF
L_{kSC}	30 μH
E_d	4.16 kV
C_f	105 mF
R_f	.05 Ω
L_f	0.73 mH

9.3   A comprehensive Decentralized Energy Management

This section illustrates a decentralized controller, where each of the storage units has its own controller. The controller decides on the reference current based on the local measurements only. This reduces the complexity of the controller and results in a faster response. In addition, it is not vulnerable to cyber-attacks. The main objectives of the controller are ensuring constant voltage on the MVDC bus, proper load sharing, and proper use of the storage units. Proper use of the storage units means that the high ramping supercapacitors should be used during the transient periods due to their high-power density, while high-energy density components, such as the batteries, should be used during the steady state periods, when there is power deficit or surplus. Also, proper use means that the controller should avoid the overcharging or undercharging of the storage unit.

To achieve the abovementioned objectives, the controller consists of four main parts, as shown in Figure 9.3. These parts are the outer adaptive droop controller, state machine logic, mathematical morphological gradient algorithm (MMGA), and PI-based current controller. It is worth mentioning that the MMGA is used only for the management of the supercapacitors.

The purpose of the MMGA of the supercapacitor is to provide fast detection of the transient changes, and to clarify whether it is a load insertion or removal. MMGA is not used in the management of the batteries because steady state voltage changes can easily be detected by the state-machine logic, as it will be shown later.

Generally, the controller collects the voltage of the MVDC bus and the state of charge (SOC) of the storage unit. Then, it decides on the initial reference value I_{refx}. This value

is forwarded as one of the inputs to the state machine logic. The purpose of the state machine logic is to decide if this value will be passed or blocked based on the nature of the change in voltage, whether it is a transient or steady state change, and based on the limits imposed on the SOC of the storage unit. Once the final reference current $I_{ref,final}$ is obtained from the state machine logic, it will be compared to the output current of the storage unit $I_{inj,x}$. Finally, the error will be passed to a PI controller that will force the DC-DC converter to follow the reference value $I_{ref,final}$.
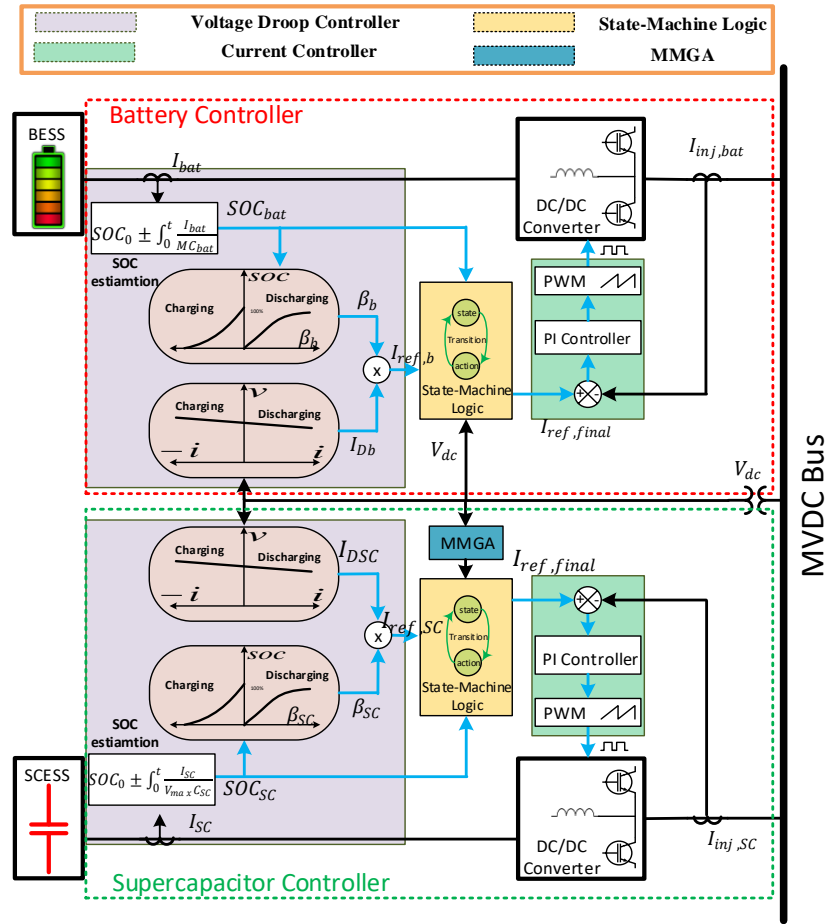
Figure 9.3: Controller schematic for the hybrid energy storage

Details about the different components of the controller are as follow:

9.3.1 Mathematical Morphological Gradient Algorithm

In order to detect the fast changes in the load, the MMGA is used to extract the high-frequency components of the voltage signal. Compared to the passive filter methods and integral based-techniques, the MMGA requires a smaller time window of few samples to capture the transients. In addition, the integral algorithms, such as Fourier Transform (FT) and Wavelet Transform (WT), depend on the conversion to the frequency domain, while MMGA deals directly with the time domain. MMGA depends on the set theory and uses the shape of the signal to extract the relevant feature structure. It has many applications in image processing [210].

MMGA has two basic morphological operators, dilation and erosion, which form a dual transform. The dilation operation is an expanded form of the input signal shape using a Structuring Element (SE). The erosion operation is a shrinking form of the input signal using the SE. The SE is a small set (shape) used to probe the signal. The SE has many shapes, like flat, square, circle and diamond. The selection of the SE shape depends on the application. In this work, as a signal processing tool, the flat shape is adopted as a structuring element (SE). The flat shape is a single dimension vector, where the length of the SE is chosen according to the required captured feature.

Mathematically, let f be an input signal with p samples and g is the SE with s samples, which is a fraction number of p. The dilation and erosion are defined as given in relations (9.1) and (9.2).

$$(f \oplus g)(p) = \max\{f(p + s) + g(s) \mid (p + s) \in D_f, s \in D_g\} \qquad (9.1)$$

$$(f \ominus g)(p) = \min\{f(p+s) - g(s) \,|\, (p+s) \in D_f, s \in D_g\} \tag{9.2}$$

where $\oplus$ and $\ominus$ are the dilation and erosion, respectively. The processed signal and the structuring element sampling are defined in D_f and D_g domains, respectively.

To detect the high-frequency components, the morphological gradient is utilized. It is defined as the arithmetic difference between the dilation and the erosion operations with the same SE. The morphological gradient G provides a depression for the steady state components (details) and an enhancement for the high-frequency changes (edges), and it can be defined as follows:

$$G(f) = (f \oplus g) - (f \ominus g) \tag{9.3}$$

One of the main advantage of the MMGA is that the SE can be defined to discriminate between the positive changes (ascending) and the negative changes (descending), which reveals the type of the change in the input signal. Therefore, MMGA can detect the nature of the change, whether it is load insertion or removal. Furthermore, the strength of the change is reflected on the magnitude of the gradient to provide more correlation with the filtration process.

9.3.2 Modified Droop Controller

The same design of the adaptive droop controller adopted in the previous chapter is used here. The values of the different constants are chosen in a way that makes the value of the modified virtual resistance much larger than the resistance of the line connecting the converters to the MVDC bus [211] to ensure equal power sharing.

Once the reference current $I_{ref,,x}$ is obtained, it will be fed to the state machine logic, which will take the final decision to pass or block this value.

9.3.3 Extended State Machine Logic

Since the characteristics of the storage devices are different, where the supercapacitors are high-power density devices and the batteries are high-energy density devices, there is a need for a decision-making algorithm that decides which one will be used and when. Therefore, state machine logic, as a decision-making tool, is used in this work. Because supercapacitors can discharge high amounts of power within a short period of time, it is recommended that it should be the storage device that is used during the transient periods. Batteries, high-energy density devices, are more suitable to react during the steady state periods, where there is a sustained deficit/surplus power in the system. In order to utilize the battery or the supercapacitor, two different state machine logics are implemented in the controller. The first one, shown in Figure 9.4, defines the battery charging/discharging decision logic. The inputs are the previously calculated reference current $I_{ref,b}$, the battery's state of charge SOC_b and the bus voltage V_{dc}. The required output is the final value of battery reference current $I_{ref,final}$, which is initialized by zero. The algorithm has three states and each state has a decision (discharging, charging and no action). The algorithm iterates over time for the bus voltage V_{dc}. If the bus voltage $V_{dc} \leq V_{min}$ for a few microseconds, a power deficit is confirmed and a flag is up to indicate the need for power support. Then, the battery capacity is checked, and if SOC ≥ 20, the discharging process is initiated with $I_{ref,final} = I_{ref,,b}$. If there is not enough capacity, then the final battery reference is set to zero.

The discharging state is declared when $V_{dc} \geq V_{max}$ for a few microseconds. If such a state is detected, the second flag is up, and checking the battery capacity starts. If the SOC < 80, and surplus power in the system is confirmed, the charging process will start and $I_{ref,final}$ is equal to $I_{ref,b}$. The final state of no action is always active if the bus voltage is within the limits or the momentary transient occurs.

The second algorithm, shown in Figure 9.5, is applied for the supercapacitors' control. The supercapacitors' transactions mainly depend on three inputs, which are load insertion/removal detection, the pre-calculated supercapacitor's reference current and its state of charge. Like the battery logic, the supercapacitor has the same three decisions of charging, discharging and no action.

If the load insertion, through the MMGA, is confirmed and the supercapacitor has a good state of charge (SoC $\geq$ 20%), the discharging process is initiated. Otherwise, $I_{ref,final}$ is set to zero. Similarly, when the load removal is noticed, the supercapacitor's capacity is checked. If it has the ability to be charged (SoC < 80), the charging process is commenced and the final reference current is set to $I_{ref,SC}$. In case of no confirmation of the load insertion/removal, the controller assigns $I_{ref,final}$ to zero. The state machine does not have the ability to detect fast transients, therefore it needs a confirmation from the MMGA algorithm to know the time of the transient and its nature (addition/removal).

9.3.4 Stability Test

In this section, the stability of the proposed controller is investigated. A lumped state-space model of the system is given in equations (9.4) - (9.7), where $\hat{x}_x$ is the energy storage state vector, $\hat{u}_x$ is the input vector, and the major parameters are A_x and B_x.
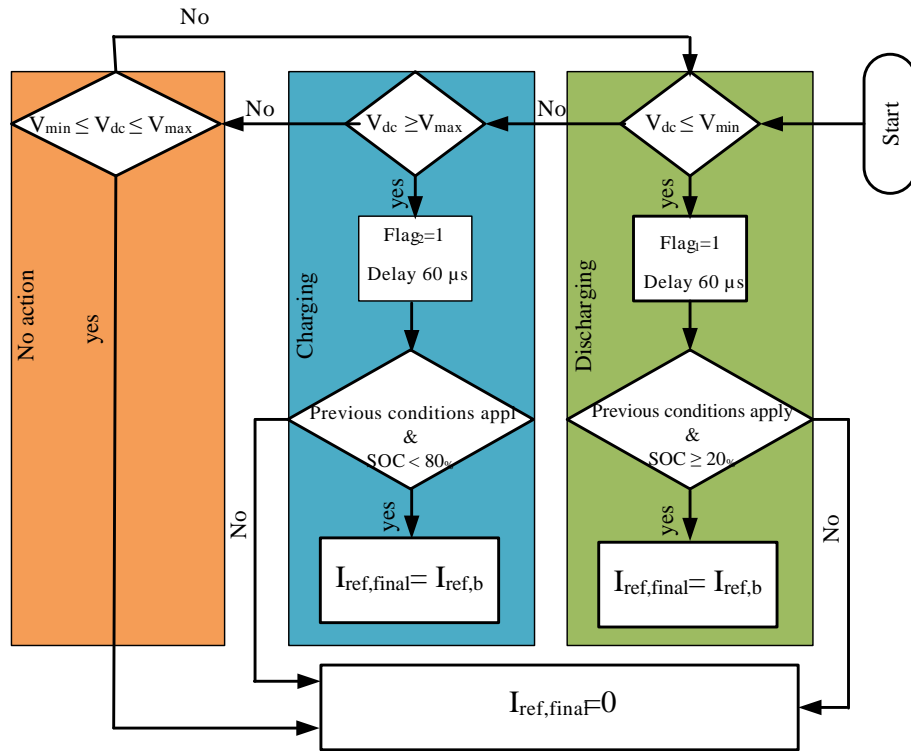
Figure 9.4: State-machine logic of the battery
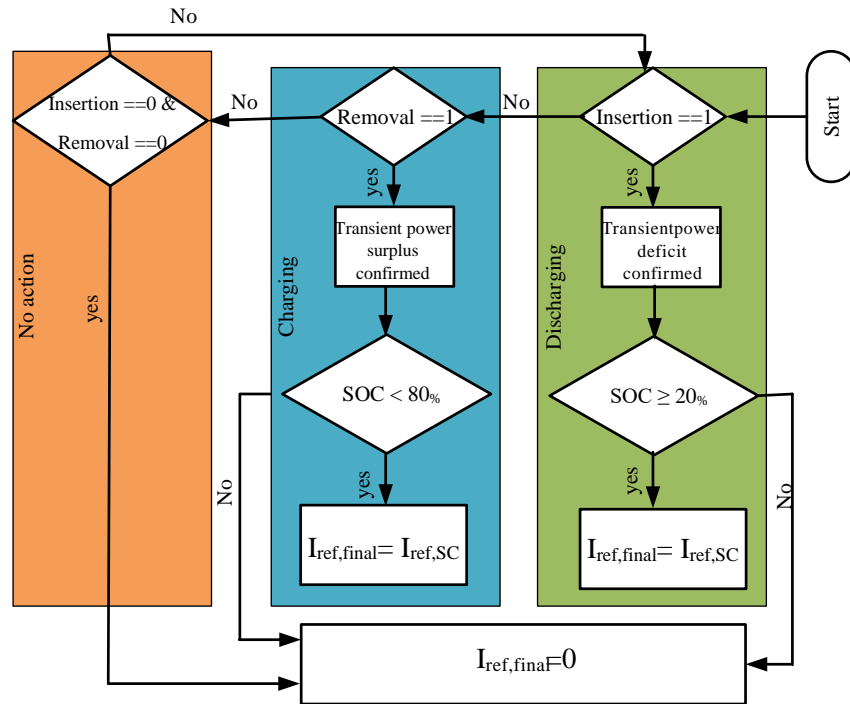
Figure 9.5: State-machine logic of the supercapacitor

$$\hat{x}_x = [\hat{I}_{Lx} \quad \hat{V}_{ix} \quad \hat{V}_x \quad \hat{I}_x]^T \tag{9.4}$$

$$\hat{u}_x = [\hat{D}_x \quad \hat{V}_{dc}]^T \tag{9.5}$$

$$A_x = \begin{bmatrix} \dfrac{-R_{Lx}}{L_x} & \dfrac{-1}{L_x} & \dfrac{\overline{D}_x}{L_x} & 0 \\[2mm] \dfrac{1}{C_{ix}} & \dfrac{-1}{R_x C_{ix}} & 0 & 0 \\[2mm] \dfrac{-\overline{D}_x}{C_{ox}} & 0 & 0 & \dfrac{1}{C_{ox}} \\[2mm] 0 & 0 & \dfrac{-1}{L_{kx}} & \dfrac{-R_{kx}}{L_{kx}} \end{bmatrix} \tag{9.6}$$

$$B_x = \begin{bmatrix} \dfrac{\overline{V}_x}{L_x} & 0 & \dfrac{-\overline{I}_{Lx}}{C_{ox}} & 0 & 0 \\[2mm] 0 & 0 & 0 & \dfrac{1}{L_{kx}} & 0 \end{bmatrix}^T \tag{9.7}$$

The subscript x can refer to the battery or the supercapacitor. In order to ensure the stability, the system is perturbed around the operating point.

Figure 9.6 and Figure 9.7 show a comparison of bode plots for the small-signal model before and after applying the proposed controller for the battery and the supercapacitor, respectively. In Figure 9.6, the bode plot for the battery output voltage to duty cycle transfer function depicts that the system is unstable before applying the controller by recording $12.2\ dB$ for the Gain Margin (G.M) and $-72.3°$ for the Phase Margin (P.H). After applying the controller, the system becomes stable and the bode margins G.M and P.M are $11\ dB$ and $89.9°$, respectively. The bode diagram of the current control loop is shown in Figure 9.6 (b). It is modelled by the transfer function of the battery output current to the duty cycle. The figure shows the stable behavior of the current controller.
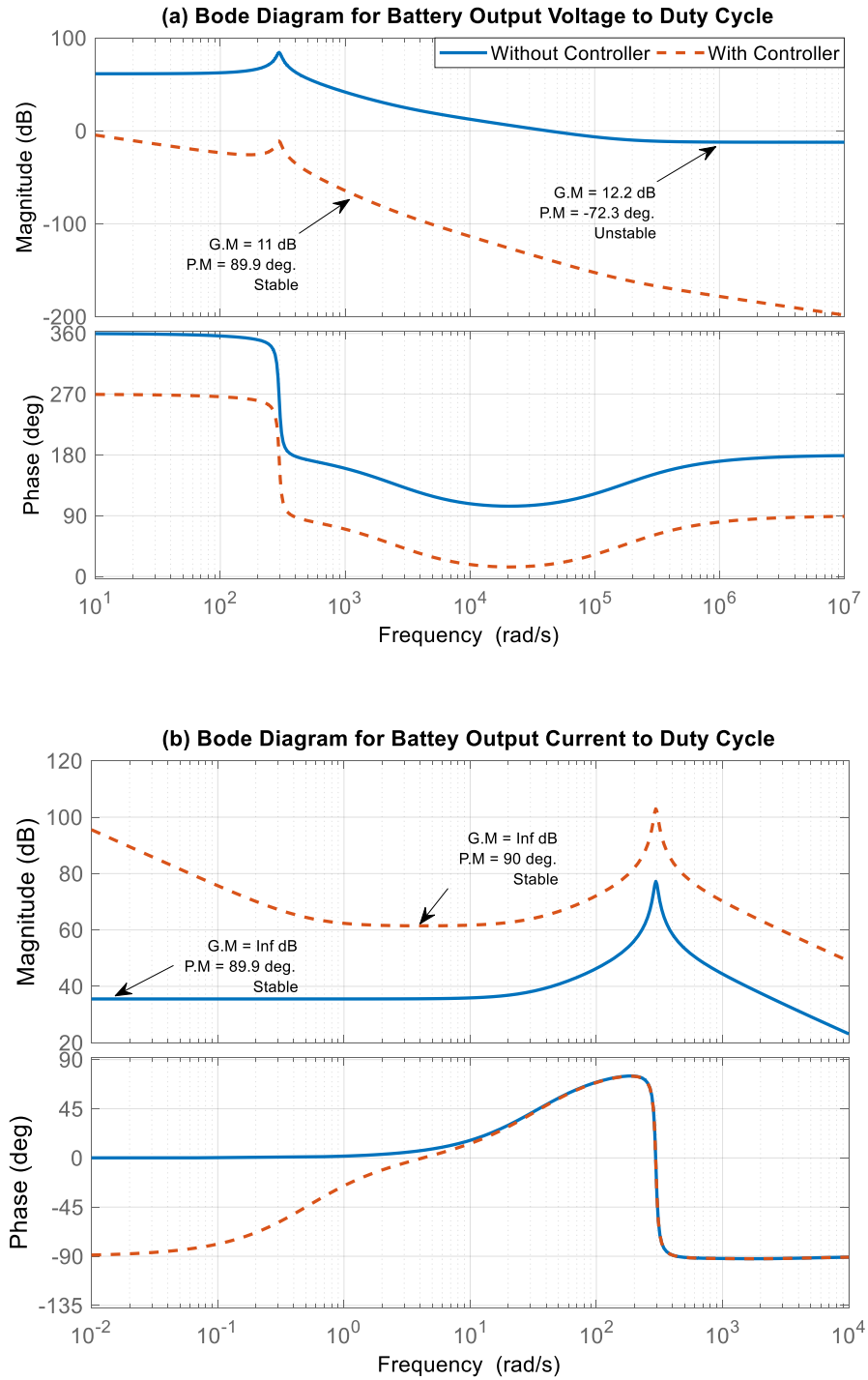
Figure 9.6: Bode plots for the battery storage stability performance before and after the controller

(a) Bode Diagram for Supercapacitor Output Voltage to Duty Cycle

G.M = 23.1 dB
P.M = 89.9 deg.
Stable

G.M = 12.2 db
P.M = -62.1 deg.
Unstable

(b) Bode Diagram for Supercapacitor Output Current to Duty Cycle

G.M = Inf dB
P.M = 90 deg.
Stable

G.M = Inf dB
P.M = 90 deg.
Stable
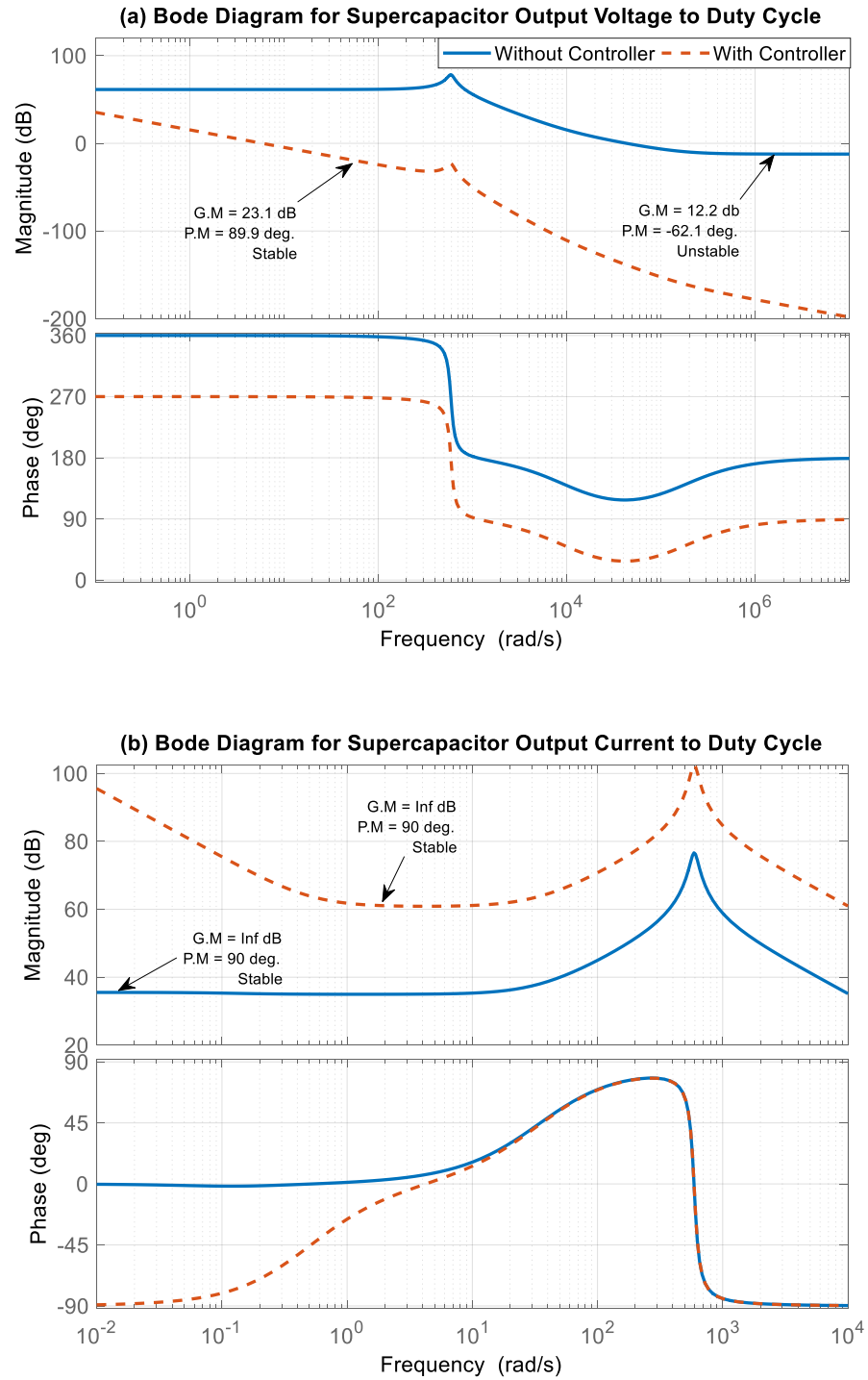
Figure 9.7: Bode plots for the supercapacitor storage stability performance before and after the controller

Similarly, the supercapacitor stability behavior is analyzed by deriving the transfer functions of the output voltage to duty cycle and the output current to duty cycle from the small-signal state-space model. Figure 9.7 (a) illustrates the unstable performance of voltage with respect to duty cycle change before applying the controller. Then, the controller reshapes the model to obtain a stable operation and approximately doubles the G.M and derives the P.M back to around 90°. The current control loop is already stable before the controller, but the steady state error is slightly improved after applying the controller, as shown in Figure 9.7 (b).

9.4   Results

The proposed controller is validated through FPGA in the loop, where the control algorithm is embedded on the FPGA chip, while the power components are on Matlab/Simulink. The connection between the FPGA and the PC is done through the JTAG connection. The used FPGA chip is a low-cost, small-sized FPGA module integrating a Xilinx Artix-7 and Quad-SPI flash memory for configuration and operation [212]. The numbers of look-up tables, flip flops and DSP capability, which are required for controlling one battery unit, are shown in Table 9.3. The complete design is composed in standard Vivado using VHDL for the Xilinx Artix-7 35T Arty FPGA. The top-level design of the controller in Vivado is shown in Figure 9.8. The FPGA is provided with a 25 MHz (40 ns) clock source to serve as the primary clock for all internal logic. All numerical operations in the engine are performed with fixed-point logic.

To show the merits of the proposed controller, it is compared to a conventional droop controller with a fixed pre-designed slope. The slope of the conventional droop controllers

213

is done assuming the existence of multiple storage units (two of each type in this work). The proposed and the conventional controllers are tested under the same loading conditions and SOCs of the storage units. Two cases are presented in this section to validate the performance of the controller.

9.4.1 Controller Performance in the Presence of Overcharged/Undercharged Batteries

In this case, one battery has 85% initial state of charge while the other one has 15% state of charge. The supercapacitors have equal SOCs of 50%. This is done to test the ability of the controller in maintaining the steady state voltage of the MVDC bus under extreme conditions.

Table 9.3: Resource usage of the proposed controller on the FPGA

Type	Utilization	%
LUT	5632	27.08
FF	5901	14.19
DSP	27	30
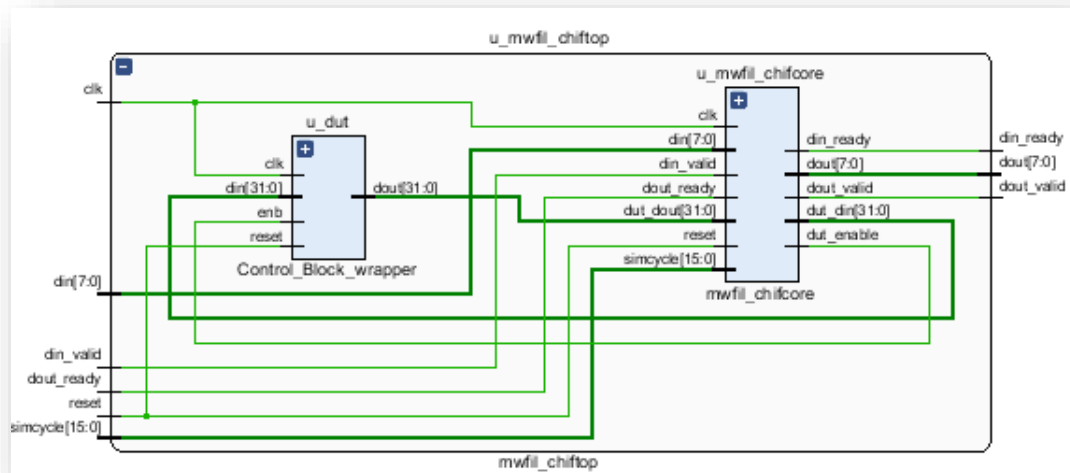
Figure 9.8: Top level design of the controller in Vivado

The loading conditions are shown in Figure 9.9 (a). The changes in the figure correspond to load additions at times t=0.7, 1.5, and 2 sec and load removals at t=3 and 3.5 sec. It should be noted that during the period t= 2 to 3 sec, a pulsed load of 1 MW is added, and the total system loading is beyond the capabilities of the generators.

Figure 9.9 (b) depicts the voltage of the MVDC bus under the different loading conditions. From the figure, it is obvious that the proposed modified droop controller results in a better steady state bus voltage especially during the period t=2-3 sec, while the conventional droop results in less voltage. This happens due to the steady state contribution of the batteries during this period, which is shown in Figure 9.10. Since one of the batteries (Battery 2) has 15% initial SOC, it cannot help support the system during this period. Therefore, the first battery needs to support as much as possible.

Since the conventional droop controller does not take into consideration the SOC of the storage units, its reference value depends only on the pre-designed slope. It is worth mentioning that the conventional droop controller is designed assuming the existence of two batteries. Therefore, the reference value of the first battery with the 85% SoC is of moderate current of 1000 A, which is not sufficient to support the system and maintain the MVDC bus at 5 kV. Unlike the conventional controller, the proposed approach takes into consideration the SOC of the battery and has a variable slope line. Since Battery 1 has sufficient energy, the reference current is set to a very high discharging rate of 1500 A. This is shown in Figure 9.10.

The advantages of taking the SOC into consideration also appear during the period t= 3.5-4.5 sec, where two loads were removed at t= 3 sec and t= 3.5 sec, which results in a power surplus in the system. During this period, the proposed controller charges the

215

undercharged battery (Battery 2) at a high rate compared to the conventional one, which is desirable. This shows the superiority of the proposed controller in maintaining the steady state MVDC bus voltage under severe conditions and achieving proper power sharing among the batteries.

During the period t=3- 3.5 sec, the currents of batteries are zero because the generation is equal to the load. The SOCs of the batteries are shown in Figure 9.11, where the effect of the differences in the reference currents is clear. The figure illustrates that the decrease in the SOC of Battery 1 is higher, in the case of the modified controller, during the period t= 2-3 sec, since the discharging current is higher. Also, the increase in the SOC of Battery 2 during the period t=3.5- 4.5 sec is higher because the charging current is higher.
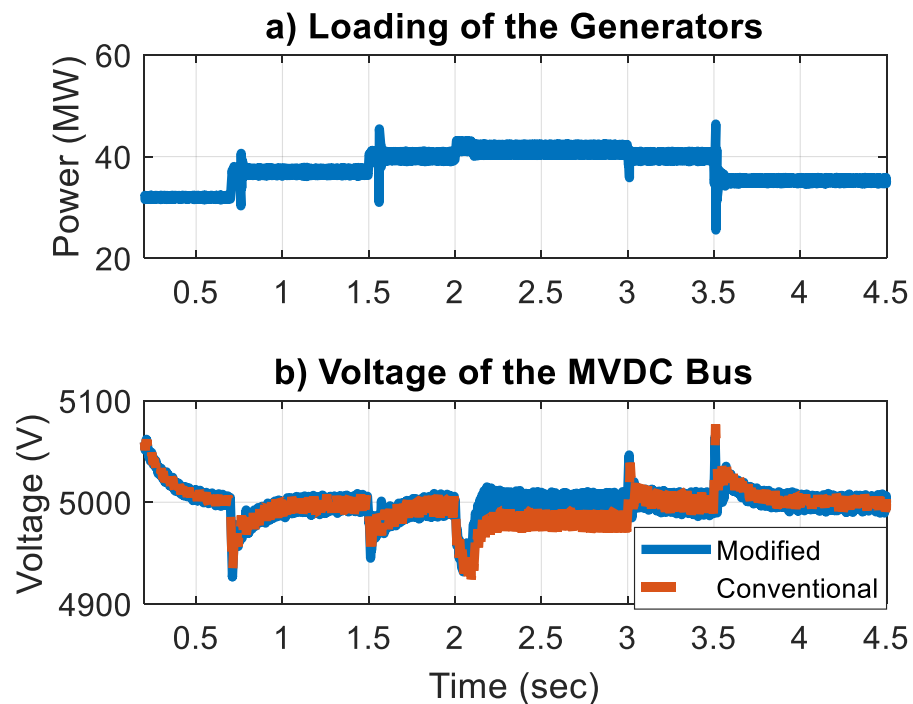
Figure 9.9: a) Loading Power.   b) MVDC bus voltage.

216
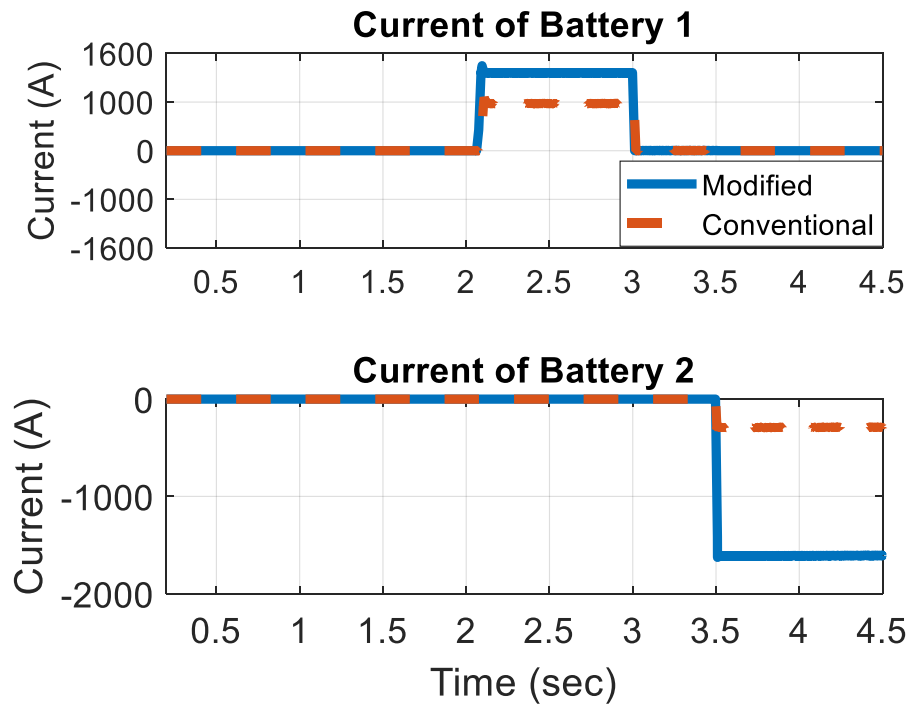
Figure 9.10: Output currents of the batteries
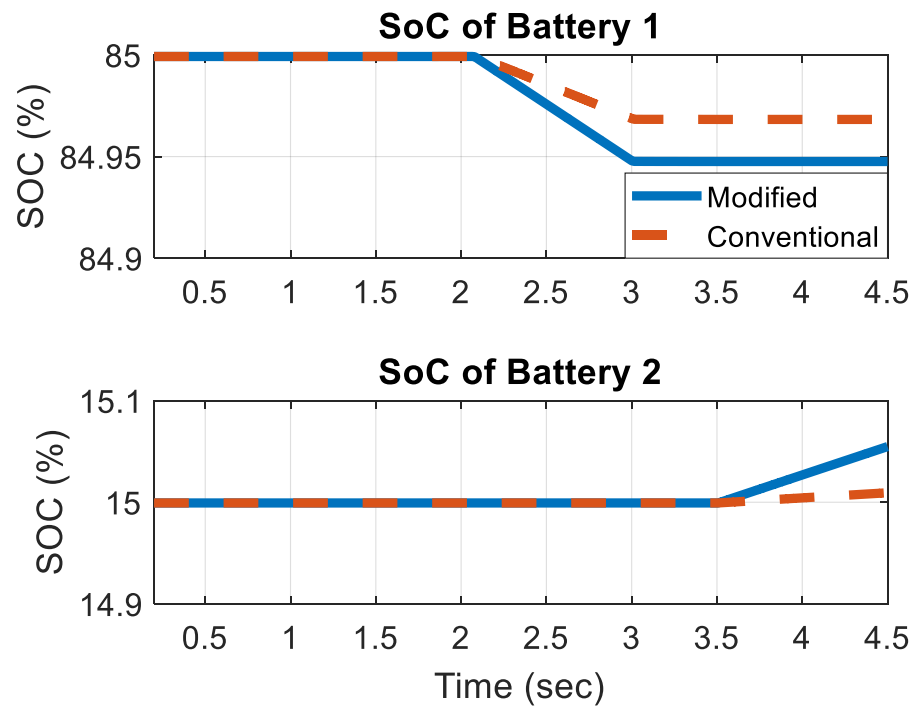
Figure 9.11: State of charge of the batteries

To show the functionalities of the state-machine logic and the current control loop, a comparison between the reference and the actual currents is shown in Figure 9.12. The figure illustrates how the actual discharging current of Battery 1 smoothly follows the reference signal coming from the state-machine logic. The same applies for the current of Battery 2 as well during the charging mode.

The performance of the supercapacitors is depicted in Figure 9.13 (a). The figure shows that the proposed algorithm is successful in achieving fast detection of the transient periods and the nature of load changes (load additions or removals). The figure shows that during the periods of load additions at t= 0.7, 1.5 and 2 sec, the supercapacitor discharges a high current to support the system, and during the period of surplus power at t=3.5 sec, it charges with a high current to absorb the surplus power.
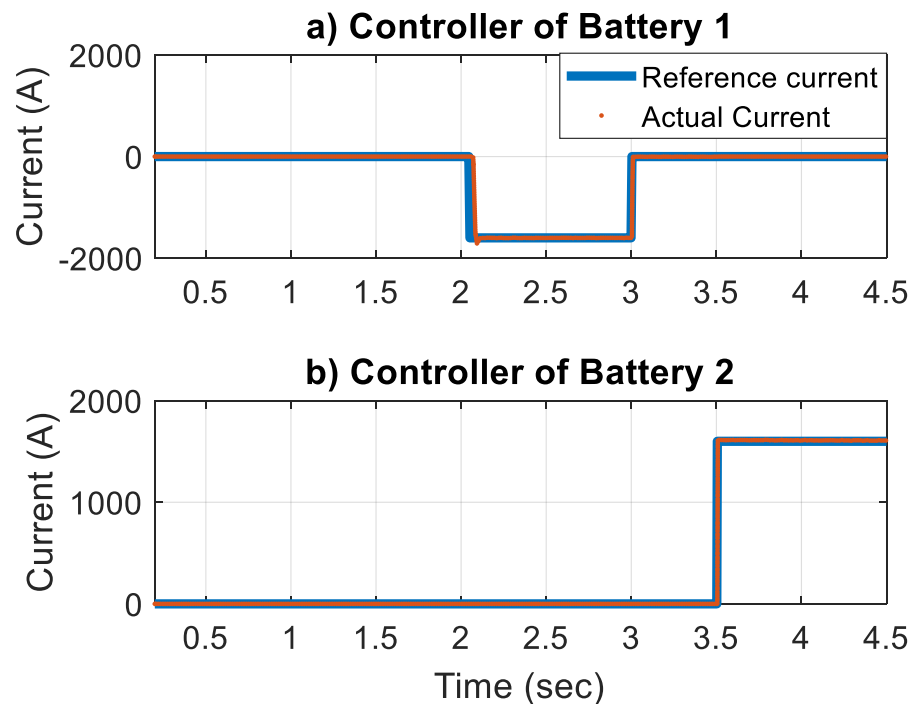
Figure 9.12: Reference and actual currents of the batteries for the case of the proposed controller

The conventional controller followed the same pattern as the proposed controller, with less currents except at t=2 sec, where the conventional droop sent a zero reference.

The SOC of the supercapacitor is shown in Figure 9.13 (b). The figure shows that the modified controller results in higher discharging/ charging current than the conventional controller. The results of one supercapacitor is shown here because both supercapacitors have the same behavior since they have the same initial SOCs.

To show the functionalities of the state-machine logic and the MMGA, Figure 9.14 illustrates the performance of the different blocks of the proposed controller of the supercapacitors. Figure 9.14 shows the reference current coming from the voltage droop control phase of the proposed controller, the final reference signal coming from the state-machine logic to the PI controller, and the actual current from the supercapacitor. Also, the triggering signal coming from the MMGA to the state machine logic is provided.
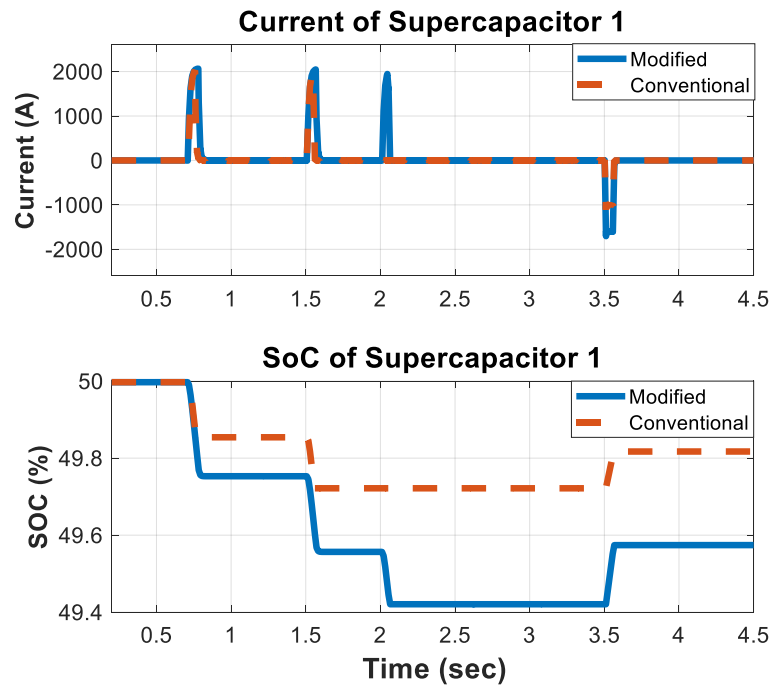
Figure 9.13: a) Output currents of the supercapacitors. b) state of charge of the supercapacitors

219
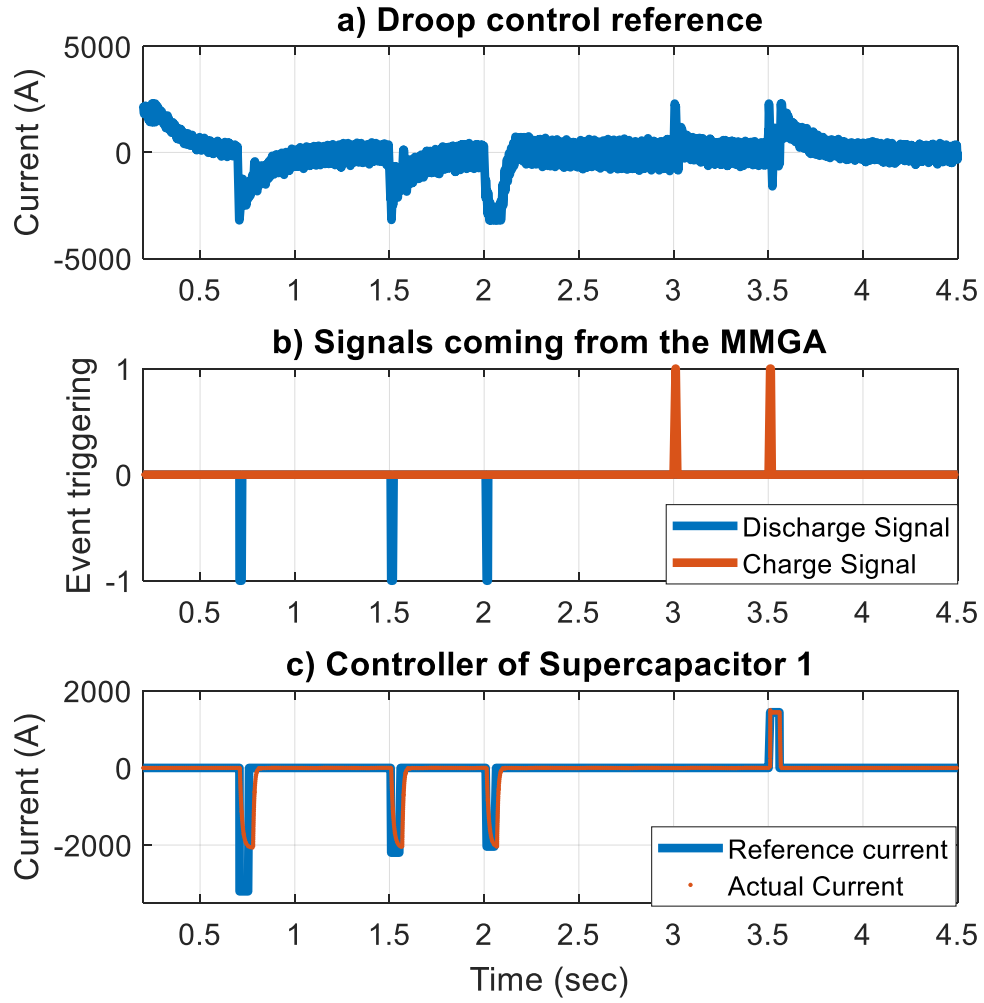
Figure 9.14: a) Output of the voltage droop block. b) Triggering of the MMGA block. c) Reference and actual currents of the batteries for the case of the proposed controller

Generally speaking, the supercapacitor is a high-power density storage device that should support the system during the transient period, where there is a high ramping load added/removed, and there is a need for the high power storage to match this high ramping.

Figure 9.14 (a) shows that the droop phase of the control algorithm always produces a reference signal, and this reference has high values during the load addition/removal instants at t= 0.7 , 1.5, 2, 3, 3.5 sec. Figure 9.14 (b) shows the triggering signals coming

from the MMGA to the state-machine logic. The function of the MMGA is to perform fast signal processing and to detect the transient changes and their types, whether it is a load addition or removal. The figure clearly shows that the MMGA is successful in detecting the load addition instants at t =0.7, 1.5, 2 second, as shown in blue in Figure 9.14 (b). Also, the MMGA is successful in detecting the load removal instants at t= 3, 3.5 sec, as shown in orange. This is reflected in generating the reference signals from the state-machine logic at the right instants and with the right mode (discharging or charging), as depicted in Figure 9.14 (c).

The state-machine logic does not generate a reference signal at t= 3 sec regardless of the fact that the coming signal from the MMGA is to insert and charge the supercapacitor, considering that there will be power surplus due to the load removal at this time instant. This happens because at this time instant, not only is there a load reduction, but also Battery 1 at this point is turned off because there is no need for supporting the system anymore. This reduces the amount of extra power in the system. In other words, the disconnection of Battery1 counteracts the load removal, making the total surplus power almost zero. Therefore, the MVDC voltage at this time instant witnesses a small and very fast over-voltage spike. This does not need any kind of support from the supercapacitor. That is why the state-machine logic produces a zero-reference signal during this time instant.

In terms of the comparison between the actual current of the supercapacitor and the reference signal, the actual current generally follows the reference signal at all the time instants except at t=0.7 sec. This exception happens because at this time instant, the state-machine logic results in a very high reference current that is beyond the maximum current that can be obtained from the supercapacitor. Since there is a saturation imposed over the

221

PI controller, it does not follow the reference signal and remains within the permissible level. It is worth mentioning that the PI controller is designed to give a maximum current of the supercapacitor of ±2100 A, while the coming signal from the state machine is -3200 A. The reference value of the state machine is based on the droop control phase that does not have any kind of constraints on the reference values. The saturation of the PI controller helps protect the storage device from discharging/charging excessive amounts of currents. This helps increase the lifetime of the storage device.

9.4.2   Controller performance in case of middle levels of SOCs

In this case, one battery has 65% initial state of charge, while the other one has 40% state of charge. The same applies for the supercapacitors. This is done to test the ability of the controller to maintain the voltage of the MVDC bus, and ensure proper power sharing among the storage units. The same loading conditions are applied here and shown in Figure 9.15   (a). As illustrated in Figure 9.15 (b), both the conventional and the proposed controllers are able to maintain the voltage of the MVDC bus.

However, a careful look at Figure 9.16 shows the advantage of the proposed controller. Since the first battery (Battery 1) has a higher initial SOC of 65%, it is expected that this battery will discharge more current when supporting the system is needed and be charged less in case of power surplus. Figure 9.16 shows that although the conventional droop controller maintains the voltage of the MVDC bus, it does not ensure proper power sharing among the batteries. Both batteries discharge/charge with the same currents (600 A), which is not desirable.

Unlike the conventional controller, the proposed one maintains the voltage of the MVDC

bus and ensures proper power sharing, where the highly charged battery discharges 887 A

during the period t =2-3 sec compared to 443 A from the less charged battery. During the

period t =3.5-4.5 sec, where there is a power surplus, the highly charged battery1 charges

at 857 A, while the less charged one is charged at 1413A. This is shown in Figure 9.16,

and its effect on the SOC of the batteries is witnessed in Figure 9.17.
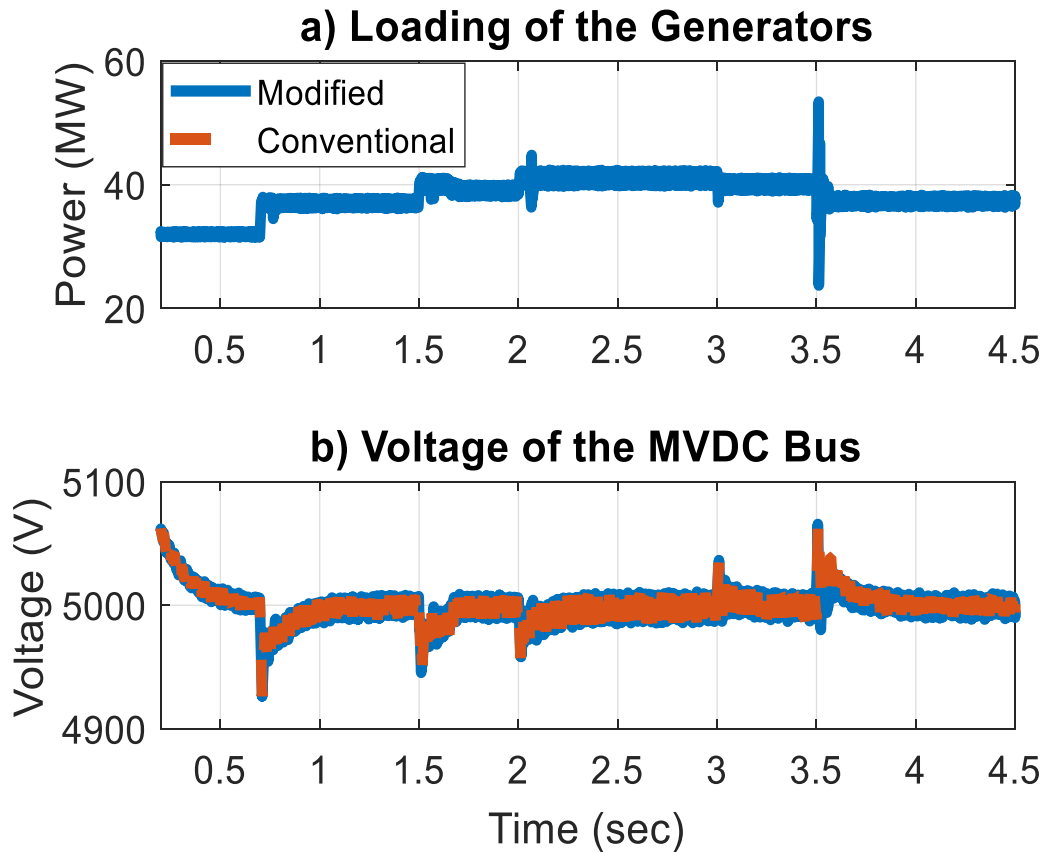
Figure 9.15: a) Loading Power.   b) MVDC bus voltage.
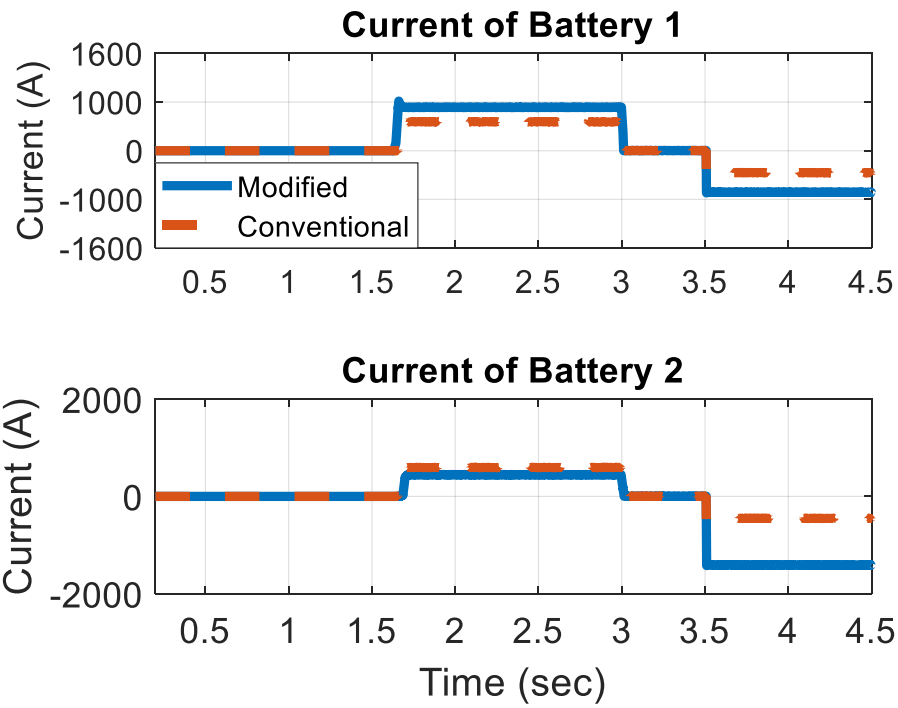
Figure 9.16: Output currents of the batteries
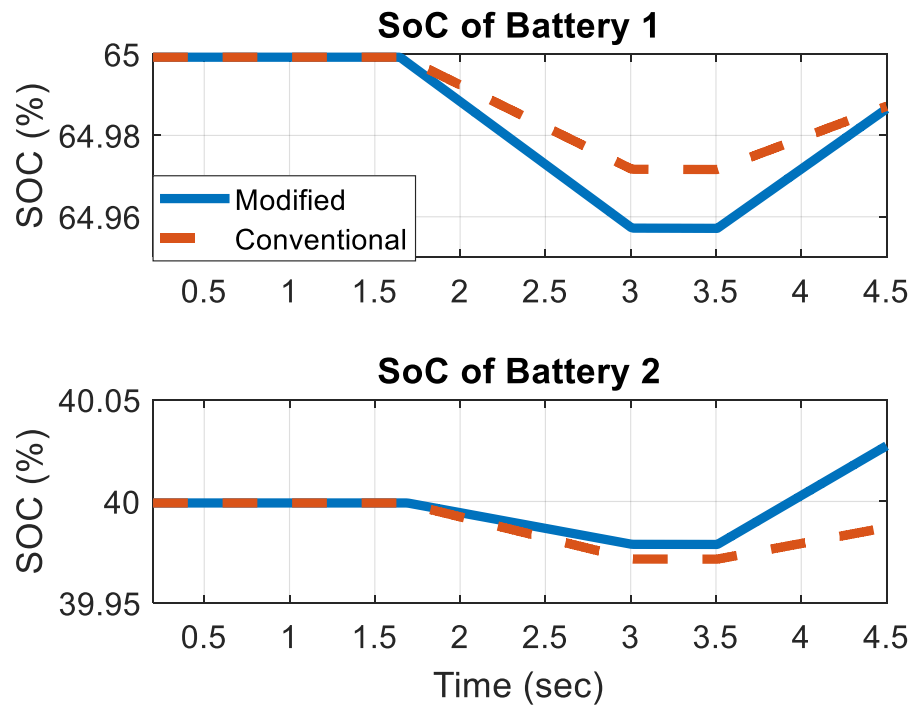
Figure 9.17: State of charge of the batteries

For the transient periods, Figure 9.18 depicts that the supercapacitors are inserted in the proper times and a good current sharing among them is also achieved using the proposed controller, where the highly charged supercapacitor discharges more current during the power deficit period and charges less current during the power surplus period compared to the less charged supercapacitor. The conventional controller followed the same pattern as the proposed controller, with less currents, neglecting the differences in the SOCs, except at t=2 sec, where the conventional droop sent a zero-reference value neglecting the small fast transient instant. Finally, the SOCs of the supercapacitors are shown in Figure 9.19, where the difference in the reference currents affected the rate of change of the SOC of the supercapacitors.
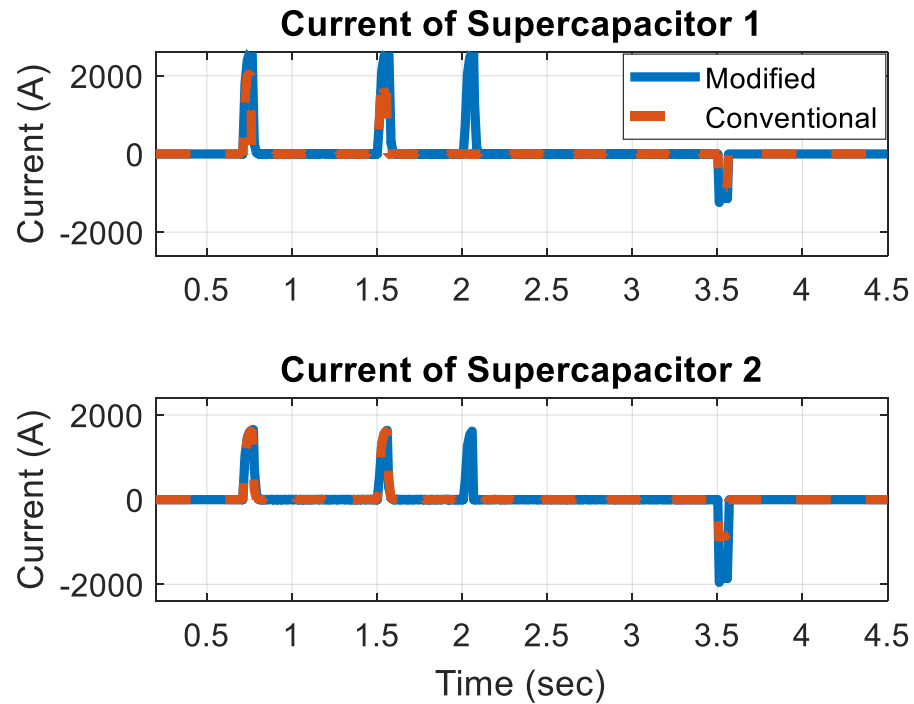
Figure 9.18: Output currents of the supercapacitors
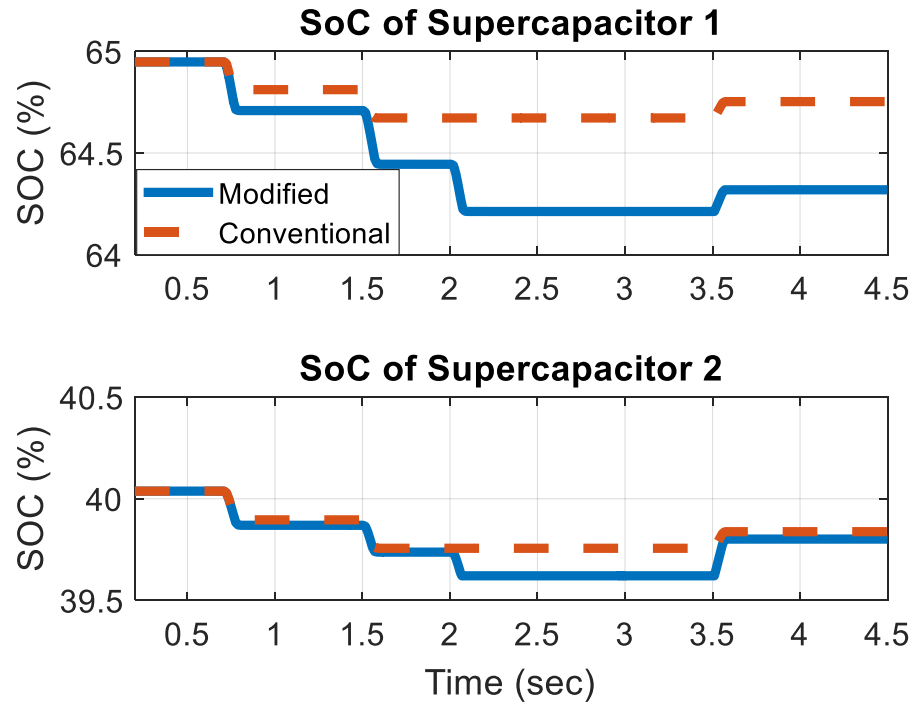
Figure 9.19: State of charge of the supercapacitors

9.5 Conclusions

In this chapter, a decentralized control strategy for the hybrid energy storage system, connected to a MVDC shipboard, is introduced. The proposed controller takes decisions on the local levels based on the SOC of the storage unit and the signature of the voltage at the MVDC bus. The controller employs MMGA and state machine logics to detect changes and decide on the addition/removal of the storage unit. The results showed the capability of the proposed approach in maintaining the voltage and ensuring proper power sharing among the storage devices. Also, it can successfully insert/remove the appropriate storage device during the transient and the steady state periods. In addition, the proposed controller was able to maintain the voltage of the MVDC bus in case of overcharged/undercharged storage unit, while not negatively affecting the storage devices.

Chapter 10   Intelligent Power Management for the Hybrid Energy Storage of the Ship Power System

This chapter tries to avoid the complexity of designing the adaptive droop-based controller by replacing it with a more intelligent fuzzy-based controller. Unlike the droop-controller, the fuzzy controller is easier to design through IF-THEN conditioning rules. In addition, the design of the fuzzy controller is done to differentiate between the normal conditions of the storage units and the case of overcharged/undercharged unit. This highly simplifies the design of the state machine logic in the next stage, removing the need of the state machine logic to check on the state of charge of the storage unit.

Also, the proposed technique in this chapter replaces the mathematical morphology methodology that was introduced before with a simple high-pass filtering process. This reduces the complexity of the computation and processing time of the controller.

The proposed algorithm is presented and validated on the same notional MVDC system introduced in the previous chapters with the same loading and operating conditions.

10.1 Introduction

Given the economic aspects and the slow response time of the gas-driven generators on the ship compared to the nature of pulsed loads, energy storage devices will be a corner stone in the successful operation of MVDC ship power systems.

In this chapter, an intelligent decentralized energy management algorithm for the onboard hybrid storage system is proposed. The chapter provides an alternative intelligent technique to the droop-based controller that was provided in the previous chapter. In addition, the proposed intelligent algorithm replaces the mathematical morphology algorithm by using

a simple high-pass filter to differentiate between the high and low frequency components of the voltage signal. The objective of the algorithm, in this chapter, is to ensure load-generation balance in the presence of pulsed loads and maintain the voltage of the MVDC bus within acceptable limits, according to the IEC 60092-101 standards[192][193][194]. Also, the proposed technique aims at ensuring proper power sharing among the storage devices and avoiding deep-discharging or over-charging of the storage devices using the intelligent fuzzy system. The proposed technique is validated on a notional MVDC power system that involves different sources and loads.

10.2 A comprehensive Decentralized Energy Management

Due to the inevitable presence of pulsed-loads on an AES MVDC bus, to maintain load-generation balance, the management strategy is required to have certain functionalities. As mentioned earlier, gas-driven generators are not cost-effective when used to feed temporarily pulsed loads. Also, they have a slow response time, in the range of 8-12 secs. Therefore, energy storage systems will be the main source for feeding the pulsed-loads. It is, thus, necessary that under all operating conditions, the strategy maintains load-generation balance, ensures proper power sharing among the storage devices on the ship, ensures the proper use of the storage type, and avoids unnecessary charging/discharging of the storage unit (to increase their lifetime).

To satisfy the aforementioned requirements, in this chapter, an intelligent decentralized controller is proposed. A decentralized controller was implemented due to its ability to make decisions on the local level (in the test system, by processing the local voltage and SOC measurements of energy storage devices) without the need to communicate with other

components of the system. The decentralized nature of the proposed controller reduces the computation burden, the fact that makes it adequate for real-time operation.

As shown in Figure 10.1, the proposed controller is composed of three parts. The first part is a Fuzzy Inference System (FIS). The FIS decides on the charging/discharging reference set-points of the batteries and the supercapacitors. The second part is the filtered voltage signal. In this work, a high-pass filter is used to distinguish between the high-frequency transient needs and the low-frequency steady state needs. On one hand, the output signal after filtering the voltage of the MVDC bus (V_{HP}) is used to control the insertion/removal of the supercapacitor. This is done because supercapacitors are high-power components, which have the ability to charge/discharge high currents to support the system during the transient times.

On the other hand, the difference (V_{diff}) between the original voltage measurement of the MVDC bus and the filtered one will represent the steady state needs. Therefore, it is used to control the insertion/removal of the batteries, which are high-energy density. The third part of the controller is the state-machine logic. This part of the controller is important because it is responsible for the further processing of the output of the FIS and the filtered signals, deciding if the charging/discharging processes will actually occur based on the need of the system or not to avoid unnecessary usage of the energy storage devices.
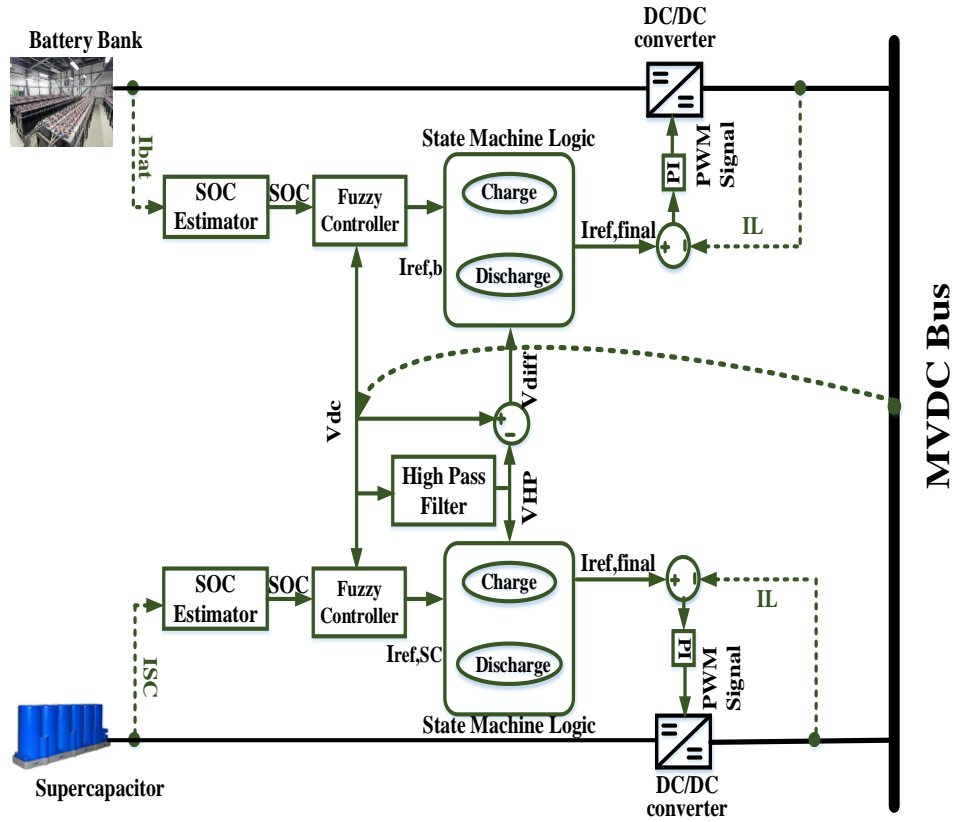
Figure 10.1: Proposed controller block diagram

Details about the different components of the proposed strategy and their design are presented in the following sections:

10.2.1 Intelligent Fuzzy Inference System

First, a fuzzy controller is selected because of its ability to handle all possible uncertainties in the system via a simplistic IF-THEN approach. The proposed FIS takes the SOC of the battery/supercapacitor and the original voltage of the MVDC bus as inputs, as shown in Figure 10.1.

The FIS gives the current $I_{ref,x}$ as its output, which represents the charging/discharging set-point of the batteries/supercapacitors. The subscript x can refer to a battery or a

supercapacitor. The decision of the fuzzy output set-point is a result of processing the inputs through the two groups of membership functions.

As seen in Table 10.1, the voltage membership functions are divided into three levels: Low (L), Medium (M), and High (H). This is done to ensure that the voltage of the MVDC bus is kept constant. Low voltage levels are selected to trigger the discharging process to support the system. Medium voltage levels ensure that no action is required. High voltage levels trigger the charging process to absorb the surplus power.

Similarly, the membership functions for the SOC are divided into three levels. This is done to ensure proper power sharing and avoid the undercharging/overcharging of the storage device. It is required that the storage unit with higher state of charge contributes more in the discharging processes, whereas the one with lower state of charge has charging favorability over the others. This helps increase the lifetime of the storage system's devices. The different membership functions are shown in Figure 10.2.

Figure 10.3 is a rule surface, which represents the rules that govern the decision of the FIS.

Table 10.1: Ranges of Membership Functions

	L	M	H
V (V)	$V < 4975$	$4975 \leq V < 5025$	$V \geq 5025$
$\boldsymbol{SOC_x}$ **(%)**	$SOC < 25$	$25 \leq SOC < 70$	$70 \leq SOC \leq 100$

- In case of low voltage on the MVDC bus, the batteries/supercapacitors are discharging. However, the contribution of each battery/supercapacitor is decided based on its SOC.

- In case of high voltage on the MVDC bus, the batteries/supercapacitors are charging. However, the rate of charge of each battery/supercapacitor is prioritized based on its SOC.

- In case of the medium MVDC bus voltage levels, which are around 5KV, the batteries/supercapacitors remain idle.

- In case of overcharged storage unit, it will not participate in the charging process. Similarly, in case of undercharged unit, this unit will not participate in the discharging process.
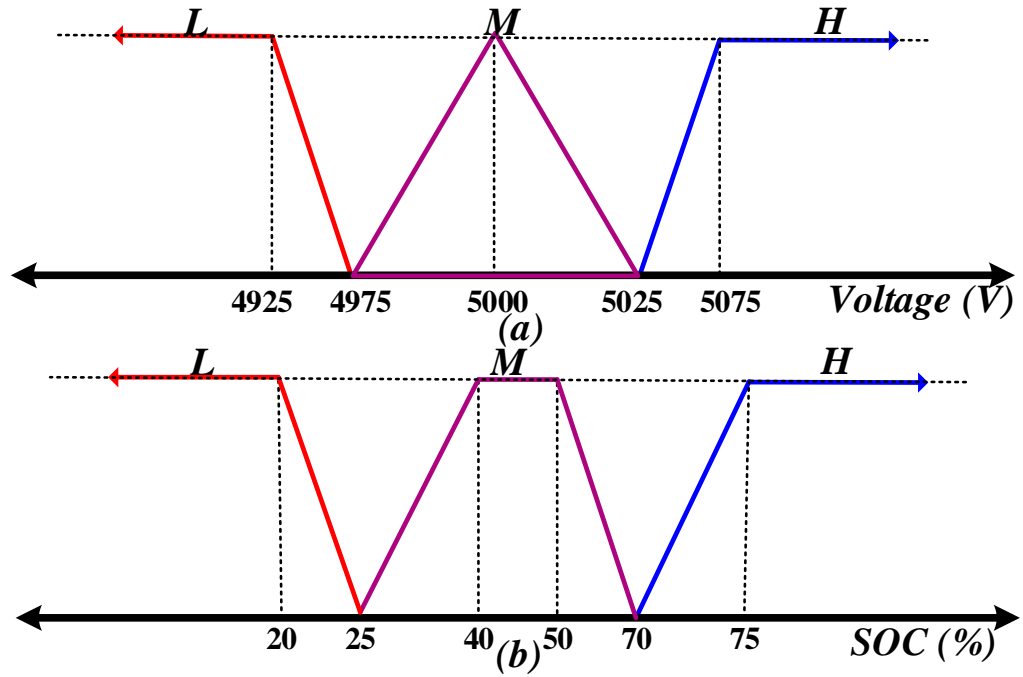
Figure 10.2: Fuzzy membership functions
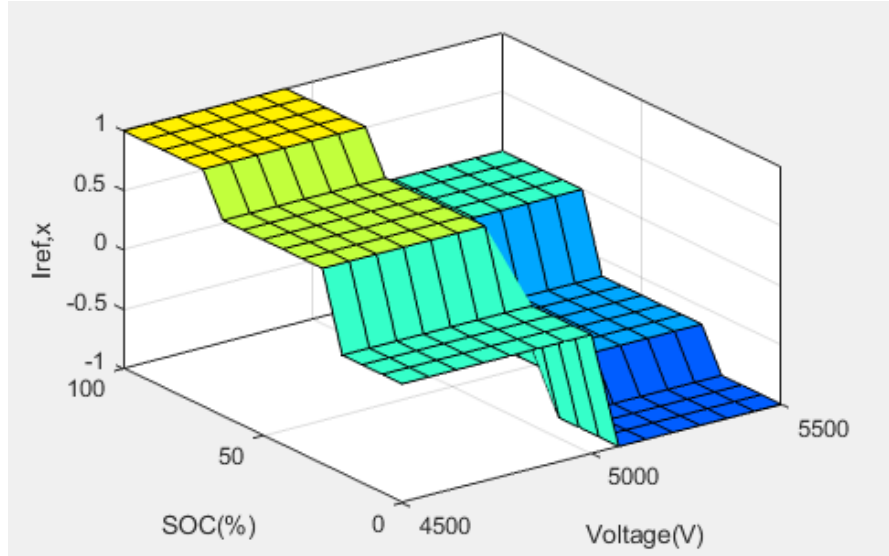
Figure 10.3: Fuzzy rule surface ($I_{ref,x}$ in p.u)

10.2.2 High-Pass Filtering

A high-pass filter, with a cut-off frequency of 20 Hz, is used as a mean to separate the high-frequency components of the voltage of the MVDC bus. The voltage of the MVDC contains valuable information about the system status, where each load addition or removal will be reflected on the voltage, causing either a momentarily change or steady-state change in case of power deficit or surplus. By extracting the momentarily changes (transient moments), the proper use of the supercapacitors can be ensured.

The difference between the original signal and the filtered one is assumed to represent the steady-state needs. This information is used to control the insertion/ removal of the batteries.

Although the reference signal is obtained from the FIS and the distinction of the transient and steady-state is obtained by the filter, there is a need for a decision-making

tool to read these values and to compare the filtered signal to certain limits to decide on the final reference value $I_{ref,final}$ for each storage unit.

10.2.3 State Machine Logic

The battery storage operation mode is defined according to the state machine logic in Figure 10.4. Typically, the control logic is continuously affected by the system requirements based on voltage low-frequency component V_{diff}. The controller modes of operation include discharging, charging and no action. First, the final reference current is initialized as $I_{ref,final}$ to zero, then the low-frequency component of the voltage is compared with minimum threshold voltage and if $V_{diff} \leq V_{min}$, the voltage deficit status is detected. A delay of 60 µs is used to make sure that the change is a real steady-state need. After the delay, the voltage V_{diff} is checked again, and if it is less than the minimum threshold, the power deficit is confirmed, and the reference current is assigned to be the value that is calculated by the fuzzy controller.

Similarly, the mode of operation in the charging is activated when $V_{diff} > V_{max}$ and the power surplus case is confirmed. Then, the reference current is captured from the fuzzy controller. For both the charging and the discharging modes, if the condition does not hold, the final reference is set to zero. In addition, if the voltage $V_{min} \leq V_{diff} \leq V_{max}$, the mode is no action and the final reference is set to zero.

Figure 10.5 illustrates the state machine logic of the supercapacitor operation. By the same approach, after initialization, the high-pass filtered voltage V_{HP} is compared to lower and upper thresholds. If the V_{HP} is less than or equal to the lower threshold V_{lower}, the

234

discharging mode is activated. However, if V_{HP} is larger than the upper threshold V_{upper}, the discharging mode is launched. Finally, if V_{HP} recorded a value that is within the lower and the upper thresholds, the mode becomes no action with a zero-reference current.
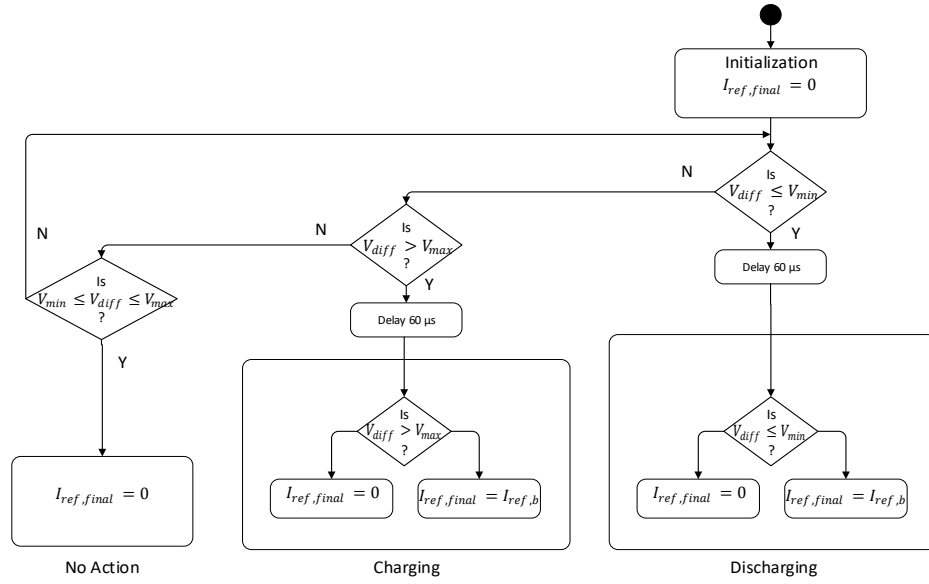
Figure 10.4: Battery state machine logic
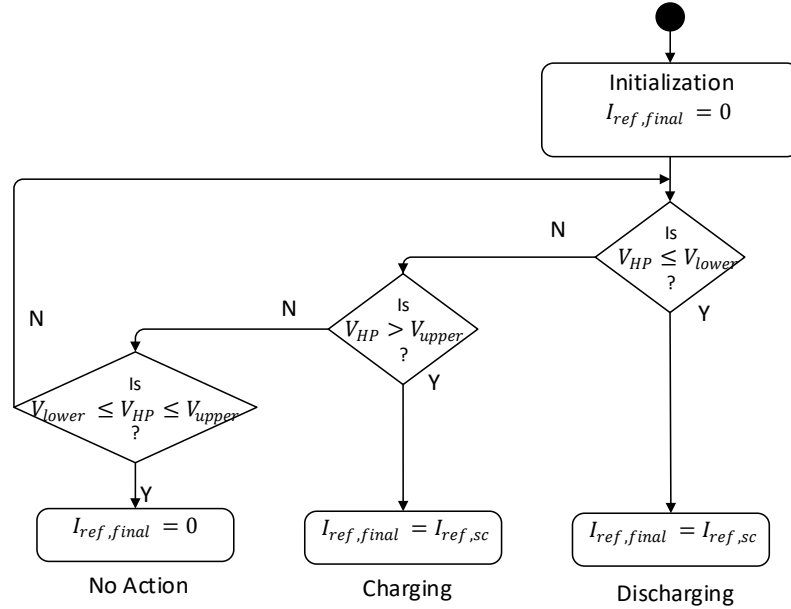
Figure 10.5: Supercapacitor state machine logic

Finally, the PI controller receives difference between the final reference $I_{ref,final}$ and the converter current I_L, and forces the converter to follow the reference value.

10.3 Results

The proposed controller is validated through simulations using the notional MVDC ship power system presented in the previous chapter. The same loads and sources, with the same ratings, are used. The maximum current that can be obtained from the generators is 8000 A, which is enough to supply the propulsion system, radar system and the service loads. However, it is not enough to supply the pulsed loads. Otherwise, a voltage drop will occur. Also, it is not economical to oversize the generators to feed the loads that consume energy for only a few seconds. Therefore, a hybrid storage system that consists of two batteries and two supercapacitors is used to supply the pulsed load. A hybrid system is used because of its ability to combine the advantages of the supercapacitors and the batteries, meeting the transient and steady state needs. The output current of the storage system is controlled using the PWM of the DC-DC converters.

The proposed controller is validated under different loading conditions and different levels of the SOCs. In this study, the initial SOCs of the batteries are chosen to be 85% and 15%, to validate the performance of the proposed controller in the case of extreme conditions, such as an overcharged/undercharged battery. The initial SOCs of the supercapacitors are chosen to be 50% each. This is done to show the ability of the controller in ensuring equal power sharing when the storage devices have the same SOC.

The stepwise loading profile, depicted in Figure 10.6 (a), shows the loading conditions at different time steps, where the propulsion system is first connected, then at t= 0.7 sec,

service loads are connected, followed by the radar system at t= 1.5 sec, and the pulsed load at t= 2 sec. The pulsed load is connected for one second, up to t= 3 sec, then it is disconnected, followed by another partial disconnection of some of the service loads at t= 3.5 sec.

Figure 10.6 (b) shows that the voltage of the MVDC bus is maintained almost constant and within the IEC 60092-101 standards regardless of the different loading conditions.

To show a detailed explanation of the different stages of the proposed methodology, in this section, the obtained reference value from the FIS block, the final reference value obtained from the state machine logic, and the actual current that is drawn by the storage devices, are shown.

Figure 10.7 (a) shows the output of the fuzzy block of the first battery. The figure shows that the fuzzy generates a discharging signal at t= 2 sec due to the low voltage, of the MVDC bus, caused by the insertion of the pulsed load. Figure 10.7 (b) shows the final reference signal that is processed by the state machine logic and the actual current that is discharged by the battery. Figure 10.7 (b) shows that the state machine logic generates the appropriate reference signal for the right time period. Since at t= 2 sec, there is a power deficit, and the first battery has 85% SOC, this means that the battery has enough capacity and should support the system. Therefore, the state machine logic generates the maximum possible discharging current from the battery, which is 1600 A. The figure also shows that the reference value is not generated instantly at t= 2 sec. This delay occurs because the state machine logic waits for a few microseconds, and then observes the bus voltage one more time before it decides to insert the battery. This action is required to ensure that the

battery will not be used during the transient periods. Only when there is a steady state power deficit, the battery should be used.
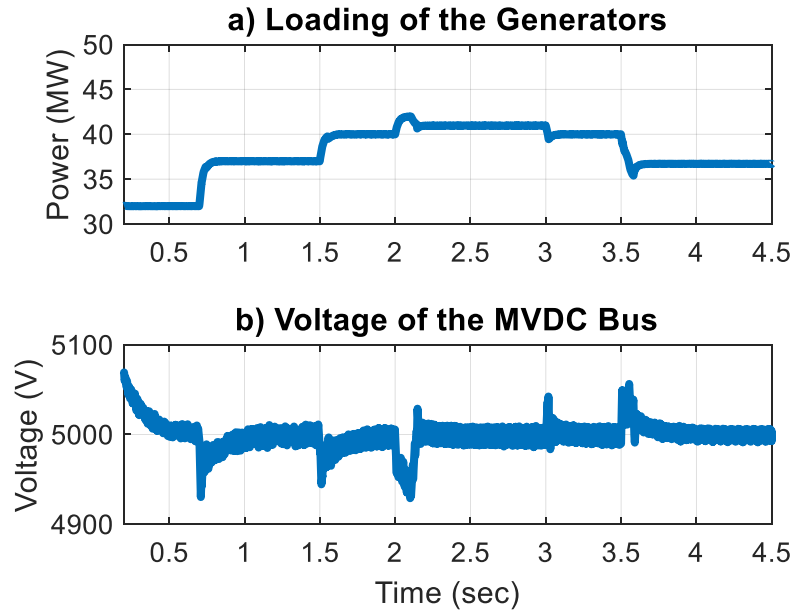
Figure 10.6:   a) Loading power.   b) MVDC bus voltage.
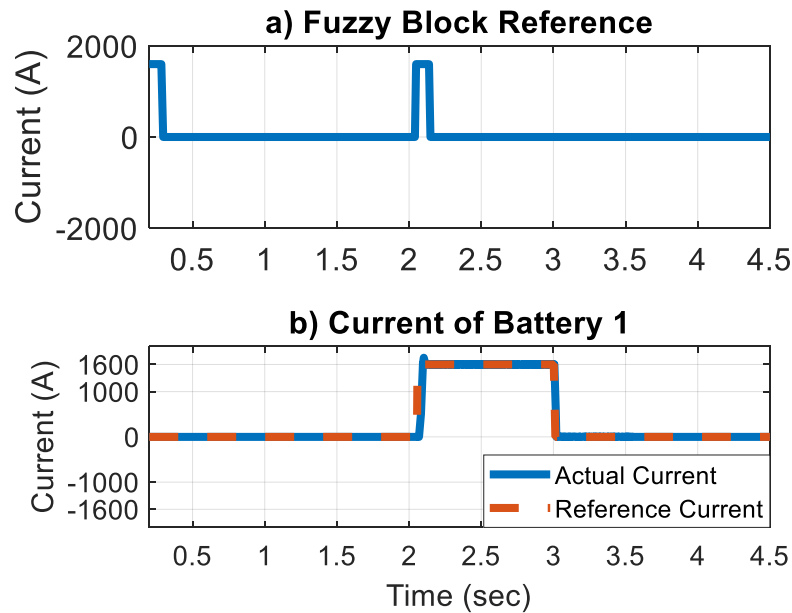
Figure 10.7: Output currents of the different stages for the first battery controller

When the pulsed load is disconnected at t = 3 sec, and the generators can supply the loads, the reference value becomes zero, and the battery is disconnected. At t= 3.5 sec, another load is disconnected. Regardless of the voltage increase at t = 3.5 sec, the fuzzy logic generates a zero-reference value because the first battery is almost fully charged (85% SOC), and it cannot support the system during this period of power surplus. Otherwise, the lifetime of the battery will be degraded. This zero-reference value is generated by the fuzzy logic block.

In addition, Figure 10.7 (b) shows that the actual current follows the reference value, and the PI-based current controller can provide fast response and support the system, ensuring constant voltage of the MVDC bus.

For the second battery, which has 15% SOC, Figure 10.8 (a) shows that the fuzzy logic only generates a reference value when there is a power surplus at t= 3.5 sec, and the battery should absorb this extra power. The fuzzy reference signal is zero at the point of inserting the pulsed load at t= 2 sec because the second battery is undercharged and cannot support the system during the power deficit phase. Figure 10.8 (b) shows that the final reference value generated by the state machine logic starts at t= 3.6 sec until the end of the simulation, when there is a power surplus in the system. The state machine logic generates a very high reference current of -1600 A because the battery has a low SOC and can absorb a large amount of power. The state machine logic waits for few microseconds before deciding on the final reference value to make sure that it is a steady state surplus power, and not a quick transient case. The figure also shows that the actual current of the battery follows the reference value.

Figure 10.9 shows the progress of the SOCs for the two batteries during the simulation period. It shows the decrease in the SOC of the first battery during the discharging phase (t = 2-3 sec), and the increase in the SOC of the second battery during the charging phase (t = 3.5 -4.5 sec). During the other periods, the batteries are idle, either because there is no action required or the battery cannot charge/discharge during certain periods.

These results show the ability of the controller in taking the correct fast response of charging/discharging, while not mitigating the lifetime of the batteries or the voltage of the MVDC bus.

The response of the supercapacitors is shown in Figure 10.10 - Figure 10.12. Figure 10.10 shows the details of the controller of the first supercapacitor. The figure shows that the fuzzy block responds to any transient voltage oscillation and provides a reference value. However, the state machine logic, with the help of the signal that is coming from the high-pass filter and the thresholds, decides which signal to pass or to block.

Since there is a transient with each load addition at t = 0.7, 1.5, and 2 sec, the state machine inserts and passes the discharging signals during these time instants, as shown in Figure 10.10 (b). The supercapacitor, a high-power density storage, can provide a high and fast current. This is shown in the figure, where the supercapacitor discharges a high pulsating current of 2000 A.
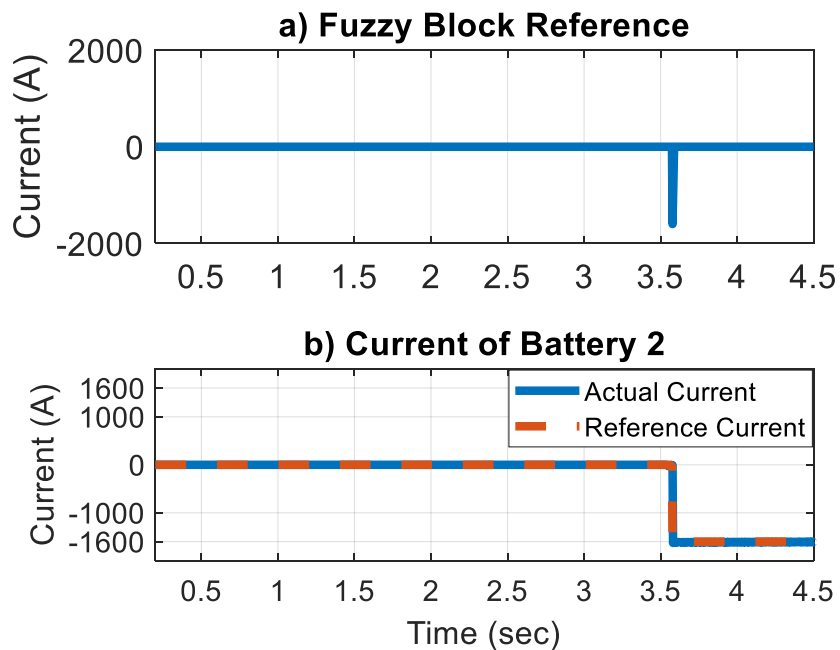
Figure 10.8: Output currents of the different stages for the second battery controller
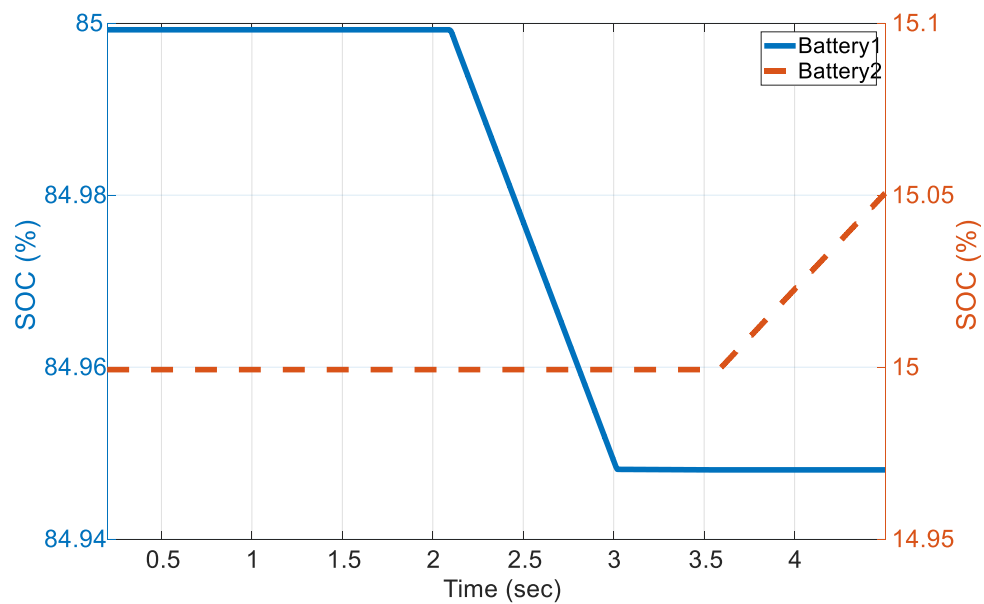
Figure 10.9: State of charge of the batteries

For the load removal instants at t= 3 and 3.5 sec, the state machine also provides a high charging current of -2000 A at t= 3.5 sec. The state machine does not provide a reference signal at t= 3 sec, regardless of the input signal that is coming from the fuzzy block, because the voltage oscillation at this instant is not high. This happens because during this time instant, a load is disconnected and also the first battery that was supporting the system is disconnected as well. Therefore, the effect of load disconnection is counteracted by the disconnection of the first battery, making the voltage oscillation small.

Since the capacitor has 50 % SOC, it supports the system with almost the same current value during the discharging and the charging phases. This guarantees a good utilization of the supercapacitor.

Figure 10.10 (b) also shows that the actual current can successfully track the reference value, providing appropriate support for the system.

Figure 10.11 shows that the second supercapacitor follows the same trend as the first one because both supercapacitors have the same initial SOCs. This validates the ability of the proposed technique in ensuring equal power sharing when the storage devices have the same energy capacity.

This is also demonstrated by Figure 10.12 that shows the SOC progress of the two supercapacitors. The figure shows that both supercapacitors have the same SOC progress, which is desirable and helps increase the overall lifetime of the storage system.
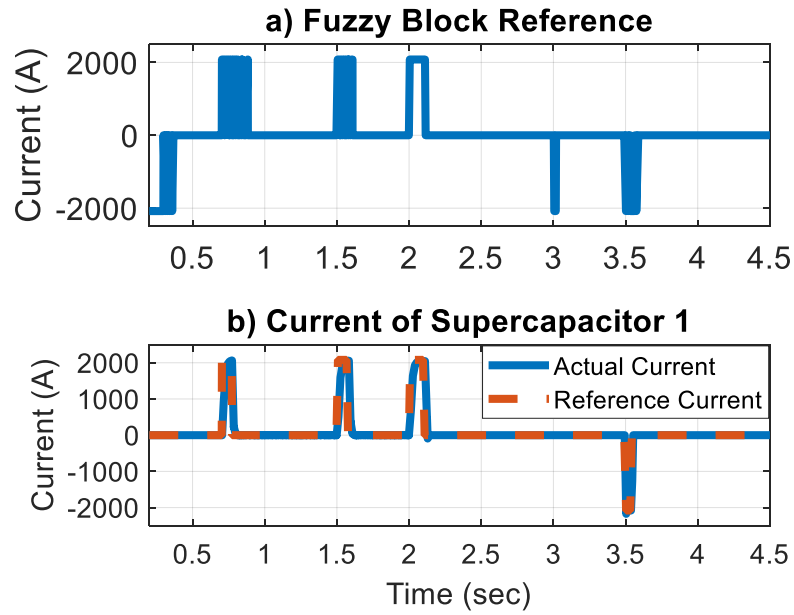
Figure 10.10: Output currents of the different stages for the first supercapacitor controller
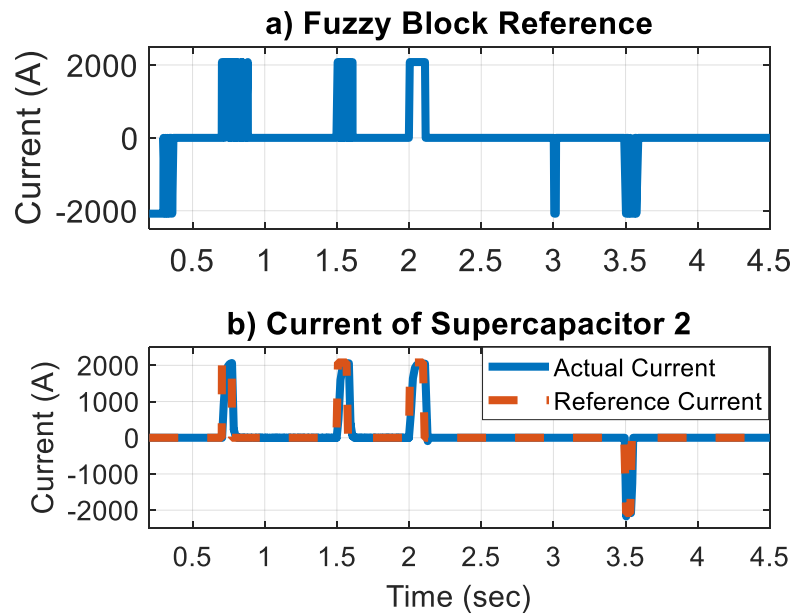
Figure 10.11: Output currents of the different stages for the second supercapacitor controller
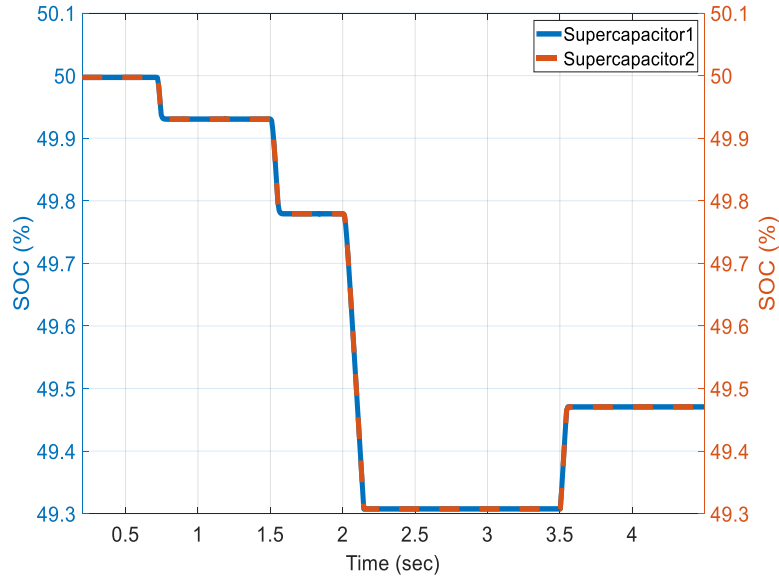
Figure 10.12: State of charge of the supercapacitors

10.4 Comparison Between the Proposed Fuzzy and the Modified Droop Algorithms

In this section, a comparison is done to compare the proposed intelligent technique in this chapter and the modified droop-based controller that was proposed in the previous chapter.

Figure 10.13 shows that both techniques are able to maintain the voltage of the MVDC bus to be within the standards. Both techniques result in almost the same voltage profile.

Similarly, Figure 10.14 shows that both techniques almost result in the same reference currents for the battery, except a minor time delay in the current of the second battery. This delay does not affect the acceptable performance of the system.

Figure 10.15 shows the currents of the supercapacitors for the two techniques. The currents are the same, except for the fact that the modified droop controller does not insert

the second supercapacitor at t = 2 sec. This also does not affect the acceptable performance of the system.
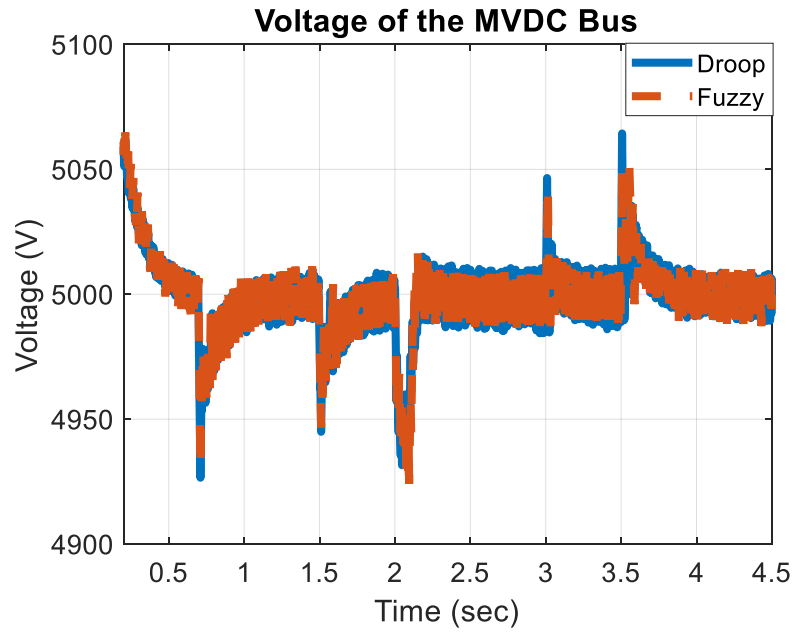
Figure 10.13: MVDC bus voltage for the droop and fuzzy-based controllers
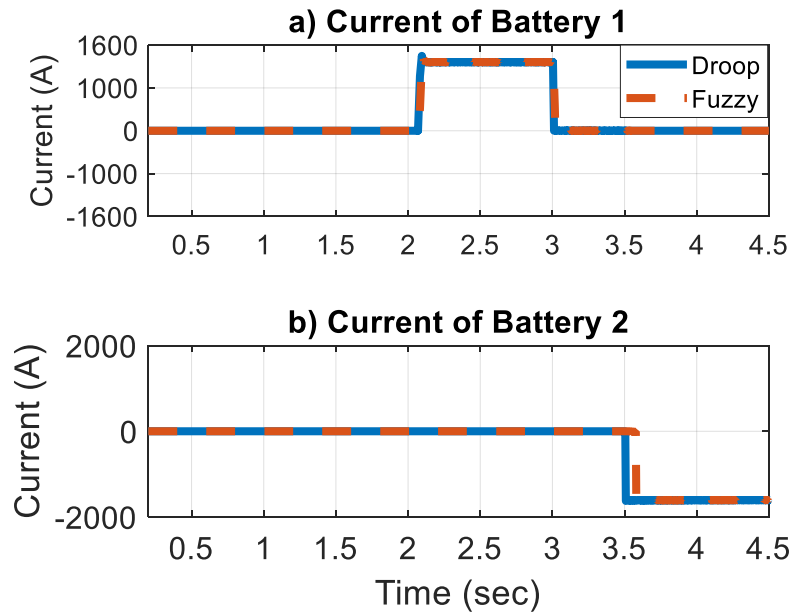
Figure 10.14: Comparison of the batteries' currents for the droop and fuzzy-based controllers
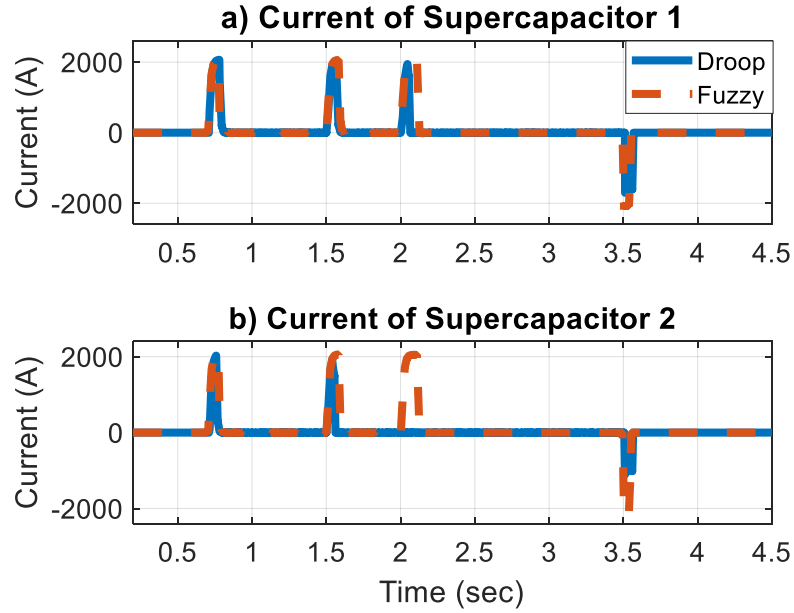
Figure 10.15: Comparison of the supercapacitors' currents for the droop and fuzzy-based controllers

Although both controllers bring about almost the same performance, there are significant differences in the complexity of the design and operation time. On one hand, the fuzzy controller is easier to adjust through simplistic conditioning rules. Also, the replacement of the mathematical morphology by a simple high-pass filter reduces the complexity of the distinction process between the steady-state and transient needs, which results in a simpler design of the state-machine logic in the next stage of the controller. On the other hand, although the fuzzy is easier to design and adjust, it is more complex in terms of the computation burden and the needed memory to allocate the control design.

To summarize, each of the proposed techniques has its pros and cons. If an easier, flexible design is required, the intelligent technique will be helpful. However, if the

memory allocation or the processing time is a barrier, the modified droop controller will be helpful in that case.

10.5 Conclusions

This chapter proposed a decentralized intelligent strategy for the onboard hybrid energy storage system to ensure the load-generation balance of the isolated MVDC ship power system. The strategy makes decisions on the local level without the need to communicate with other components of the system. The technique takes into consideration the voltage of the MVDC bus and the state of charge of the storage devices. The performance was validated under different loading conditions and SOCs of the storage devices, and the results showed the ability of the technique to ensure load-generation balance, maintain the voltage of the MVDC bus constant, and ensure the proper power sharing among the storage devices. The results showed the ability of the controller to ensure healthy operation of the storage system by avoiding undercharging/overcharging and ensuring equal power sharing among the storage devices that have the same SOCs.

The proposed intelligent controller is also compared to the adaptive droop controller. Although both controllers bring about almost the same performance, there are significant differences in the complexity of the design and operation time.

The proposed intelligent fuzzy controller is easy to design, and the operating condition rules are more flexible and can be modified using a semi-natural language. The main disadvantage of the fuzzy controller is its memory allocation size that needs to be more to accommodate the different rules and conditions.

Chapter 11   Conclusions and Recommendations for Future Work

11.1 Conclusions

This dissertation provided different solutions related to the control and optimization aspects of energy storage devices in the AC and DC power grids. Regarding the use of the energy storage in the AC power grid, this dissertation investigated, from different perspectives, how electric vehicles will reshape the future of the power systems by introducing new challenges and opportunities.

Firstly, the impact of the uncontrolled charging of EVs on the distribution system was evaluated. The results showed how the active and reactive powers of the system will be affected by the charging of the EVs. It was found that uncontrolled charging can cause a significant increase in the line loadings and power losses.

So far, the experimental study of the impact of EVs on the distribution systems did not get enough investigation in the literature. In [121], an experimental study and control was done on a real-estate feeder capacity during the charging of an EV. However, the impacts of charging the EVs on the system level were not investigated. Therefore, the experimental verification of the impacts of EVs was considered in this dissertation.

The experimental results demonstrated that future charging stations must follow the standard charging arrangements at unity or 0.95 capacitive power factors. Otherwise, high amounts of reactive power will be drawn from the system, leading to severe voltage sags, and will cause considerable and repetitive use of the voltage support units in the system.

The voltage sags will be witnessed the most at the downstream end-users, far from the substation, where the voltages might be below the minimum standard limit.

Secondly, to manage the charging of a mass number of dispersed electric vehicles into the distribution systems, which do not have mature communication infrastructure, an autonomous EV controller was developed. Unlike the droop controller in [69], the fairness of charging among different EVs, where the charging process is very sensitive to the charging location, was considered. Also, state of charge dependency was taken into consideration as well. The charger took into consideration the owner's requirements and mitigated overloading and under-voltage problems in the distribution system. The controller and the charger were tested on a large-scale system through simulation.

Also, the performance of the controller was evaluated in the presence of renewable distributed generation. It was found that the proposed controller was able to take advantage of the local generation by increasing the charging rate whenever there is available local generation.

In addition, the sensitivity of the proposed controller was tested. Two cases were evaluated, which are the sensitivity of the controller to changes in the maximum required final state of charge SOC_{max}, and the sensitivity of the controller to design parameters $(\Delta V_c, I_c)$. The results showed that the control algorithm was not affected by the maximum limit SOC_{max}. This limit only affected how much energy is required from the system. The more the required energy is, the more the stress on the system is, and the longer the charging time is.

It was also shown that parameters (ΔV_c, I_c) represent a compromise between the speed of the charging process and the fairness among the EVs. Since there are variations in the voltages at different buses of the system, where the upstream buses have much higher voltage compared to the downstream ones, it was important to charge the EVs within reasonable times and in a non-discriminatory way as well. Since the proposed work in chapter 3 was concerned with EVs at the residential sector, where most of the EVs charge during night times, the priority was given to the fairness issue more than the speed of charging.

In terms of actual validation, the proposed control algorithm was successfully verified through a laboratory-scale experimental distribution system with multiple dynamic loads, rectifiers, DC-DC converters and an inverter-based distributed generation. The algorithm achieved a good performance by charging the li-ion batteries without any negative impacts on the grid. The results confirmed the superiority of the proposed autonomous controller compared to other autonomous controllers that are reported in the literature.

To consider the control of dispersed electric vehicle, participating in the demand-side management (DSM) in distribution systems that have a mature communication infrastructure, a decentralized fuzzy-based controller was proposed to successfully integrate and coordinate the charging of EVs. The objective of the controller was to ensure a fair charging of EVs at different point of connections in the distribution grid, where voltage conditions might not be the same.

The proposed fuzzy-based controller, while requiring minimum real-time communication that already exists in the current DSM infrastructure, effectively

coordinated the charging process among the different EVs connected to the system in a fair manner. The controller took into consideration the customer's charging requirements, the system voltage, and the cost of customer bills, depending on the coming price signal from the system. The results proved that a better valley filling can be obtained, and the voltage can be maintained within the standard limits.

In addition to the control strategy, the successful deployment of DSM programs in residential distribution systems needs more attention because it is not appropriate to perform direct actuation on loads since it will represent an invasion of the user privacy. Moreover, direct load actuation will need large investments to provide the required additional communication infrastructure and control technologies for each user. Therefore, a new DSM scheme that is capable of benefiting from EVs as prosumers, without invading the privacy, was proposed. The new scheme effectively helped mitigate the system peaking, and avoided introducing new peaks "the rebound effect." The new scheme is compatible with the current DSM infrastructure and does not need any further investments.

This dissertation also proposed an improvement to the existing decentralized AIMD algorithm that was recently used to manage the charging of EVs while ensuring the best utilization and safety of the power system. None of the reported work in the literature, that used the AIMD algorithm, considered the network dynamics and the under-voltage problems that might occur in the grid. To take the grid voltage-constraints into consideration in addition to the power limit constraint, the authors in [187], [188] proposed an enhanced AIMD that charges the EVs in a fair manner, taking into consideration the grid voltage and transformer power constraints. Although the authors have described the

functionality of the proposed algorithm, they did not describe the physical implementation of the communication infrastructure, which is needed to support the proposed algorithm. Also, they did not consider the customer's preferences. Similar concepts of the AIMD that take the local voltages into consideration were used for the management of battery storage devices that support the grid in [189]. Due to the scope of the work, the effects of the owner preference were not considered.

This dissertation proposed an improved algorithm that took into consideration the system loading limits, as well as the voltage limits at the different buses. In addition, the proposed algorithm took the preferences of the owners of EVs into account. The proposed algorithm was validated through a co-simulation platform, where the power components are simulated using MATLAB/Simulink and is linked to embedded microcontrollers over a real-time communication network via the Data Distribution Service (DDS) middleware. The results showed that the proposed algorithm was able to charge the different EVs without overloading the system or causing any voltage sags at any of the buses. The preferences of the owners of the EVs were also ensured by the proposed algorithm.

When it comes to the charging of a large number of EVs that are located and charging from the same parking lot (PL), the allocation and sizing of the EV parking lot need to be carefully considered.

Some researchers tried to consider that problem in the literature. Optimal coordination for operational planning of EVs in the microgrid was considered in [163]. The authors used an economic method called Sortino ratio to maximize the profits per unit risk, while the size and location of the EVs were assumed as a priori. In [164], an Analytic Hierarchy

252

Process (AHP) was used to determine the optimal weighting coefficient for each objective in a mutli-objective problem to determine the optimal site and size of parking lots. In [165], the authors developed a two stage multi-objective formulation to optimally allocate a PL, taking network constraints into consideration. However, the optimal profit of the PL was obtained in the first stage, then optimal allocation and sizing were done in the second stage. This neglects the mutual effect that the optimal sizing and allocation might have on be profits in the first stage.

To consider that problem, a bi-layer multi-objective optimization for the sizing and allocation of a commercial parking lot was developed. The formulation looked at both the economic aspects, trying to maximize the parking lot profits, as well as the technical aspects, trying to minimize the losses and voltage deviations in the distribution system at the same time. Pareto-based optimization was used to generate the different possible solutions. Then, a statistics-based decision-making algorithm was used to select the optimal solution among the different compromises. The problem formulation was also solved as three different single objective problems, and a comparison and analysis among the different obtained solutions were presented. A final optimal size and location was obtained.

It was found that, under the current available prices and incentives, the investment in commercial parking lots does not seem to be profitable. This is mainly due to the very high initial investments and the required maintenance. This means that the government or the EV manufacturers will need to provide more incentives to make the investment in parking lots more profitable. Another possible solution to consider is how the profits will be

253

impacted if the parking lot investor tries to use the parked EVs as energy storage devices and participates in the ancillary services market.

In addition to the control and optimization of the energy storage in the AC grid, the dissertation also considered the control of the hybrid energy storage devices in the DC power grid.

Due to the nature of the emerging pulsed load connected to the medium voltage direct current (MVDC) power system, conventional generators are not able to respond to the high ramping rate for this type of loads. In that domain, the control of the storage devices on a MVDC ship power system was investigated. To that end, an overview of the different components of the ship power system was presented. Then, different control algorithms of a hybrid energy storage system, consisting of batteries and supercapacitors, were designed and validated.

Generally, centralized and hierarchical controllers ensure the optimal use of resources on the ship. However, the cost and the complexity of the controller increase nonlinearly as the number of system components increases. Also, there is always the risk of communication failure with the higher-level controller. This is of significant importance in mission-oriented applications, especially in the presence of the current issues of cyber-attacks. Therefore, decentralized controllers have become a potential solution for these issues.

In that domain, an adaptive droop controller was proposed to maintain the voltage of the MVDC bus while ensuring proper use of the different energy storage devices.

Insertion/removal of the storage devices, such as batteries and supercapacitors, was made according to the mathematical morphology-based voltage processing and state-machine logic algorithms. The controller was validated through processor in the loop simulation. The controller could successfully insert/remove the appropriate storage device during the transient and the steady state periods and ensured proper power sharing among the different devices.

In addition to the adaptive droop controller, an artificial intelligence-based controller was proposed to achieve the same control objectives by using simpler if-then fuzzy based rules. The fuzzy controller was also able to achieve smooth and reliable operation of the ship. While the fuzzy controller is easier in its design and can provide more flexibility in the design options, it requires a larger processing time and memory allocation to achieve the same objectives that can be easily realized using the adaptive droop controller.

11.2 Recommendations for Future Work

This dissertation covered several aspects related to the control and optimization of energy storage devices. Despite the proposed solutions in this dissertation and the influx of research activities on the topic of controlling the energy storage and EVs in recent years, a number of interesting questions are yet to be addressed properly and comprehensively.

Most of the works either ignored, or only partly addressed, the impacts of the communication infrastructure on EV charge management. The integration of more thorough models for the communication infrastructure into the EV charge strategies is still needed. This detailed communication modeling is especially important for EV charge management policies that facilitate the provision of ancillary services to the grid. The

255

issues of communication channel bandwidth limitation, latency, and bit rate, among others, can have a profound impact on the EV responsiveness.

Another pressing issue is the development of reliable planning tools for EV charge control, aggregation, and EV-rich system modeling. For example, distribution systems' planning models for utilities that anticipate a significant penetration of EVs into their system is yet to be developed. These models are instrumental for distribution system planners to help them make more informed long-term decisions, such as sizing and siting of distribution substations, sizing and routing of medium voltage feeders, sizing and siting of volt/var control devices, and so on. An EV aggregation investment planning model that addresses the concerns of an investor interested in EV aggregation is also largely absent.

Another issue that is only partially addressed is the interaction of the stochastic natures of EVs, renewable energies, especially wind and solar energy, and conventional unit commitment. Due to the stochastic nature of renewable energies and EVs, old conventional methods for optimal unit commitment should be re-adapted to consider these stochastic entities to ensure the optimal and reliable operation of the grid.

Moreover, for electric vehicles participating in the DSM programs, proper incentives should be given to the EV owners. The investigation of constructing these incentives to be effective for both the utility operator and the customers will be an interesting point to study. Since the residents of some areas will be high-income residents while other areas might have middle or lower-income residents, the design of the incentive structure must include the social studies and other related disciplines to ensure a proper structure that will be fair for all the customers.

Also, driver-less EVs are expected to be a disruptive technology in the coming years. Although some research activities have lately dealt with driver-less EVs, very little has been reported on the impact of a large fleet of these EVs on the local grid. The possibility of utilizing driver-less EVs to the grid advantage is a ripe research area. Charge strategies that are suitable for this type of EVs, considering their unique characteristics and limitations, are greatly needed. For example, for a fleet of shared autonomous EVs, when to dispatch each EV for transportation purposes and when to park it for charging is an interesting question yet to be addressed properly. The fact that autonomous EVs can be re-located effortlessly provokes the thought of using them as mobile sources for power injection to improve the distribution system's resilience.

When it comes to the use of the hybrid energy storage to ensure load-generation balance in MVDC ship power system, there is a great lack of a comprehensive modelling of the future MVDC ships. Comprehensive modelling is needed, especially the behavior of the constant power loads and pulsed loads, and how they can mitigate the stability of the ship power system when both are active. Any control functionality cannot be fully validated without a comprehensive modelling of the different components on the ship.

Also, fault-ride through capabilities on the system level is largely absent for the MVDC AES. The control and protection schemes need to be developed and studied, taking into consideration the zonal isolation protection and the presence of fast switching power electronics components.

List of References

[1]   P. W. Parfomak, "Energy Storage for Power Grids and Electric Transportation: A Technology Assessment," *Congressional Research Service*, March 2012.

[2]   Brittney Becker, Myriam Elisa *et al*, "European Energy Storage Technology Development Roadmap." *European Energy Research Alliance*, 2017.

[3]   P. Ralon, M. Taylor, A. Ilas, H. Diaz-Bone, and K.-P. Kairies, "Electricity storage and renewables: Costs and markets to 2030," *International Renewable Energy Agency*, Oct. 2017.

[4]   "Tracking Progress - Energy Storage," *California Energy Commission*, Aug. 2018.

[5]   J. M. Carrasco *et al.*, "Power-Electronic Systems for the Grid Integration of Renewable Energy Sources: A Survey," *IEEE Trans. Ind. Electron.*, vol. 53, no. 4, pp. 1002–1016, Jun. 2006.

[6]   S. Vazquez, S. M. Lukic, E. Galvan, L. G. Franquelo, and J. M. Carrasco, "Energy Storage Systems for Transport and Grid Applications," *IEEE Trans. Ind. Electron.*, vol. 57, no. 12, pp. 3881–3895, Dec. 2010.

[7]   Z. Jin, G. Sulligoi, R. Cuzner, L. Meng, J. C. Vasquez, and J. M. Guerrero, "Next-Generation Shipboard DC Power System: Introduction Smart Grid and dc Microgrid Technologies into Maritime Electrical Netowrks," *IEEE Electrification Mag.*, vol. 4, no. 2, pp. 45–57, Jun. 2016.

[8]   "COP 21 Paris France Sustainable Innovation Forum 2015 working with UNEP." [Online]. Available: http://www.cop21paris.org/. [Accessed: 07-May-2017].

[9]   unfccc.com, "List of 175 Signatories to Paris Agreement15 States Deposit Instruments of Ratification," *UNFCCC*. [Online]. Available: http://newsroom.unfccc.int/paris-agreement/175-states-sign-paris-agreement/. [Accessed: 06-Oct-2017].

[10]   "Global EV Outlook 2017," International Energy Agency, 2017.

[11]   A. Ghavami, K. Kar, and A. Gupta, "Decentralized Charging of Plug-in Electric Vehicles With Distribution Feeder Overload Control," *IEEE Trans. Autom. Control*, vol. 61, no. 11, pp. 3527–3532, Nov. 2016.

[12]   M. A. Masoum, P. S. Moses, and S. Hajforoosh, "Distribution transformer stress in smart grid with coordinated charging of Plug-In Electric Vehicles," in *Innovative Smart Grid Technologies (ISGT), 2012 IEEE PES*, 2012, pp. 1–8.

[13]   E. Sortomme, M. M. Hindi, S. D. J. MacPherson, and S. S. Venkata, "Coordinated Charging of Plug-In Hybrid Electric Vehicles to Minimize Distribution System Losses," *IEEE Trans. Smart Grid*, vol. 2, no. 1, pp. 198–205, Mar. 2011.

[14]   P. Richardson, D. Flynn, and A. Keane, "Impact assessment of varying penetrations of electric vehicles on low voltage distribution systems," in *Power and Energy Society General Meeting, 2010 IEEE*, 2010, pp. 1–6.

[15]   K. De Craemer, S. Vandael, B. Claessens, and G. Deconinck, "An Event-Driven Dual Coordination Mechanism for Demand Side Management of PHEVs," *IEEE Trans. Smart Grid*, vol. 5, no. 2, pp. 751–760, Mar. 2014.

[16]   M. R. Sarker, Y. Dvorkin, and M. A. Ortega-Vazquez, "Optimal Participation of an Electric Vehicle Aggregator in Day-Ahead Energy and Reserve Markets," *IEEE Trans. Power Syst.*, vol. 31, no. 5, pp. 3506–3515, Sep. 2016.

[17]   H. Zhang, Z. Hu, Z. Xu, and Y. Song, "Evaluation of Achievable Vehicle-to-Grid Capacity Using Aggregate PEV Model," *IEEE Trans. Power Syst.*, vol. 32, no. 1, pp. 784–794, Jan. 2017.

[18]   M. N. Mojdehi and P. Ghosh, "An On-Demand Compensation Function for an EV as a Reactive Power Service Provider," *IEEE Trans. Veh. Technol.*, vol. 65, no. 6, pp. 4572–4583, Jun. 2016.

[19]   E. Borden, "Electric Vehicles and Public Charging Infrastructure: Impediments And Opportunities For Success In The United States." *Center for Transportation Research*, Jul-2013.

[20]   S. O. G. Pelletier, Jabali,Laporte, "Battery Electric Vehicles for Goods Distribution: A Survey of Vehicle Technology, Market Penetration, Incentives and Practices." Interuniversity Research Centre on Enterprise Networks, Logistics and Transportation, Sep-2014.

[21]   "Compare Electric Cars and Plug-in Hybrids - List of Features, Price, Range, Model | PluginCars.com." [Online]. Available: http://www.plugincars.com/cars. [Accessed: 10-Oct-2017].

[22]   New West Technologies, "Costs Associated With Non-Residential Electric Vehicle Supply Equipment," Nov. 2015.

[23]   G. M. A. Akhtar, A. T. Al-Awami, E. Sortomme, M. A. Abido, and M. W. Ahmed, "Autonomous electric vehicle charging management over real time digital simulator," in *2014 IEEE PES General Meeting | Conference Exposition*, 2014, pp. 1–5.

[24]   M. Ansari, A. T. Al-Awami, E. Sortomme, and M. A. Abidoeric, "Coordinated Bidding of Ancillary Services for Vehicle-to-Grid Using Fuzzy Optimization," *IEEE Trans. Smart Grid*, vol. 6, no. 1, pp. 261–270, Jan. 2015.

[25] J. E. Contreras-Ocana, M. R. Sarker, and M. A. Ortega-Vazquez, "Decentralized Coordination of a Building Manager and an Electric Vehicle Aggregator," *IEEE Trans. Smart Grid*, pp. 1–1, 2016.

[26] D. Thomas, C. S. Ioakimidis, V. Klonari, F. Vallée, and O. Deblecker, "Effect of electric vehicles' optimal charging-discharging schedule on a building's electricity cost demand considering low voltage network constraints."

[27] D. Wu, H. Zeng, C. Lu, and B. Boulet, "Two-Stage Energy Management for Office Buildings With Workplace EV Charging and Renewable Energy," *IEEE Trans. Transp. Electrification*, vol. 3, no. 1, pp. 225–237, Mar. 2017.

[28] P. You and Z. Yang, "Efficient optimal scheduling of charging station with multiple electric vehicles via v2v," in *Smart Grid Communications (SmartGridComm), 2014 IEEE International Conference on*, 2014, pp. 716–721.

[29] L. Cheng, Y. Chang, and R. Huang, "Mitigating Voltage Problem in Distribution System With Distributed Solar Generation Using Electric Vehicles," *IEEE Trans. Sustain. Energy*, vol. 6, no. 4, pp. 1475–1484, Oct. 2015.

[30] J. Zhong *et al.*, "Coordinated control for large-scale EV charging facilities and energy storage devices participating in frequency regulation," *Appl. Energy*, vol. 123, pp. 253–262, Jun. 2014.

[31] J. R. Pillai and B. Bak-Jensen, "Integration of Vehicle-to-Grid in the Western Danish Power System," *IEEE Trans. Sustain. Energy*, Jan. 2010.

[32] E. Sortomme and M. A. El-Sharkawi, "Optimal Scheduling of Vehicle-to-Grid Energy and Ancillary Services," *IEEE Trans. Smart Grid*, vol. 3, no. 1, pp. 351–359, Mar. 2012.

[33] W. Kempton and S. E. Letendre, "Electric vehicles as a new power source for electric utilities," *Transp. Res. Part Transp. Environ.*, vol. 2, no. 3, pp. 157–175, Sep. 1997.

[34] W. Su, H. Eichi, W. Zeng, and M.-Y. Chow, "A Survey on the Electrification of Transportation in a Smart Grid Environment," *IEEE Trans. Ind. Inform.*, vol. 8, no. 1, pp. 1–10, Feb. 2012.

[35] J. A. Peças Lopes, S. A. Polenz, C. L. Moreira, and R. Cherkaoui, "Identification of control and management strategies for LV unbalanced microgrids with plugged-in electric vehicles," *Electr. Power Syst. Res.*, vol. 80, no. 8, pp. 898–906, Aug. 2010.

[36] J. C. Mukherjee and A. Gupta, "A Review of Charge Scheduling of Electric Vehicles in Smart Grid," *IEEE Syst. J.*, vol. 9, no. 4, pp. 1541–1553, Dec. 2015.

[37] M. Moeini-Aghtaie, A. Abbaspour, M. Fotuhi-Firuzabad, and P. Dehghanian, "Optimized Probabilistic PHEVs Demand Management in the Context of Energy Hubs," *IEEE Trans. Power Deliv.*, vol. 30, no. 2, pp. 996–1006, Apr. 2015.

[38] D. Steen, L. A. Tuan, O. Carlson, and L. Bertling, "Assessment of Electric Vehicle Charging Scenarios Based on Demographical Data," *IEEE Trans. Smart Grid*, vol. 3, no. 3, pp. 1457–1468, Sep. 2012.

[39] D. Wu, D. C. Aliprantis, and L. Ying, "Load Scheduling and Dispatch for Aggregators of Plug-In Electric Vehicles," *IEEE Trans. Smart Grid*, vol. 3, no. 1, pp. 368–376, Mar. 2012.

[40] Z. Xu, W. Su, Z. Hu, Y. Song, and H. Zhang, "A hierarchical framework for coordinated charging of plug-in electric vehicles in China," *IEEE Trans. Smart Grid*, vol. 7, no. 1, pp. 428–438, 2016.

[41] J. A. Peas Lopes, F. J. Soares, and P. R. Almeida, "Identifying management procedures to deal with connection of electric vehicles in the grid," in *PowerTech, 2009 IEEE Bucharest*, 2009, pp. 1–8.

[42] C. Harris, I. Dusparic, E. Galván-López, A. Marinescu, V. Cahill, and S. Clarke, "Set point control for charging of electric vehicles on the distribution network," in *2014 IEEE Power & Energy Society Innovative Smart Grid Technologies Conference (ISGT), Washington, DC, USA*, 2014.

[43] M. Erol-Kantarci and H. T. Mouftah, "Supply and load management for the smart distribution grid using wireless networks," in *Electronics, Communications and Computers (JEC-ECC), 2012 Japan-Egypt Conference on*, 2012, pp. 145–150.

[44] A. Mohamed, V. Salehi, T. Ma, and O. Mohammed, "Real-Time Energy Management Algorithm for Plug-In Hybrid Electric Vehicle Charging Parks Involving Sustainable Energy," *IEEE Trans. Sustain. Energy*, vol. 5, no. 2, pp. 577–586, Apr. 2014.

[45] J. de Hoog, T. Alpcan, M. Brazil, D. A. Thomas, and I. Mareels, "A Market Mechanism for Electric Vehicle Charging Under Network Constraints," *IEEE Trans. Smart Grid*, vol. 7, no. 2, pp. 827–836, Mar. 2016.

[46] J. de Hoog, T. Alpcan, M. Brazil, D. A. Thomas, and I. Mareels, "Optimal Charging of Electric Vehicles Taking Distribution Network Constraints Into Account," *IEEE Trans. Power Syst.*, vol. 30, no. 1, pp. 365–375, Jan. 2015.

[47] M. I. Ghiasi, A. Hajizadeh, M. A. Golkar, and M. Marefati, "Demand and supply side management strategies for zero energy buildings," in *2017 IEEE 17th International Conference on Ubiquitous Wireless Broadband (ICUWB)*, 2017, pp. 1–5.

[48] N. G. Paterakis, A. Tascikaraoglu, O. Erdinc, A. G. Bakirtzis, and J. P. S. Catalao, "Assessment of Demand-Response-Driven Load Pattern Elasticity Using a Combined Approach for Smart Households," *IEEE Trans. Ind. Inform.*, vol. 12, no. 4, pp. 1529–1539, Aug. 2016.

[49] E. L. Karfopoulos and N. D. Hatziargyriou, "A Multi-Agent System for Controlled Charging of a Large Population of Electric Vehicles," *IEEE Trans. Power Syst.*, vol. 28, no. 2, pp. 1196–1204, May 2013.

[50] S. D. J. McArthur *et al.*, "Multi-Agent Systems for Power Engineering Applications #x2014;Part I: Concepts, Approaches, and Technical Challenges," *IEEE Trans. Power Syst.*, vol. 22, no. 4, pp. 1743–1752, Nov. 2007.

[51] L. Gan, U. Topcu, and S. H. Low, "Optimal decentralized protocol for electric vehicle charging," *IEEE Trans. Power Syst.*, vol. 28, no. 2, pp. 940–951, May 2013.

[52] J. Hu, G. Yang, H. W. Bindner, and Y. Xue, "Application of Network-Constrained Transactive Control to Electric Vehicle Charging for Secure Grid Operation," *IEEE Trans. Sustain. Energy*, vol. 8, no. 2, pp. 505–515, Apr. 2017.

[53] X. Luo, S. Xia, and K. W. Chan, "A Decentralized Charging Control Strategy for Plug-In Electric Vehicles To Mitigate Wind Farm Intermittency and Enhance Frequency Regulation," *J. Power Sources*, vol. 248, pp. 604–614, Feb. 2014.

[54] X. Xi and R. Sioshansi, "Using Price-Based Signals to Control Plug-in Electric Vehicle Fleet Charging," *IEEE Trans. Smart Grid*, 2014.

[55] Z. Ma, D. Callaway, and I. Hiskens, "Decentralized charging control for large populations of plug-in electric vehicles," in *Decision and Control (CDC), 2010 49th IEEE Conference on*, 2010, pp. 206–212.

[56] A. H. Mohsenian-Rad, V. W. S. Wong, J. Jatskevich, R. Schober, and A. Leon-Garcia, "Autonomous Demand-Side Management Based on Game-Theoretic Energy Consumption Scheduling for the Future Smart Grid," *IEEE Trans. Smart Grid*, vol. 1, no. 3, pp. 320–331, Dec. 2010.

[57] N. Z. Xu and C. Y. Chung, "Challenges in Future Competition of Electric Vehicle Charging Management and Solutions," *IEEE Trans. Smart Grid*, vol. 6, no. 3, pp. 1323–1331, May 2015.

[58] L. Zhang and Y. Li, "A Game-Theoretic Approach to Optimal Scheduling of Parking-Lot Electric Vehicle Charging," *IEEE Trans. Veh. Technol.*, vol. 65, no. 6, pp. 4068–4078, Jun. 2016.

[59] W. Wei, F. Liu, and S. Mei, "Charging Strategies of EV Aggregator Under Renewable Generation and Congestion: A Normalized Nash Equilibrium Approach," *IEEE Trans. Smart Grid*, vol. 7, no. 3, pp. 1630–1641, May 2016.

[60] Z. Zhu, S. Lambotharan, W. H. Chin, and Z. Fan, "A Mean Field Game Theoretic Approach to Electric Vehicles Charging," *IEEE Access*, vol. 4, pp. 3501–3510, 2016.

[61] S. Stüdli, E. Crisostomi, R. Middleton, and R. Shorten, "A flexible distributed framework for realising electric and plug-in hybrid vehicle charging policies," *Int. J. Control*, vol. 85, no. 8, pp. 1130–1145, Aug. 2012.

[62] J. de Hoog *et al.*, "Electric vehicle charging and grid constraints: Comparing distributed and centralized approaches," in *Power and Energy Society General Meeting (PES), 2013 IEEE*, 2013, pp. 1–5.

[63] M. Singh, P. Kumar, and I. Kar, "Implementation of Vehicle to Grid Infrastructure Using Fuzzy Logic Controller," *IEEE Trans. Smart Grid*, vol. 3, no. 1, pp. 565–577, Mar. 2012.

[64] M. Singh, K. Thirugnanam, P. Kumar, and I. Kar, "Real-Time Coordination of Electric Vehicles to Support the Grid at the Distribution Substation Level," *IEEE Syst. J.*, vol. 9, no. 3, pp. 1000–1010, Sep. 2015.

[65] M. Liu and S. McLoone, "Enhanced AIMD-based decentralized residential charging of EVs," *Trans. Inst. Meas. Control*, Jul. 2013.

[66] P. Richardson, D. Flynn, and A. Keane, "Local Versus Centralized Charging Strategies for Electric Vehicles in Low Voltage Distribution Systems," *IEEE Trans. Smart Grid*, vol. 3, no. 2, pp. 1020–1028, Jun. 2012.

[67] M. Tokudome, K. Tanaka, T. Senjyu, A. Yona, T. Funabashi, and C. H. Kim, "Frequency and voltage control of small power systems by decentralized controllable loads," in *2009 International Conference on Power Electronics and Drive Systems (PEDS)*, 2009, pp. 666–671.

[68] J. A. P. Lopes, P. M. R. Almeida, and F. J. Soares, "Using vehicle-to-grid to maximize the integration of intermittent renewable energy resources in islanded electric grids," in *2009 International Conference on Clean Electrical Power*, 2009, pp. 290–295.

[69] N. Leemput, F. Geth, J. V. Roy, A. Delnooz, J. Büscher, and J. Driesen, "Impact of Electric Vehicle On-Board Single-Phase Charging Strategies on a Flemish Residential Grid," *IEEE Trans. Smart Grid*, vol. 5, no. 4, pp. 1815–1822, Jul. 2014.

[70] C. Gouveia, C. L. Moreira, J. A. P. Lopes, D. Varajao, and R. E. Araujo, "Microgrid Service Restoration: The Role of Plugged-in Electric Vehicles," *IEEE Ind. Electron. Mag.*, vol. 7, no. 4, pp. 26–41, Dec. 2013.

[71] Y. Ota, H. Taniguchi, T. Nakajima, K. M. Liyanage, J. Baba, and A. Yokoyama, "Autonomous Distributed V2G (Vehicle-to-Grid) Satisfying Scheduled Charging," *IEEE Trans. Smart Grid*, vol. 3, no. 1, pp. 559–564, Mar. 2012.

[72] L. Xia, I. Mareels, T. Alpcan, M. Brazil, J. de Hoog, and D. A. Thomas, "A distributed electric vehicle charging management algorithm using only local measurements," in *Innovative Smart Grid Technologies Conference (ISGT), 2014 IEEE PES*, 2014, pp. 1–5.

[73] A. T. Al-Awami and E. Sortomme, "Electric vehicle charging modulation using voltage feedback control," in *Power and Energy Society General Meeting (PES), 2013 IEEE*, 2013, pp. 1–5.

[74] "Communication free charging management of electric vehicles under grid constraints - ProQuest." [Online]. Available: https://search.proquest.com/openview/7cf2d967afa5ec35ab0da7b243741b3a/1?pq-origsite=gscholar&cbl=2026366&diss=y. [Accessed: 09-Feb-2018].

[75] A. T. Al-Awami, E. Sortomme, G. M. A. Akhtar, and S. Faddel, "A Voltage-Based Controller for an Electric-Vehicle Charger," *IEEE Trans. Veh. Technol.*, vol. 65, no. 6, pp. 4185–4196, Jun. 2016.

[76] S. Faddel, A. T. Al-Awami, and M. A. Abido, "Real time digital simulation of voltage-based controller for electric vehicle charging," in *2016 Clemson University Power Systems Conference (PSC)*, 2016, pp. 1–5.

[77] P. García-Triviño, J. P. Torreglosa, L. M. Fernández-Ramírez, and F. Jurado, "Decentralized Fuzzy Logic Control of Microgrid for Electric Vehicle Charging Station," *IEEE J. Emerg. Sel. Top. Power Electron.*, vol. 6, no. 2, pp. 726–737, Jun. 2018.

[78] A. Y. Saber and G. K. Venayagamoorthy, "Resource Scheduling Under Uncertainty in a Smart Grid With Renewables and Plug-in Vehicles," *IEEE Syst. J.*, vol. 6, no. 1, pp. 103–109, Mar. 2012.

[79] S. I. Vagropoulos and A. G. Bakirtzis, "Optimal Bidding Strategy for Electric Vehicle Aggregators in Electricity Markets," *IEEE Trans. Power Syst.*, vol. 28, no. 4, pp. 4031–4041, Nov. 2013.

[80] S. Faddel, A. T. Al-Awami, and M. A. Abido, "Fuzzy Optimization for the Operation of Electric Vehicle Parking Lots," *Electr. Power Syst. Res.*, vol. 145, pp. 166–174, Apr. 2017.

[81] W. Su and M.-Y. Chow, "Performance Evaluation of an EDA-Based Large-Scale Plug-In Hybrid Electric Vehicle Charging Algorithm," *IEEE Trans. Smart Grid*, vol. 3, no. 1, pp. 308–315, Mar. 2012.

[82] L. Jian, Y. Zheng, X. Xiao, and C. C. Chan, "Optimal Scheduling for Vehicle-to-Grid Operation with Stochastic Connection of Plug-In Electric Vehicles To Smart Grid," *Appl. Energy*, vol. 146, pp. 150–161, May 2015.

[83] X. Bai and W. Qiao, "Robust Optimization for Bidirectional Dispatch Coordination of Large-Scale V2G," *IEEE Trans. Smart Grid*, vol. 6, no. 4, pp. 1944–1954, Jul. 2015.

[84] A. T. Al-Awami, N. Amleh, and A. Muqbel, "Optimal Demand Response Bidding and Pricing Mechanism with Fuzzy Optimization: Application for a Virtual Power Plant," *IEEE Trans. Ind. Appl.*, vol. PP, no. 99, pp. 1–1, 2017.

[85] Z. Yang, K. Li, Q. Niu, and Y. Xue, "A comprehensive study of economic unit commitment of power systems integrating various renewable generations and plug-in electric vehicles," *Energy Convers. Manag.*, vol. 132, pp. 460–481, Jan. 2017.

[86] A. T. Al-Awami and E. Sortomme, "Coordinating Vehicle-to-Grid Services with Energy Trading," *IEEE Trans. Smart Grid*, vol. 3, no. 1, pp. 453–462, Mar. 2012.

[87] L. He, J. Yang, J. Yan, Y. Tang, and H. He, "A bi-layer optimization based temporal and spatial scheduling for large-scale electric vehicles," *Appl. Energy*, vol. 168, pp. 179–192, Apr. 2016.

[88] Q. Cai, F. Wen, Y. Xue, and J. Xin, "An SCUC-based optimization approach for power system dispatching with plug-in hybrid electric vehicles," *Dianli Xitong ZidonghuaAutomation Electr. Power Syst.*, vol. 36, no. 1, pp. 38–46, 2012.

[89] M. A. Ortega-Vazquez, "Optimal scheduling of electric vehicle charging and vehicle-to-grid services at household level including battery degradation and price uncertainty," *IET Gener. Transm. Distrib.*, vol. 8, no. 6, pp. 1007–1016, Jun. 2014.

[90] W. Qi, Z. Xu, Z.-J. M. Shen, Z. Hu, and Y. Song, "Hierarchical Coordinated Control of Plug-in Electric Vehicles Charging in Multifamily Dwellings," *IEEE Trans. Smart Grid*, vol. 5, no. 3, pp. 1465–1474, May 2014.

[91] M. S. Kuran, A. C. Viana, L. Iannone, D. Kofman, G. Mermoud, and J. P. Vasseur, "A Smart Parking Lot Management System for Scheduling the Recharging of Electric Vehicles," *IEEE Trans. Smart Grid*, pp. 1–1, 2015.

[92] N. Neyestani, M. Yazdani Damavandi, M. Shafie-khah, J. P. Catalao, and J. Contreras, "Modeling the optimal behavior of PEV parking lots in energy and reserve market," in *Innovative Smart Grid Technologies Conference Europe (ISGT-Europe), 2014 IEEE PES*, 2014, pp. 1–6.

[93] AeroVirnonment EV Solutions, "Electric Vehicle Smart Charging Station," 2017.

[94] F. J. Soares, P. M. R. Almeida, and J. A. P. Lopes, "Quasi-Real-Time Management of Electric Vehicles Charging," *Electr. Power Syst. Res.*, vol. 108, pp. 293–303, Mar. 2014.

[95]   L. Yang, J. Zhang, and H. V. Poor, "Risk-Aware Day-Ahead Scheduling and Real-time Dispatch for Electric Vehicle Charging," *IEEE Trans. Smart Grid*, vol. 5, no. 2, pp. 693–702, Mar. 2014.

[96]   Y. Huang, C. Guo, Y. Ding, L. Wang, B. Zhu, and L. Xu, "A Multi-Period Framework for Coordinated Dispatch of Plug-in Electric Vehicles," *Energies*, vol. 9, no. 5, p. 370, May 2016.

[97]   L. He, C. Li, Y. Cao, Z. Yu, and B. Fang, "Synergistic and priority control for electric vehicles power allocation in participating in AGC," in *2013 Chinese Automation Congress*, 2013, pp. 81–86.

[98]   S. I. Vagropoulos, D. K. Kyriazidis, and A. G. Bakirtzis, "Real-Time Charging Management Framework for Electric Vehicle Aggregators in a Market Environment," *IEEE Trans. Smart Grid*, vol. 7, no. 2, pp. 948–957, Mar. 2016.

[99]   R. Wang, Y. Li, P. Wang, and D. Niyato, "Design of a V2G aggregator to optimize PHEV charging and frequency regulation control," in *2013 IEEE International Conference on Smart Grid Communications (SmartGridComm)*, 2013, pp. 127–132.

[100] R. Wang, P. Wang, and G. Xiao, "Two-Stage Mechanism for Massive Electric Vehicle Charging Involving Renewable Energy," *IEEE Trans. Veh. Technol.*, vol. 65, no. 6, pp. 4159–4171, Jun. 2016.

[101] W. Y. Chiu, H. Sun, J. Thompson, K. Nakayama, and S. Zhang, "IoT and Information Processing in Smart Energy Applications," *IEEE Commun. Mag.*, vol. 55, no. 10, pp. 44–44, Oct. 2017.

[102] "ITU Internet Reports 2005: The Internet of Things." [Online]. Available: https://www.itu.int/osg/spu/publications/internetofthings/. [Accessed: 14-Feb-2018].

[103] E. Borgia, "The Internet of Things vision: Key features, applications and open issues," *Comput. Commun.*, vol. 54, pp. 1–31, Dec. 2014.

[104] Shanzhi Chen, Hui Xu, Dake Liu, Bo Hu, and Hucheng Wang, "A Vision of IoT: Applications, Challenges, and Opportunities With China Perspective," *IEEE Internet Things J.*, vol. 1, no. 4, pp. 349–359, Aug. 2014.

[105] L. Yao, Y. Q. Chen, and W. H. Lim, "Internet of Things for Electric Vehicle: An Improved Decentralized Charging Scheme," in *2015 IEEE International Conference on Data Science and Data Intensive Systems*, 2015, pp. 651–658.

[106] V. Monteiro, J. C. Ferreira, and J. L. Afonso, "Smart Platform towards Batteries Analysis Based on Internet-of-Things," *Procedia Technol.*, vol. 17, pp. 520–527, 2014.

[107] D. A. Chekired and L. Khoukhi, "Smart Grid Solution for Charging and Discharging Services Based on Cloud Computing Scheduling," *IEEE Trans. Ind. Inform.*, vol. 13, no. 6, pp. 3312–3321, Dec. 2017.

[108] M. Tao, K. Ota, and M. Dong, "Foud: Integrating Fog and Cloud for 5G-Enabled V2G Networks," *IEEE Netw.*, vol. 31, no. 2, pp. 8–13, Mar. 2017.

[109] J. Chen *et al.*, "Service-Oriented Dynamic Connection Management for Software-Defined Internet of Vehicles," *IEEE Trans. Intell. Transp. Syst.*, vol. 18, no. 10, pp. 2826–2837, Oct. 2017.

[110] V. P. Singh, N. Kishor, and P. Samuel, "Load Frequency Control with Communication Topology Changes in Smart Grid," *IEEE Trans. Ind. Inform.*, vol. 12, no. 5, pp. 1943–1952, Oct. 2016.

[111] A. Bose, "Smart Transmission Grid Applications and Their Supporting Infrastructure," *IEEE Trans. Smart Grid*, vol. 1, no. 1, pp. 11–19, Jun. 2010.

[112] C. P. Nguyen and A. J. Flueck, "Modeling of communication latency in smart grid," in *2011 IEEE Power and Energy Society General Meeting*, 2011, pp. 1–7.

[113] P. Kansal and A. Bose, "Bandwidth and Latency Requirements for Smart Transmission Grid Applications," *IEEE Trans. Smart Grid*, vol. 3, no. 3, pp. 1344–1352, Sep. 2012.

[114] Ş. Sönmez, S. Ayasun, and C. O. Nwankpa, "An Exact Method for Computing Delay Margin for Stability of Load Frequency Control Systems With Constant Communication Delays," *IEEE Trans. Power Syst.*, vol. 31, no. 1, pp. 370–377, Jan. 2016.

[115] G. Binetti, A. Davoudi, D. Naso, B. Turchiano, and F. L. Lewis, "Scalable Real-Time Electric Vehicles Charging With Discrete Charging Rates," *IEEE Trans. Smart Grid*, vol. 6, no. 5, pp. 2211–2220, Sep. 2015.

[116] P. Rezaei, J. Frolik, and P. D. H. Hines, "Packetized Plug-In Electric Vehicle Charge Management," *IEEE Trans. Smart Grid*, vol. 5, no. 2, pp. 642–650, Mar. 2014.

[117] E. Sortomme and K. W. Cheung, "Intelligent dispatch of Electric Vehicles performing vehicle-to-grid regulation," in *2012 IEEE International Electric Vehicle Conference*, 2012, pp. 1–6.

[118] M. Singh, P. Kumar, and I. Kar, "Implementation of Vehicle to Grid Infrastructure Using Fuzzy Logic Controller," *IEEE Trans. Smart Grid*, vol. 3, no. 1, pp. 565–577, Mar. 2012.

[119] M. Singh, K. Thirugnanam, P. Kumar, and I. Kar, "Real-Time Coordination of Electric Vehicles to Support the Grid at the Distribution Substation Level," *IEEE Syst. J.*, vol. 9, no. 3, pp. 1000–1010, Sep. 2015.

[120] G. M. Asim Akhtar, A. T. Al-Awami, E. Sortomme, M. A. Abido, and M. W. Ahmed, "Autonomous electric vehicle charging management over real time digital simulator," in *PES General Meeting| Conference & Exposition, 2014 IEEE*, 2014, pp. 1–5.

[121] A. Rautiainen, K. Lummi, P. Järventausta, V. Tikka, and A. Lana, "Control of electric vehicle charging in domestic real estates as part of demand response functionality," in *CIRED Workshop 2016*, 2016, pp. 1–4.

[122] F. Geth, N. Leemput, J. Van Roy, J. Buscher, R. Ponnette, and J. Driesen, "Voltage droop charging of electric vehicles in a residential distribution feeder," in *Innovative Smart Grid Technologies (ISGT Europe), 2012 3rd IEEE PES International Conference and Exhibition on*, 2012, pp. 1–8.

[123] T. Sansawatt, L. F. Ochoa, and G. P. Harrison, "Smart Decentralized Control of DG for Voltage and Thermal Constraint Management," *IEEE Trans. Power Syst.*, vol. 27, no. 3, pp. 1637–1645, Aug. 2012.

[124] E. Sortomme, A. I. Negash, S. S. Venkata, and D. S. Kirschen, "Multistate voltage dependent load model of a charging electric vehicle," in *Transportation Electrification Conference and Expo (ITEC), 2012 IEEE*, 2012, pp. 1–5.

[125] C. R. Lashway and O. A. Mohammed, "Adaptive Battery Management and Parameter Estimation Through Physics-Based Modeling and Experimental Verification," *IEEE Trans. Transp. Electrification*, vol. 2, no. 4, pp. 454–464, Dec. 2016.

[126] American National Standard for Electrical Power Systems and Equipment, "ANSI C84.1-2006, Voltage Ratings (60 Hertz)," 2006.

[127] J. Belt, V. Utgikar, and I. Bloom, "Calendar and PHEV cycle life aging of high-energy, lithium-ion cells containing blended spinel and layered-oxide cathodes," *J. Power Sources*, vol. 196, no. 23, pp. 10213–10221, Dec. 2011.

[128] J. Jaguemont, L. Boulon, and Y. Dubé, "A comprehensive review of lithium-ion batteries used in hybrid and electric vehicles at cold temperatures," *Appl. Energy*, vol. 164, pp. 99–114, Feb. 2016.

[129] Cooper Power Systems, *Electrical Distribution-System Protection, Cooper Industries*, 3rd ed. Cooper Power Systems, 1990.

[130] "Load Profiling." [Online]. Available: http://www.ercot.com/mktinfo/loadprofile. [Accessed: 25-Nov-2017].

[131] A. Dubey, S. Santoso, and M. P. Cloud, "A practical approach to evaluate voltage quality effects of electric vehicle charging," in *2013 International Conference on Connected Vehicles and Expo (ICCVE)*, 2013, pp. 188–194.

[132] O. M. F. Camacho, P. B. Norgard, N. Rao, and L. Mihet-Popa, "Electrical Vehicle Batteries Testing in a Distribution Network Using Sustainable Energy," *IEEE Trans. Smart Grid*, vol. 5, no. 2, pp. 1033–1042, Mar. 2014.

[133] E. Voumvoulakis, E. Leonidaki, G. Papoutsis, and N. Hatziargyriou, "Evaluation of the impact of plug-in electric vehicles in Greek distribution network," *CIRED - Open Access Proc. J.*, vol. 2017, no. 1, pp. 2270–2274, Oct. 2017.

[134] A. Dubey and S. Santoso, "Electric Vehicle Charging on Residential Distribution Systems: Impacts and Mitigations," *IEEE Access*, vol. 3, pp. 1871–1893, 2015.

[135] A. C. Melhorn, K. McKenna, A. Keane, D. Flynn, and A. Dimitrovski, "Autonomous plug and play electric vehicle charging scenarios including reactive power provision: a probabilistic load flow analysis," *IET Gener. Transm. Distrib.*, vol. 11, no. 3, pp. 768–775, Feb. 2017.

[136] V. Salehi, A. Mohamed, A. Mazloomzadeh, and O. A. Mohammed, "Laboratory-Based Smart Power System, Part I: Design and System Development," *IEEE Trans. Smart Grid*, vol. 3, no. 3, pp. 1394–1404, Sep. 2012.

[137] A. T. Elsayed, T. A. Youssef, and O. A. Mohammed, "Modeling and Control of a Low-Speed Flywheel Driving System for Pulsed-Load Mitigation in DC Distribution Networks," *IEEE Trans. Ind. Appl.*, vol. 52, no. 4, pp. 3378–3387, Jul. 2016.

[138] A. Elsayed, A. F. Ebrahim, H. Mohammed, and O. A. Mohammed, "Design and implementation of AC/DC active power load emulator," in *SoutheastCon 2015*, 2015, pp. 1–5.

[139] K. H. S. V. S. Nunna and S. Doolla, "Responsive End-User-Based Demand Side Management in Multimicrogrid Environment," *IEEE Trans. Ind. Inform.*, vol. 10, no. 2, pp. 1262–1272, May 2014.

[140] V. C. Gungor *et al.*, "A Survey on Smart Grid Potential Applications and Communication Requirements," *IEEE Trans. Ind. Inform.*, vol. 9, no. 1, pp. 28–42, Feb. 2013.

[141] E. Lannoye, D. Flynn, and M. O'Malley, "Evaluation of Power System Flexibility," *IEEE Trans. Power Syst.*, vol. 27, no. 2, pp. 922–931, May 2012.

[142] P. Samadi, H. Mohsenian-Rad, V. W. S. Wong, and R. Schober, "Tackling the Load Uncertainty Challenges for Energy Consumption Scheduling in Smart Grid," *IEEE Trans. Smart Grid*, vol. 4, no. 2, pp. 1007–1016, Jun. 2013.

[143] B. Hayes, I. Hernando-Gil, A. Collin, G. Harrison, and S. Djokić, "Optimal Power Flow for Maximizing Network Benefits From Demand-Side Management," *IEEE Trans. Power Syst.*, vol. 29, no. 4, pp. 1739–1747, Jul. 2014.

[144] C. O. Adika and L. Wang, "Demand-Side Bidding Strategy for Residential Energy Management in a Smart Grid Environment," *IEEE Trans. Smart Grid*, vol. 5, no. 4, pp. 1724–1733, Jul. 2014.

[145] F. D. Silva and O. Mohammed, "Demand Side Load Control with Smart Meters," in *2013 IEEE Power Energy Society General Meeting*, 2013, pp. 1–5.

[146] B. Hayes, I. Melatti, T. Mancini, M. Prodanovic, and E. Tronci, "Residential Demand Management using Individualised Demand Aware Price Policies," *IEEE Trans. Smart Grid*, pp. 1–1, 2016.

[147] S. Tong, T. Fung, and J. W. Park, "Reusing Electric Vehicle Battery for Demand Side Management Integrating Dynamic Pricing," in *2015 IEEE International Conference on Smart Grid Communications (SmartGridComm)*, 2015, pp. 325–330.

[148] H. Aburub, W. T. Jewell, and J. E. Price, "Assessment of the use of CAISO wholesale grid state indicator to schedule storage," in *2013 North American Power Symposium (NAPS)*, 2013, pp. 1–6.

[149] J. E. Price and H. Sanders, "Concepts for a wholesale grid state indicator to enable price responsive demand," in *2013 IEEE Power Energy Society General Meeting*, 2013, pp. 1–5.

[150] M. Muratori and G. Rizzoni, "Residential Demand Response: Dynamic Energy Management and Time-Varying Electricity Pricing," *IEEE Trans. Power Syst.*, vol. 31, no. 2, pp. 1108–1117, Mar. 2016.

[151] "Residential rates, clauses and storm factors," 2017. [Online]. Available: https://www.fpl.com/rates/pdf/Jan2017-Residential.pdf.

[152] NorthWestern Energy, "Residential customer profile." [Online]. Available: http://www.northwesternenergy.com/forsuppliers/customerload-profiles/residential-customer-profile. Accessed on: Jan. 16, 2017.

[153] "Solar Power Data for Integration Studies | Grid Modernization | NREL." [Online]. Available: https://www.nrel.gov/grid/solar-power-data.html. [Accessed: 19-Oct-2017].

[154] Margaret Smith and Jonathan Castellano, "Costs Associated with Non-Residential Electric Vehicle Supply Equipment," Nov. 2015.

[155] G. H. Fox, "Electric Vehicle Charging Stations: Are We Prepared?," *IEEE Ind. Appl. Mag.*, vol. 19, no. 4, pp. 32–38, Jul. 2013.

[156] T. Ma and O. A. Mohammed, "Optimal Charging of Plug-in Electric Vehicles for a Car-Park Infrastructure," *IEEE Trans. Ind. Appl.*, vol. 50, no. 4, pp. 2323–2330, Jul. 2014.

[157] S. X. Chen, H. B. Gooi, and M. Q. Wang, "Sizing of Energy Storage for Microgrids," *IEEE Trans. Smart Grid*, vol. 3, no. 1, pp. 142–151, Mar. 2012.

[158] S. Kahrobaee, S. Asgarpoor, and W. Qiao, "Optimum Sizing of Distributed Generation and Storage Capacity in Smart Households," *IEEE Trans. Smart Grid*, vol. 4, no. 4, pp. 1791–1801, Dec. 2013.

[159] X. Han, T. Ji, Z. Zhao, and H. Zhang, "Economic evaluation of batteries planning in energy storage power stations for load shifting," *Renew. Energy*, vol. 78, pp. 643–647, Jun. 2015.

[160] E. Nasrolahpour, S. J. Kazempour, H. Zareipour, and W. D. Rosehart, "Strategic Sizing of Energy Storage Facilities in Electricity Markets," *IEEE Trans. Sustain. Energy*, vol. 7, no. 4, pp. 1462–1472, Oct. 2016.

[161] K. W. Chan, X. Luo, M. Qin, T. Wu, and C. Y. Chung, "Optimal planning and operation of energy storage systems in radial networks for wind power integration with reserve support," *IET Gener. Transm. Distrib.*, vol. 10, no. 8, pp. 2019–2025, May 2016.

[162] Y. Zheng, Z. Y. Dong, F. J. Luo, K. Meng, J. Qiu, and K. P. Wong, "Optimal Allocation of Energy Storage System for Risk Mitigation of DISCOs With High Renewable Penetrations," *IEEE Trans. Power Syst.*, vol. 29, no. 1, pp. 212–220, Jan. 2014.

[163] V. Mohan, J. G. Singh, and W. Ongsakul, "Sortino Ratio Based Portfolio Optimization Considering EVs and Renewable Energy in Microgrid Power Market," *IEEE Trans. Sustain. Energy*, vol. 8, no. 1, pp. 219–229, Jan. 2017.

[164] M. Moradijoz, M. Parsa Moghaddam, M. R. Haghifam, and E. Alishahi, "A multi-objective optimization problem for allocating parking lots in a distribution network," *Int. J. Electr. Power Energy Syst.*, vol. 46, pp. 115–122, Mar. 2013.

[165] N. Neyestani, M. Y. Damavandi, M. Shafie-Khah, J. Contreras, and J. P. S. Catalao, "Allocation of Plug-In Vehicles' Parking Lots in Distribution Systems Considering Network-Constrained Objectives," *IEEE Trans. Power Syst.*, vol. 30, no. 5, pp. 2643–2656, Sep. 2015.

[166] M. H. Amini and A. Islam, "Allocation of electric vehicles' parking lots in distribution network," in *Innovative Smart Grid Technologies Conference (ISGT), 2014 IEEE PES*, 2014, pp. 1–5.

[167] R. Baños, F. Manzano-Agugliaro, F. G. Montoya, C. Gil, A. Alcayde, and J. Gómez, "Optimization methods applied to renewable and sustainable energy: A review," *Renew. Sustain. Energy Rev.*, vol. 15, no. 4, pp. 1753–1766, May 2011.

[168] H. A. Mostafa, R. El-Shatshat, and M. M. A. Salama, "Multi-Objective Optimization for the Operation of an Electric Distribution System With a Large Number of Single

Phase Solar Generators," *IEEE Trans. Smart Grid*, vol. 4, no. 2, pp. 1038–1047, Jun. 2013.

[169] I. Das and J. E. Dennis, "A closer look at drawbacks of minimizing weighted sums of objectives for Pareto set generation in multicriteria optimization problems," *Struct. Optim.*, vol. 14, no. 1, pp. 63–69, Aug. 1997.

[170] P. Zhang *et al.*, "Multi-Objective Tradeoffs in the Design Optimization of a Brushless Permanent-Magnet Machine With Fractional-Slot Concentrated Windings," *IEEE Trans. Ind. Appl.*, vol. 50, no. 5, pp. 3285–3294, Sep. 2014.

[171] K. Deb, A. Pratap, S. Agarwal, and T. Meyarivan, "A fast and elitist multiobjective genetic algorithm: NSGA-II," *IEEE Trans. Evol. Comput.*, vol. 6, no. 2, pp. 182–197, Apr. 2002.

[172] D. S. Kirschen, J. Ma, V. Silva, and R. Belhomme, "Optimizing the flexibility of a portfolio of generating plants to deal with wind generation," in *2011 IEEE Power and Energy Society General Meeting*, 2011, pp. 1–7.

[173] W. Su and M. Y. Chow, "Performance Evaluation of an EDA-Based Large-Scale Plug-In Hybrid Electric Vehicle Charging Algorithm," *IEEE Trans. Smart Grid*, vol. 3, no. 1, pp. 308–315, Mar. 2012.

[174] "Day-Ahead Market." [Online]. Available: http://www.ercot.com/mktinfo/dam. [Accessed: 27-Mar-2017].

[175] "CVX: Matlab Software for Disciplined Convex Programming | CVX Research, Inc." [Online]. Available: http://cvxr.com/cvx/. [Accessed: 27-Mar-2017].

[176] "pg_tca30bus." [Online]. Available: http://www2.ee.washington.edu/research/pstca/pf30/pg_tca30bus.htm. [Accessed: 27-Mar-2017].

[177] R. D. Zimmerman, C. E. Murillo-Sanchez, and R. J. Thomas, "MATPOWER: Steady-State Operations, Planning, and Analysis Tools for Power Systems Research and Education," *IEEE Trans. Power Syst.*, vol. 26, no. 1, pp. 12–19, Feb. 2011.

[178] "Backcasted (Actual) Load Profiles -- Historical." [Online]. Available: http://www.ercot.com/mktinfo/loadprofile/alp. [Accessed: 27-Mar-2017].

[179] J. A. P. Lopes, F. J. Soares, and P. M. R. Almeida, "Integration of Electric Vehicles in the Electric Power System," *Proc. IEEE*, vol. 99, no. 1, pp. 168–183, Jan. 2011.

[180] S. Stüdli, E. Crisostomi, R. Middleton, and R. Shorten, "A flexible distributed framework for realising electric and plug-in hybrid vehicle charging policies," *Int. J. Control*, vol. 85, no. 8, pp. 1130–1145, Aug. 2012.

[181] C. Gouveia, C. L. Moreira, J. A. P. Lopes, D. Varajao, and R. E. Araujo, "Microgrid Service Restoration: The Role of Plugged-in Electric Vehicles," *IEEE Ind. Electron. Mag.*, vol. 7, no. 4, pp. 26–41, Dec. 2013.

[182] N. Leemput, F. Geth, J. V. Roy, A. Delnooz, J. Büscher, and J. Driesen, "Impact of Electric Vehicle On-Board Single-Phase Charging Strategies on a Flemish Residential Grid," *IEEE Trans. Smart Grid*, vol. 5, no. 4, pp. 1815–1822, Jul. 2014.

[183] D.-M. Chiu and R. Jain, "Analysis of the increase and decrease algorithms for congestion avoidance in computer networks," *Comput. Netw. ISDN Syst.*, vol. 17, no. 1, pp. 1–14, Jun. 1989.

[184] S. Studli, E. Crisostomi, R. Middleton, and R. Shorten, "AIMD-like algorithms for charging electric and plug-in hybrid vehicles," 2012, pp. 1–8.

[185] S. Stüdli, R. H. Khan, R. H. Middleton, and J. Y. Khan, "Performance analysis of an AIMD based EV charging algorithm over a wireless network," in *2013 Australasian Universities Power Engineering Conference (AUPEC)*, 2013, pp. 1–6.

[186] C. Harris, I. Dusparic, E. Galvan-Lopez, A. Marinescu, V. Cahill, and S. Clarke, "Set point control for charging of electric vehicles on the distribution network," 2014, pp. 1–5.

[187] M. Liu and S. McLoone, "Enhanced AIMD-based decentralized residential charging of EVs," *Trans. Inst. Meas. Control*, vol. 37, no. 7, pp. 853–867, Aug. 2015.

[188] I. Beil and I. Hiskens, "Coordinated PEV charging and its effect on distribution system dynamics," 2014, pp. 1–7.

[189] M. Zangs, P. Adams, T. Yunusov, W. Holderbaum, and B. Potter, "Distributed Energy Storage Control for Dynamic Load Impact Mitigation," *Energies*, vol. 9, no. 8, p. 647, Aug. 2016.

[190] T. A. Youssef, A. T. Elsayed, and O. A. Mohammed, "Data Distribution Service-Based Interoperability Framework for Smart Grid Testbed Infrastructure," *Energies*, vol. 9, no. 3, p. 150, Mar. 2016.

[191] T. A. Youssef, M. E. Hariri, A. T. Elsayed, and O. A. Mohammed, "A DDS-Based Energy Management Framework for Small Microgrid Operation and Control," *IEEE Trans. Ind. Inform.*, vol. 14, no. 3, pp. 958–968, Mar. 2018.

[192] Institute of Electrical and Electronics Engineers and IEEE-SA Standards Board, *IEEE recommended practice for 1 kV to 35 kV medium-voltage DC power systems on ships*. New York: Institute of Electrical and Electronics Engineers, 2010.

[193] N. L. Diaz, D. Wu, T. Dragicevic, J. C. Vasquez, and J. M. Guerrero, "Fuzzy droop control loops adjustment for stored energy balance in distributed energy storage system," 2015, pp. 728–735.

[194] U. Javaid, F. D. Freijedo, D. Dujic, and W. van der Merwe, "Dynamic Assessment of Source–Load Interactions in Marine MVDC Distribution," *IEEE Trans. Ind. Electron.*, vol. 64, no. 6, pp. 4372–4381, Jun. 2017.

[195] Z. Jin, G. Sulligoi, R. Cuzner, L. Meng, J. C. Vasquez, and J. M. Guerrero, "Next-Generation Shipboard DC Power System: Introduction Smart Grid and dc Microgrid Technologies into Maritime Electrical Netowrks," *IEEE Electrification Mag.*, vol. 4, no. 2, pp. 45–57, Jun. 2016.

[196] G. Sulligoi, A. Vicenzutti, and R. Menis, "All-Electric Ship Design: From Electrical Propulsion to Integrated Electrical and Electronic Power Systems," *IEEE Trans. Transp. Electrification*, vol. 2, no. 4, pp. 507–521, Dec. 2016.

[197] M. Cupelli, L. Zhu, and A. Monti, "Why Ideal Constant Power Loads Are Not the Worst Case Condition From a Control Standpoint," *IEEE Trans. Smart Grid*, vol. 6, no. 6, pp. 2596–2606, Nov. 2015.

[198] H. Park *et al.*, "Real-Time Model Predictive Control for Shipboard Power Management Using the IPA-SQP Approach," *IEEE Trans. Control Syst. Technol.*, vol. 23, no. 6, pp. 2129–2143, Nov. 2015.

[199] J. Shi, R. Amgai, and S. Abdelwahed, "Modelling of shipboard medium-voltage direct current system for system level dynamic analysis," *IET Electr. Syst. Transp.*, vol. 5, no. 4, pp. 156–165, Dec. 2015.

[200] M. M. S. Khan, M. O. Faruque, and A. Newaz, "Fuzzy Logic Based Energy Storage Management System for MVDC Power System of All Electric Ship," *IEEE Trans. Energy Convers.*, vol. 32, no. 2, pp. 798–809, Jun. 2017.

[201] M. M. S. Khan and M. O. Faruque, "Management of hybrid energy storage systems for MVDC power system of all electric ship," in *North American Power Symposium (NAPS), 2016*, 2016, pp. 1–6.

[202] J. Hou, J. Sun, and H. Hofmann, "Interaction analysis and integrated control of hybrid energy storage and generator control system for electric ship propulsion," in *2015 American Control Conference (ACC)*, 2015, pp. 4988–4993.

[203] J. Hou, J. Sun, and H. Hofmann, "Integrated control of power generation, electric motor and hybrid energy storage for all-electric ships," in *2016 American Control Conference (ACC)*, 2016, pp. 6797–6802.

[204] R. Mo and H. Li, "Hybrid Energy Storage System With Active Filter Function for Shipboard MVDC System Applications Based on Isolated Modular Multilevel DC/DC Converter," *IEEE J. Emerg. Sel. Top. Power Electron.*, vol. 5, no. 1, pp. 79–87, Mar. 2017.

[205] E. D. Din, H. A. B. Siddique, M. Cupelli, A. Monti, and R. W. D. Doncker, "Voltage Control of Parallel-Connected Dual-Active Bridge Converters for Shipboard

Applications," *IEEE J. Emerg. Sel. Top. Power Electron.*, vol. PP, no. 99, pp. 1–1, 2017.

[206] J. Neely, L. Rashkin, M. Cook, D. Wilson, and S. Glover, "Evaluation of power flow control for an all-electric warship power system with pulsed load applications," in *Applied Power Electronics Conference and Exposition (APEC), 2016 IEEE*, 2016, pp. 3537–3544.

[207] Z. Jin, L. Meng, J. C. Vasquez, and J. M. Guerrero, "Frequency-division power sharing and hierarchical control design for DC shipboard microgrids with hybrid energy storage systems," in *Applied Power Electronics Conference and Exposition (APEC), 2017 IEEE*, 2017, pp. 3661–3668.

[208] T. V. Vu, D. Gonsoulin, D. Perkins, F. Diaz, H. Vahedi, and C. S. Edrington, "Predictive energy management for MVDC all-electric ships," in *2017 IEEE Electric Ship Technologies Symposium (ESTS)*, 2017, pp. 327–331.

[209] T. V. Vu, D. Gonsoulin, D. Perkins, B. Papari, H. Vahedi, and C. S. Edrington, "Distributed control implementation for zonal MVDC ship power systems," in *2017 IEEE Electric Ship Technologies Symposium (ESTS)*, 2017, pp. 539–543.

[210] A. A. Saad, M. F. El-Naggar, and E. H. Shehab_Eldin, "Modeling and testing of multi-resolution morphological gradient distance relay algorithm," *Energy Procedia*, vol. 14, pp. 271–279, Jan. 2012.

[211] X. Lu, J. M. Guerrero, K. Sun, and J. C. Vasquez, "An Improved Droop Control Method for DC Microgrids Based on Low Bandwidth Communication With DC Bus Voltage Restoration and Enhanced Current Sharing Accuracy," *IEEE Trans. Power Electron.*, vol. 29, no. 4, pp. 1800–1812, Apr. 2014.

[212] "FPGA Board Reference Manual," [Online]. Available: https://reference.digilentinc.com/_media/reference/programmable logic/arty/arty_rm.pdf. [Accessed: 25-Aug-2018].

Appendices

Operating the Charge Control Algorithm for Electric Vehicles

1. Introduction

In order to test the developed control algorithm for the charging of electric vehicles without risk and prevent any mistakes, one should follow the complete procedure explained in this section. The first step is to check all the physical connections of the batteries, the grid, the loads and control boards. Then, the software on both the LabVIEW and the dSPACE 1104 should run and start collecting the measurements.

2. Hardware Connection of the System

As shown in Figure 1, the system under study consists of two dynamic loads, two Lithium-Ion batteries that are connected using two three phase Diode rectifiers and DC-DC converters. The way to connect the system is as follows:

2. Make sure you disconnect Generator 1 and connect the 3-phase utility connection instead. In this study, the effect of electric vehicles on the distribution system is studied and controlled. Therefore, a utility connection should be used.

3. Make sure that the high-side terminals of the batteries are connected to the DC side of the rectifiers.

4. Double check that the positive terminal of rectifier is connected to the positive terminal of DC-DC converter as shown in Figure 2. The same applies for the negative terminal. Wrong connection might damage the DC-DC converter.
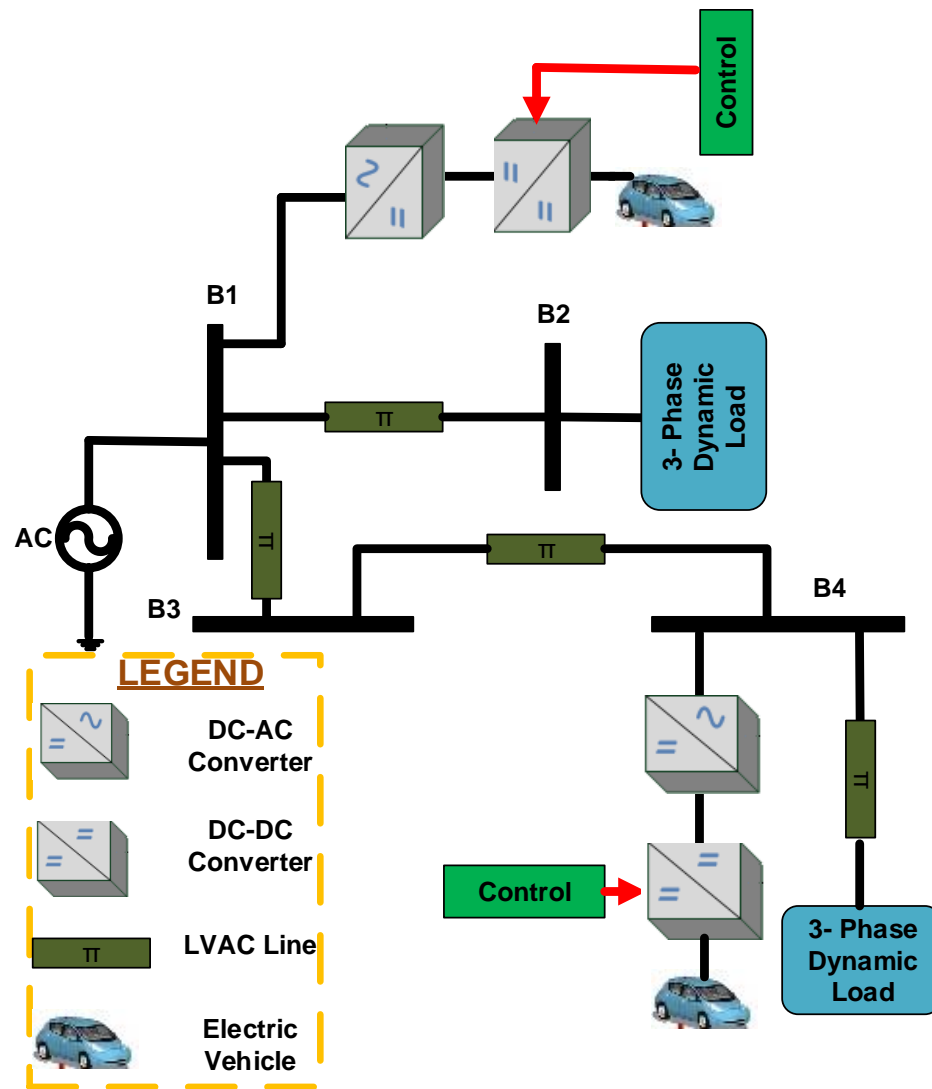
Figure 1: System Schematic

Note that the positive terminal of the rectifier is the black wire while the negative terminal is the white wire.

5. Connect the 3-phase terminal of one of the rectifiers directly to the utility through the solid-state switch 0320A. The 3-phase connection of the other rectifier is connected far from the utility connection through the solid-state switch 0380C.
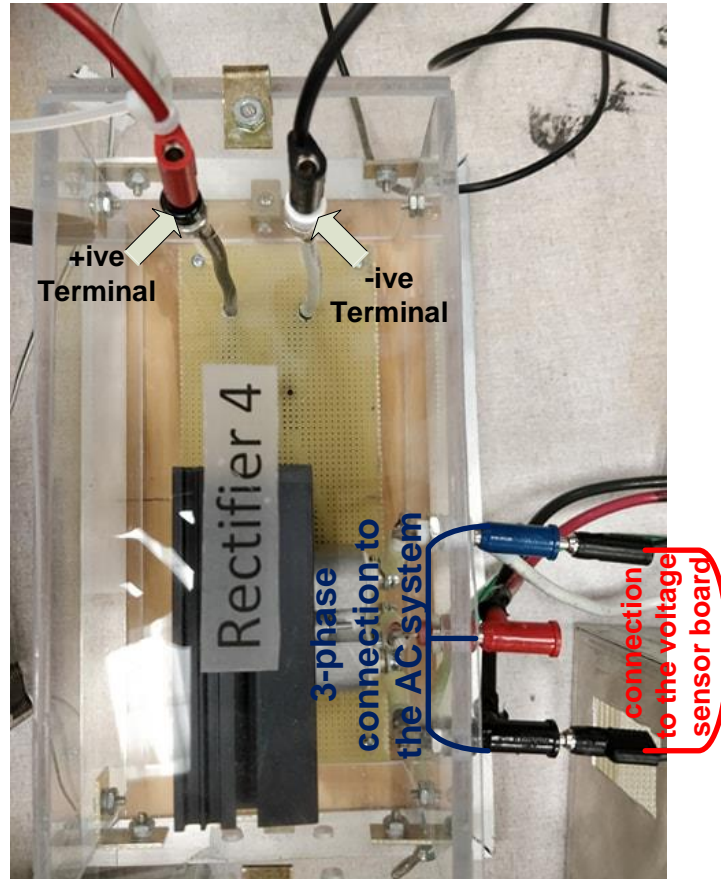
Figure 2: 3-phase Rectifier Connection

Make sure to connect the rectifiers at the correct side of the solid-state switch to have a control on its insertion and removal through the LabVIEW. Otherwise, the rectifier will be directly connected to the AC source.

6. As shown in Figure 2, to collect the voltage of the AC side and feed it to the dSPACE, a voltage sensor board is connected to measure the line-line voltage of the AC side. The sensor's connection to the rectifier is shown in Figure 2.

7. Connect the voltage and current measurements on each of the DC-DC converter to the ADCH ports of the dSPACE, shown in Figure 3. These measurements are

collected using the sensors that are embedded on the DC-DC converter. As shown in Figure 4, the DC-DC converter has two current measurements for the input and output currents and a voltage measurement of the battery side. These sensors are connected to the sensor terminals, shown on the right side of Figure 4. These terminals should be connected to three different ADCH points on the dSPACE.

8. From the dSPACE, two connections are taken from the PWM ports to a voltage amplifying circuit, shown in Figure 5. This circuit is used to amplify the PWM signals, coming from the dSPACE, to the level that is required by the driver circuit of the DC-DC converter.

9. The output of the amplifying circuit should be connected to the PWM ports on the DC-DC converter.

It is worth mentioning that only the buck-mode PWM port (the bottom one of the PWM ports in Figure 4) is used. The other PWM is connected directly to the ground.
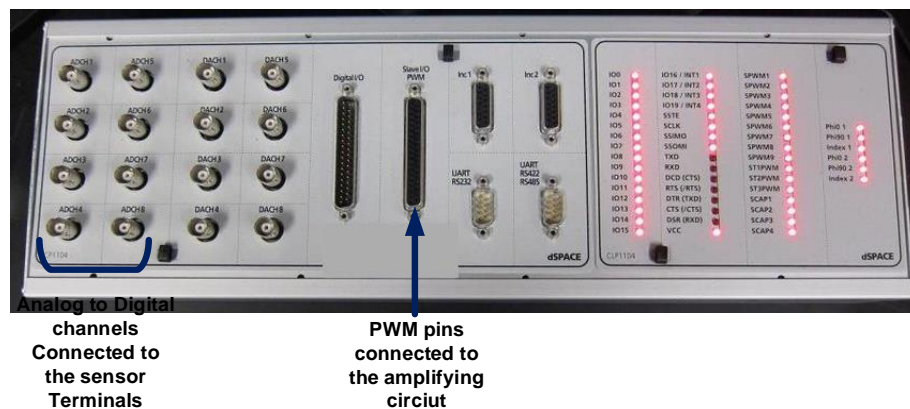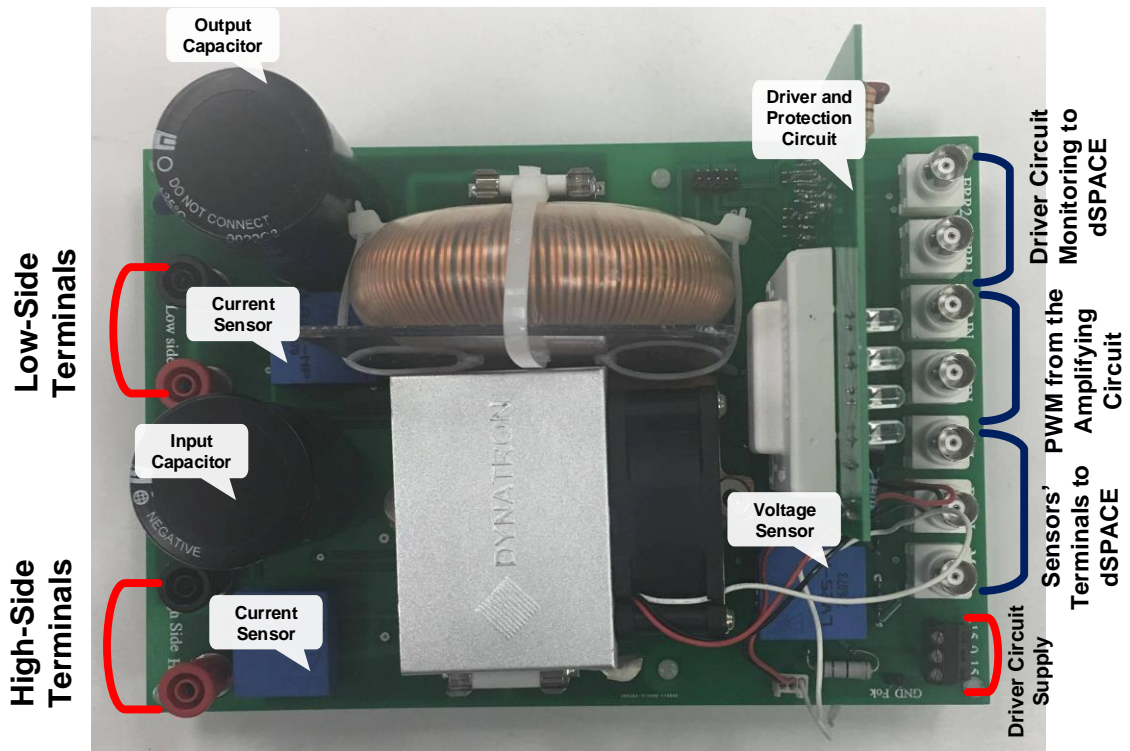

Figure 3: dSPACE 1104

Figure 4: DC-DC converter Terminals

10. Connect a two port DC supply to the driver circuit supply ports on the DC-DC converters. The DC supply should be adjusted to give +15, 0, -15 Volt. <u>Increase the voltage gradually till you reach these values. If the supply voltage increased abruptly and became higher than 15 volts value, the driver circuit will be damaged.</u>

11. Once the rectifiers and the measurements are well connected, the low voltage sides of the DC-DC converters can be connected to the batteries.

Since this experiment focuses on the effect of charging the electric vehicles, each of the batteries is connected to the low-voltage side of the DC-DC converter through a diode. The diode should be in the forward-bias mode during the charging mode of
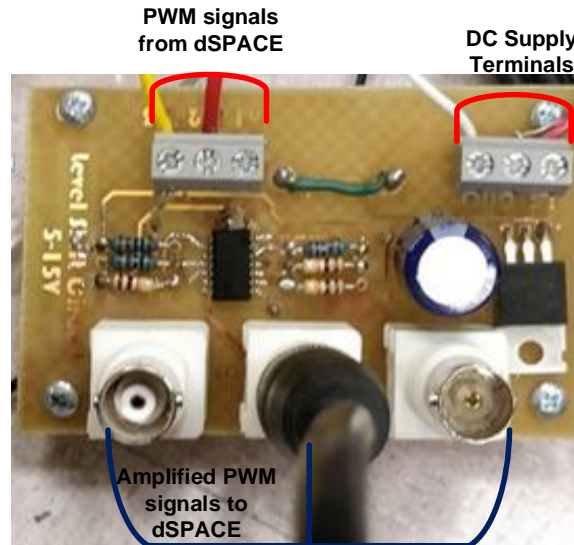
Figure 5: A circuit for amplifying the PWM signal

the batteries (from the grid to the battery), and in the reverse-bias mode during the discharging. This is done to prevent the batteries from supplying the output capacitors of the converters, which might represent a hazard of discharging into the user when the experiment is not into operation.

12. <u>Again, double check that the positive terminal of battery is connected to the positive terminal of the low-voltage side of the DC-DC converter through the diode.</u> Note that the positive terminals of the DC-DC converters are red while the negative terminals are black. The same applied to the batteries.

After making sure that all the hardware connections are done appropriately, you can go to the software part and make sure that the appropriate loads and control algorithm are used.

3. The Software Part of the Algorithm

13. From the main computer of the testbed, open the LabVIEW and select the file Hariri that contains the appropriate programmed interface for this experiment.

14. From that file, open the SCADA file, the DAQ file and generation control file. The SCADA file should be as shown in Figure 6.

15. From the Window tab in the SCADA interface, open the Block Diagram to see the programming of this interface.
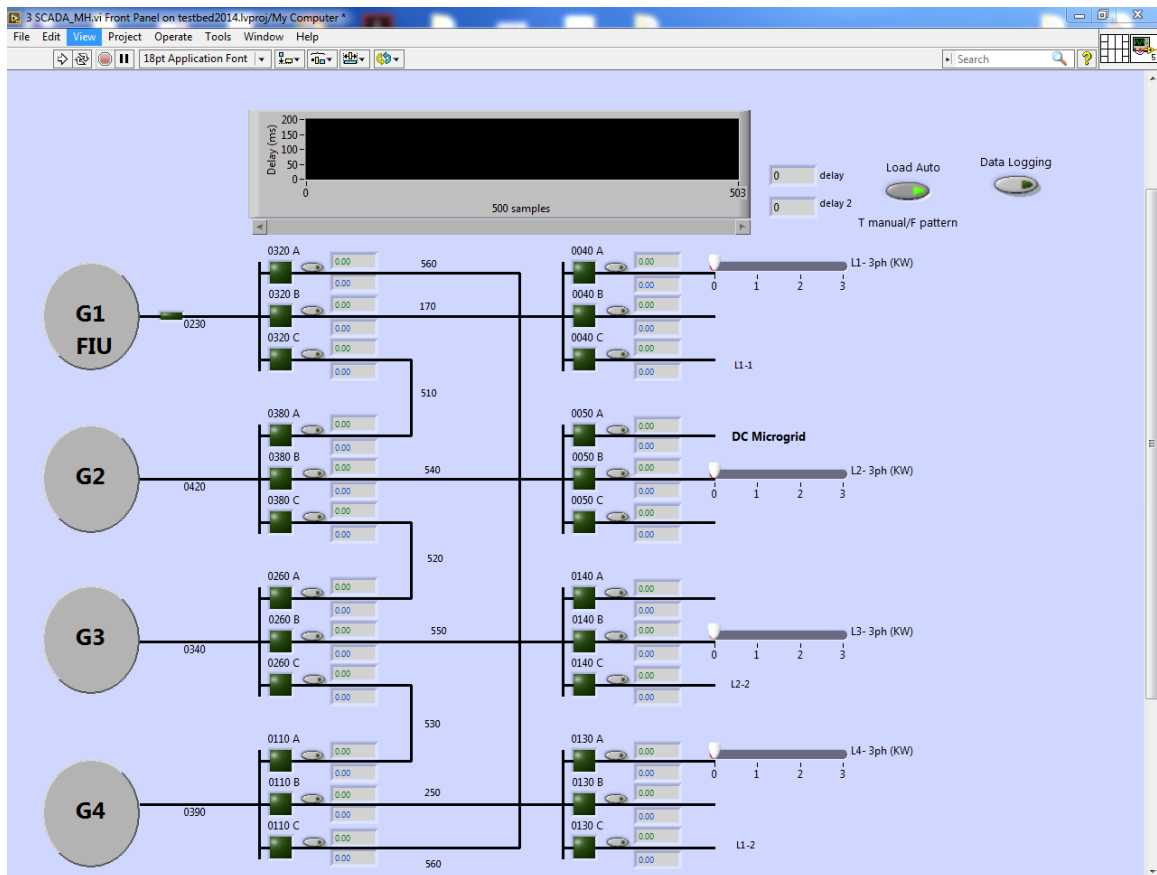

Figure 6: SCADA interface of the testbed

16. In the Block Diagram window, double check that there are two while loops for the loads L1 and L2. These loops are designed to generate variable automatic load profiles during the experiment. It should be as shown in Figure 7.

17. To make sure that the data are collected and saved during the experiment, the Block Diagram window should contain data collection blocks, as shown in Figure 8.

The data collecting is designed to collect the active and reactive powers and the three-phase voltages (Magnitudes and Angles) at the sensors 0320A, 0040A, 0380C, and 0050B.

18. After making sure that the dSPACE is programmed and you ready to start the experiment, from the LabVIEW, you should turn on the appropriate solid-state switches 0320A, 0320B, 0230C, 0040B, 0380A, 0380B, 0380C, and 0050B.

19. Also, using the load auto switch, shown in Figure 6, you should select the pattern mode.

20. To start logging the data, you should turn on the data logging switch, shown in Figure 6.
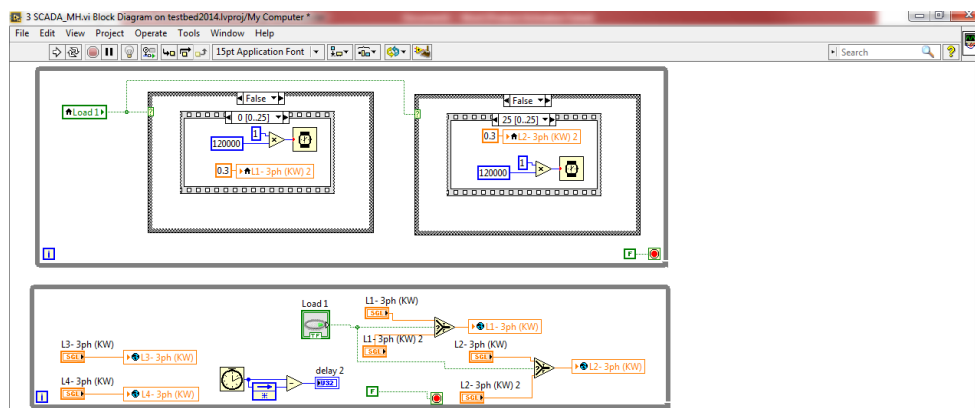

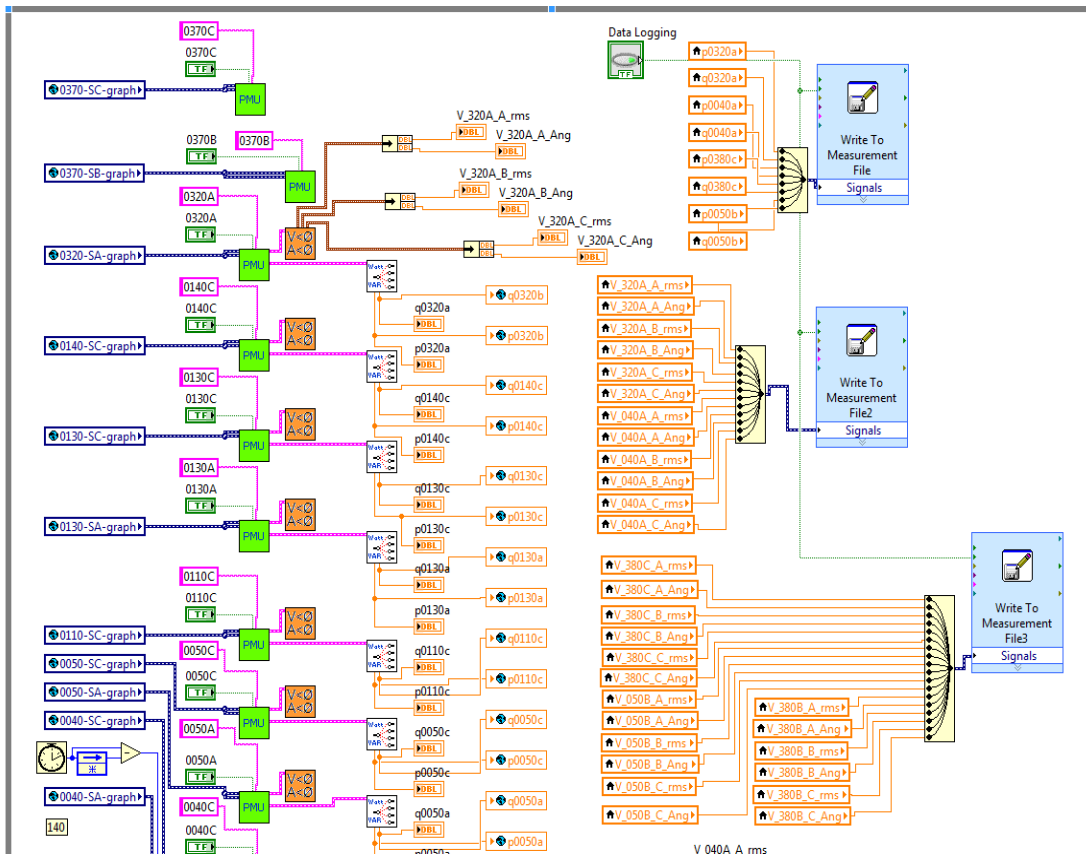Figure 7: Loops to generate automatic variable load profiles

Figure 8: Data collecting blocks for saving the real-time measurements

21. To make sure that the dSPACE is ready, open MATLAB/SIMULINK at the computer that the dSPACE cable is connected to.

22. Open the SIMULINK file that contains the control algorithm. It should be like Figure 9. This Figure shows the upper layer of the algorithm and shows all the input and output ports from the measurements and to the PWM block.

This layer contains the measurements that are calibrated to reflect the actual values before the analog to digital conversion, the voltage and current protection of the battery, the control algorithm, and the PI current controller.
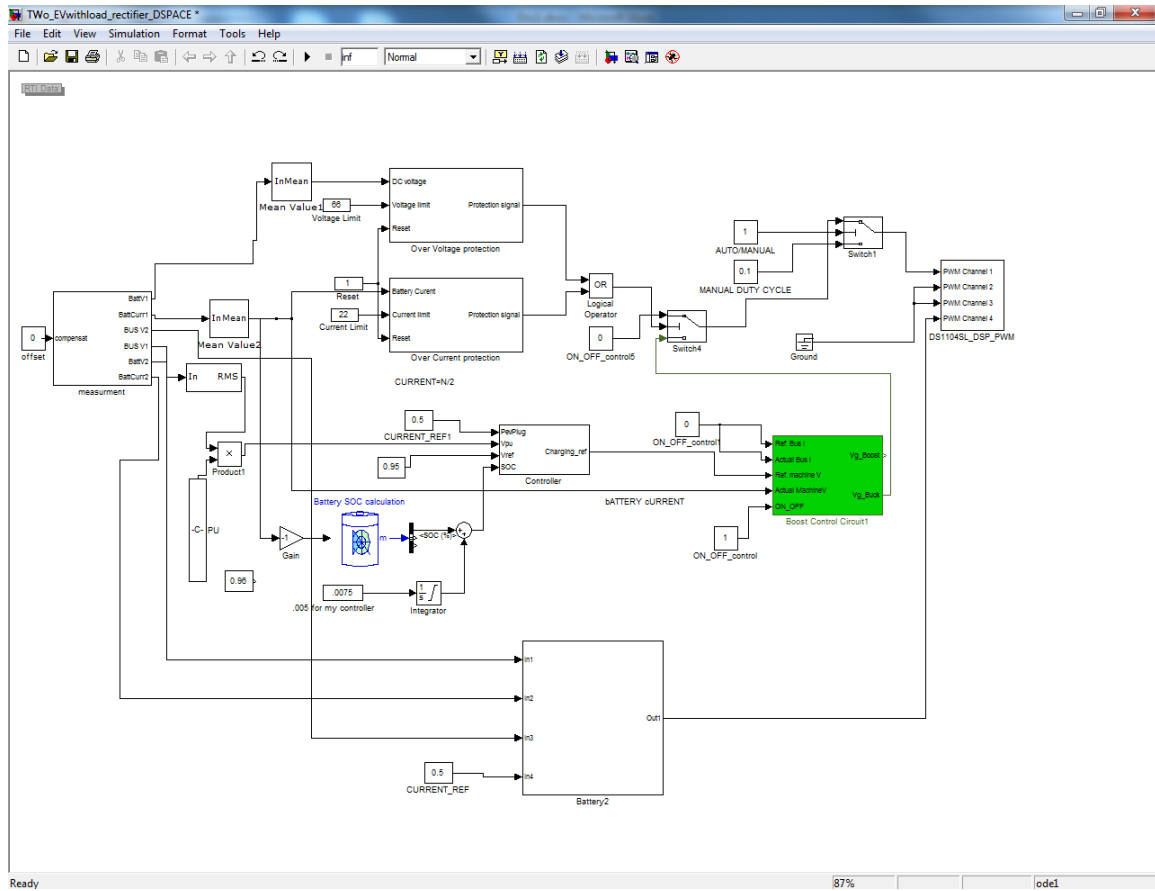
Figure 9: Upper layer of the algorithm in MATLAB/SIMULINK

23. Build this model to embed it on the dSPACE.

24. From the start menu, open the control desk.

25. From the file tab in the control desk, open the appropriate experiment file. It should open the window that is shown in Figure 10.

26. Start the dSPACE program from the control desk.

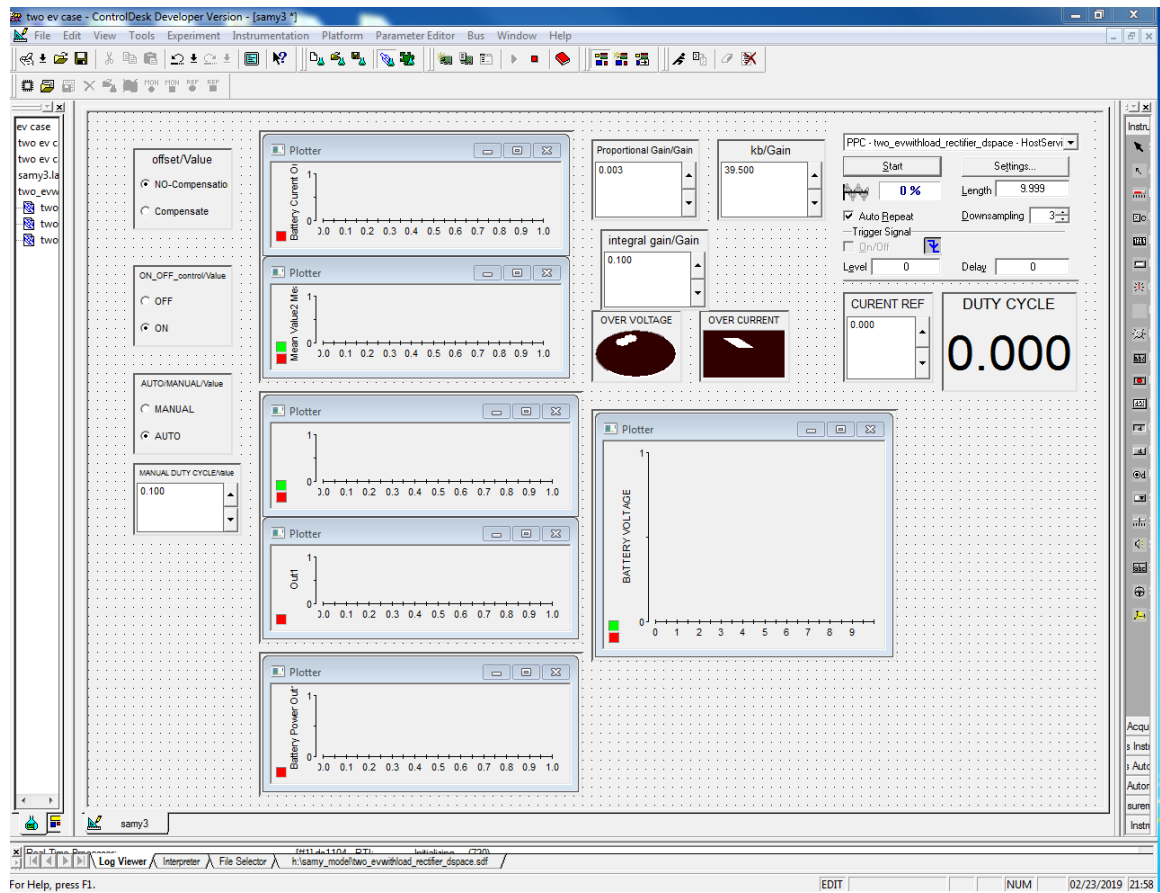27. To start collecting the result, start the animation mode.

Figure 10: Control desk of the developed algorithm

VITA

SAMY GAMAL FADDEL MOHAMED

Born, Qena, Egypt

2007-2011	B.Sc., Electrical Engineering, Assiut University, Egypt
2012-2013	Electrical Engineer, General Authority of Educational Buildings, Egypt
2013-2015	M.Sc., Electrical Engineering, King Fahd University of Petroleum & Minerals, KSA
2015-2016	Research Assistant, King Fahd University of Petroleum & Minerals, KSA
2016-2018	Graduate Teaching Assistant, Florida International University, Miami, Florida, USA
2018-2019	Dissertation Year Fellowship, Florida International University, Miami, Florida, USA

SELECTED PUBLICATIONS AND PRESENTATIONS
Format: Journal [J-*n*], Conference [C-*n*], Patent [P-*n*]

[J-1]   Samy Faddel, Ahmed A.S Mohamed and O. Mohammed, "Fuzzy Logic-Based Autonomous Controller for Electric Vehicles Charging under Different Conditions in Residential Distribution Systems," in *Electric Power Systems Research*, vol. 148, pp. 48-58, July 2017.

[J-2]   Samy Faddel, A. T. Al-Awami and O. Mohammed, "Charge Control and Operation of Electric Vehicles in Power Grids: A Review," in *Energies*, vol. 11, no. 4, p. 701, Mar. 2018.

[J-3]   Samy Faddel, Ahmed T. Elsayed and O. Mohammed, "Bi-Layer Multi-Objective Optimal Allocation and Sizing of Electric Vehicle Parking Garage," in *IEEE Transactions on Industry Applications*, vol. 54, no. 3, pp. 1992-2001, June 2018.

[J-4]   Hassan H. Eldeeb, Samy Faddel and O. Mohammed, "Multi-Objective Optimization Technique for the Operation of Grid Tied PV Powered EV Charging Station," in *Electric Power Systems Research*, vol. 164, pp. 201–211, Nov. 2018.

[J-5]   Samy Faddel, Tarek Youssef, Ahmed T. Elsayed and O. Mohammed, "An Automated Charger for Large Scale Adoption of Electric Vehicles," in *IEEE*

Transaction on Transportation Electrification, vol. 4, no. 4, pp. 971-984, Dec. 2018.

[J-6]   Ahmed A. Saad, Samy Faddel, Tarek Youssef and O. Mohammed, "Small-Signal Model Predictive Control Based Resilient Energy Storage Management Strategy for All Electric Ship MVDC Voltage stabilization," in *Journal of Energy Storage*, vol. 21, pp. 370-382, Feb. 2019.

[J-7]   Samy Faddel and O. Mohammed, "Automated Distributed Electric Vehicle Controller for Residential Demand Side Management," in *IEEE Transactions on Industry Applications*, vol. 55, no. 1, pp. 16-25, Jan.-Feb. 2019.

[J-8]   Samy Faddel, Ahmed A. Saad, Tarek Youssef and O. Mohammed, "Decentralized Control Algorithm for Hybrid Energy Storage System on Shipboard Power System," in *IEEE Journal of Emerging and Selected Topics in Power Electronics*, Early Access.

[C-1]   Samy Faddel, Ahmed A.S Mohamed and O. Mohammed, "Linear Autonomous Control of Electric Vehicles Charging in Distribution Systems," 2017 IEEE Power & Energy Society General Meeting, Chicago, IL, 2017, pp. 1-5.

[C-2]   Samy Faddel, Tarek Youssef and O. Mohammed, "Decentralized Controller for Energy Storage Management on MVDC Ship Power System with Pulsed Loads," 2018 IEEE Transportation Electrification Conference and Expo (ITEC), Long Beach, CA, USA, 2018, pp. 254-259.

[C-3]   Samy Faddel, Mohamad El Hariri and O. Mohammed, "Intelligent Control Framework for Energy Storage Management on MVDC Ship Power System," the 18th International Conference on Environment and Electrical Engineering 2018 (EEEIC), Palermo, Italy, 2018, pp. 1-6.

[C-4]   Samy Faddel, Tarek Youssef, Ahmed T. Elsayed and O. Mohammed, "Experimental Verification of the Effect of Uncoordinated Charging of Electric Vehicles on Power Grids," the 2019 IEEE PES Innovative Smart Grid Technologies Conference, In press.